ISSN 2433-2232(Online)
JAXA-SP-21-002

宇宙航空研究開発機構特別資料

JAXA Special Publication

Seventh Aerodynamics Prediction Challenge（APC-7）

開催日：2021年6月30日

開催場所：オンライン開催

2021年11月

宇宙航空研究開発機構

Japan Aerospace Exploration Agency

目　次

Aerodynamics Prediction Challenge (APC) 企画趣意書

1983 年に初回が開催された航空宇宙技術研究所(当時)の航空機計算空気力学シンポジウムが，我が国の航空宇宙分野における計算空気力学技術の発展を牽引したことは論じるまでもありません。第 1 回のシンポジウム論文集(NAL SP-1)の巻頭言では，当時の武田峻所長が「各分野の研究者や技術者の皆様に研究発表と意見交換の場を提供し，それによって航空機設計技術の発展に寄与する」と記しています。その意思は 30 年以上経過した現在においても航空宇宙数値シミュレーション技術シンポジウム(ANSS)に引き継がれています。しかし，膨大な技術情報へのアクセスを容易に実現するインターネットの発達は，学生や研究者と民間技術者の交流の機会を減少させ，近年の計算空気力学研究が航空機設計開発現場の求める研究課題や方向性を見失う一因になっているのではないかと危惧されます。

今日の計算空気力学手法は，80 年代には想像できなかった計算機ハードウェアの著しい発展と数々の新しい計算技術に支えられ，航空機設計開発に不可欠なツールと認識されるまでに至りました。しかし一方，計算空気力学手法の成熟度が高まるに連れて，定常流れ場に対する計算空気力学手法はある種のスタンダードが認知浸透し，設計開発現場では宇宙航空研究開発機構(JAXA)の標準コードや商用コードの活用も進められるなど，計算空気力学研究に停滞感が出てきているのも事実です。計算空気力学の停滞は，空気力学研究のパートナーである風洞技術の高度化にも影響を与えかねません。この停滞感を打破し，いま一度新たな高みを目指すには，航空機設計開発現場の求める研究課題や方向性が具体的に示されることが重要だと思われます。

この APC と名付けられたワークショップでは，実機開発に活用されている計算空気力学課題や将来の利用が期待されるテーマを選定し，JAXA で取得された風洞試験データとの詳細な比較を行うことによって，計算空気力学ならびに風洞技術の発展に求められる新たな課題を抽出しその解決を共同で模索することを目指します。APC 参加者による新たな課題への挑戦は，計算空気力学研究や風洞技術開発を活性化させ，機会の減少が懸念される産官学交流を促し，最終的には我が国の航空宇宙産業の発展と欧米に次ぐ第 3 極としてのプレゼンス向上に貢献することが期待されます。産官学がそれぞれの立場から APC を活用していただくことを望んでいます。

澤田恵介，APC 有識者会議 前代表（全体）
今村太郎，APC 有識者会議 現代表（全体）
青山剛史，APC 有識者会議 代表（CFD）
浜本滋，　APC 有識者会議 代表（風洞試験）

Seventh Aerodynamics Prediction Challenge (APC-7) の開催について

流力 ANSS は当初対面での開催が検討されましたが，コロナの感染状況が改善せず，昨年度に引き続き，オンラインでの開催となりました。そのため，ANSS の企画セッションとして開催される APC-7 についても，オンラインで実施されました。それにも関わらず，JAXA，大学，産業界から 10 件の発表申込みがあり，ほぼ例年通りの発表件数が集まりました。また，当日は，多くの方にご聴講いただき，盛況に終えることができました。APC-7 の開催にご協力いただいた，発表者，学会参加者，実行委員会の皆様に，深く感謝申し上げます。

APC-7 の課題は，APC-6 に続き，NASA-CRM の低速・高迎角流の予測を対象としました。低速・高迎角時に主翼で剥離して失速したり，主翼の後流が尾翼に干渉して機体が振動したりする場合は，それらがフライトエンベロープを定める為，現象を正確に予測することが求められます。また，レギュレーションによる安全性要求として，不意に失速しても急激なピッチアップにならないことが求められており，失速付近でのピッチングモーメント傾向予測も重要となります。このように，巡航，離陸，着陸のいずれの形態でも低速・高迎角時の空力特性予測は重要であることを踏まえ，APC ではそれらのベース形状である巡航形態の低速・高迎角特性を対象とし，CFD と実験を比較することで，現状の CFD の予測精度を把握することを目的としました。

APC-7 では，APC-6 で明らかになった課題に取り組むため，フォーカスポイントを設定し，主翼剥離に対する計算手法の影響，及び主翼後流の尾翼干渉に対する計算手法の影響を重点的に調査することにしました。参加者によるオンラインによる事前ミーティングを開催し，この開催趣旨を共有し，疑問点などを質問できる場を設けました。そのため，データの提出や集計作業が従来よりも円滑にできたと思います。これをきっかけに，今後は事前ミーティングも積極的に活用していきたいと思います。

本資料では，APC-7 の成果を公開するため，JAXA 特別資料として出版します。JAXA，大学，産業界を含む All-Japan のチームで，CFD の難題に挑んだ成果です。参加者全員の発表資料と集計データを掲載しました。これらの成果が，今後の CFD や空気力学研究の発展に寄与することを期待しています。

APC 有識者会議

Aerodynamics Prediction Challenge 有識者会議　委員名簿

代表	今村太郎	東京大学大学院 工学研究科 航空宇宙工学専攻
代表	青山剛史	JAXA　航空技術部門　数値解析技術研究ユニット
代表	浜本滋	JAXA　航空技術部門　空力技術研究ユニット
委員	松島紀佐	富山大学大学院　理工学研究部　機械知能システム工学専攻
委員	佐々木大輔	金沢工業大学　工学部　航空システム工学科
委員	吉本稔	三菱重工業（株）総合研究所　流体研究部　流体第三研究室
委員	上野陽亮	川崎重工業（株）航空宇宙ｼｽﾃﾑｶﾝﾊﾟﾆｰ　技術統括部 技術開発部 空力技術課
委員	中北和之	JAXA　航空技術部門　空力技術研究ユニット
委員	村山光宏	JAXA　航空技術部門　航空システム研究ユニット
委員【事務局】	香西政孝	JAXA　航空技術部門　空力技術研究ユニット
委員【事務局】	橋本敦	JAXA　航空技術部門　数値解析技術研究ユニット

APC-7 プログラム

（2021 年 6 月 30 日第 53 回流力講演会／第 39 回 ANSS 内で開催）

14:45-14:55	APC-7 の課題説明 橋本 敦(JAXA)，APC 有識者会議
14:55-15:05	APC-7 における NASA-CRM の低速・高迎角時の風洞試験データ 香西 政孝（JAXA）
15:05-15:20	FaSTAR を用いた低速・高迎角条件における NASA-CRM 解析の格子依存性調査 橋本 敦，小島 良実，金森 正史（JAXA），松﨑 智明（アドバンスソフト），中元 啓太，林 謙司（菱友システムズ）
15:20-15:35	Cflow による NASA 巡航 CRM の低速高迎角剥離流れの予測 上野 陽亮，安田 英将，澤木 悠太（川崎重工）
15:35-15:50	階層型直交格子と再帰的なフィッティングを用いた低速・高迎角条件における NASA-CRM 巡航形態の空力予測 菅谷 圭祐，原 惇，今村 太郎（東大院）
15:50-16:05	階層型直交格子と埋め込み境界法を用いた低速・高迎角条件における NASA-CRM 巡航形態の空力予測 原 惇，菅谷 圭祐，今村 太郎（東大院）
16:05-16:20	休憩
16:20-16:35	壁面応力モデルを適用した直交カットセル法による NASA-CRM まわりの圧縮性流れの数値解析 髙橋 佑太（岩手大院），竹田 裕貴（岩手大），松原 夏鈴（岩手大院），上野 和之（岩手大）
16:35-16:50	NASA CRM 低速バフェットの非定常流体解析における乱流モデルと数値流束関数の比較 安村 祐哉，北村 圭一，古澤 善克（横国大），金森 正史，橋本 敦（JAXA）
16:50-17:05	Flux-Reconstruction 法と壁面モデルを用いた NASA-CRM の低速・高迎角流の非定常解析 坂井 玲太郎，芳賀 臣紀，福島 裕馬，村山 光宏（JAXA），雨宮 孝（QuickMesh），伊藤 浩之（菱友システムズ）
17:05-17:20	APC-7 の集計結果 橋本 敦(JAXA)，APC 有識者会議
17:20-18:00	ディスカッション

The 53th Fluid Dynamics Conference/ The 39th Aerospace Numerical Simulation Symposium
30th June 2021

APC-7の課題説明

Test cases of Seventh Aerodynamics Prediction Challenge (APC-7)

橋本敦（JAXA）, APC有識者会議
Atsushi Hashimoto (JAXA), APC committee

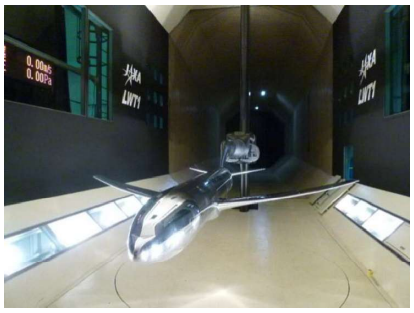

Objective

- Predicting aerodynamic characteristics at low speeds and high angles of attack of aircraft is an important research subject. At low speeds and high angles of attack, a flow above the main wing is separated and this causes stall of aircraft, or a wake of the main wing interferes with the tail wing. If the aircraft vibrates, this determines the flight envelope, so it is required to accurately predict the phenomenon. In addition, as a safety requirement due to regulation, it is required that the pitch angle does not rise sharply even if the aircraft suddenly stalls. Therefore, it is also important to predict the pitching moment tendency near the stall.
- Since the aerodynamic prediction at low speeds and high angles of attack is important in any configurations of cruising, takeoff, and landing, the APC-7 targets the characteristics of the cruise, which is the base shape of these configurations. The objective of APC-7 is to understand the prediction accuracy of the current CFD by comparing the CFD with the experiment.

Test cases of APC-7

- Aerodynamics prediction of NASA-CRM

  Case1 : Steady computation

  Case2 : Unsteady computation

- Geometry

  NASA-CRM (Wing/Body/Horizontal Tail)

- Flow conditions

  M = 0.168, Re_c = 1.06 x 10^6, T_{ref}=310K

3

Case1 : Steady computation

- Aims
  - Understand the prediction accuracy of aerodynamic performance such as CL, CD, Cm at low speeds and separation characteristics (beginning of separation, separated area).
  - Understand the dependency of turbulence model, grid.

- Conditions
  - M = 0.168, Re_c = 1.06 x 10^6, T_{ref}=310K
  - AoA=-3.22, -0.67, 2.89, 5.95, 9.01, 10.03, 11.05, 12.06, 13.08, 14.08, 18.08deg

4

Case2 : Unsteady computation

- Aims
  - Understand the prediction accuracy of unsteady computation by comparing the unsteady computation with the steady computation.
  - Understand the dependency of turbulence model, grid, time step.

- Conditions
  - M = 0.168, Re_c = 1.06 x 10^6, T_{ref}=310K
  - AoA=11.05, 13.08deg

5

Point of focus

- The test cases of APC-7 are same as those of APC-6. In APC-7, we focus on the following points. The participants are expected to investigate the sensitivities of the phenomena and propose a best practice. Application of AI, ML, and data mining techniques are also encouraged.
  - **Prediction of the main-wing separation**
    - Effect of numerical methods on the leading-edge separation
    - Effect of numerical methods on the trailing-edge separation
  - **Prediction of the interference between main-wing wake and tail wing**
    - Effect of numerical methods on the wake

<u>Examples of the numerical methods:</u>

- Type of grids (mixed-element or hexahedral), grid resolution(number of nodes or cells)
- Accuracy and dissipation of the numerical schemes
- Turbulence models (Steady: SA, SST, Unsteady: DES, IDDES, WMLES)
- Conditions of unsteady computation: Initial conditions (Uniform flow or lower-AoA solution), time step, number of inner iteration, time evolution method(local time step or global time step)

6

Submitted Data

Test Case	Value	AoA	Remark
1	Grid	-	Picture Image (Only for custom grids)
	Aerodynamic coefficients	All angles	Data for plots Converged value (decomposed by pressure and skin friction, by components)
	Surface Cp	All angles	Data for plots Converged value Cross sections on main and tail wings.
	Surface streamline	11.05, 13.08deg	Picture image Converged value Surfaces of main and tail wings.
	Velocity contours		Picture image Converged value
2	Grid	-	Picture Image (Only for custom grids)
	Aerodynamic coefficients	11.05, 13.08deg	Data for plots Converged value (decomposed by pressure and skin friction, by components)
	Surface Cp		Data for plots Averaged and RMS values Cross sections on main and tail wings.
	Surface streamline		Picture image Averaged value Surfaces of main and tail wings.
	Velocity contours		Picture image Averaged values

Cross sections for Cp distributions

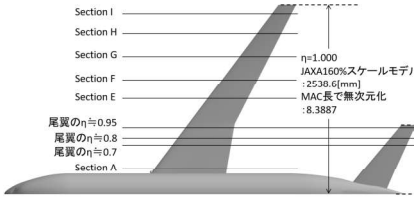

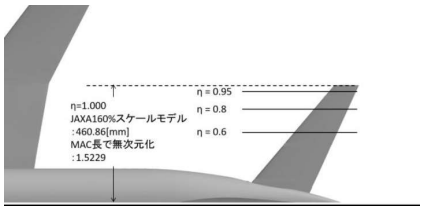

7

Submitted Data

Test Case	Value	AoA	Remark
1	Grid	-	Picture Image (Only for custom grids)
	Aerodynamic coefficients	All angles	Data for plots Converged value (decomposed by pressure and skin friction, by components)
	Surface Cp	All angles	Data for plots Converged value Cross sections on main and tail wings.
	Surface streamline	11.05, 13.08deg	Picture image Converged value Surfaces of main and tail wings.
	Velocity contours		Picture image Converged value
2	Grid	-	Picture Image (Only for custom grids)
	Aerodynamic coefficients	11.05, 13.08deg	Data for plots Converged value (decomposed by pressure and skin friction, by components)
	Surface Cp		Data for plots Averaged and RMS values Cross sections on main and tail wings.
	Surface streamline		Picture image Averaged value Surfaces of main and tail wings.
	Velocity contours		Picture image Averaged values

Cross sections for velocity contours

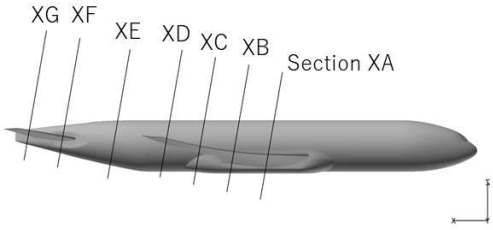

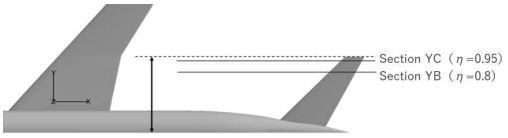

The data of cross sections are provided as csv and plot3d formats

8

APC Website

- Geometry (formats: stl)
  - NASA-CRM geometry data are available
- Grid (formats: fsgrid, cgns)
  - HexaGrid and BOXFUN grids are available
- Please see the APC website for more information
  - https://cfdws.chofu.jaxa.jp/apc/

1A-14　APC-7におけるNASA-CRMの低速・高迎角時の風洞試験データ
NASA Common Research Model (CRM) wind tunnel data at low speed and high angle of attack conditions in APC-7

香西政孝（JAXA）
KOHZAI Masataka (JAXA)

The 53rd Fluid Dynamics Conference/ The 39th Aerospace Numerical Simulation Symposium, 30th June 2021

Outline

- Explain NASA CRM data measured at JAXA 6.5m×5.5m low speed wind tunnel provided to APC-7.
- Please refer to ‘2A03’ at this symposium, if you want to know details of the wind tunnel results.

- Contents
  - Wind tunnel tests description
    - Wind tunnel and Model description
    - Measurement items and wind tunnel condition
  - Wind tunnel test data
    - Forces and moments
    - Surface pressure data of main wing and h-tail (Steady and Unsteady)
    - Vibration data of main wing and h-tail
    - Oil flow visualization
    - Stereo PIV

JAXA 6.5m × 5.5m low speed wind tunnel (JAXA LWT1)

- Type: Closed circuit（Atmospheric）
- Test section: 6.5m height 5.5m width （Octagonal with corner truncated 1m）
- Maximum Flow speed: 70m/s
- Constructed: 1965

Blockage ratio : 0.29%

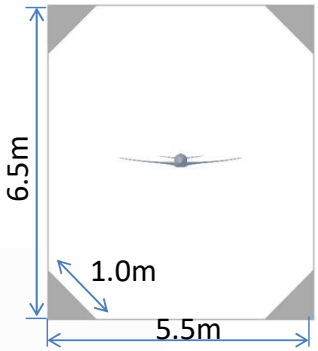

Sting Cart

Strut Cart

Blower
ϕ9.3m

Electric Motor
3,000kW

Strut Cart at JAXA LWT1

- Models are supported with two struts.
- Forces and moments are measured with pyramid-type 6 component balance.

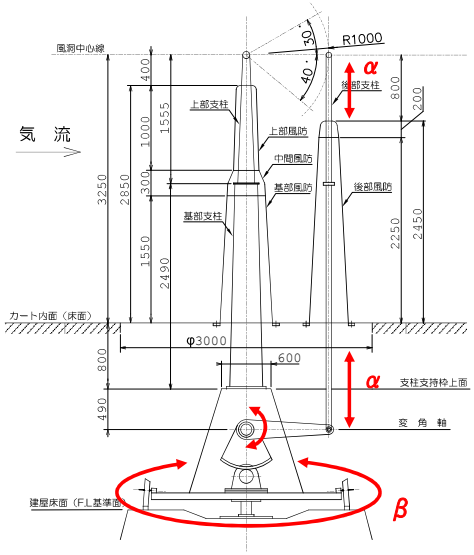

Strut support

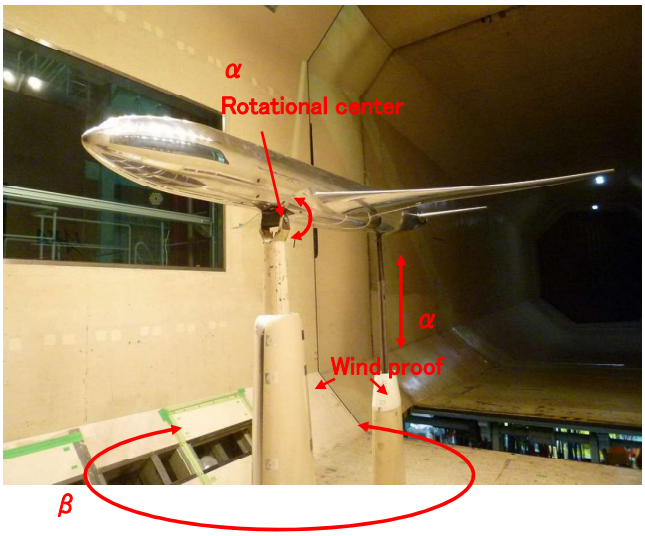

Wind tunnel model

- NASA Common Research Model
  - Scale to assumed aircraft：4.32%
  - Length: 2.711m
  - Span length: 2.539m
  - Reference area: 0.716m^2
  - Reference cord: 0.303m
  - Applied trip dots
    - ✓ Location ：Wing, horizontal tail, Nose.
    - ✓ Height：11.4 [in/1000]

- Used horizontal tail with pressure transducers
  - ✓ Pressure taps: 12
  - ✓ Kulite transducers: 10
- Bonded Kulite transducers on the main wing
  - ✓ Kulite transducers: 4

5

Locations of pressure taps, kulite transducers, and strain gages on the main wing and horizontal tail

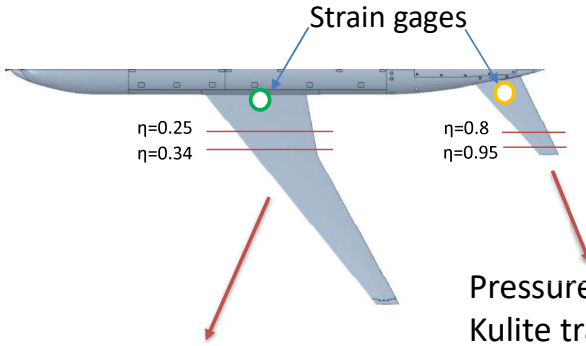

Kulite transducers on the wing

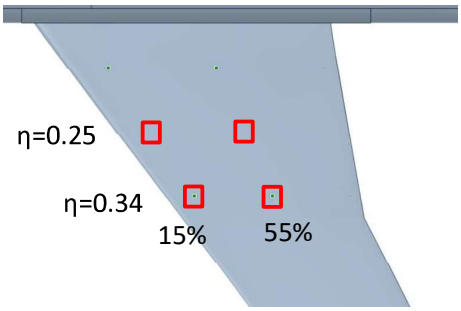

Pressure taps and Kulite transducers on the horizontal tail

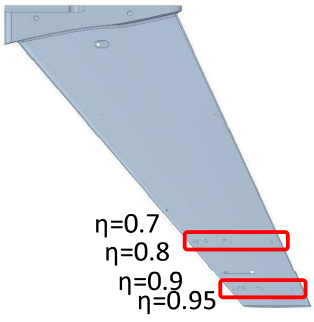

Pressure Tap			
Port	η	Location	Cord, %
1	0.8	Leading edge	0
2	0.8	Upper	5
3	0.8	Upper	10
4	0.8	Upper	20
5	0.8	Upper	45
6	0.8	Upper	90
7	0.95	Leading edge	0
8	0.95	Upper	5
9	0.95	Upper	10
10	0.95	Upper	20
11	0.95	Upper	45
12	0.95	Upper	85

Kulite			
Port	η	Location	Cord, %
1	0.7	Upper	5
2	0.8	Leading edge	0
3	0.8	Upper	10
4	0.8	Upper	20
5	0.8	Upper	40
6	0.9	Lower	12.5
7	0.95	Leading edge	0
8	0.95	Upper	15
9	0.95	Upper	20
10	0.95	Upper	40

6

Measurement data sets

Test id	Model	Test conditions	Measurement items	Provided to APC
Sting Cart Test	NASA CRM	V=60m/s Re=1.06 × 10^6	Forces and Moments Oil flow visualization PIV（x-z Section）	APC6 APC6 APC7
1st Strut Cart Test	NASA CRM Main wing：Kulite transducers horizontal tail :pressure taps and Kulite transducers	V=53-60m/s Re=1.06 × 10^6	Forces and Moments Oil flow visualization Steady pressures Unsteady pressures Vibration of the wings	APC7
2nd Strut Cart Test	NASA CRM	V=53-58m/s Re=1.06 × 10^6	Stereo PIV （y-z Section）	APC7

7

Wind tunnel results

- Stall characteristic at high AoA
  - Forces and Moments
  - Oil flow visualization
- Steady and Unsteady pressures, and vibrations of wing and h-tail
  - Steady pressures on wing and h-tail
  - Unsteady pressures on wing and h-tail
  - Vibration of wing and h-tail
- Velocity distributions between wake of main wing and h-tail
  - PIV（x-z section）
  - Stereo PIV（y-z section）

8

Comparisons of aerodynamic data between two supports

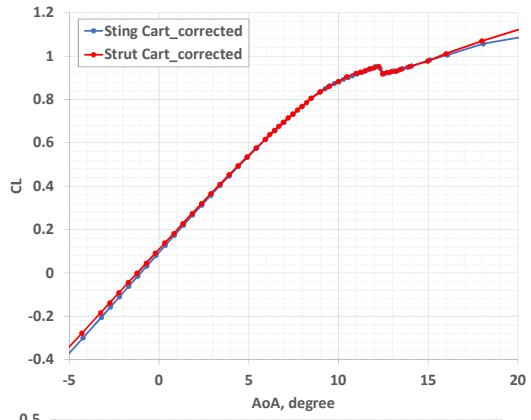

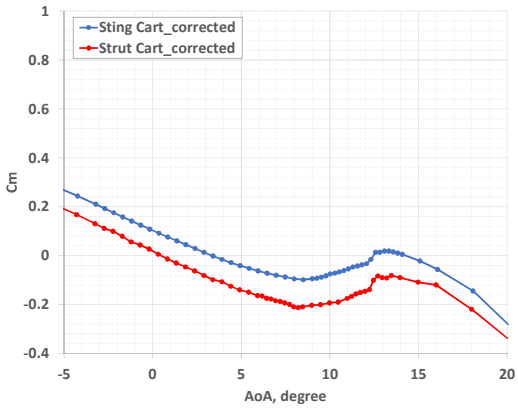

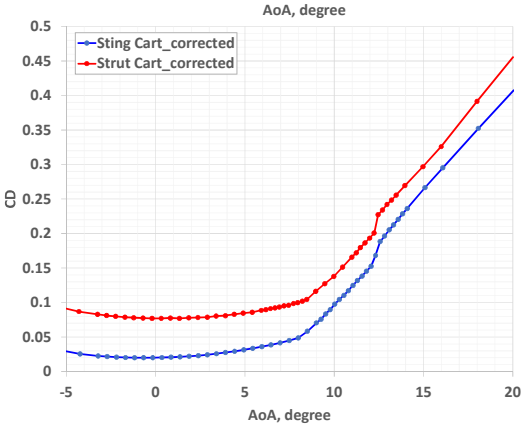

- CL increases linearly to 8.5 degrees, and CL decreases drastically at AoA=12.5.
- The tendency is almost the same for sting cart data and strut cart data. The difference of CD and Cm are influenced on aerodynamic forces received at the strut.
- The repeatability of CL, CD, and Cm are 0.005, 0.001, and 0.01 respectively.

※Sting cart data are referred to AIAA2019-2190

Oil flow visualization at AoA=8-13 degrees

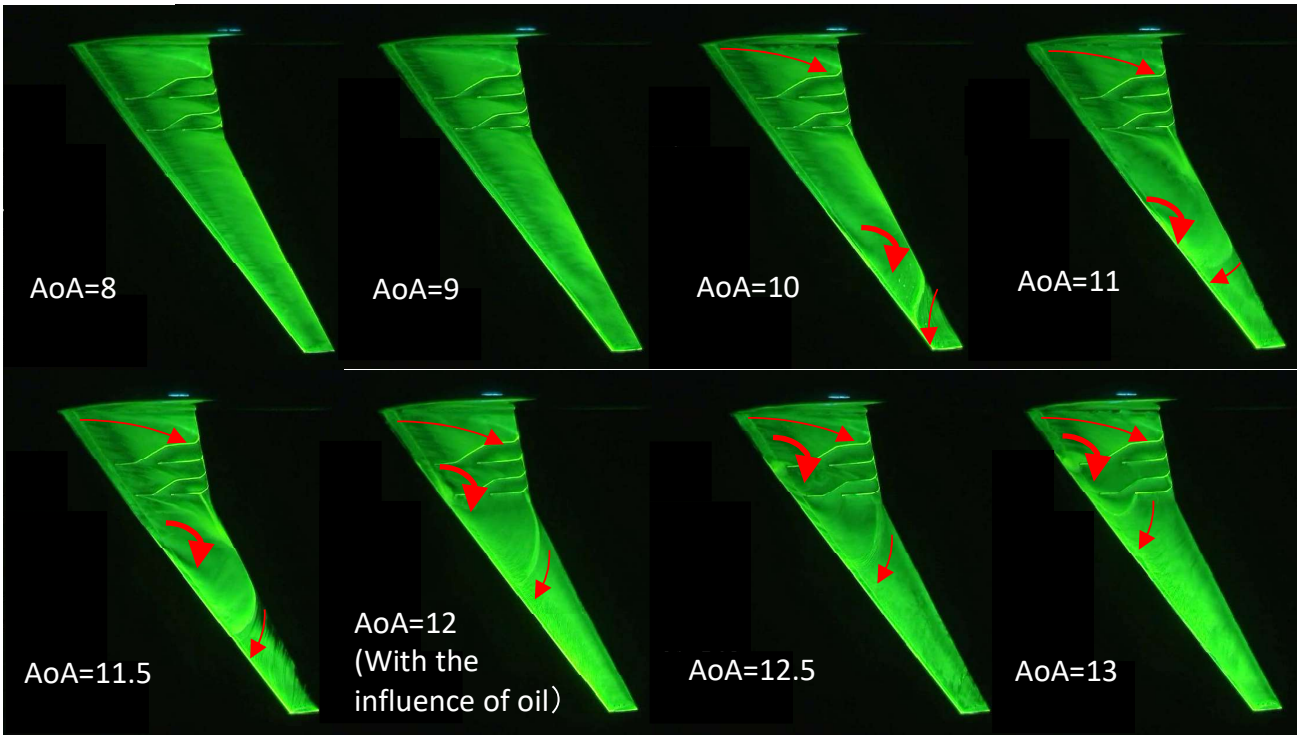

Though the separation area is outside of the kink on the main wing at AoA=11.5degree, the separation area spreads near wing root at stall angle.

Pressure distributions on h-tail

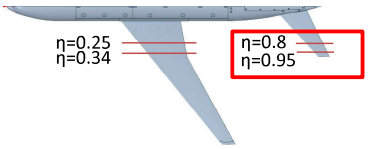

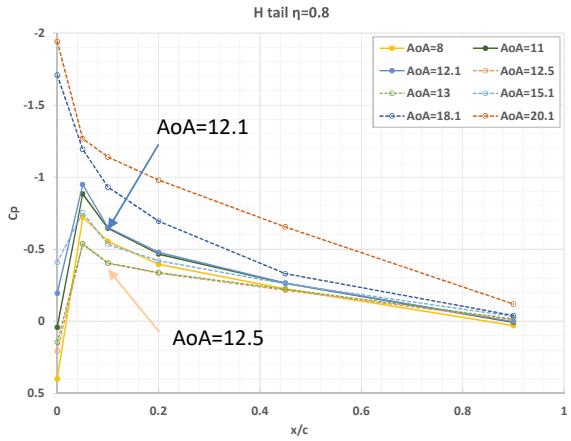

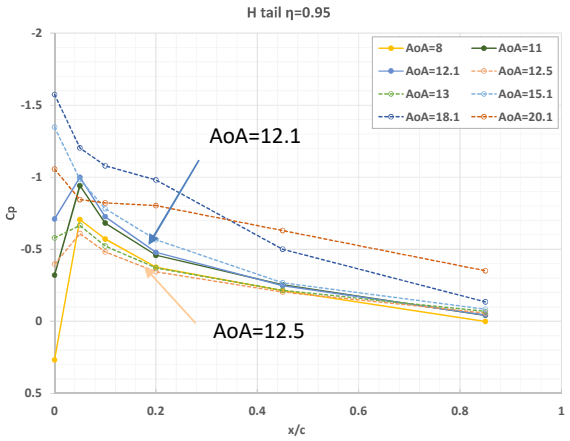

- At the stall angle, the lift of the h-tail is reduced.

Pressure distributions on main wing

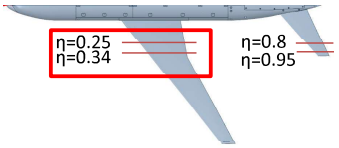

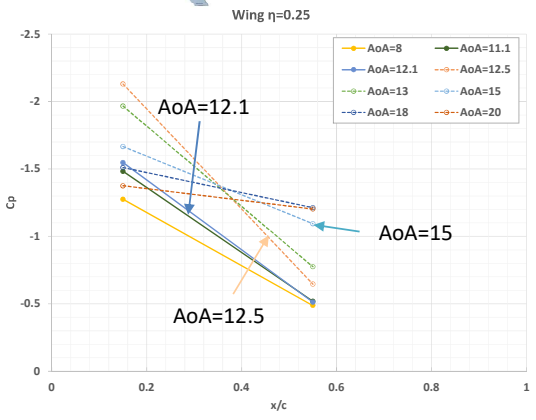

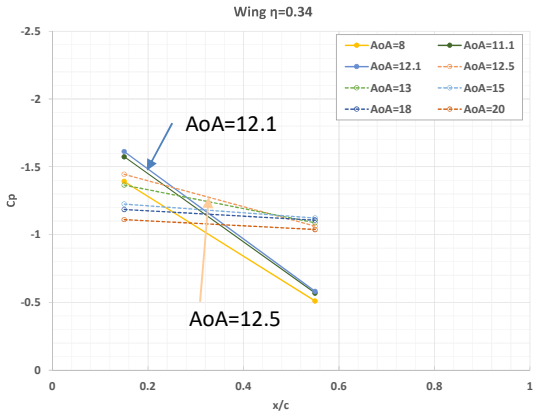

- At the stall angle, the suction is reduced, so that the flow separation on the main wing is confirmed.

※The data is interfered with existence of the Kulite transducers.

RMS variations of unsteady pressures and vibrations of wing and h-tail

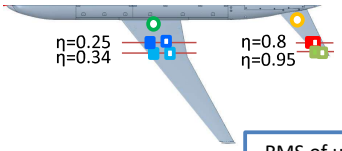

RMS of unsteady pressures

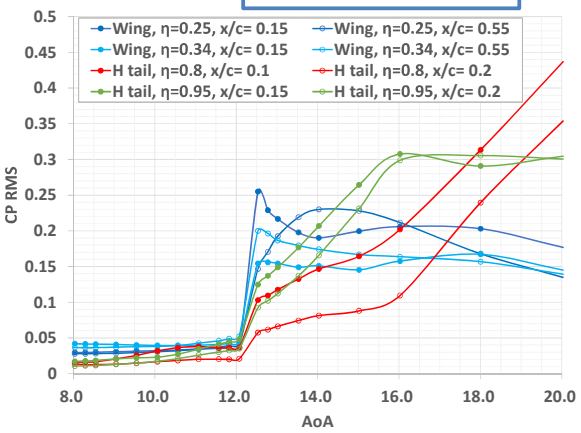

RMS of vibrations

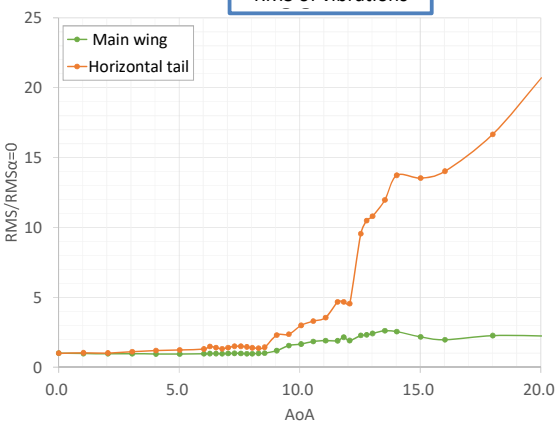

- The RMS of unsteady pressures of wing and h-tail increases drastically at the stall angle of 12.5 degrees. With that increases, vibration of h-tail increases.
- Vibration of main wing increases from angles of 9 degrees. H-tail vibrates slightly also.

PIV results at the sting cart test

☐ At the sting cart test, PIV measurements are conducted. At the post stall angles, we confirmed separation flow effects on η=0.8 and 0.9 of the horizontal tail.

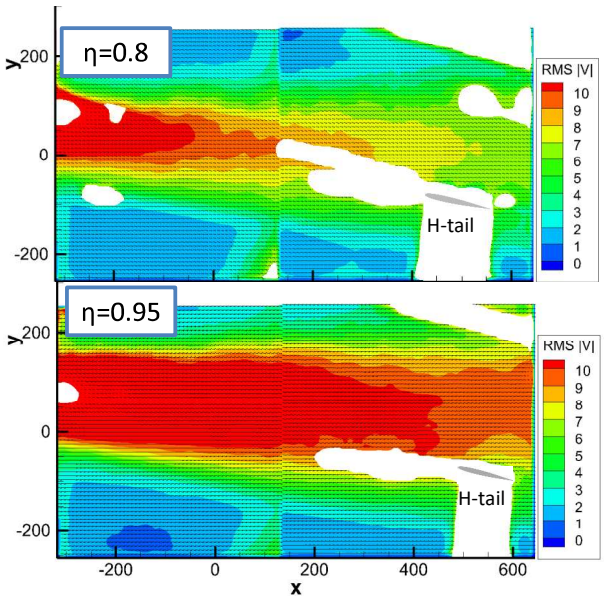

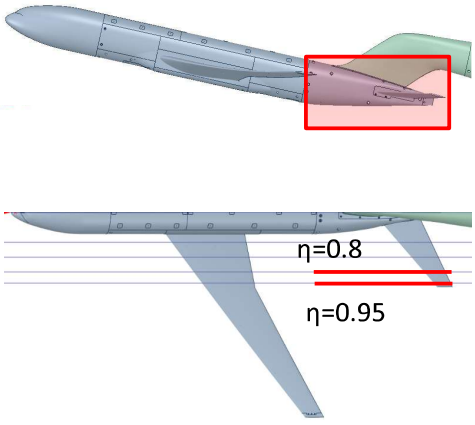

V=60m/s, AoA=12.5degrees

Horizontal tails with pressure taps and Kulite transducers at η=0.8,0.95 are manufactured.

Stereo PIV results

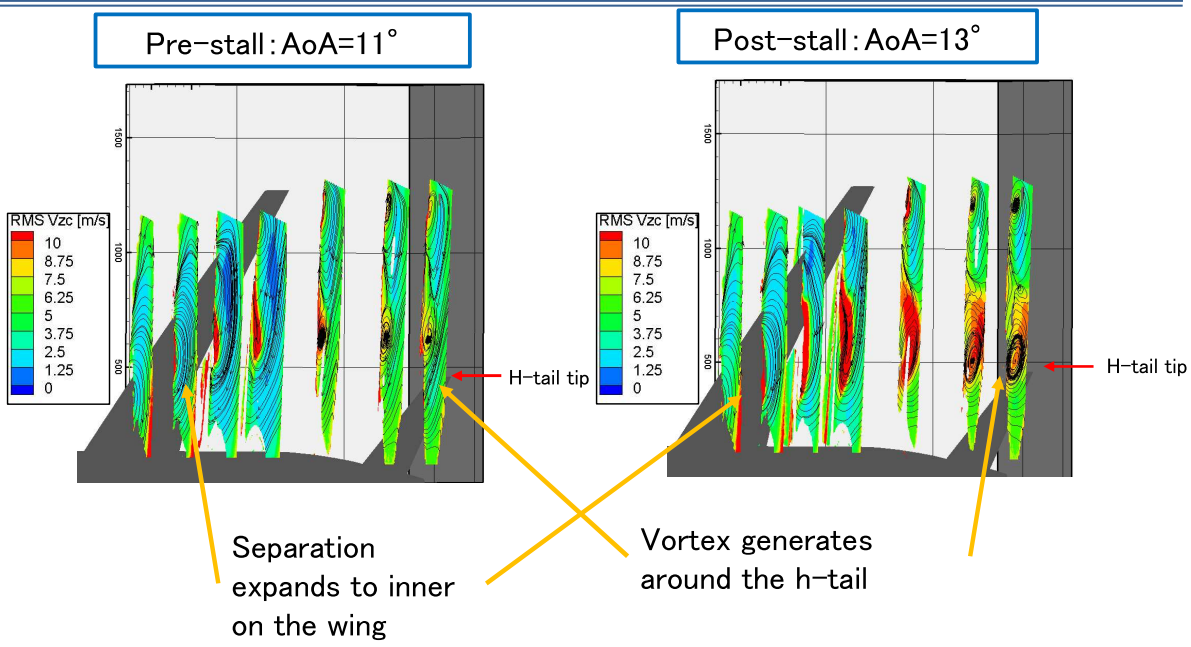

- PIV data are measured at pre-stall and post-stall angle of attack.
- At post-stall, separation flow on the main wing interfere with the h-tail.

The 53th Fluid Dynamics Conference/ The 39th Aerospace Numerical Simulation Symposium
30th June 2021

FaSTARを用いた低速・高迎角条件における NASA-CRM解析の格子依存性調査

Grid dependency Study on NASA-CRM computation with FaSTAR at low speeds and high angles of attack

橋本 敦, 小島良実、金森 正史(JAXA),
松﨑 智明(アドバンスソフト),
中元 啓太, 林 謙司(菱友システムズ)
Hashimoto Atsushi, Kojima Yoimi, Kanamori Masashi (JAXA),
Matsuzaki Tomoaki(AdvanceSoft),
Nakamoto Keita, Hayashi Kenji(Ryoyu Systems)

Computational Grid

- The following three grids are used.

BOXFUN grid (Hexahedral unstructured grid provided at APC-6): 39M cells

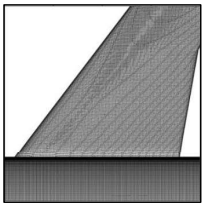
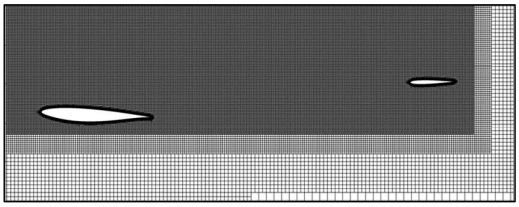

MEGG3D grid (Mixed-element unstructured grid provided at APC-3): 35M nodes

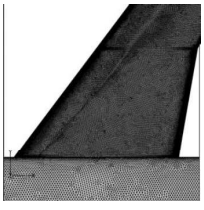
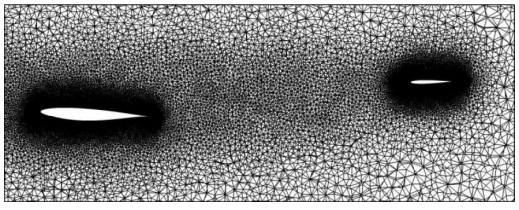

UPACS grid (Structured grid provided at APC-3): 30M cells

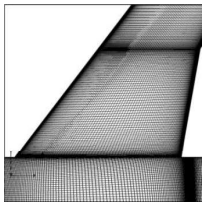
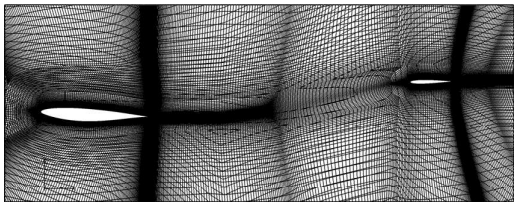

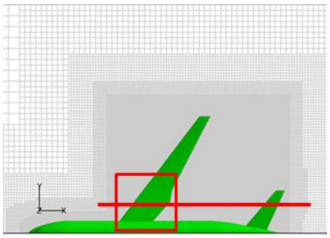

Computational conditions, methods

- Computational conditions
  - M = 0.168, Re_c = 1.06 x 10^6, T_{ref}=310K
  - AoA = 9.01˚, 10.03˚, 11.05˚, 13.08˚ for steady computation
  - AoA = 11.05˚ for unsteady computation
- Computational methods
  - Code: FaSTAR
    - Discretization: Cell-center for BOXFUN and UPACS grids
      Cell-vertex for MEGG3D grid
    - Inviscid flux: SLAU
    - Gradient: GLSQ, Limiter: Hishida(van Leer)
    - Spatial accuracy: Second order with MUSCL
    - Time integration: LU-SGS
    - Turbulence model:
      SST-2003 and SA-noft2-R for steady computation,
      SST-2003-IDDES and SA-noft2-R-IDDES for unsteady computation

3

CL-alpha

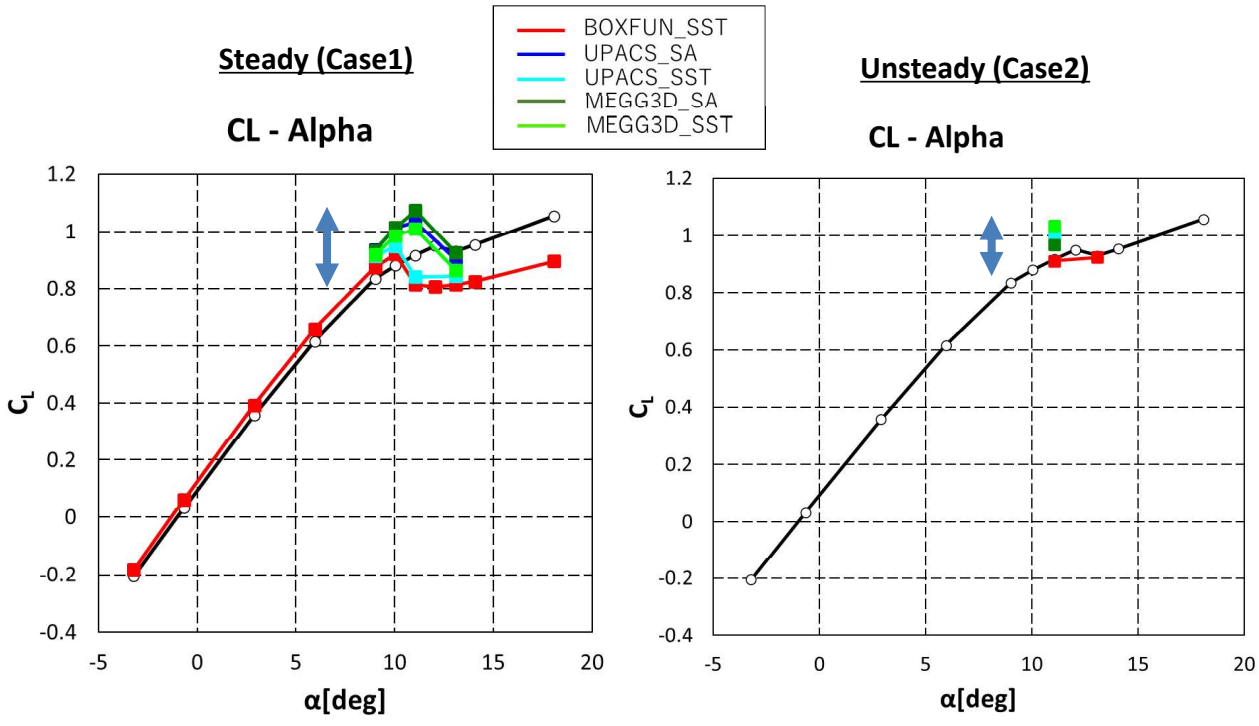

- The lift is affected by the grids and turbulence models.
- The range of prediction is reduced by using the unsteady computation.

Surface streamline(11.05deg)

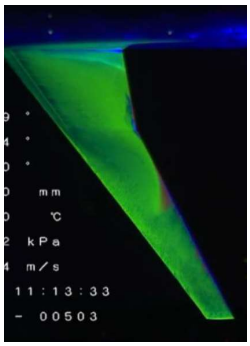

T. Uchiyama, et al.,
AIAA 2019-2190

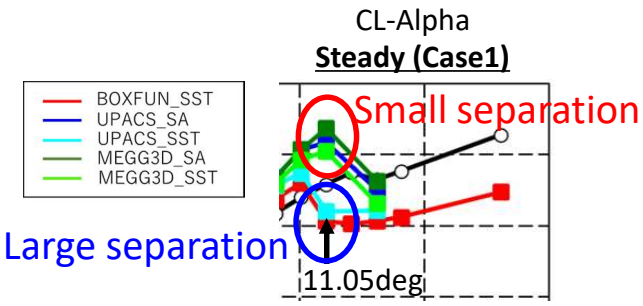

Steady (Case1)

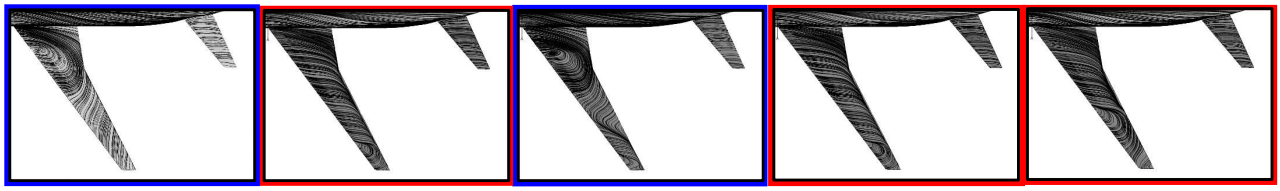

BOXFUN_SST UPACS_SA UPACS_SST MEGG3D_SA MEGG3D_SST

- The large separation is observed for SST model
- The small separation is observed for MEGG3D grid

5

Surface streamline(11.05deg)

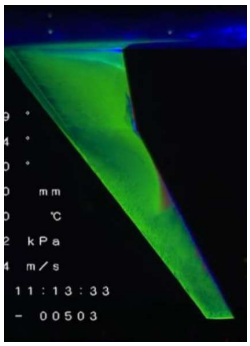

T. Uchiyama, et al.,
AIAA 2019-2190

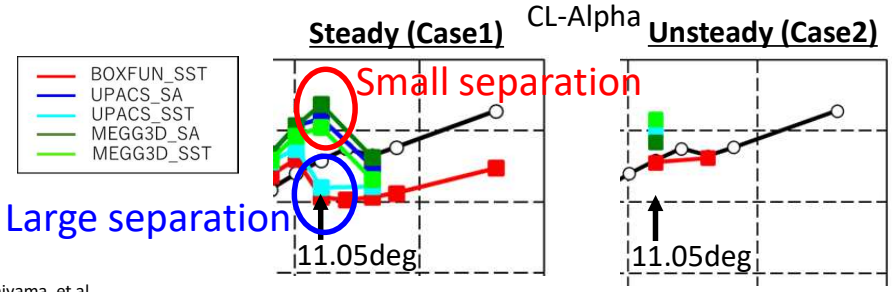

The separation region is reduced by the unsteady computation

Steady (Case1)

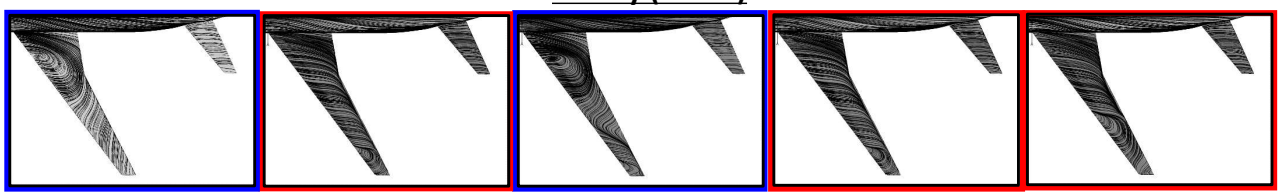

Unsteady (Case2)

BOXFUN_SST UPACS_SA UPACS_SST MEGG3D_SA MEGG3D_SST

6

Surface streamline(13.08deg)

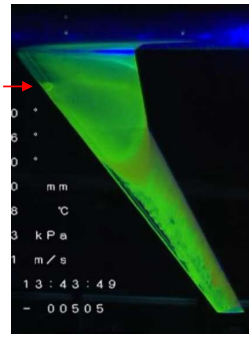

T. Uchiyama, et al.,
AIAA 2019-2190

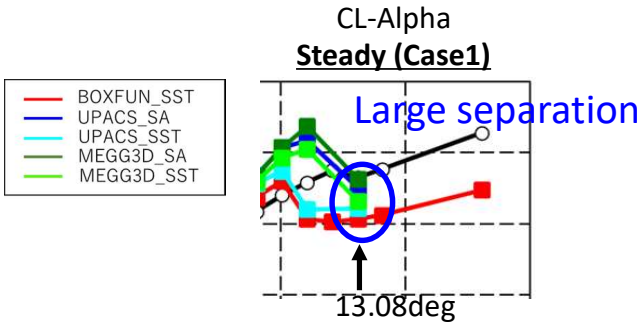

Steady (Case1)

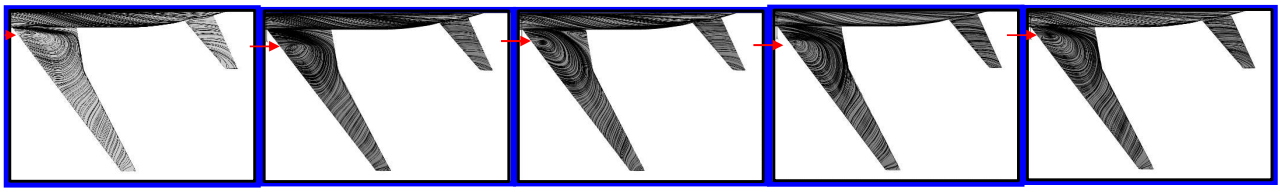

BOXFUN_SST UPACS_SA UPACS_SST MEGG3D_SA MEGG3D_SST

7

Surface streamline(13.08deg)

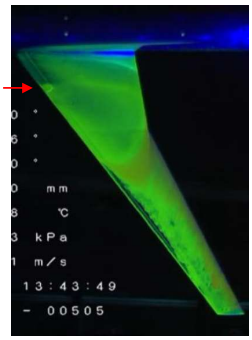

T. Uchiyama, et al.,
AIAA 2019-2190

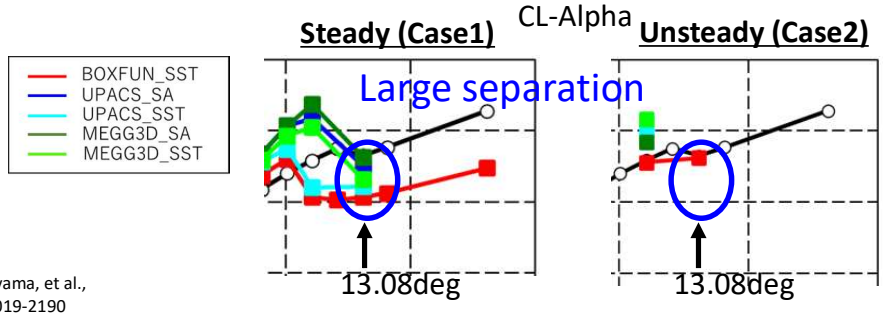

Steady (Case1)

Unsteady (Case2)

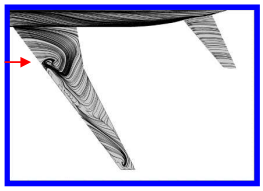

The separation region is reduced by the unsteady computation

BOXFUN_SST UPACS_SA UPACS_SST MEGG3D_SA MEGG3D_SST

8

Wake interference with tail (11.05deg)

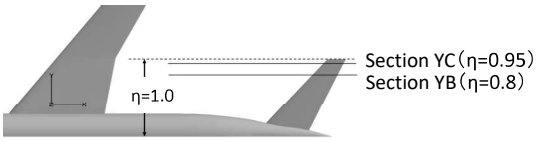

Steady (Case1)

Large separation

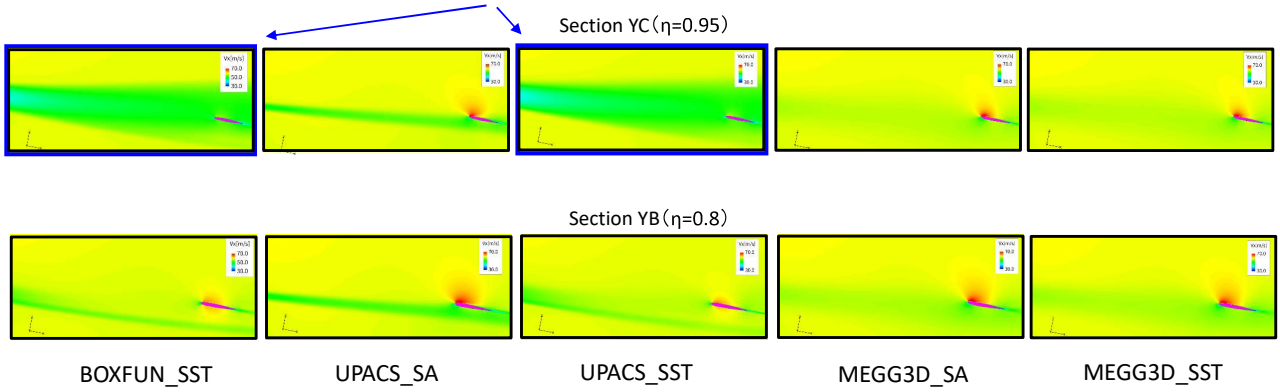

- The large separation is observed for SST model
- The wake is diffused for MEGG3D grid

9

Wake interference with tail (11.05deg)

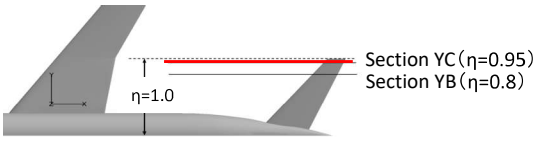

Large separation

Steady (Case1)

Unsteady (Case2)

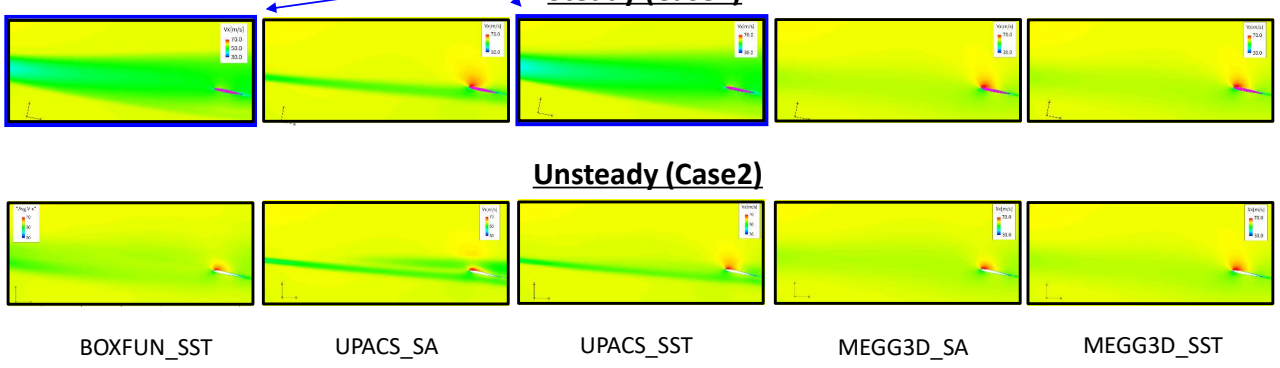

The separation region is reduced by the unsteady computation

10

Wake interference with tail (13.08deg)

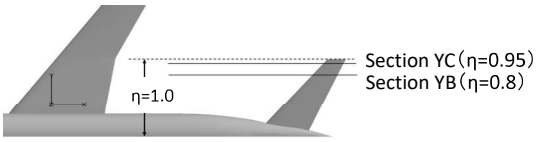

Steady (Case1)

Section YC(η=0.95)

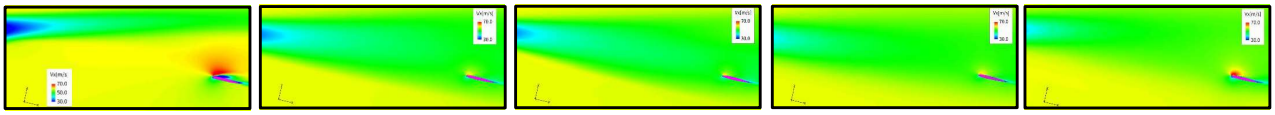

Section YB(η=0.8)

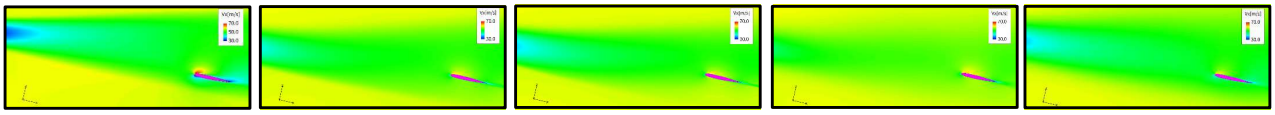

BOXFUN_SST UPACS_SA UPACS_SST MEGG3D_SA MEGG3D_SST

- The wake velocity distributions are similar except for BOXFUN grid

11

Velocity contours (13.08deg)

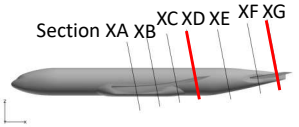

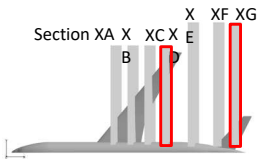

Section XD

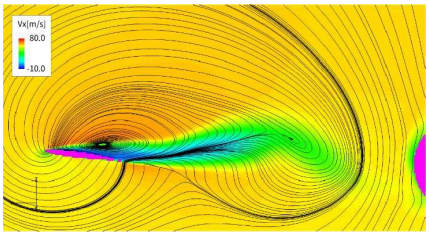

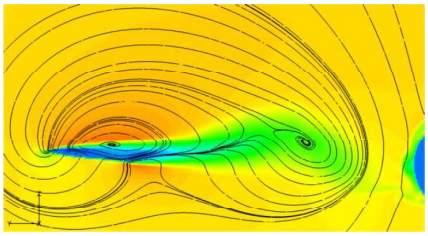

Section XG

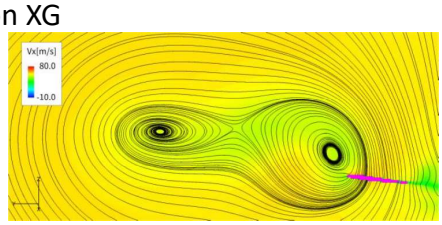

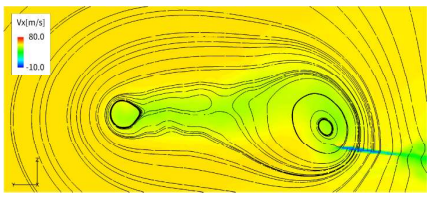

MEGG3D_SA_STEADY BOXFUN_SST_UNSTEADY

12

We selected the two cases that the predicted lift is close to the experiment.
The almost same velocity contours are shown.

Summary

- The stall prediction is largely affected by the grid type and turbulence model. The separation is large when the hexahedral grid is used. The SST model predicts the stall at lower AoA than the SA model.
- The range of predicted CL is reduced by using the unsteady computation. Generally, the separation region is smaller when the unsteady computation is used.
- The wake is diffused for the mixed-element grid. The hexahedral or a finer mixed-element grid is recommended to simulate the wake interaction.

13

Grid（Wing, Section C）

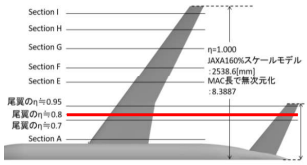

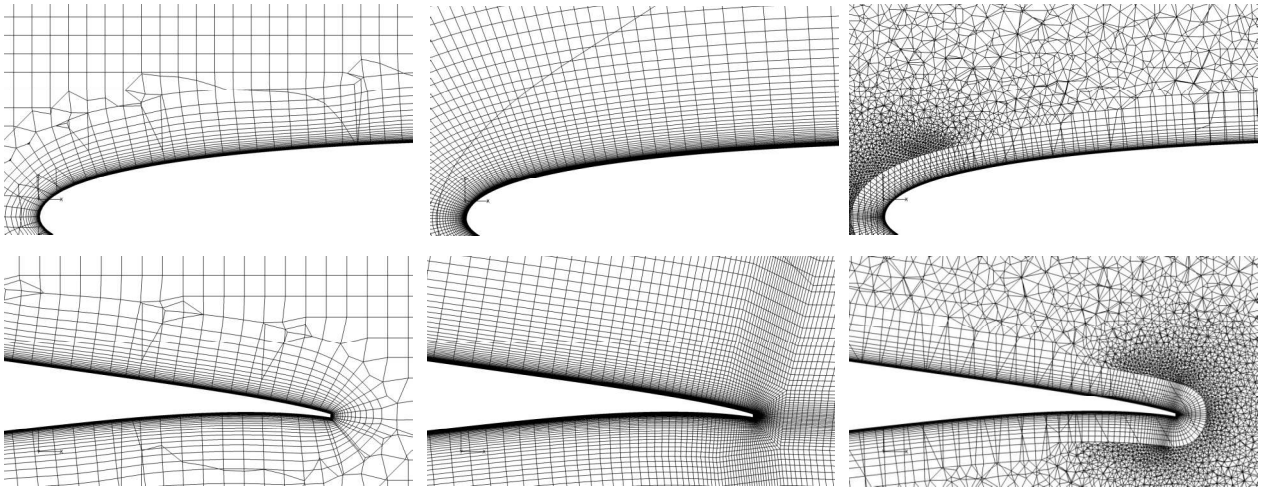

BOXFUN UPACS MEGG3D

14

AoA=11.05deg

A1-BO-SST A2-UP-SA A3-UP-SST A4-ME-SA A5-ME-SST

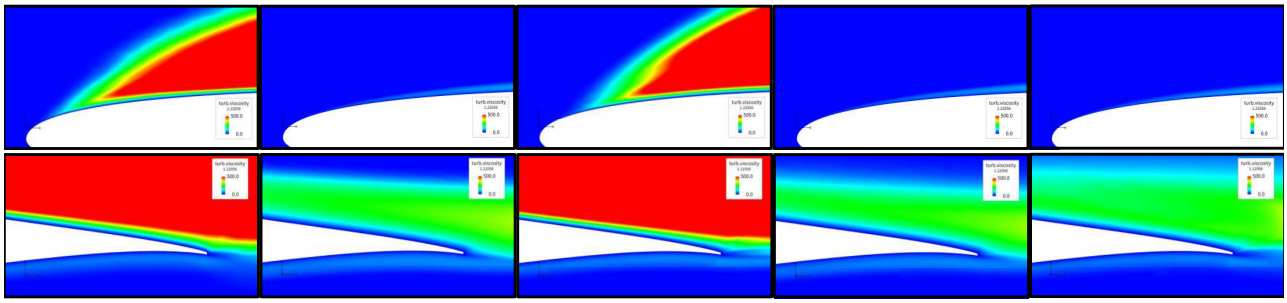

AoA=13.08deg

SAの方が厚い

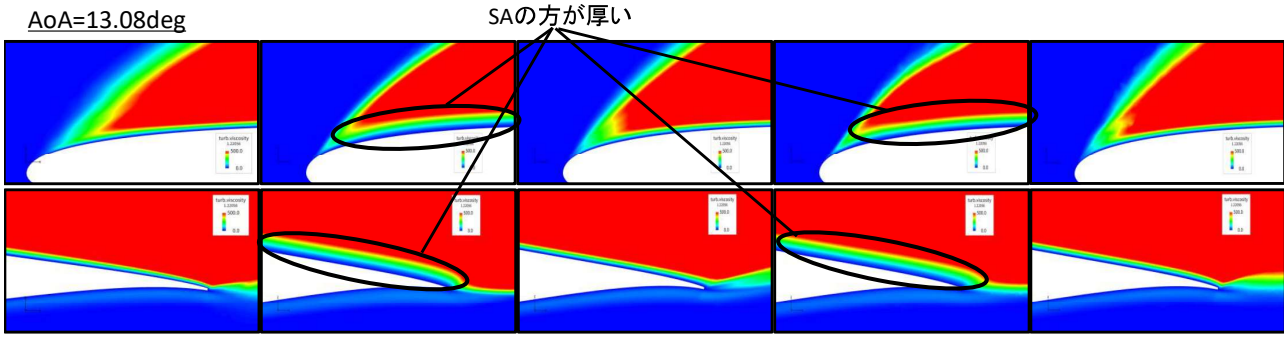

15

CD-alpha, CM-alpha

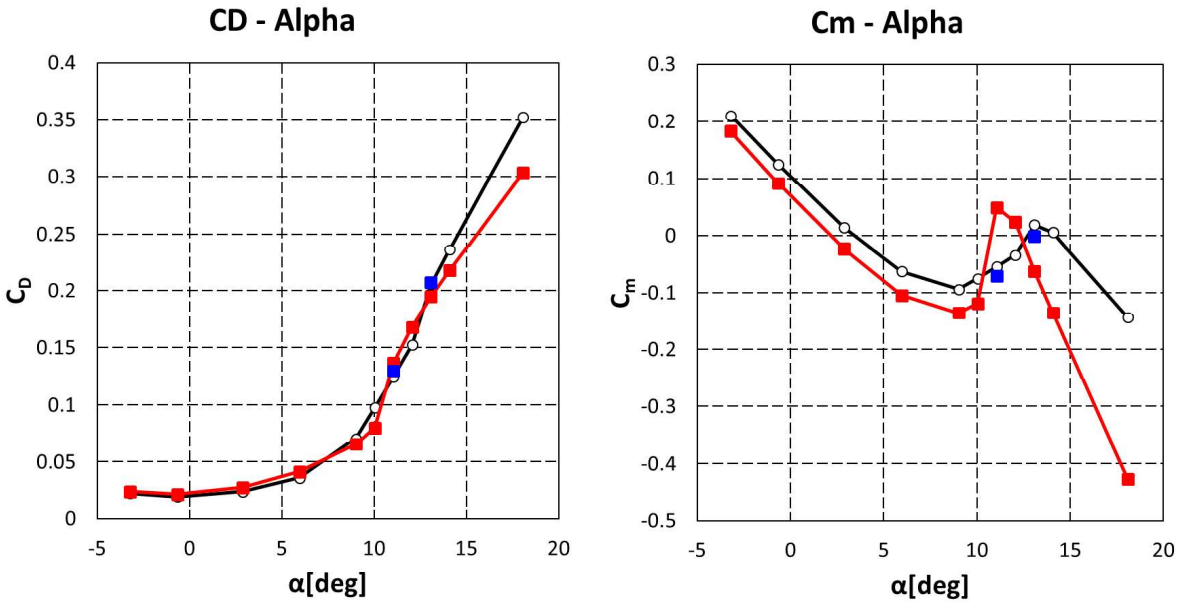

The accuracy of drag and pitching moment prediction is also improved with unsteady computation.

Streamline (Steady)

9.01deg

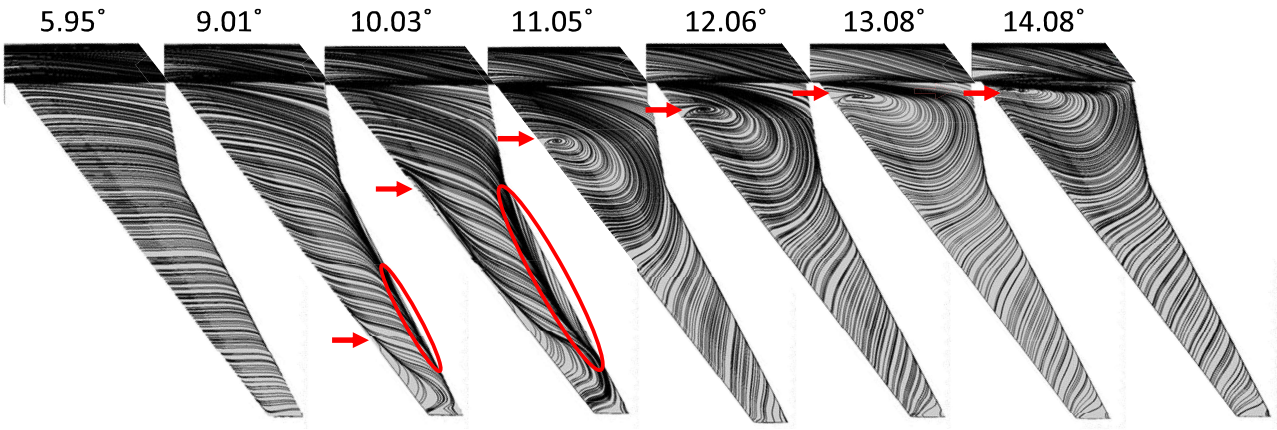

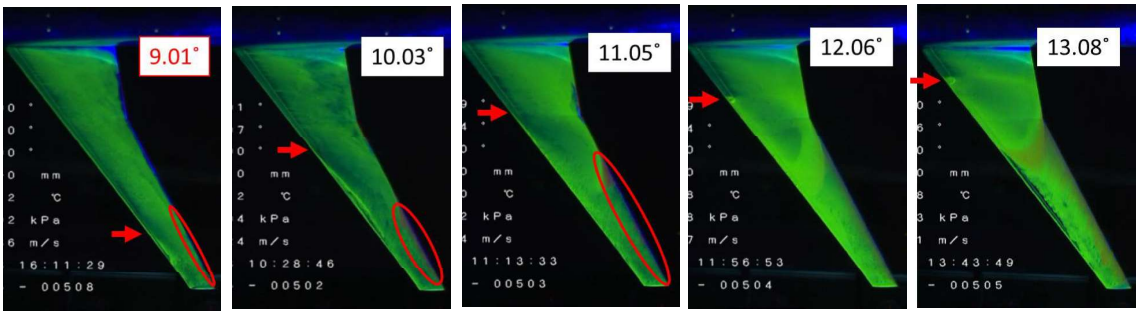

17

Streamline (Steady vs Unsteady)

9.01deg

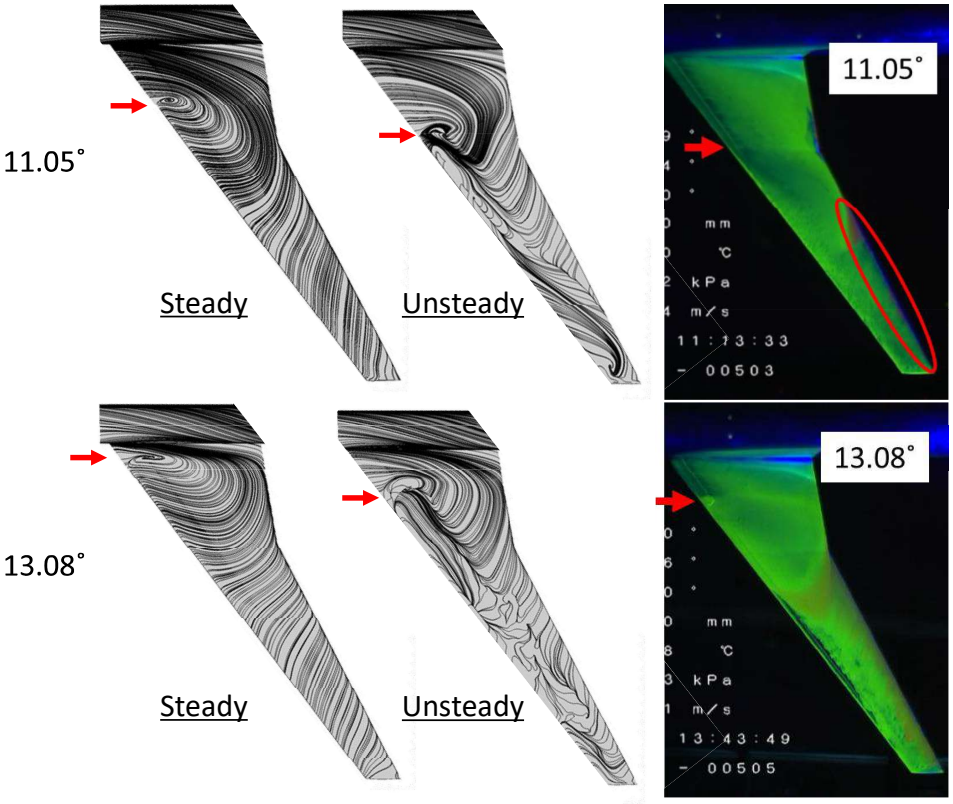

18

Q criterion

11.05deg

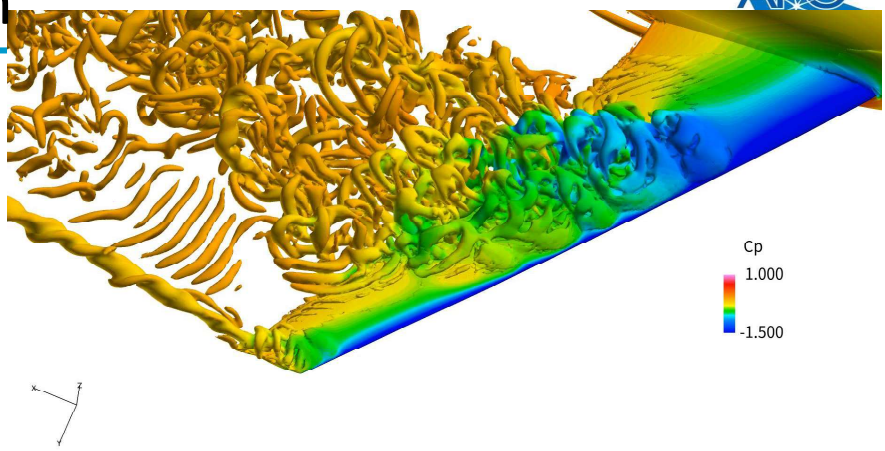

13.08deg

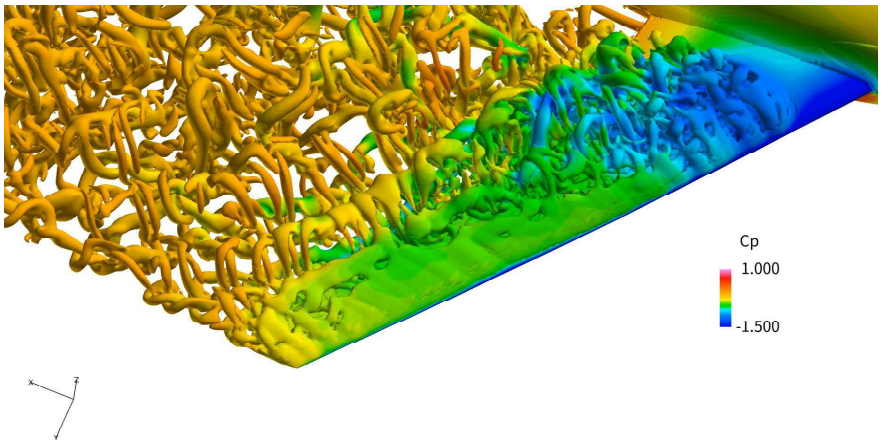

Q criterion

11.05deg

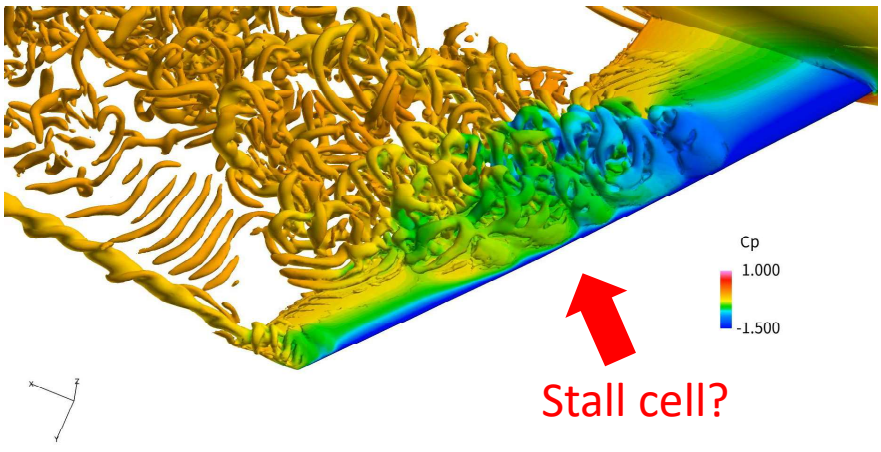

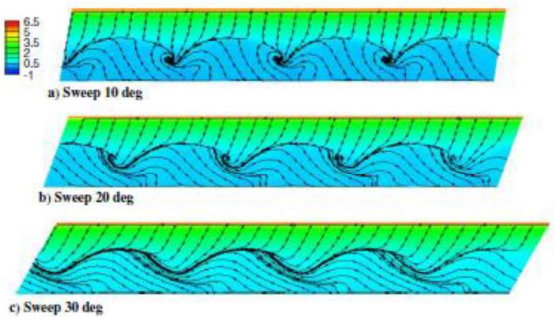

Frédéric Plante, et al., “Similarities Between Cellular Patterns Occurring in Transonic Buffet and Subsonic Stall,” AIAA JOURNAL Vol. 58, No. 1, January 2020.

Case1: Steady Computation

21

BOXFUN_SST

AoA=11.05deg

CDの収束は，
(a) グラフ全体を見て値が一定になっていること
(b) グラフの最小値と最大値を変更して，
振動が0.1～0.2cnt以内程度に収まっていること

CLの収束は，
(a) グラフ全体を見て値が一定になっていること
(b) グラフの最小値と最大値を変更して，
振動が1cnt以内程度に収まっていること

1cnt=0.0001

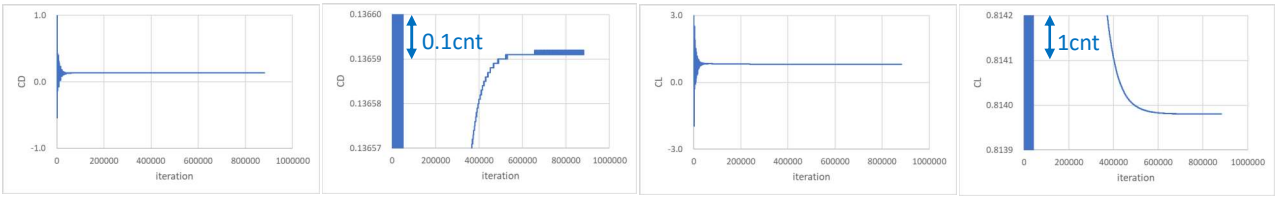

AoA=13.08deg

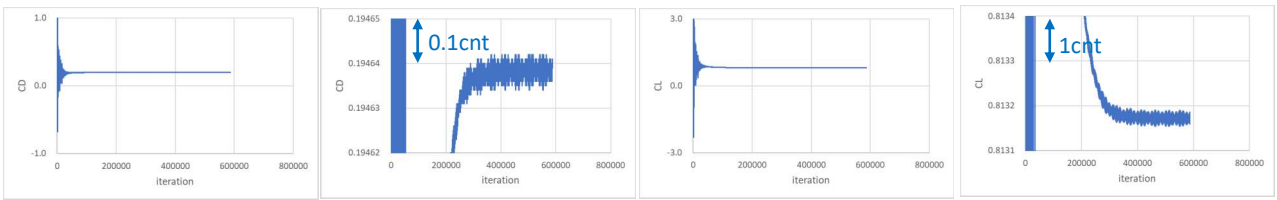

22

UPACS_SA

1cnt=0.0001

AoA=11.05deg

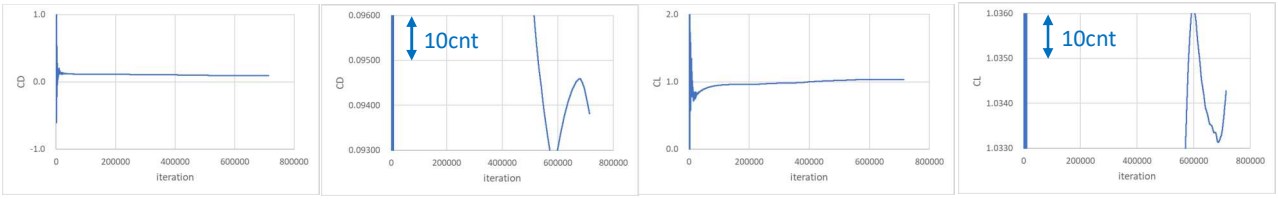

AoA=13.08deg

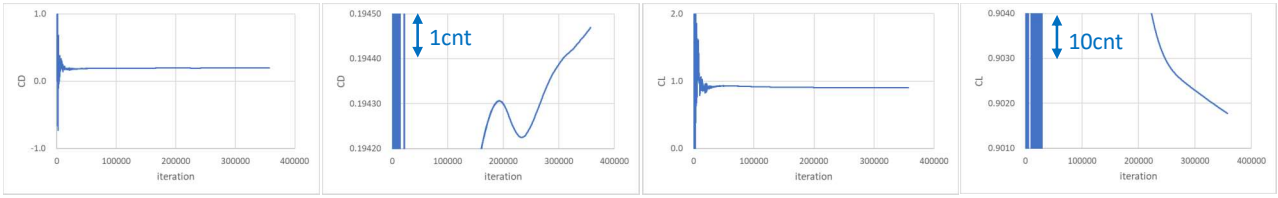

23

UPACS_SST

1cnt=0.0001

AoA=11.05deg

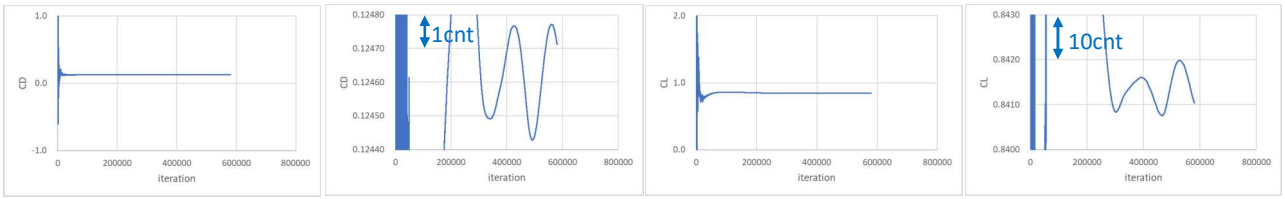

AoA=13.08deg

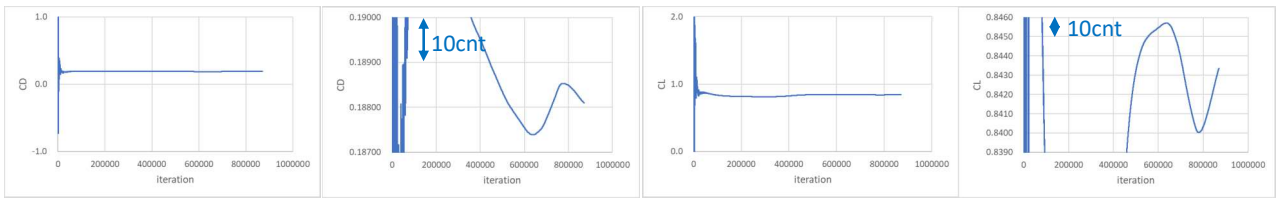

24

MEGG3D_SA

1cnt=0.0001

AoA=11.05deg

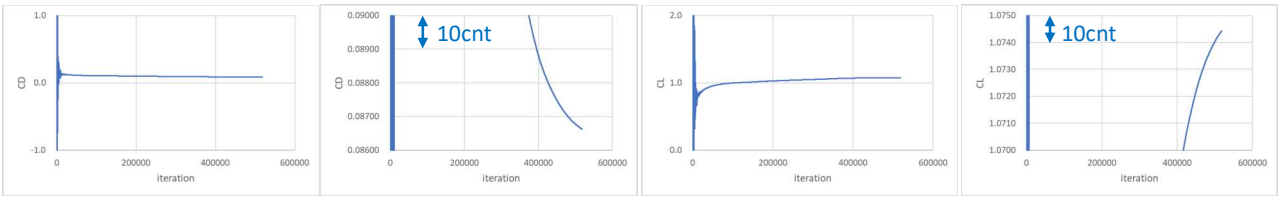

AoA=13.08deg

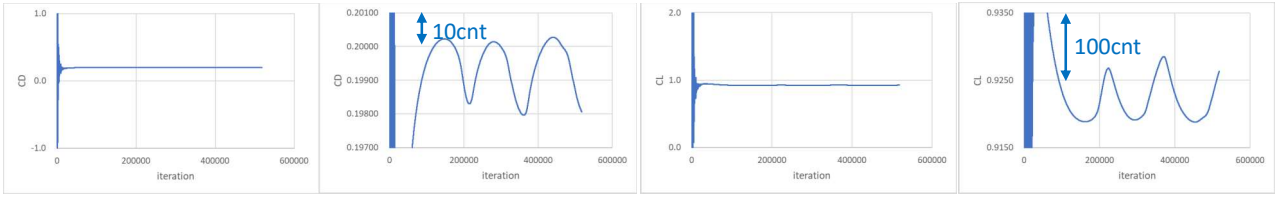

25

MEGG3D_SST

1cnt=0.0001

AoA=11.05deg

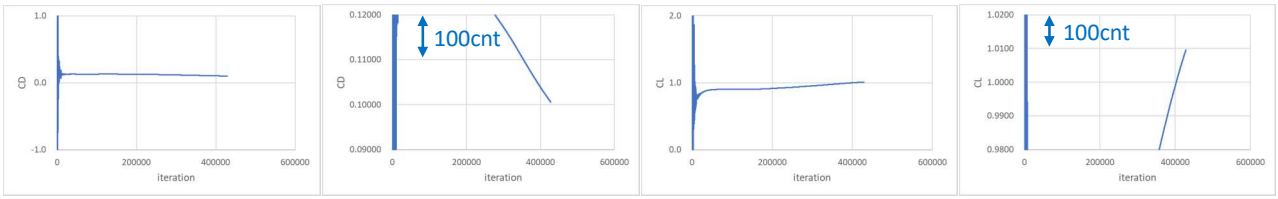

AoA=13.08deg

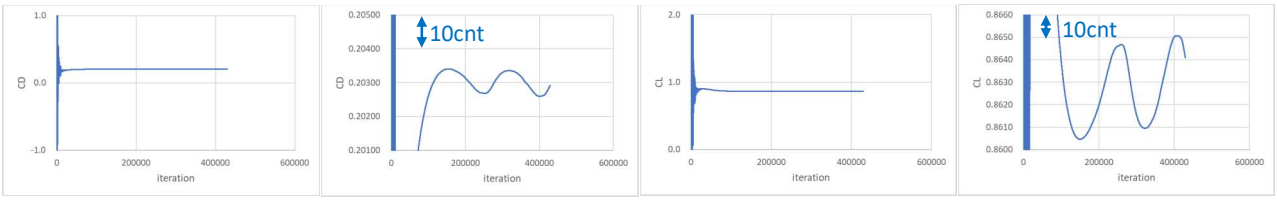

26

Case2:Unsteady Computation

27

BOXFUN_SSTIDDES

1cnt=0.0001

AoA=11.05deg

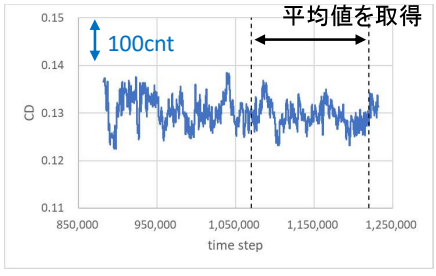

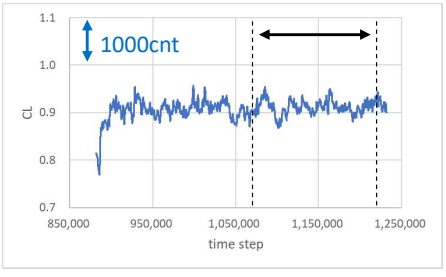

AoA=13.08deg

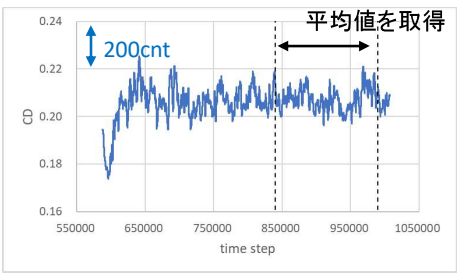

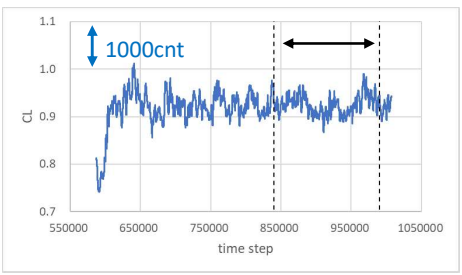

28

UPACS_SADDES AoA=11.05deg 1cnt=0.0001

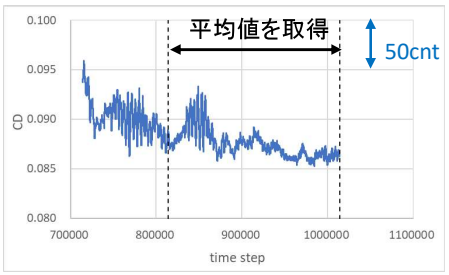

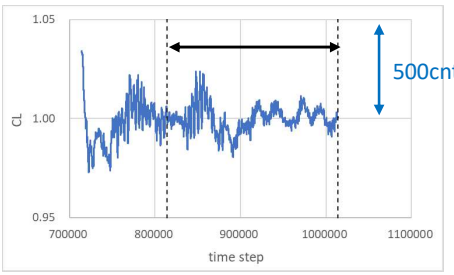

UPACS_SSTDDES AoA=11.05deg

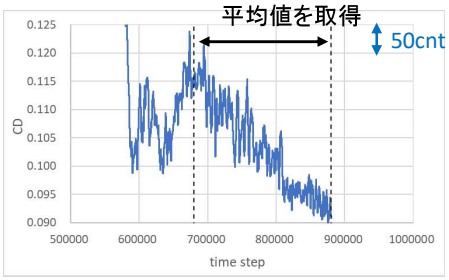

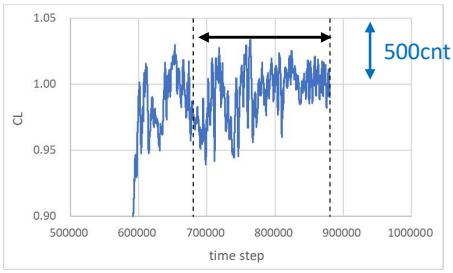

29

MEGG3D_SADDES AoA=11.05deg 1cnt=0.0001

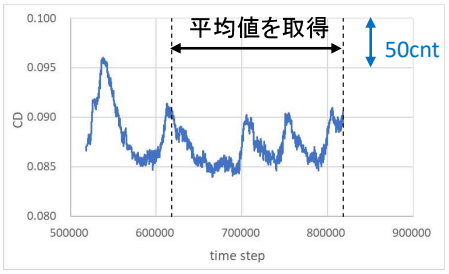

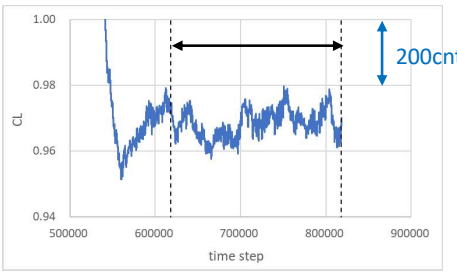

MEGG3D_SSTDDES AoA=11.05deg

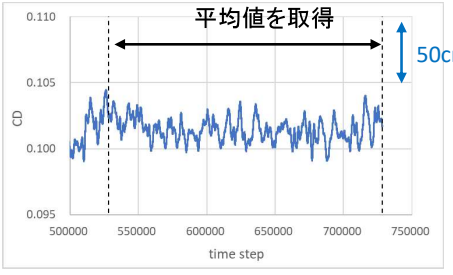

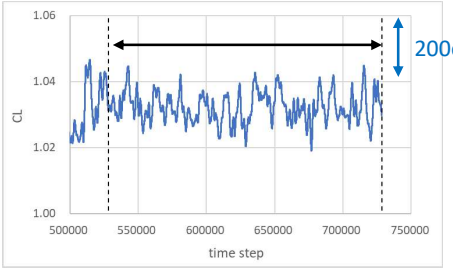

30

21KT009601

APC-7 （講演番号:1A16）

CflowによるNASA巡航CRMの低速高迎角剥離流れの予測 [課題1]

Prediction of Low-speed, High-angle-of-attack Separated Flows for the NASA-CRM Cruise Configuration using Cflow

上野 陽亮、安田 英将、澤木 悠太
Yosuke Ueno, Hidemasa Yasuda, Yuta Sawaki
川崎重工業（株） 航空宇宙システムカンパニー

2021年6月30日（水）
第53回流力講演会/第39回ANSS@オンライン

Kawasaki
Powering your potential

Outline

- **Outcome of APC-6**
  - Effect of **grid** (Provided vs Cflow)
- **Focus of APC-7**
  1. Effect of **turbulence model** (SA-noft2 vs SA-neg*)
  2. Effect of **time integration** (Local vs Global time step)
  3. Effect of **initial condition** (Impulsive vs Lower AoA)
- Summary

* The reason for using SA-neg in APC-7 is that SA-neg is used in another CFD workshop (AIAA HLPW-4) and has already been verified in our Cflow solver.

Outcome of APC-6

M=0.168
Re=1.06×10⁶

- **Effect of grid**
  - ✓ Provided grids overpredict stall angle and CL_{max}.
  - ✓ Cflow grids underpredict stall angle and CL_{max}.

APC-7

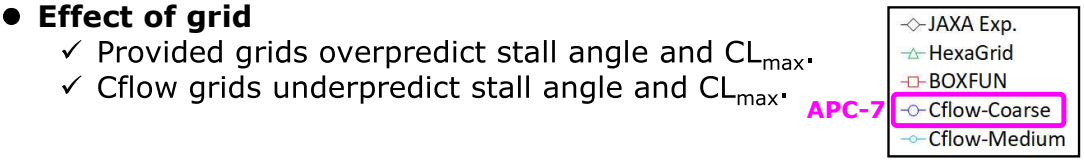

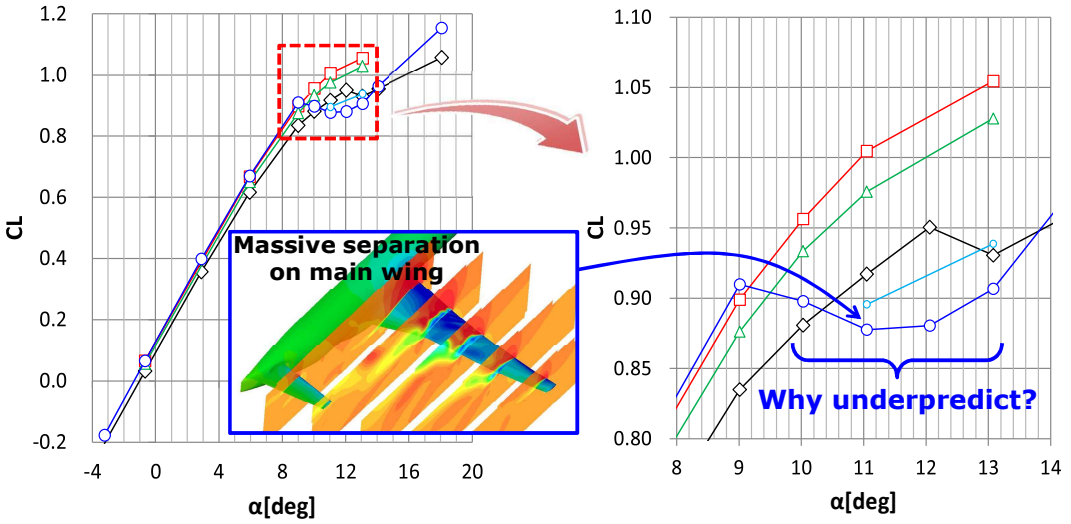

Grid Comparison

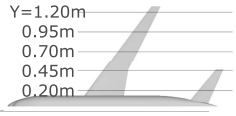

18.3M cells
Cell size: **6.8mm**

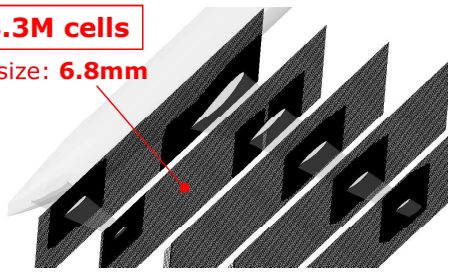

HexaGrid

42.6M cells
Cell size: **3.7mm**

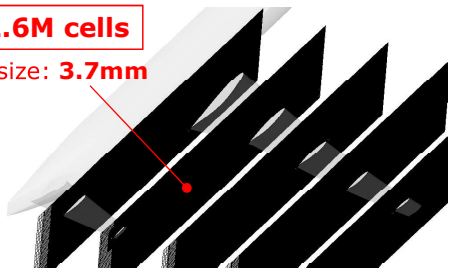

BOXFUN

APC-7

12.6M cells
Cell size: **12.5mm**
(Level=8)

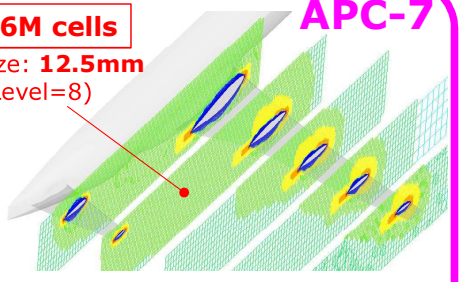

Cflow-Coarse
(for Case1)

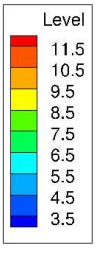

24.8M cells
Cell size: **3.1mm**
(Level=10)

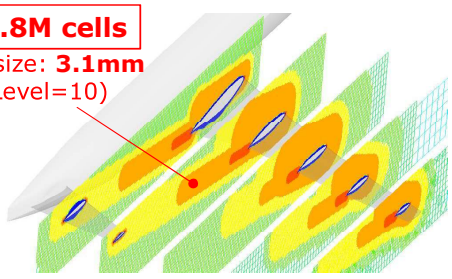

Cflow-Medium
(for Case2)

Numerical Method

CFD tool	Cflow (KHI in-house)
Governing Equations	**Three-dimensional compressible Navier-Stokes equations**
Spatial Discretization	Cell-centered finite volume method with 2rd-order accurate reconstruction based on MUSCL
Inviscid Flux	**SLAU** (Simple Low-dissipation AUSM scheme)
Viscous Flux	2nd-order accurate central difference
Turbulence Modeling	**SA-neg** (Negative Spalart-Allmaras One-Equation Model) ***SA-noft2@APC-6**
Time Integration	**MFGS implicit method with local/global time stepping**
Parallelization	Domain decomposition method with MPI

References for ***Cflow*** details

1. Ueno, Y. and Ochi, A., ***"Airframe Noise Prediction Using Navier-Stokes Code with Cartesian and Boundary-fitted Layer Meshes,"*** 25th AIAA/CEAS Aeroacoustics Conference, (AIAA 2019-2553).
2. Atsushi Hashimoto, Takashi Aoyama, Yuichi Matsuo, Makoto Ueno, Kazuyuki Nakakita, Shigeru Hamamoto, Keisuke Sawada, Kisa Matsushima, Taro Imamura, Akio Ochi, and Minoru Yoshimoto, ***"Summary of First Aerodynamics Prediction Challenge (APC-I),"*** 54th AIAA Aerospace Sciences Meeting, AIAA SciTech, (AIAA 2016-1780).
3. Yasushi Ito, Mitsuhiro Murayama, Atsushi Hashimoto, Takashi Ishida, Kazuomi Yamamoto, Takashi Aoyama, Kentaro Tanaka, Kenji Hayashi, Keiji Ueshima, Taku Nagata, Yosuke Ueno and Akio Ochi, ***"TAS Code, FaSTAR and Cflow Results for the Sixth Drag Prediction Workshop,"*** *Journal of Aircraft*, Vol. 55, No. 4, pp. 1433-1457, 2018.
4. Yasushi Ito, Mitsuhiro Murayama, Yuzuru Yokokawa, Kazuomi Yamamoto, Kentaro Tanaka, Tohru Hirai, Hidemasa Yasuda, Atsushi Tajima and Akio Ochi, ***"Japan Aerospace Exploration Agency's and Kawasaki Heavy Industries' Contribution to the Third High Lift Prediction Workshop,"*** 2018 AIAA Aerospace Sciences Meeting, AIAA SciTech, (AIAA 2018-1034).

Focus of APC-7 (1)
Effect of turbulence model

M=0.168
Re=1.06×10⁶

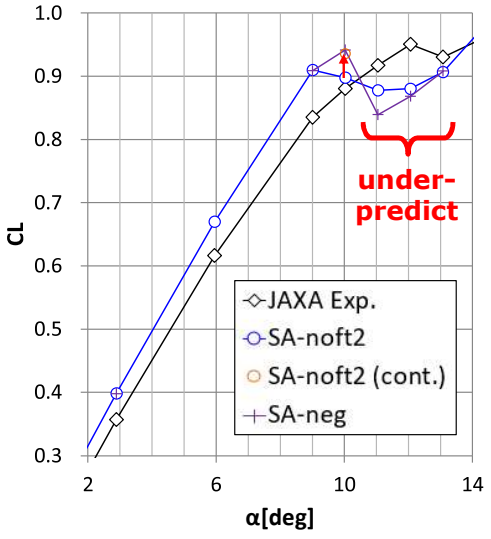

CL history

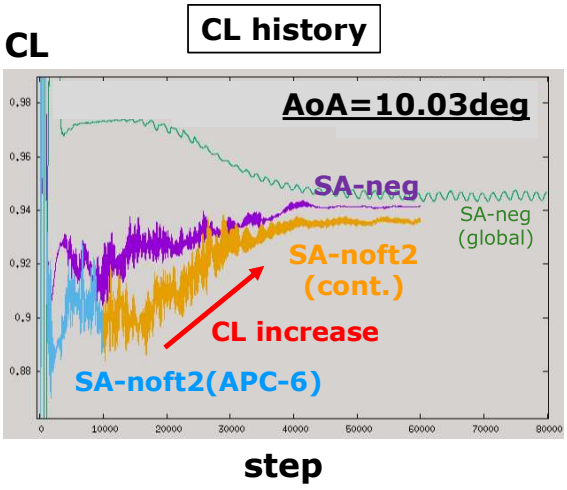

*APC-6: SA-noft2, only 10,000 steps
*APC-7: SA-neg, more than 50,000 steps

- SA-neg and SA-noft2 bring similar results for this case
- Further investigation on QCR and RC effects is needed

Focus of APC-7 (2)
Effect of time integration

M=0.168
Re=1.06×10⁶

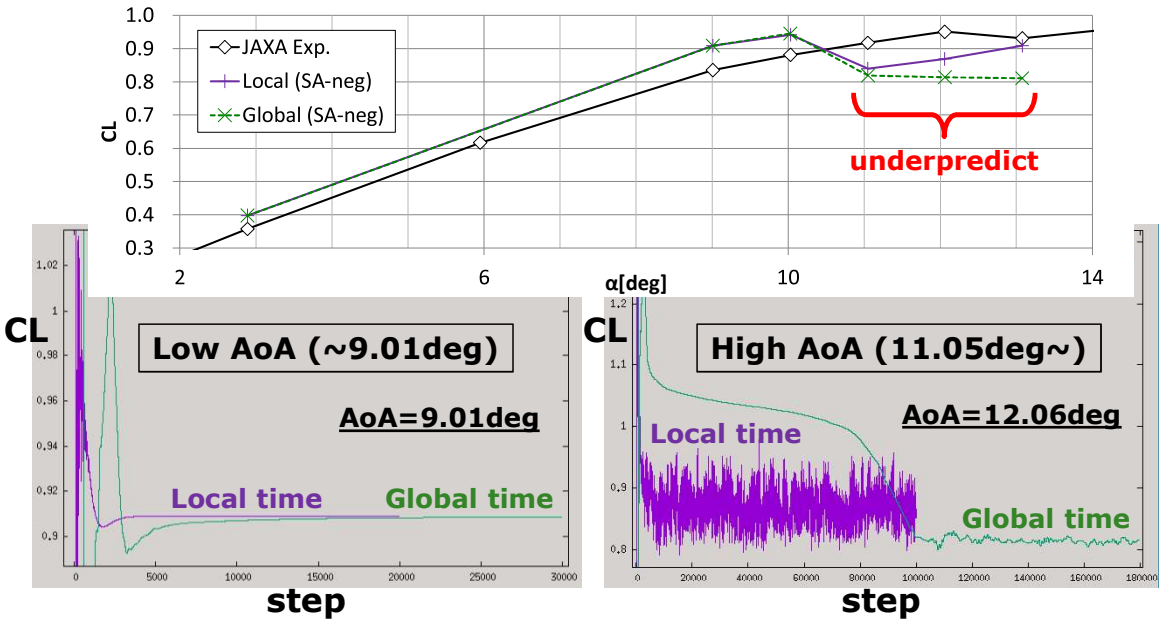

- Converge to same result (steady flow)
- Global needs more time steps

- Not converge (unsteady flow)
- Global needs more time steps

Focus of APC-7 (3)
Effect of initial condition

M=0.168
Re=1.06×10⁶

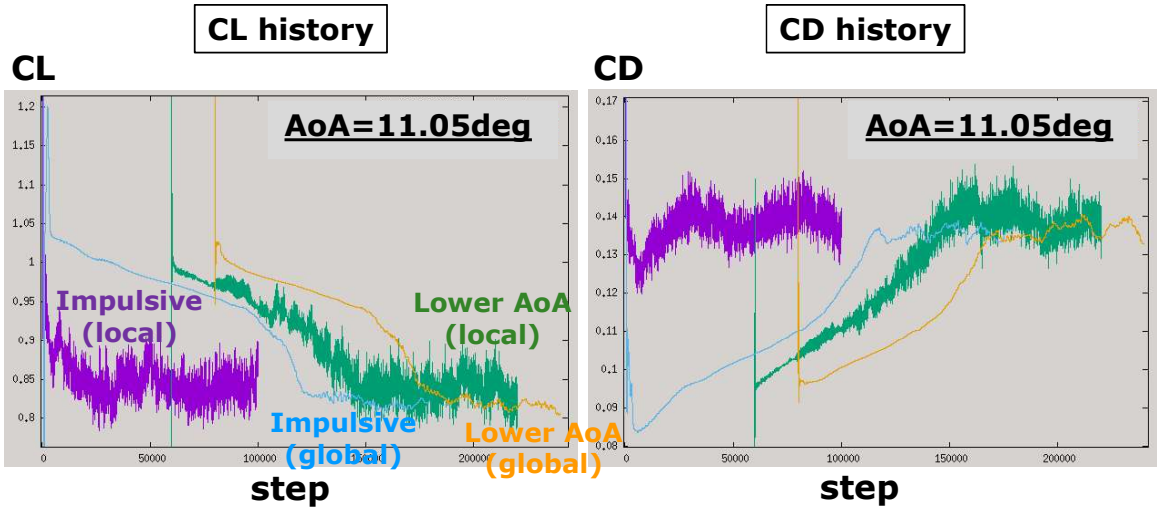

- Restart from the lower-AoA result (warm start) brings the same result as impulsive (cold start) both in local and global time steps

Summary

- For steady-state RANS computations with Cflow-Coarse grid used in APC-6, the effects of several computational parameters were investigated to improve predictive capability in low-speed high-angle-of-attack aerodynamics.

- **Lessons Learned: not improved…**
  - ✓ **Effect of turbulence model (SA-noft2 vs SA-neg):**
    little effect, need further investigation on QCR and RC effects
  - ✓ **Effect of time integration (Local vs Global time step):**
    similar results, global needs more time steps
  - ✓ **Effect of initial condition (Impulsive vs Lower AoA):**
    similar results (investigated only for AoA=11deg)

- Future work
  - ✓ Establish **"best practices"** (trade-off between accuracy and cost)
  - ✓ More complicated high-lift configuration (**CRM-HL**, see **2C09**)

【補足】提出データについて

- ローカルタイムステップの定常解析結果は、高迎角（≧11deg）で解が収束せずに振動しているが、APC-6同様に今回事務局に提出したデータ（カデータ、可視化図）は最終ステップの瞬時値である。
- 一方、本資料に示したカデータ（CL, CD, Cm）は、圧力分と摩擦分を足し合わせたものであり、Cflowの解析ログから平均化して求めたものである。
- よって、APC事務局作成のまとめ資料と本資料のカデータは若干異なる。

提出データの一例

収束していない結果（p.8のCL履歴参照）の
最終ステップの瞬時値であるため斑な分布

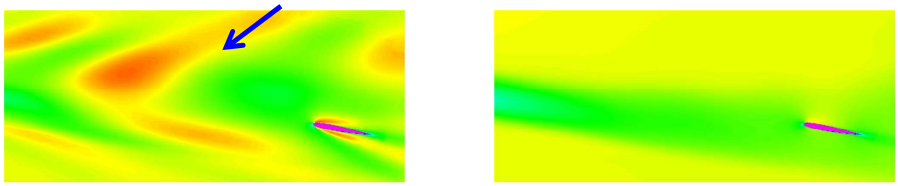

Local time step　　Global time step

断面流速分布（Section YB, AoA=11.05deg）

Motivation

- **Practical use** of CFD in the aircraft design
- **Validation** of KHI in-house CFD tool for low-speed aerodynamics
- **Facilitation** of CFD-WTT collaboration

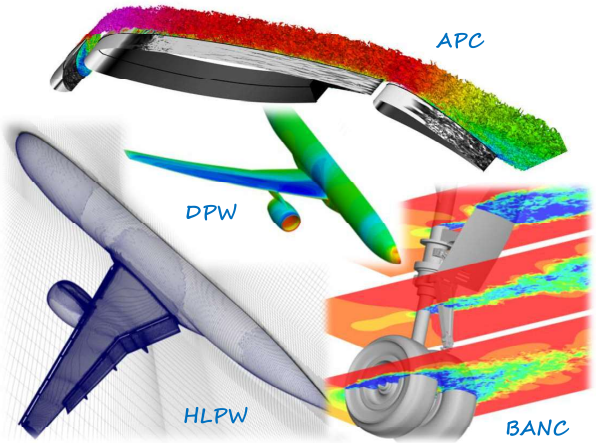

KHI in-house CFD tool "*Cflow*"
(highly complicated geometry, unsteady, large-scale)

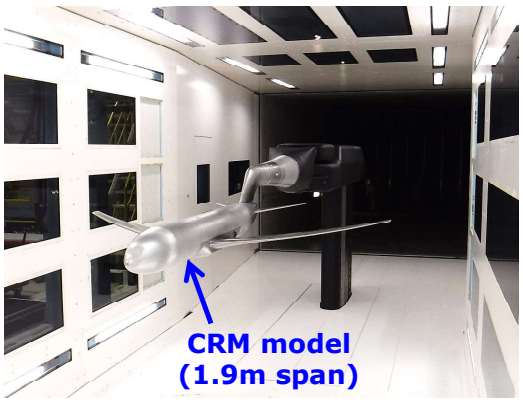

KHI new wind tunnel
(low-speed, low-noise)

Cflow (KHI in-house CFD tool)

✓ **Kawasaki** originally developed ***"Cflow"***

Cflow = Grid Generator + Flow Solver

highly complicated | large-scale | unsteady

✓ Cflow has been validated in various workshops.

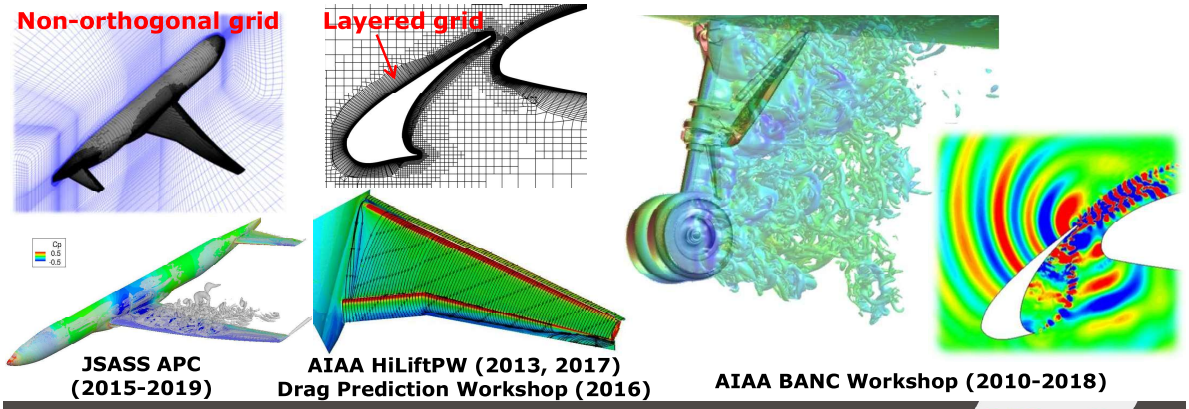

Grid Generation Procedure in *Cflow*

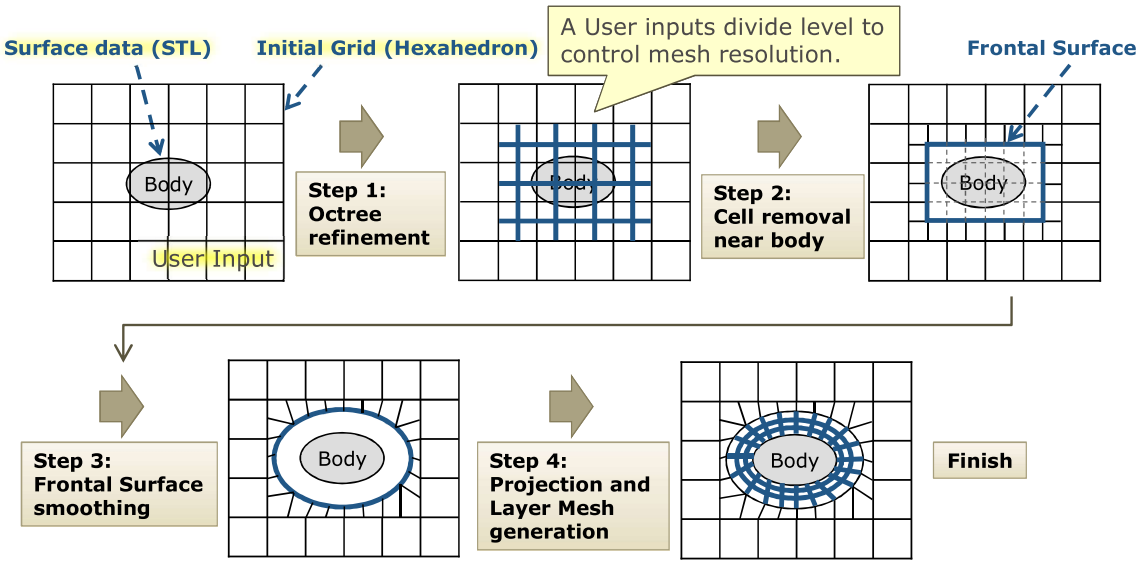

Cflow automatically generates body-fitted layered grids on no-slip walls to resolve boundary layers and hexahedral grids in the other regions.

Initial Grid of *Cflow*

There are 2 options for initial grid of *Cflow*.

Cartesian Grid

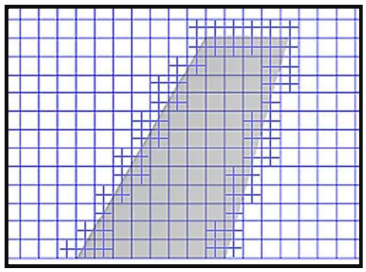

- grid generation robustness
- unsteady simulation (resolving vortices)
- acoustic wave propagation

Noise prediction from complicated geometry

or

Non-orthogonal Grid

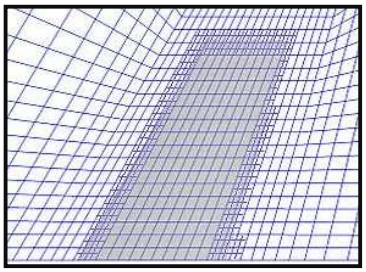

- reduction of total cells (high aspect ratio)
- sweptback cells
- oblique shock wave

Steady simulations

Grid (HexaGrid)

空間セル数： 1830万セル
最小格子幅： 8.3×10^{-6} m

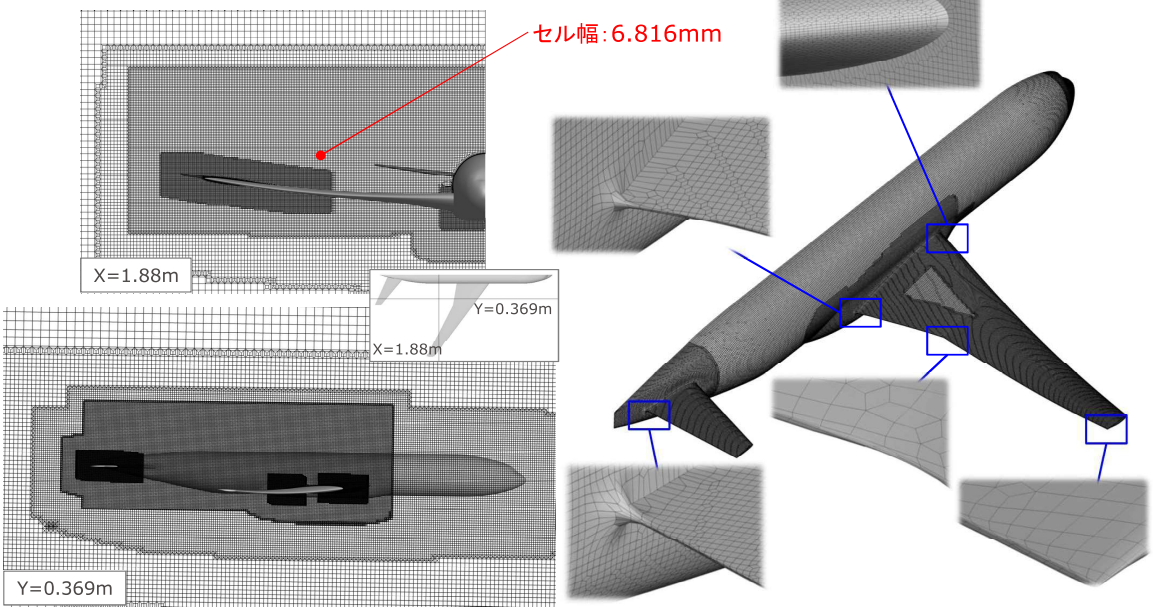

Grid (BOXFUN)

空間セル数： 4260万セル
最小格子幅： 5.2×10^{-6} m

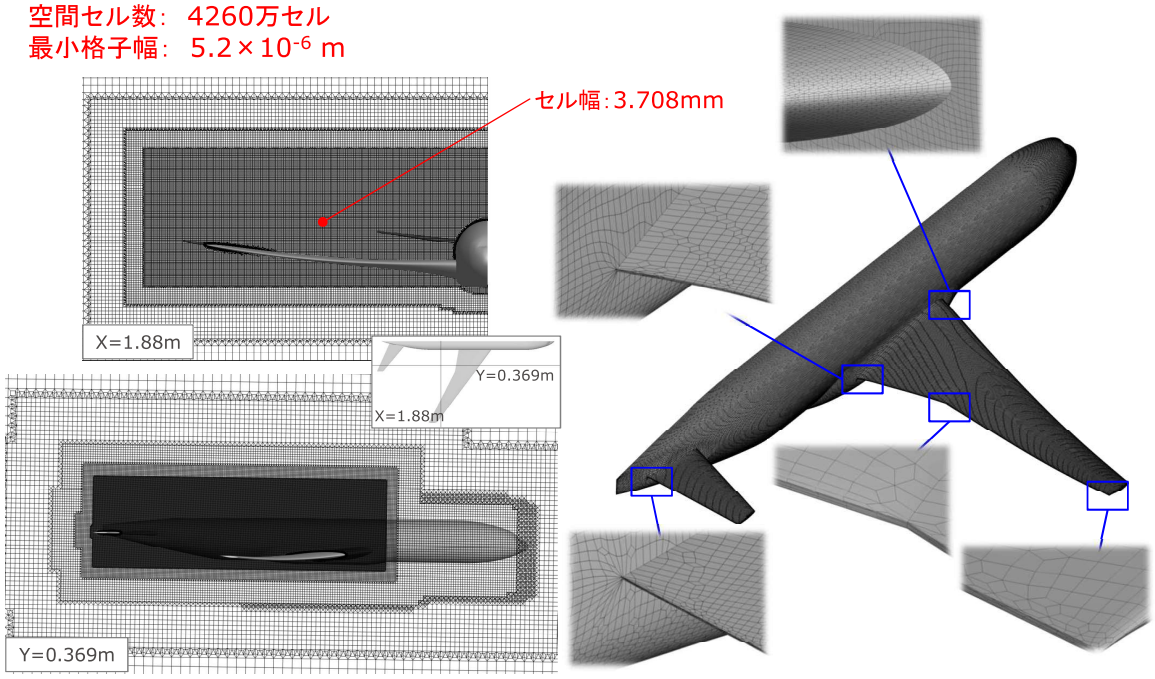

Grid (Cflow-Coarse)

空間セル数： 1260万セル
最小格子幅： 8.0×10^{-6} m

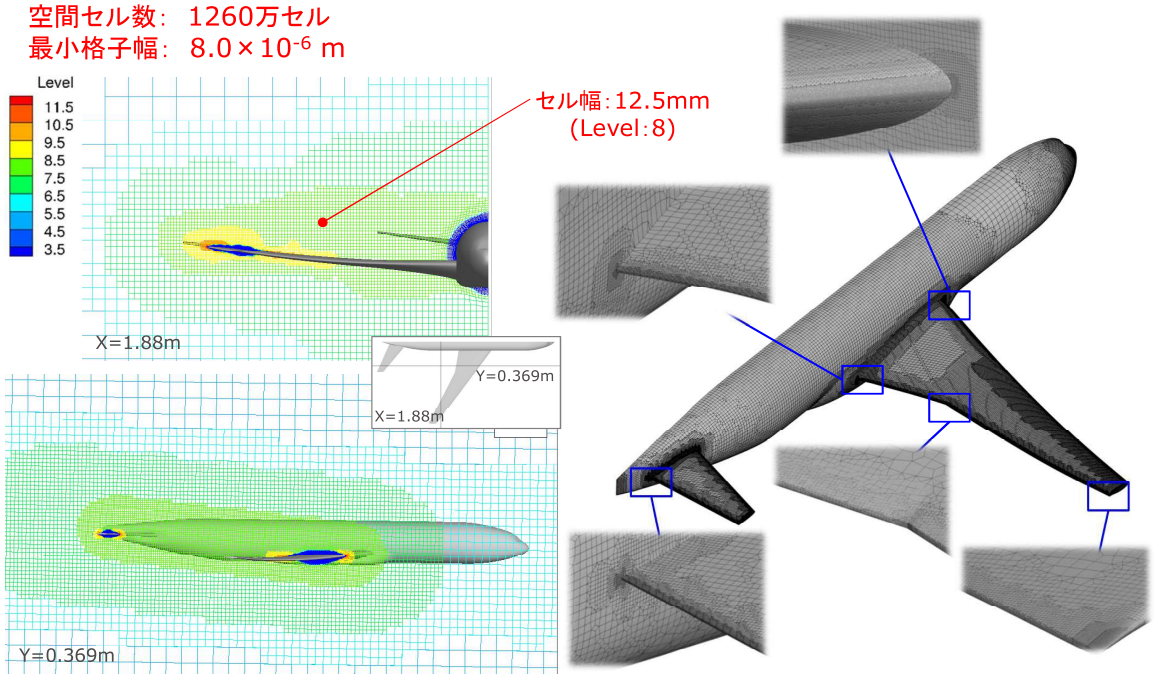

Grid (Cflow-Medium)

空間セル数： 2480万セル
最小格子幅： 8.0×10^{-6} m

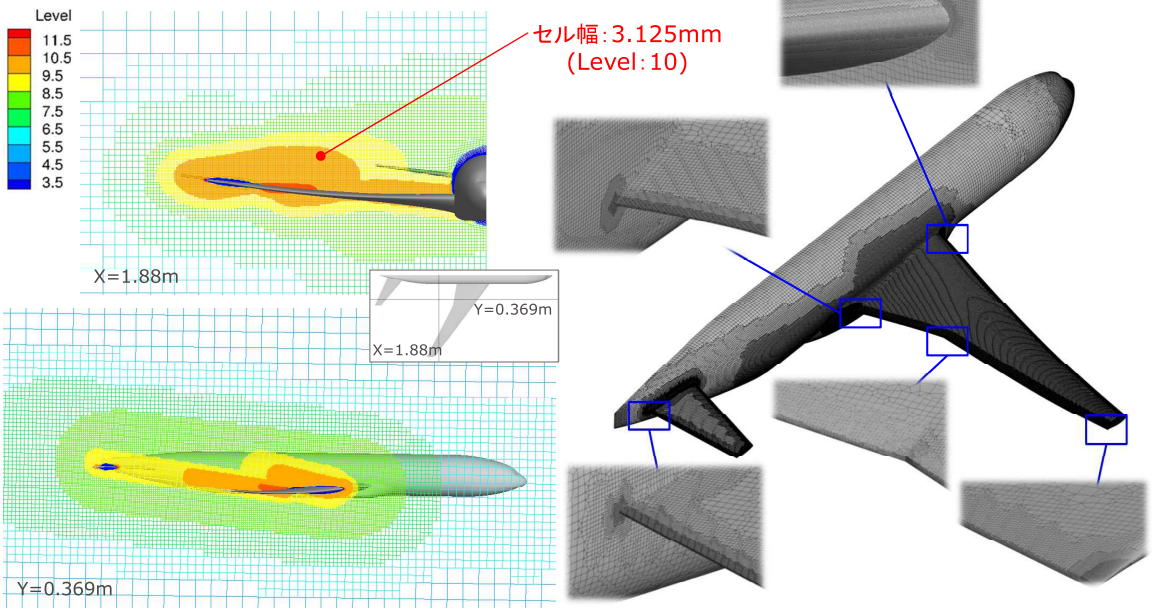

Seventh Aerodynamics Prediction Challenge (APC-7)
2021/06/30, Online

Aerodynamic Analysis of NASA-CRM at Low Speed and High Angle of Attack conditions Using Hierarchical Cartesian Mesh and Recursive Fitting Method

階層型直交格子と再帰的なフィッティングを用いた
低速・高迎角条件におけるNASA-CRM巡航形態の空力予測

○Keisuke Sugaya, Atsushi Hara, Taro Imamura
(The University of Tokyo)

東京大学 THE UNIVERSITY OF TOKYO

Background

- Development of **UTCart** for aerodynamic designing of aircraft.
  - Automatic grid generation based on octree structure.
  - Compressible RANS/DDES simulation with wall function.
  - Immersed Boundary method (**IBM**) on stair-step grids.
  - Simulation on cut-cell like grid is also developed[1,2] .

NASA N2A HWB
(Data from VSP Hangar)

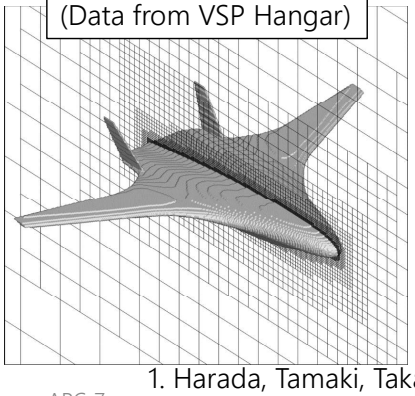

Immersed boundary method
with wall function

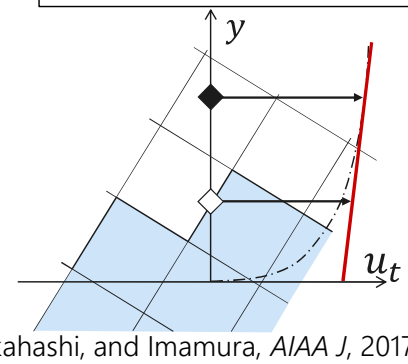

Automatic generation of
Cut-cell like grid

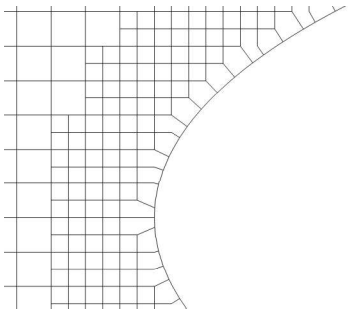

1. Harada, Tamaki, Takahashi, and Imamura, *AIAA J*, 2017.
2. 菅谷 and 今村, *日本航空宇宙学会論文集*, 2020.

Results of APC-6* (IBM simulation)

- A fair agreement of aerodynamics between UTCart and experiment at low AoA.
- Large *CL* than that of experiment at high AoA.
- **Influence of numerical methods on aerodynamics prediction needs to be investigated.**
- Further study of dependency on grid size is necessary.

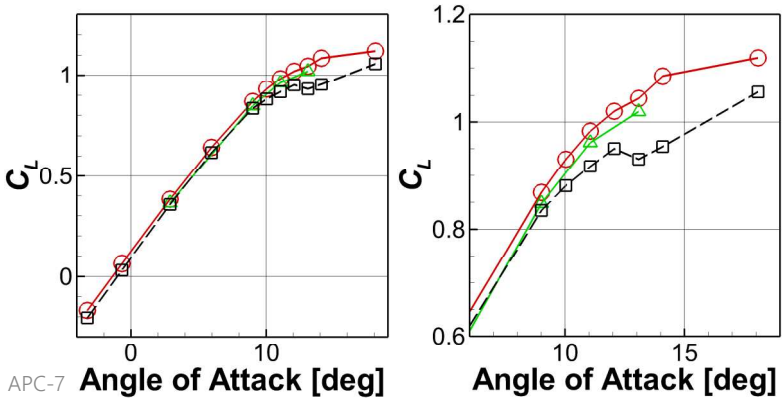

* Yoshinaga, Sugaya, and Imamura, APC-6, 2020.

Objective

Investigate prediction accuracy of flow simulation around NASA-CRM using Recursive Fitting Method.

- Cartesian grid based automatic body-fitted grid generation.
  - **Geometric features are approximately represented.**
- Comparison with simulation using IBM (APC-6).
  - **Conservation laws are satisfied in simulation using Recursive Fitting Method (RFM)**, as opposed to IBM.

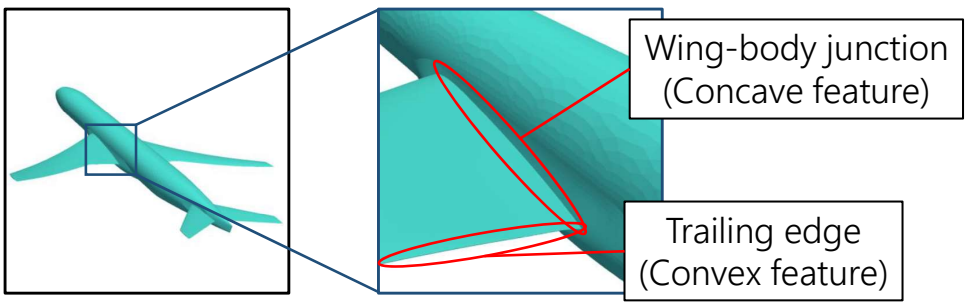

Recursive Fitting Method (RFM)*

1. Generate the stair-step grid.
2. Calculate the closest points to the vertices of the cell faces.
3. Extend fluid cells to body surfaces.

○ Automatic grid generation around two- and three-dimensional bodies.

△ Cell faces does not match body surfaces around geometric features.

- Wing-body juncture, Trailing edge,…

→ **Necessary to modify cells around features.**

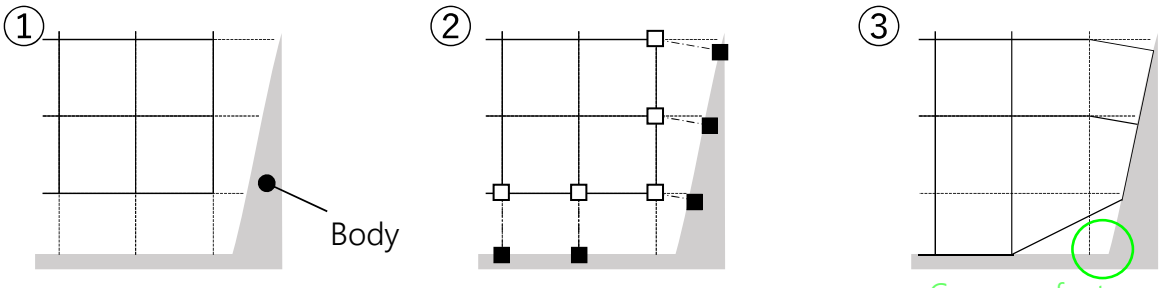

* 菅谷 and 今村, *日本航空宇宙学会論文集*, 2020.

Recursive Fitting Method (RFM)*

- Recursively fitting the wall face to body surfaces
- Modified the cell properties which is necessary for flow simulation

$$\frac{\partial (Q_C V_i)}{\partial t} + \sum_{j \in \mathrm{neighbor}(i)} F(Q_i, Q_j, \boldsymbol{n}_{ij}) s_{ij} = 0$$

  - The number of cells and cell faces are kept unchanged.
- Repeating fitting procedure recursively until the distance between wall face and wall becomes smaller than user-specified parameter.

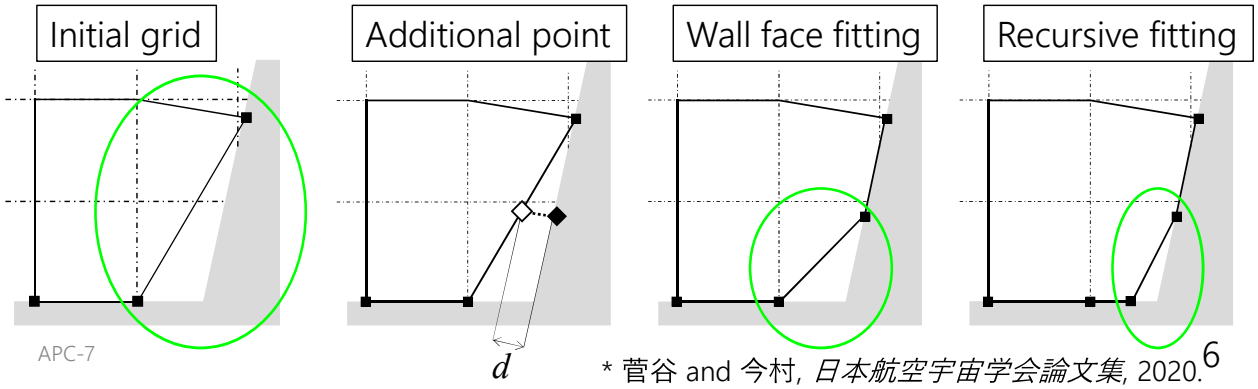

* 菅谷 and 今村, *日本航空宇宙学会論文集*, 2020.

Example of RF grid

- Grid generation around Intersecting cubes.
- Features are approximately represented in RF grid.

CAD

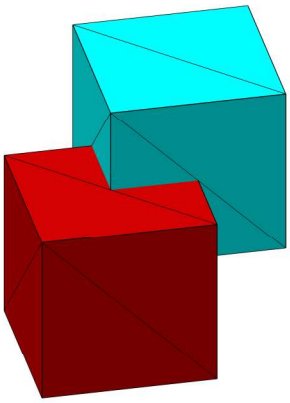

Initial grid

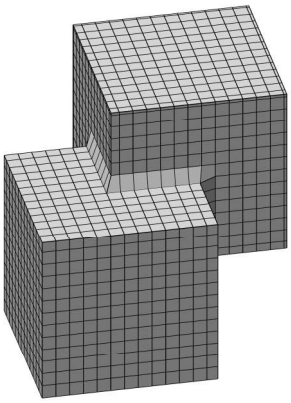

RF grid (dt=0.1dx)

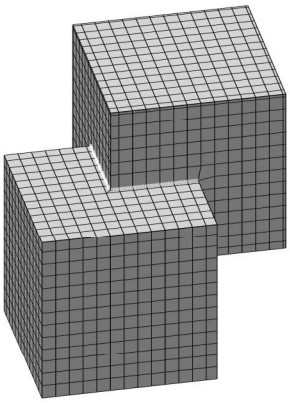

Computational Grid Setting

- Same grid setting as APC-6.
- Total cell number: 68.5 M
- $C_{MAC}/\Delta x$ ~ 655, y^+=40~100 on main wing
- Uniformly refined region between main wing and tail.

Trailing edge-body juncture (Saddle point)

Trailing edge (Convex)

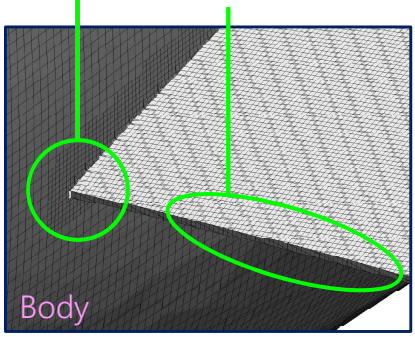

Uniformly refined region

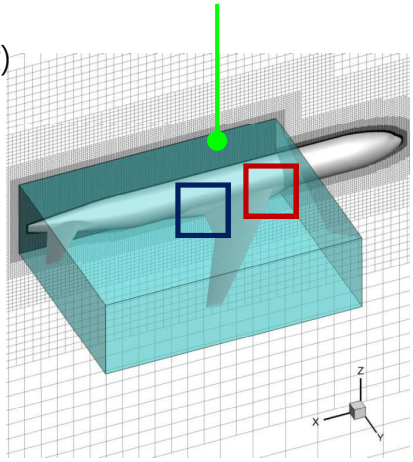

Wing-body juncture (Concave)

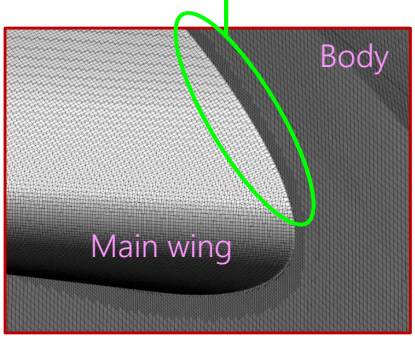

Computational Grid of NASA-CRM

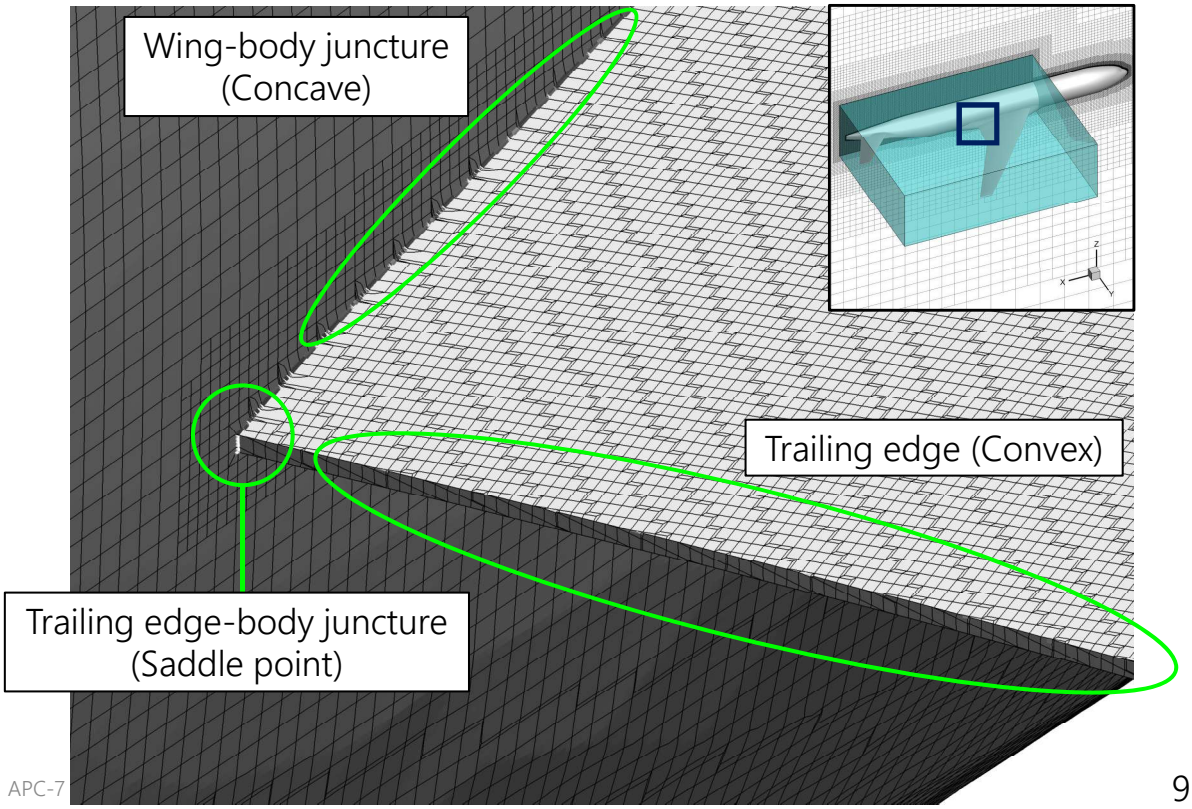

Numerical methods

- Turbulence Model (Steady) ：SA-noft2-R (Crot=1)
- Turbulence Model (Unsteady) ：DDES-protected*
  - RANS region is protected even when the stream-wise grid size is small.
- **Wall Function ：SA wall model**

- Inviscid flux ：Linear reconstruction+ SLAU
  - Limiter for recursively modified cells.
- Viscous flux ：2nd order Central difference

- Time integration(Steady) ：MFGS + Local Time Stepping
  - Start from free-stream conditions.
- Time integration(Unsteady) ：MFGS + BDF2 with 5 Inner Iteration
  - Restart form RANS results.
  - Courant number ~ 1 at wake region.

* 玉置 *et al.* ,第49期年会講演会講演集, 2018.

Case 1

Steady Simulation

Alpha sweep

- A fair agreement between RFM, IBM, and exp. at low AoA.
- Predicted *CL* and *CM* using RFM is closer to exp. than those of IBM at high AoA.
  - *CL* decrease at AoA = 13.08 to 14.08 [deg] in RFM simulation.

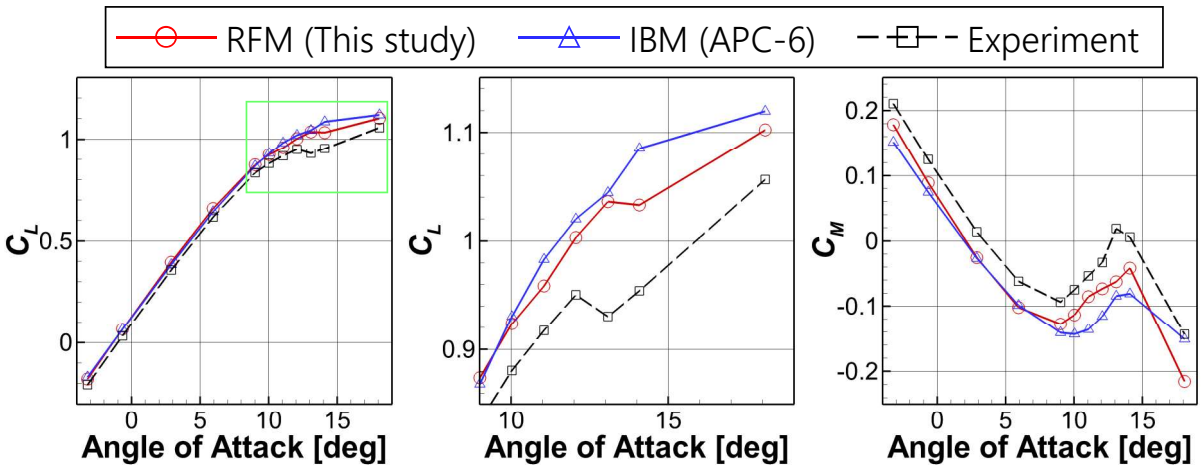

Streamline and skin friction

- Separating region (*Cfx*<0) gradually expands as AoA increases.
- Causing discrepancy of *CL* between RFM and experiment.
  - *CL* of exp. suddenly changes at AoA=12 due to large flow separation*.

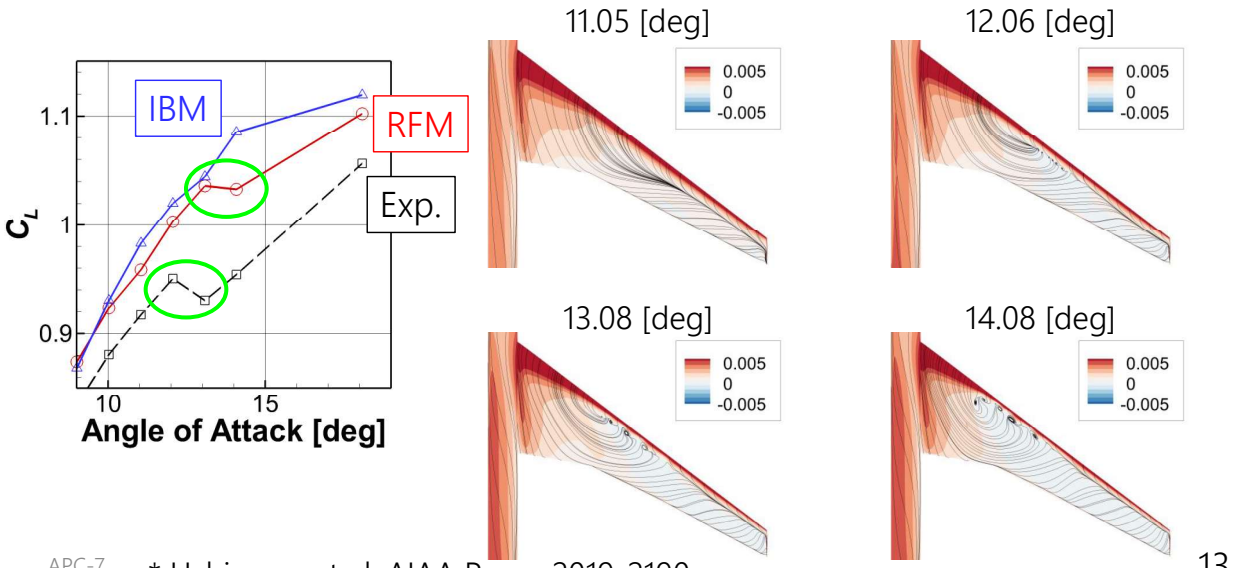

* Uchiyama et al. AIAA Paper 2019-2190.

Case 2

Unsteady Simulation

Comparison of aerodynamics coefficients

- Reasonable prediction of *CL* and *CM*.
- Similar results to simulations of 2nd-order FVM on body-fitted grids.

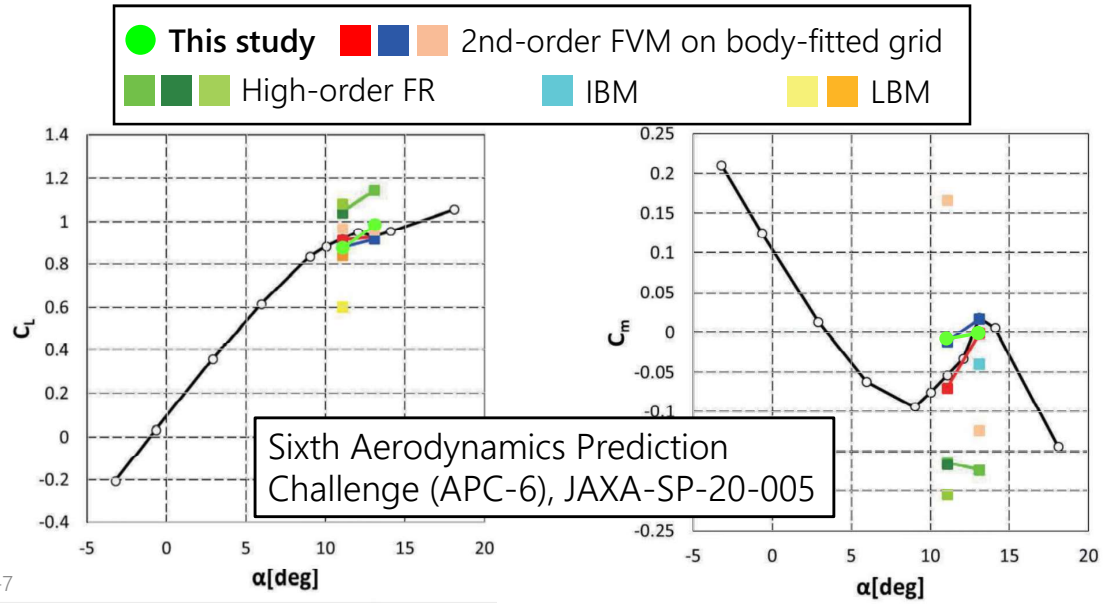

Q criterion

- Massive flow separation on main wing.
- Position of leading edge separation moves upstream as AoA increases.
- Vortices from wing-body junction.
  - Interfering with tail wing.

11.05 deg

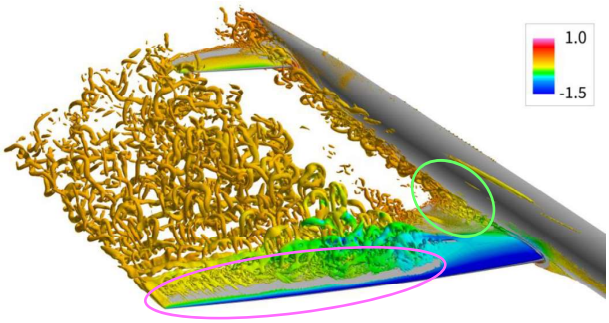

13.08 deg

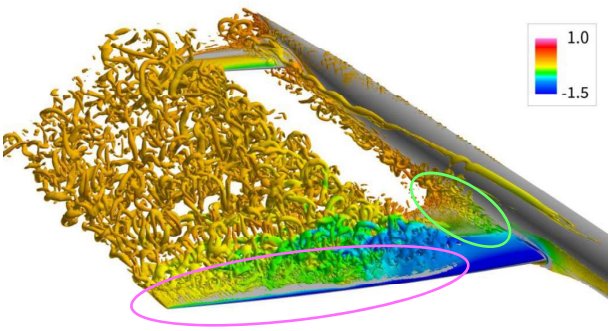

Conclusion

Turbulent flow simulation around NASA-CRM was conducted by using UTCart and Recursive Fitting Method.

- Automatic grid generation based on Cartesian grids.
- Geometric features are approximately represented.
- Conservation laws are satisfied.

- In steady simulation, *CL* and *CM* of Recursive Fitting method are closer to exp. than those of Immersed Boundary method.
- Reasonable prediction of unsteady aerodynamic coefficients
  - similar to those of 2nd-order FVM on conventional body-fitted grid.

Appendix

Details of grid setting

- Grid size
  - Main wing, tail : 0.00153 C_{MAC}
  - Body : 0.00306 C_{MAC}
  - Wake : 0.0122 C_{MAC}
- Domain size: $200C_{MAC} \times 200C_{MAC} \times 200C_{MAC}$
- Time for grid generation
  - Immersed Boundary (APC-6): 31 min.
  - Recursive Fitting Method (This study) : 49 min.

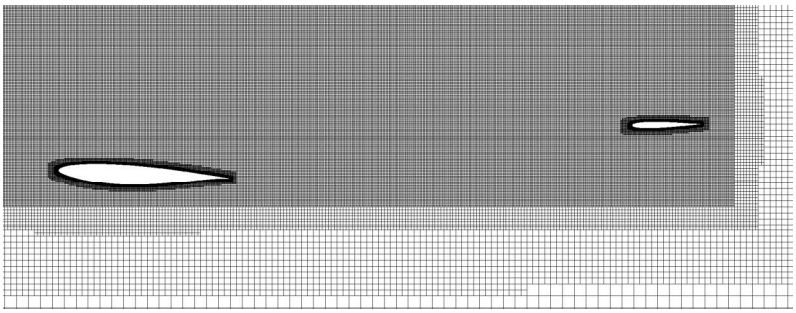

Time histories of *CL* and *CM*

- Initial conditions
  - Steady: Free stream conditions.
  - Unsteady: results of steady RANS simulation.

13.08 deg steady simulation

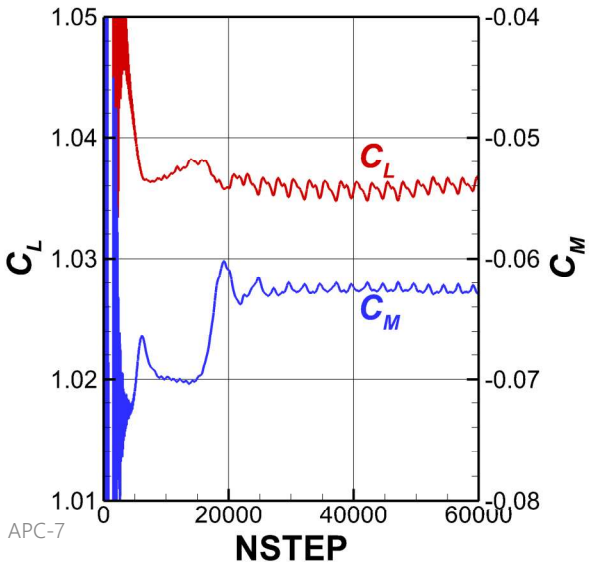

13.08 deg unsteady simulation

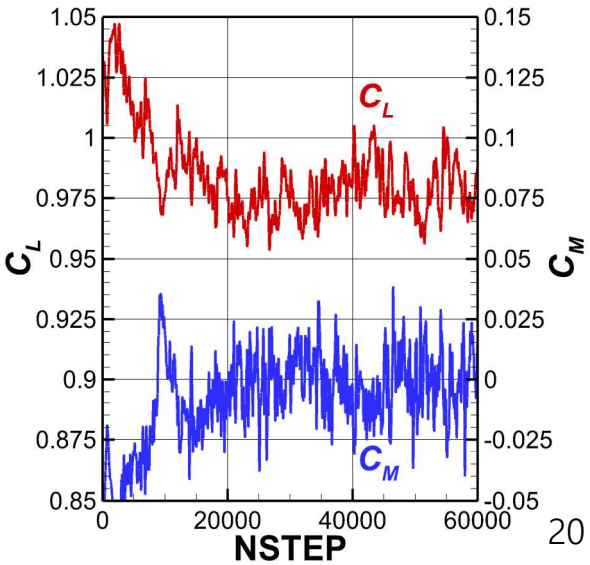

PSD of Lift coefficient (Unsteady)

- PSD becomes large as AoA increases.
- Peak of PSD of main wing around St~1 in simulation at AoA=11.05 deg.

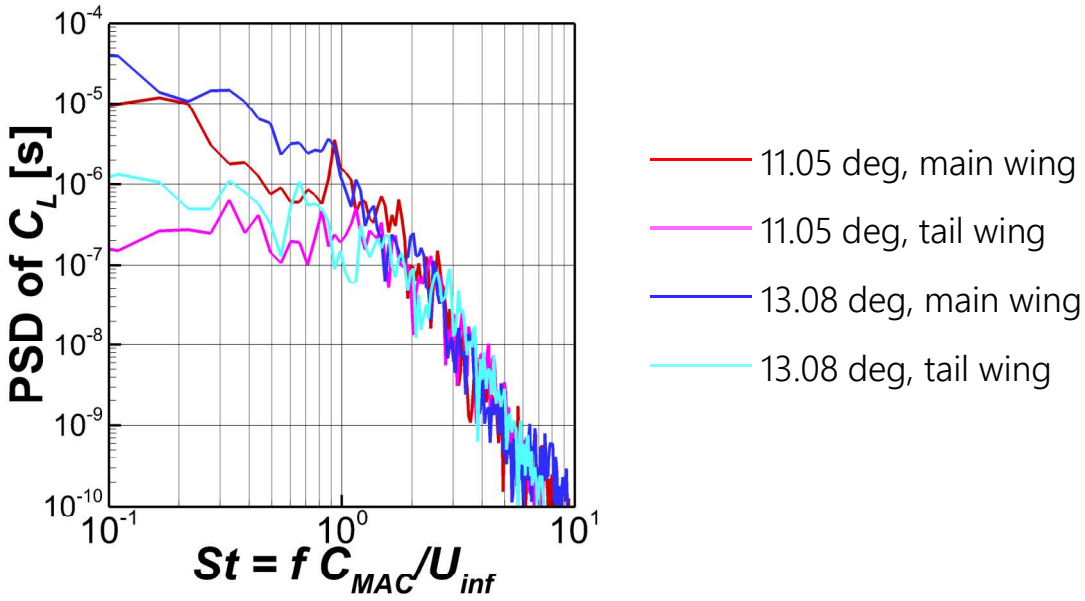

Seventh Aerodynamics Prediction Challenge (APC-7)
2021/06/30, Online

1A18: Aerodynamic Analysis of NASA-CRM at Low Speed and High Angle of Attack conditions Using Hierarchical Cartesian Mesh and Immersed Boundary Method

(階層型直交格子と埋め込み境界法を用いた低速・高迎角条件におけるNASA-CRM巡航形態の空力予測)

○Atsushi Hara, Keisuke Sugaya, Taro Imamura
(The University of Tokyo)

東京大学 THE UNIVERSITY OF TOKYO

Outline

- Background
- Objective
- Computational conditions
  - Numerical methods
  - Immersed boundary method
  - Computational grid
- Results
  - Aerodynamic coefficients
  - Time history
  - Q criterion
- Conclusion

Background

- Development of UTCart for aircraft design.
  - Grid generation + flow simulation.
  - Automatic and robust generation of hierarchical Cartesian grid.
  - Immersed boundary method (IBM) on stair step grids.
  - Compressible RANS/DDES simulation with wall function.

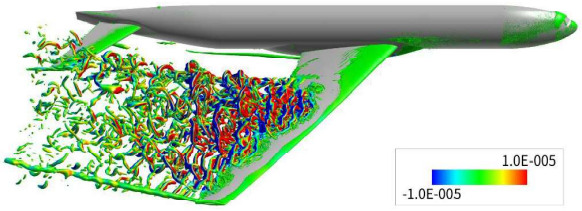

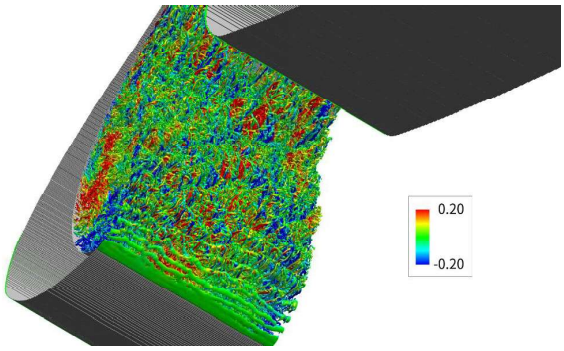

APC-7 吉永, 菅谷 and 今村, 流力ANSS2020. 菅谷 and 今村, 流力ANSS2020. 3

Results of APC-6(1) (IBM)

- A good agreement of aerodynamic coefficients between UTCart and the experiment at low angles of attack (AoA).
- At high AoA, UTCart and the experiment differ.
- **Effects of grid size needs to be investigated.**
- Further study of influence of numerical method is also necessary.

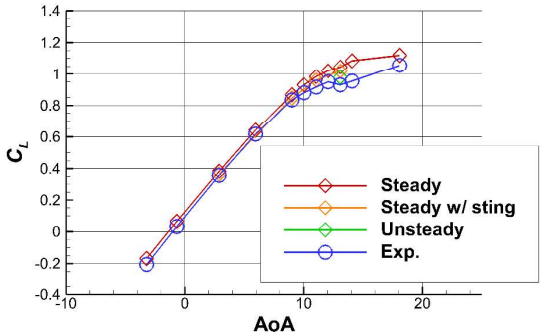

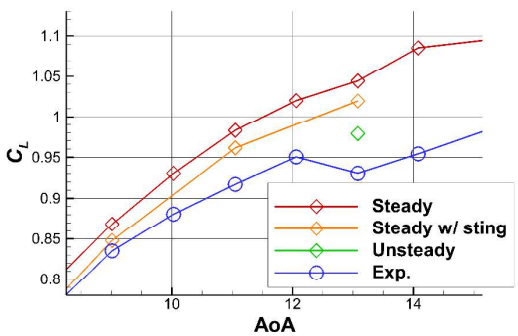

APC-7 1) Yoshinaga, H., Sugaya, K., and Imamura, T., APC-6, 2020 4

Objective

- To calculate the NASA-CRM cruising configuration at low speed with finer grids than APC-6 using IBM.
- To investigate the effect of the difference in the grid width of the wake area.
- To assess the prediction accuracy of UTCart for low speed and high AoA simulations.

Numerical method

	Steady	Unsteady
Governing equation	RANS	DDES-p(1)
Turbulence model	SA-noft2-R(2) (Crot = 1)	
Inviscid flux	SLAU + MUSCL ($\kappa = 1/3$)	
Viscous flux	2nd order central difference	
Time integration	MFGS (Local time stepping)	MFGS (Constant dt)
Initial condition	Free-stream	Restart from RANS
Wall boundary condition	IB + SA wall model	
Distance between Image Point and wall (d_{IP})	$2\Delta x$	

1) 玉置 et al., 航空宇宙学会年会, 2018.
2) Dacles-Mariani, j., et al., *AIAA J.*, 1995.

Immersed boundary method

- Flow variables on the Face Center (FC) are calculated from variables on the Image Point (IP) and wall boundary conditions.
- Assuming that tangential velocity is linear between the IP and the wall using wall functions(1).

$$u_{t,FC} = u_{t,IP} - u_\tau \left\{ \frac{\partial f_{wall}}{\partial y^+}(y_{IP}^+) \right\} (y_{IP}^+ - y_{FC}^+)$$

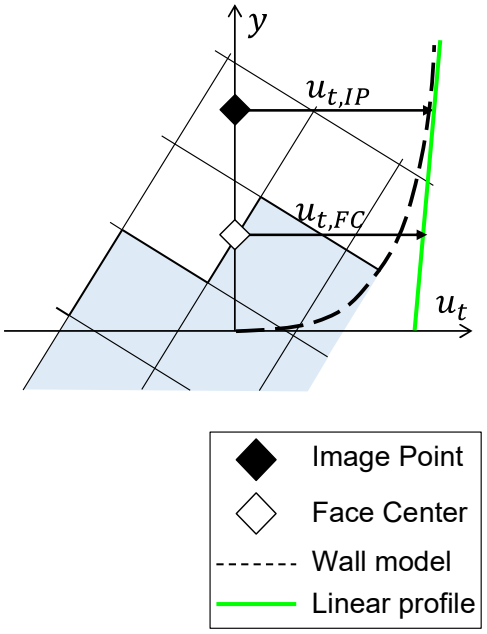

1) Tamaki, Y., Harada, M., and Imamura, T., *AIAA J.*, Vol 55, 2017.

Computational grid

- Unstructured hierarchical Cartesian grid.
- Two grids are used in both steady simulations and unsteady simulations.

	Grid #1 (140M)	Grid #2 (90M)
Total cell number	1.37×10^8	9.02×10^7
Domain size [in.]	2.76×10^4	2.76×10^4
Minimum grid size [in.]	0.281	0.281
Grid size of refinement box [in.]	2.24	4.49
MAC / Minimum grid size	981	981

Computational grid

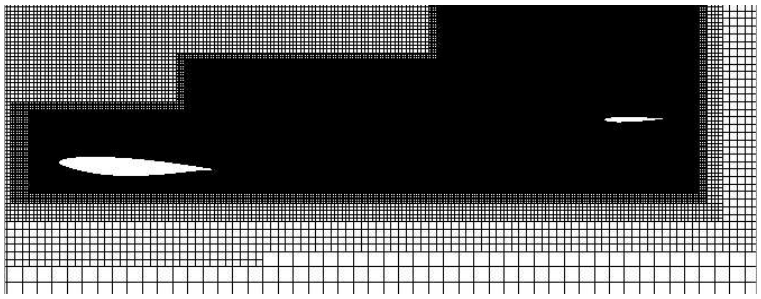

Grid #1 (140M), section YA ($y = 252$ [in.])

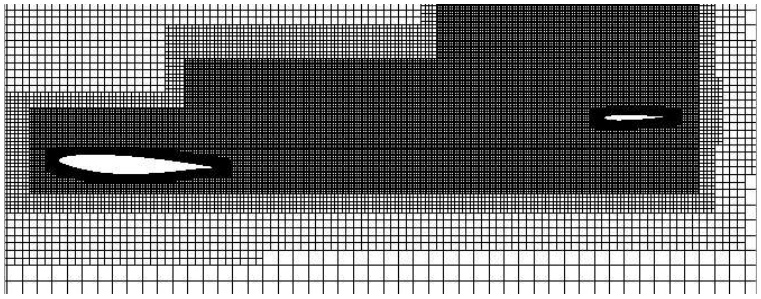

Grid #2 (90M), section YA ($y = 252$ [in.])

Computational grid

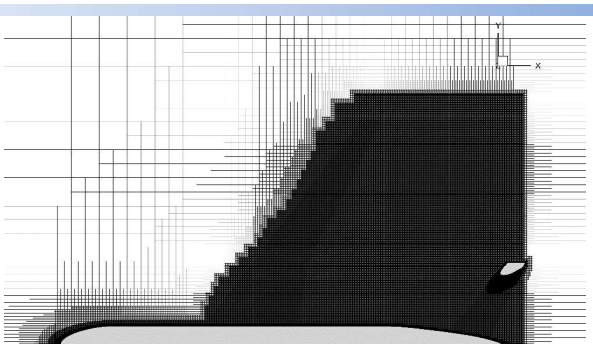

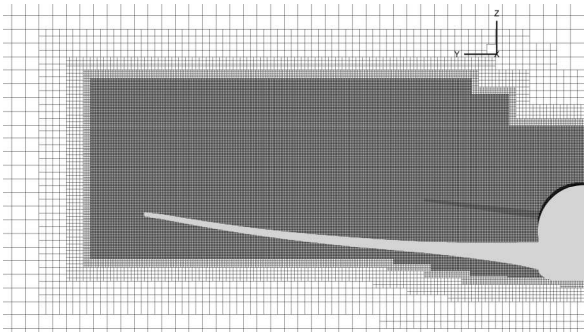

Grid #1 (140M)

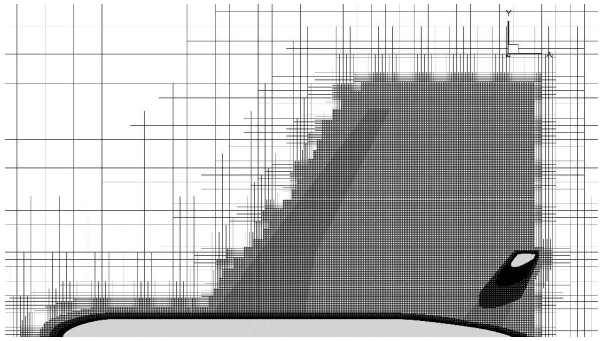

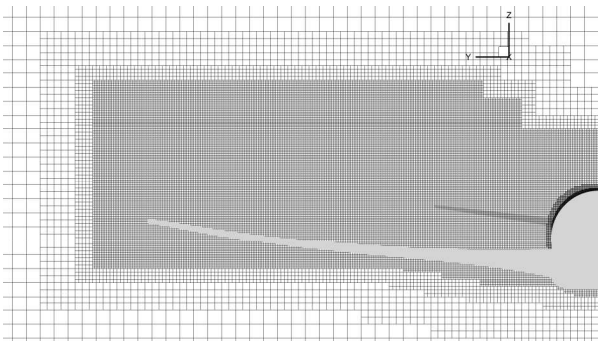

Grid #2 (90M)

Aerodynamic coefficients

- Macro trends match the experiment.
- There is little difference between steady simulation of 140M grid and 90M grid.

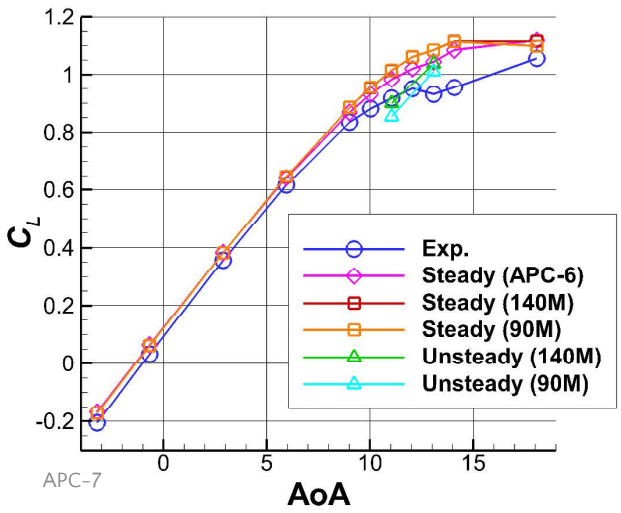

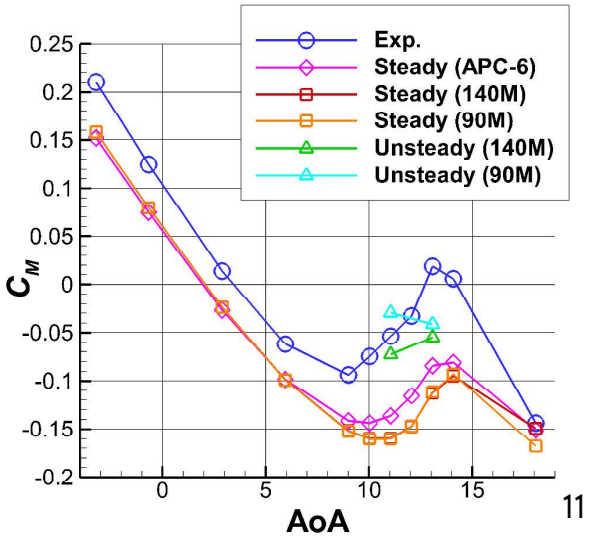

11

Aerodynamic coefficients

- Steady simulations overestimate C_L at high AoA.
  - Flow separation seems underestimated.
- Results of unsteady simulations are closer to the experimental values than steady simulations.

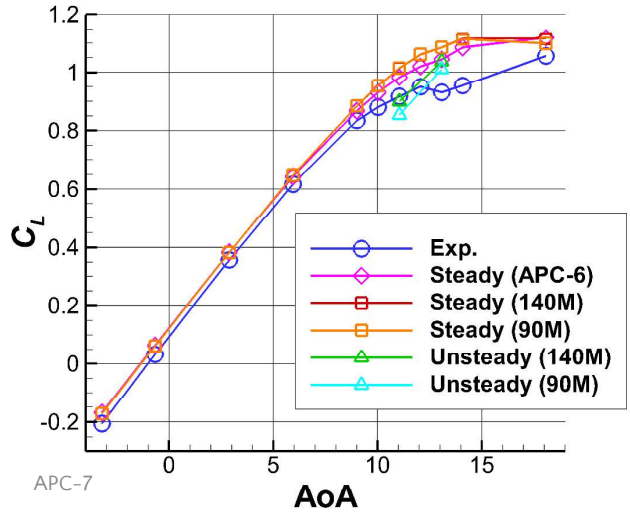

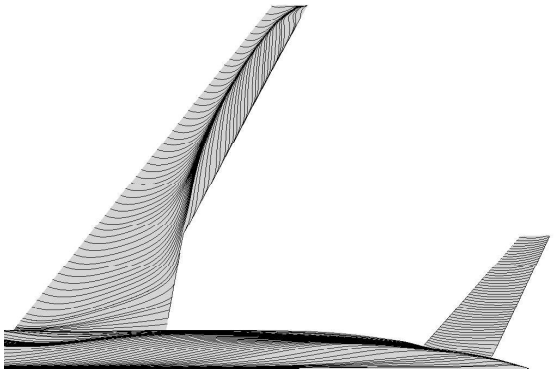

AoA = 13.08 [deg.], Steady (140M)

12

Aerodynamic coefficients

- Predicted C_D values are smaller than the experimental values at high AoA.
- C_M values are underestimated.
- Unsteady simulations are closer to the experiment.

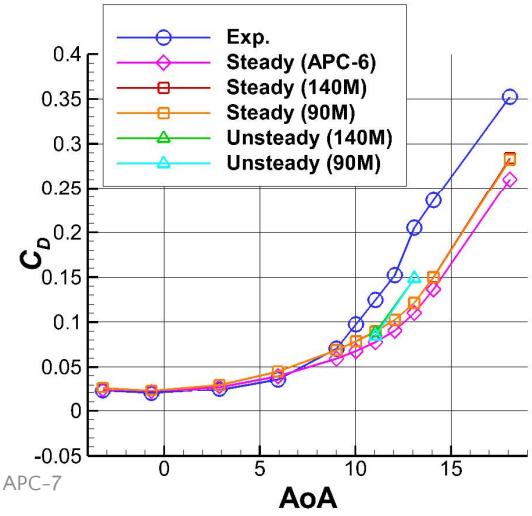

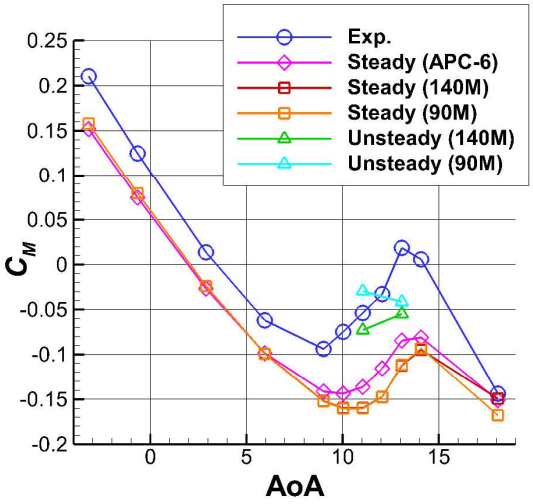

Time history

- Unsteady simulations (DDES) start after 15000 steps of steady simulations (RANS).
- The results from step 45001 to step 90000 are used in this research (about 6.15 sec.).
- $\Delta t = 1.37 \times 10^{-4}$ sec. (both 140M and 90M)

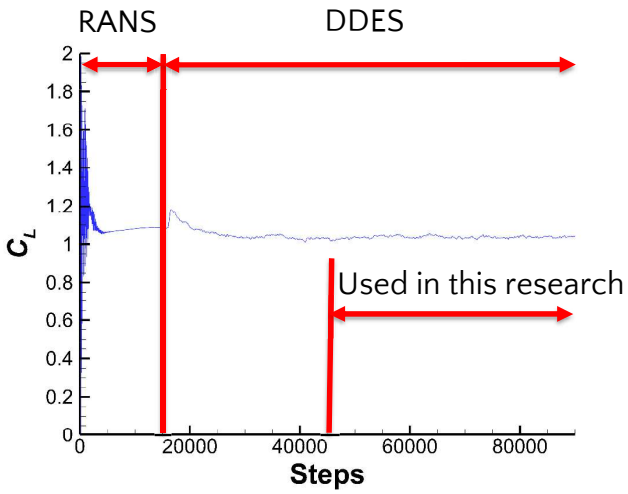

History of C_L, AoA = 11.05 [deg.], Unsteady (140M)

Time history (140M)

- Periodic oscillation is observed at AoA = 11.05 [deg.].
- Flow becomes non-periodic at AoA = 13.08 [deg.].

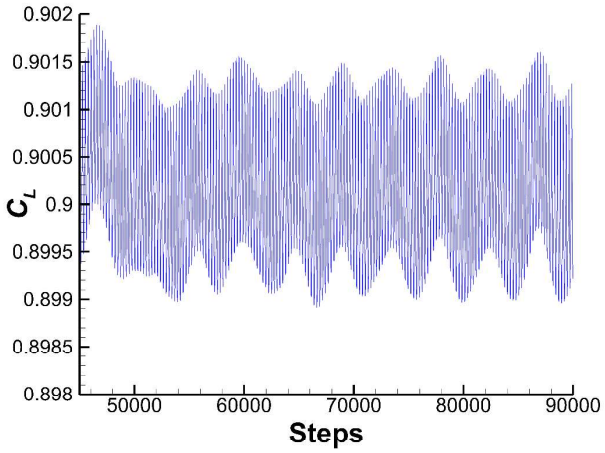

AoA = 11.05 [deg.], Unsteady (140M)

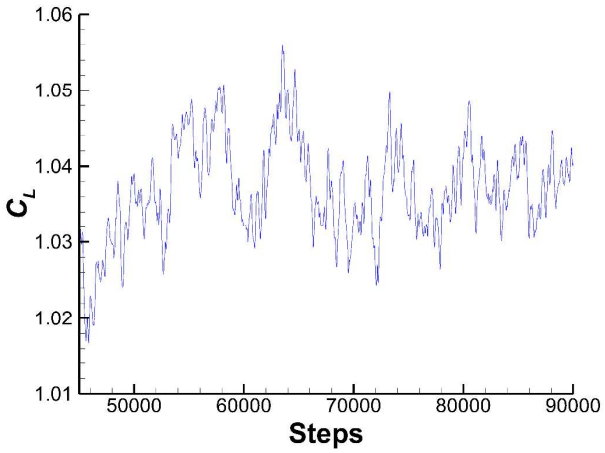

AoA = 13.08 [deg.], Unsteady (140M)

Time history (90M)

- At AoA = 11.05 [deg.], flow has both periodic and non-periodic characteristics.
- At AoA = 13.08 [deg.], flow is non-periodic.

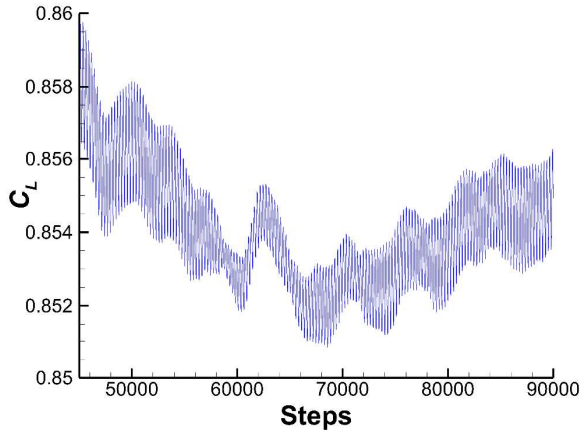

AoA = 11.05 [deg.], Unsteady (90M)

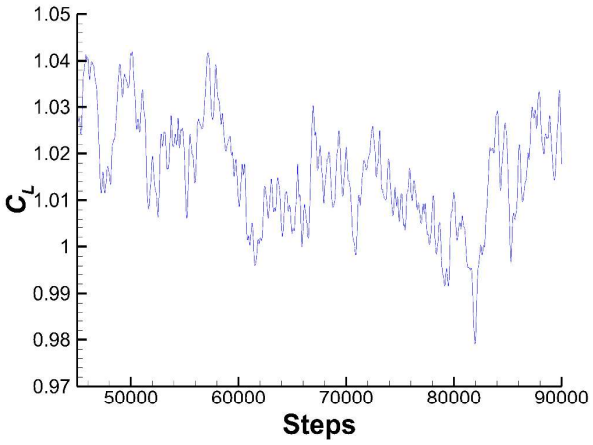

AoA = 13.08 [deg.], Unsteady (90M)

Q criterion

- There is a difference in the wake by AoA and grids.

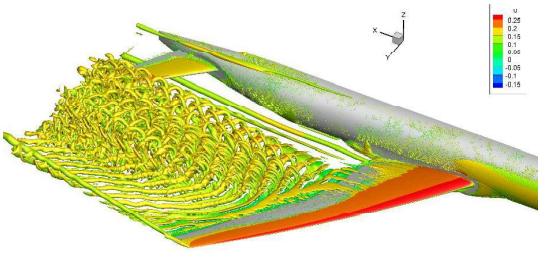

AoA = 11.05 [deg.], Unsteady (140M)

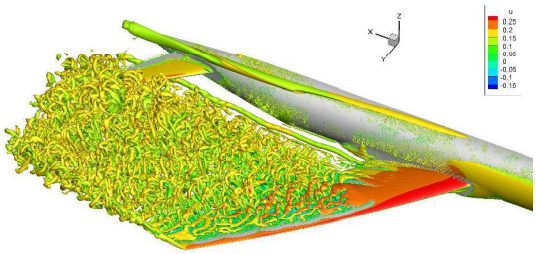

AoA = 13.08 [deg.], Unsteady (140M)

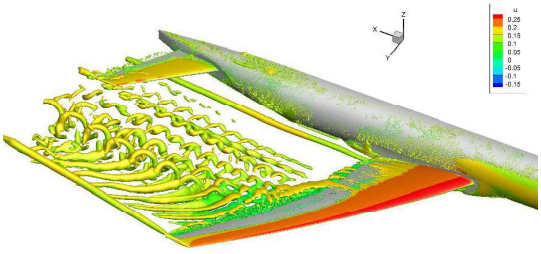

AoA = 11.05 [deg.], Unsteady (90M)

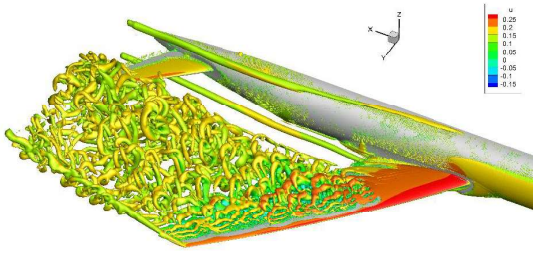

AoA = 13.08 [deg.], Unsteady (90M)

17

Q criterion

- At AoA = 13.08 [deg.], separation occurs from leading edge.

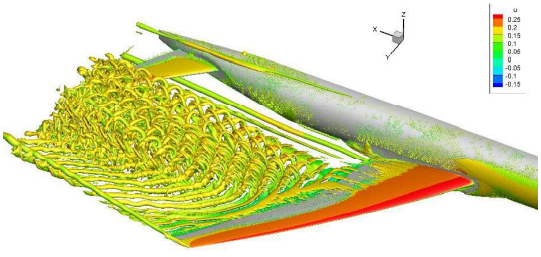

AoA = 11.05 [deg.], Unsteady (140M)

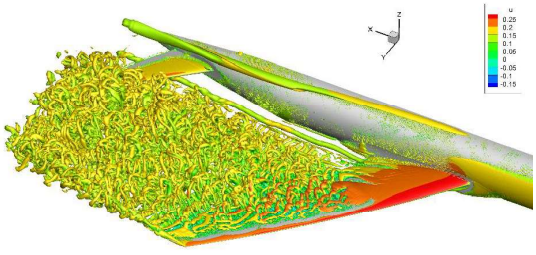

AoA = 13.08 [deg.], Unsteady (140M)

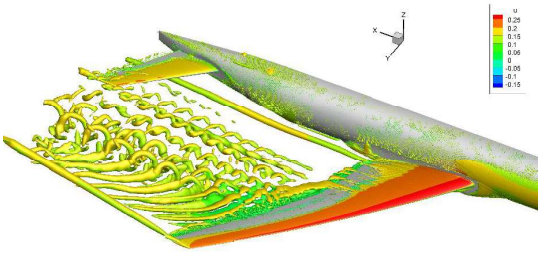

AoA = 11.05 [deg.], Unsteady (90M)

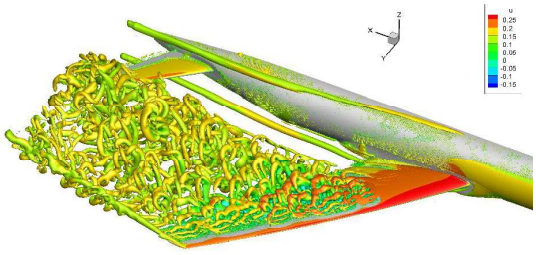

AoA = 13.08 [deg.], Unsteady (90M)

18

Conclusion

- Flow simulations for NASA-CRM at low-speed conditions are conducted by using UTCart and IBM.
  - In many cases, the effect of the difference in the grid width of the wake area is small.
  - The tendency of the aerodynamic coefficients at low angles of attack is consistent with the experimental results.
  - Flow separation at high angles of attack is underestimated in steady simulations.
  - Unsteady simulation improves the predictions of flow separation and aerodynamic coefficients.

Appendix

Coefficients of each component (Unsteady, AoA = 11.05 [deg.])

AoA = 11.05 [deg.]		C_D	C_L	C_M
140M	Main wing	4.79×10^{-2}	7.30×10^{-1}	-1.10×10^{-1}
	Fuselage	3.39×10^{-2}	1.38×10^{-1}	1.70×10^{-1}
	Tail wing	6.67×10^{-3}	3.20×10^{-2}	-1.32×10^{-1}
	Total	8.84×10^{-2}	9.00×10^{-1}	-7.26×10^{-2}
90M	Main wing	4.47×10^{-2}	6.88×10^{-1}	-7.65×10^{-2}
	Fuselage	3.35×10^{-2}	1.36×10^{-1}	1.70×10^{-1}
	Tail wing	6.41×10^{-3}	2.97×10^{-2}	-1.23×10^{-1}
	Total	8.46×10^{-2}	8.54×10^{-1}	-2.94×10^{-2}

Coefficients of each component (Unsteady, AoA = 13.08 [deg.])

AoA = 13.08 [deg.]		C_D	C_L	C_M
140M	Main wing	9.48×10^{-2}	8.29×10^{-1}	-9.41×10^{-2}
	Fuselage	4.50×10^{-2}	1.70×10^{-1}	1.94×10^{-1}
	Tail wing	8.71×10^{-3}	3.77×10^{-2}	-1.54×10^{-1}
	Total	1.49×10^{-1}	1.03	-5.48×10^{-2}
90M	Main wing	9.55×10^{-2}	8.05×10^{-1}	-8.94×10^{-2}
	Fuselage	4.49×10^{-2}	1.69×10^{-1}	1.92×10^{-1}
	Tail wing	8.56×10^{-3}	3.54×10^{-2}	-1.45×10^{-1}
	Total	1.49×10^{-1}	1.01	-4.13×10^{-2}

Computational grid of APC-6(1)

	Steady		unsteady
	w/o sting	w/ sting	
Total cell number	6.85×10^7	8.14×10^7	5.52×10^7
Domain size [in.]	2.76×10^4	2.76×10^4	2.76×10^4
Minimum grid size [in.]	0.421	0.421	0.421
Grid size of refinement box [in.]	3.37	3.37	3.37
MAC / Minimum grid size	655	655	655

1) Yoshinaga, H., Sugaya, K., and Imamura, T., APC-6, 2020

Numerical Simulations of Compressible Flow around the NASA-CRM using Cartesian Cut-Cell Method with Wall-Stress Model

壁面応力モデルを適用した直交カットセル法によるNASA-CRMまわりの圧縮性流れの数値解析

Yuta Takahashi, Yuki Takeda,
Karin Matsubara, Kazuyuki Ueno
(Iwate University)

Cartesian Grid Method

Characteristics of Cartesian grid
- Easy grid generation and full automation
- Fast and robust grid generation

→ One of the most useful computational methods for complex shaped object

Typical Cartesian grid method
- Cartesian Cut-Cell Method
- Voxel Method
- Immersed Boundary Method

Cartesian Cut-Cell Method

Cut-Cell method cuts the computation cells according to object shape.

- Smoother surface than voxel method.
- Satisfy the mass conservation law.
  (IB method is not satisfy.)

On the other hand…

- Need to be divided into a large number of cases depending on many cutting patterns.
- Problem of CFL condition in small cells.

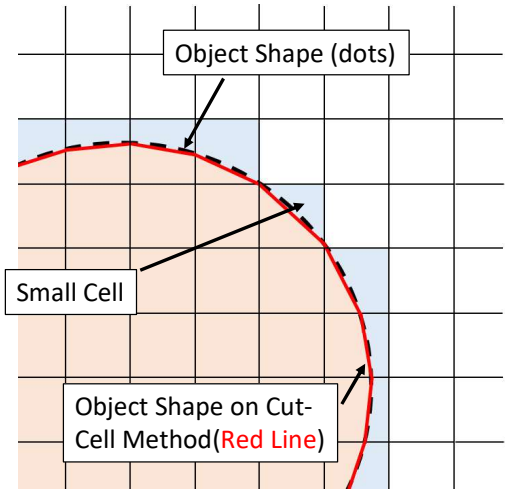

Objective

Aerodynamic prediction on the NASA-CRM using Cartesian Cut-Cell Method with Wall-Stress Model is performed.

Simulation Method

Conservation Equation	Compressible Navier-Stokes Equation
Wall Shear Stress	Wall-Stress Model[1]
Discretization Method	Cell-Centered Finite Volume Method
Wall Treatment	Cartesian Cut-Cell Method
Inviscid Flux	SLAU （5th-Order MUSCL + Thornber's Modification）
Viscous Flux	2nd-Order Central Difference
Time Integration	2nd-Order TVD Runge-Kutta Method
Turbulence Model	Implicit LES

[1] S. Kawai, J. Larsson, "Wall-modeling in large eddy simulation: Length scales, grid resolution, and accuracy ", Physics of Fluids **24**, 2012.

Wall-Stress Model for Cut-Cell Method

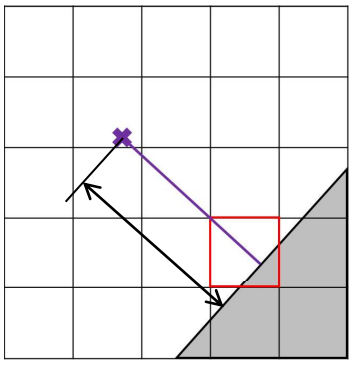

1) Extend the probe vertically from the wall.

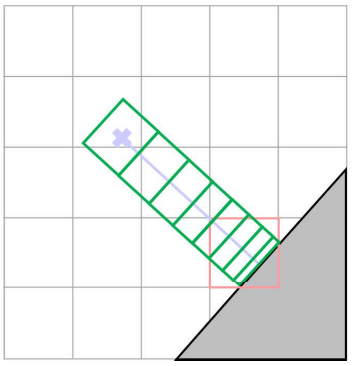

2) Generate virtual grid system (1D) in the vertical direction of the wall, based on the extended probe.

Wall-Stress Model for Cut-Cell Method

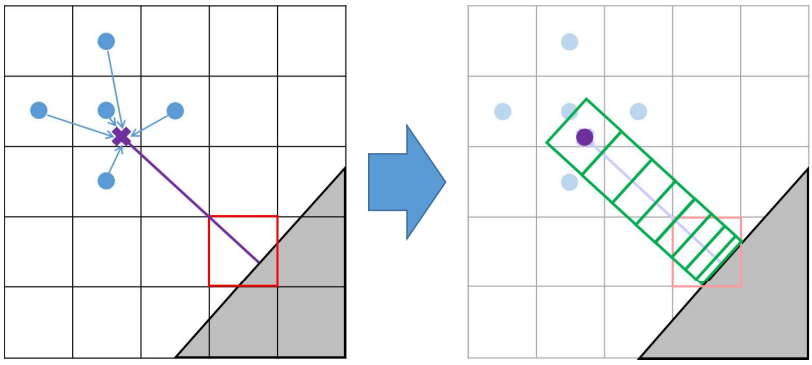

Inverse Distance Weighted Interpolation

$$Q = \frac{\sum_{i=1}^{n} w_i Q_i}{\sum_{i=1}^{n} w_i}$$

$$w_i = \frac{1}{\sqrt{(x_i - x)^2 + (y_i - y)^2 + (z_i - z)^2}}$$

3) The values at the probe tip are interpolated from the neighboring cell-centers by Inverse Distance Weighted Interpolation, and input as a boundary condition for Wall-Stress Model.

Wall-Stress Model for Cut-Cell Method

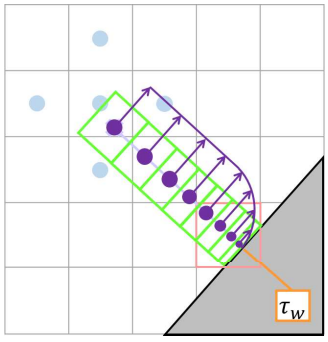

4) Solve the Wall-Stress Model Equation[1] to obtain τ_w, and apply τ_w to the Cut-Cell as the wall flux.

$$\frac{d}{d\eta}\left[(\mu + \mu_{t,\mathrm{wm}})\frac{dU_{||}}{d\eta}\right] = 0$$

$$\frac{d}{d\eta}\left[(\mu + \mu_{t,\mathrm{wm}})U_{||}\frac{dU_{||}}{d\eta}\right] + \frac{d}{d\eta}\left[c_p\left(\frac{\mu}{Pr} + \frac{\mu_{t,\mathrm{wm}}}{Pr_{t,\mathrm{wm}}}\right)\frac{dT}{d\eta}\right] = 0$$

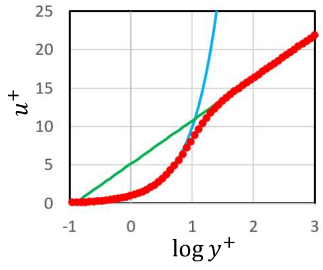

- Wall-Stress Model
- $u^+ = y^+$
- Log law

$$\mu_{t,\mathrm{wm}} = \kappa\rho y\sqrt{\frac{\tau_w}{\rho}}D \qquad D = \left[1 - \exp\left(-\frac{y^+}{A^+}\right)\right]^2$$

[1] S. Kawai, J. Larsson, "Wall-modeling in large eddy simulation: Length scales, grid resolution, and accuracy ", Physics of Fluids **24**, 2012.

Computational Conditions

Case2 : Unsteady computation

-Mach number : $M_\infty = 0.168$

-Reynolds number : $Re_c = 1.06 \times 10^6$

-Reference temperature : $T_{ref} = 310$ K

-Angle of attack : $\alpha = 11.05°$

Computational Grid

Cartesian grid（Uniform＋Non-Uniform）

	Minimum cell size Δx ($\Delta x / C_{ref}$)	Total cell number
Coarse	0.1 m (1.43×10^{-2})	54,737,280 cells（$731 \times 360 \times 208$）
Fine	0.05 m (7.14×10^{-3})	379,011,072 cells($1402 \times 704 \times 384$)

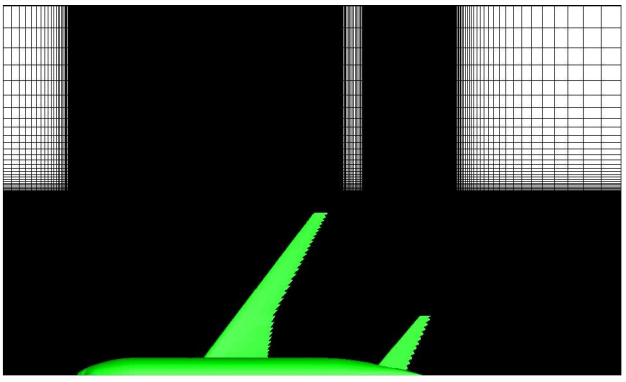

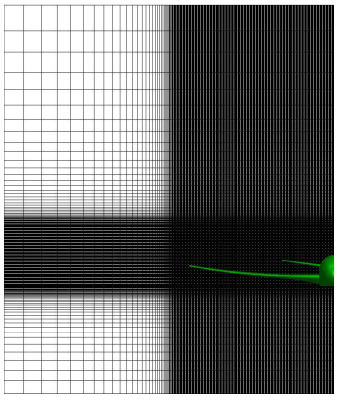

Computational Grid (Coarse)

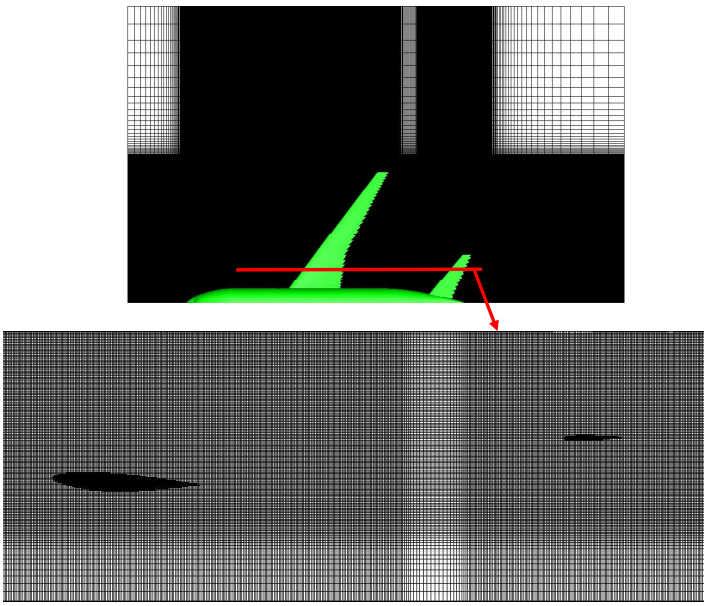

Surface grid（Main wing root）

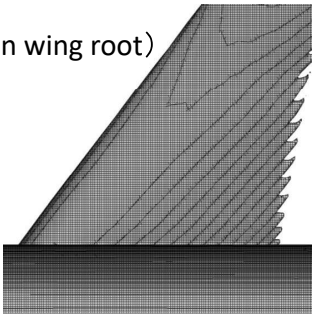

Surface grid（Tail wing）

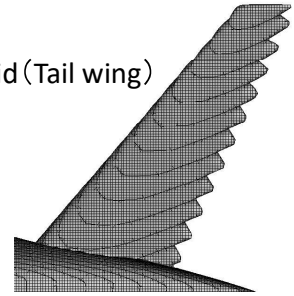

Shape of Wing Trailing Edge

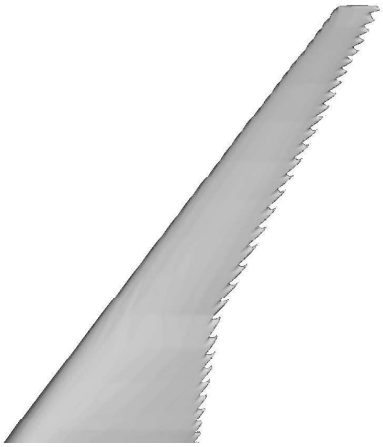

Coarse (Main wing)

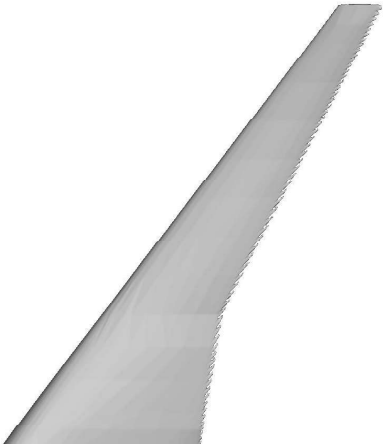

Fine (Main wing)

Coarse
(Tail wing)

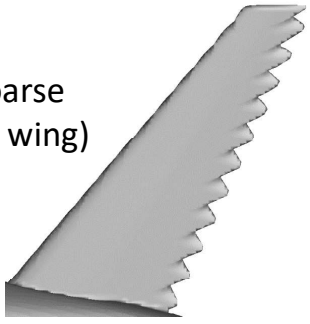

Fine
(Tail wing)

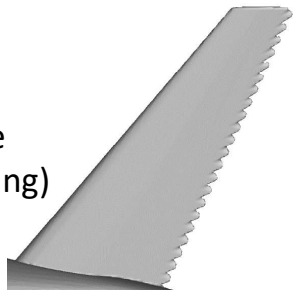

Results : Flow Field (Coarse)

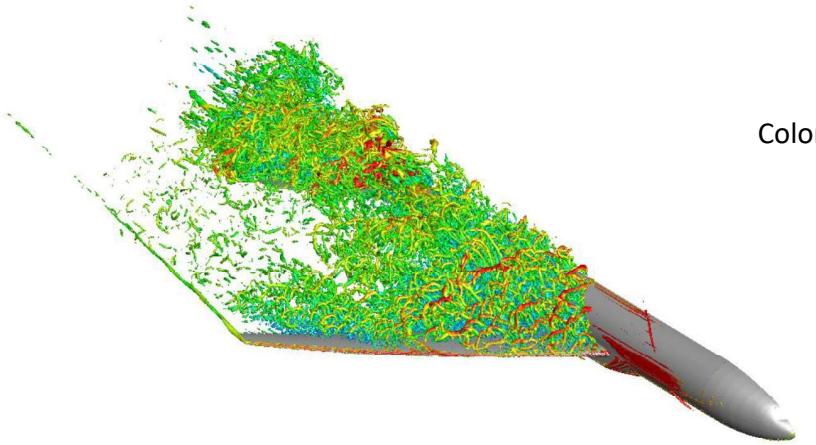

Isosurfaces of Q value
＋
Color contour of Mach number

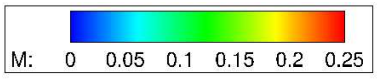

Results : Wake of Main Wing (Section YB)

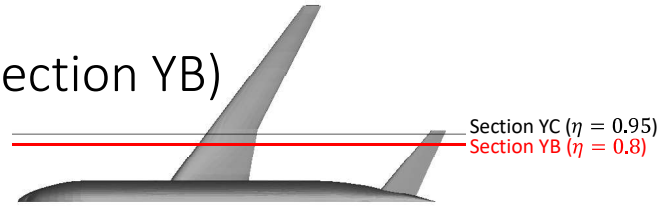

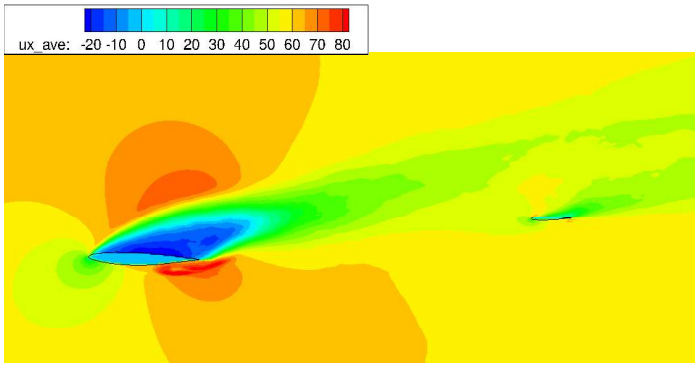

Time-averaged flow field (Coarse)

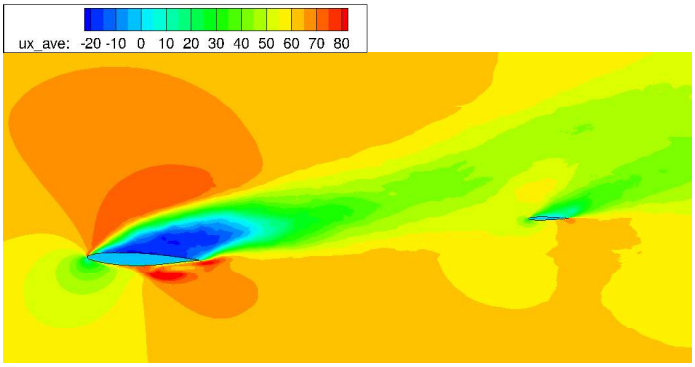

Time-averaged flow field (Fine)

Results : Wake of Main Wing (Section YC)

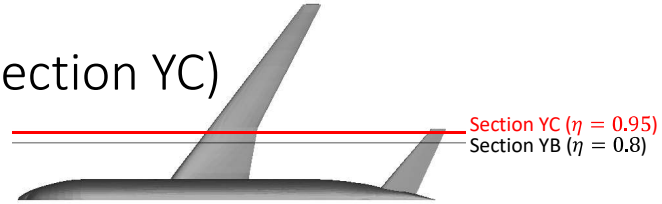

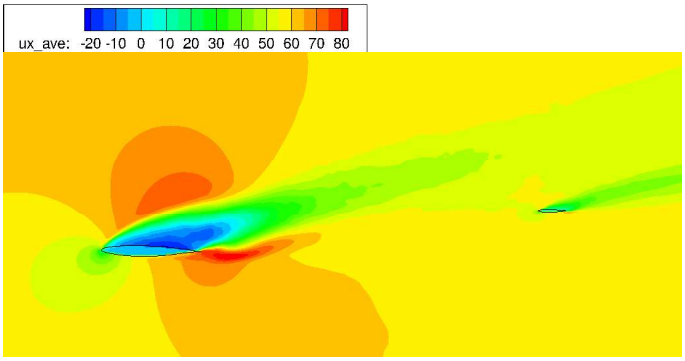

Time-averaged flow field (Coarse)

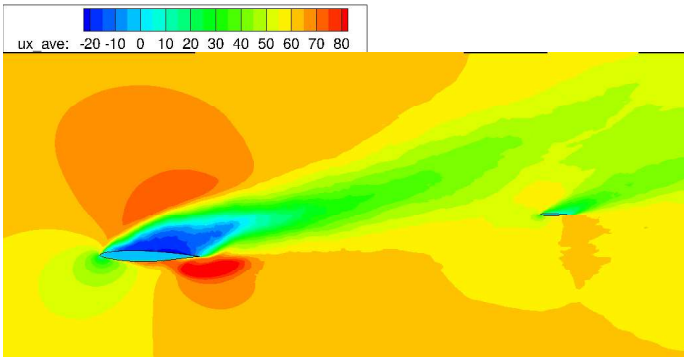

Time-averaged flow field (Fine)

Results : Surface Streamline (Time-averaged)

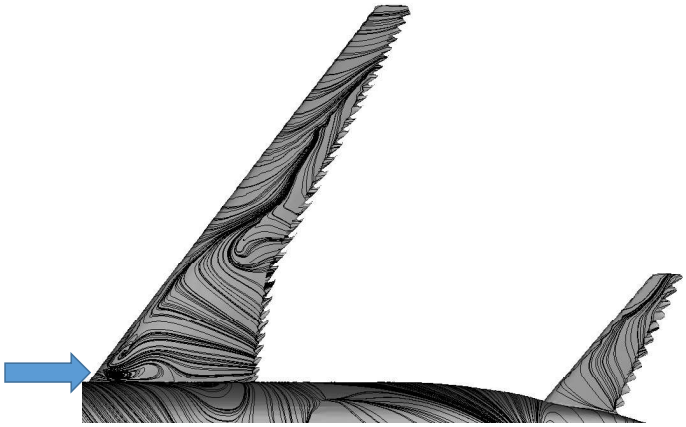

Coarse

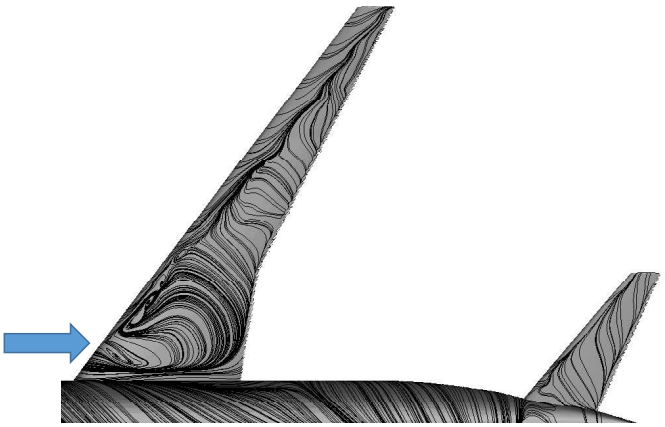

Fine

Results : Aerodynamic Coefficients (C_L, C_D, C_M)

	C_L	C_D	C_M
Exp. [2]	0.9172	0.1247	-0.0537
Coarse	0.9687	0.1440	-0.1601
Fine	1.300	0.2884	-0.4612

[2] T. Uchiyama et al. , “Experimental Investigation of 160% Scaled NASA Common Research Model at Low Speed Conditions ", 7-11 January 2019, San Diego, California, AIAA Scitech 2019 Forum, AIAA 2019-2190.

Result : Pressure Coefficient C_p

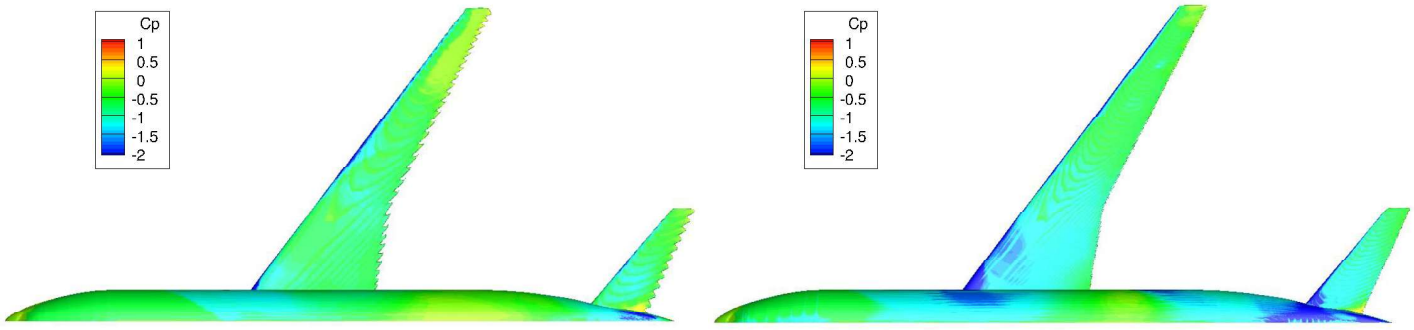

Coarse Fine

Conclusion

Numerical simulations of compressible flow around the NASA-CRM using Cartesian Cut-Cell Method with Wall-Stress Model were performed.

- The position of leading edge separation of main wing approaches the experiment by increasing grid resolution.
- Both Coarse grid and Fine grid, wake of main wing passed above the tail wing.
- Lift coefficient and Drag coefficient of Coarse grid were close to that of the experiment.
- Lift coefficient and Drag coefficient of Fine grid was overestimated compared to Coarse grid and experiment.

1A20

Comparative Study on Turbulence Models and Numerical Flux Functions in NASA CRM Unsteady Low-Speed Buffet Simulations

○Y. Yasumura and K. Kitamura, Y. Furusawa (Yokohama National University)
and
M. Kanamori and A. Hashimoto (JAXA)

Background

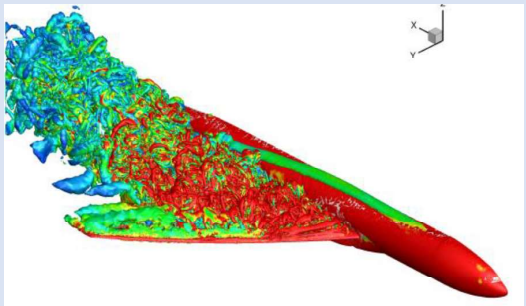

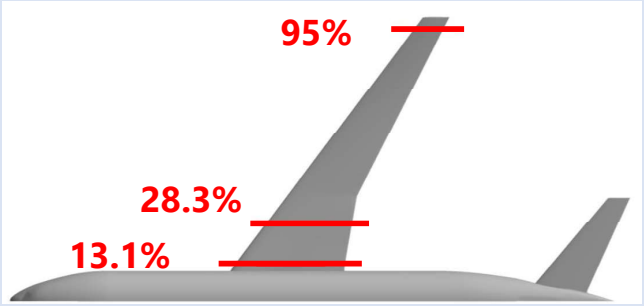

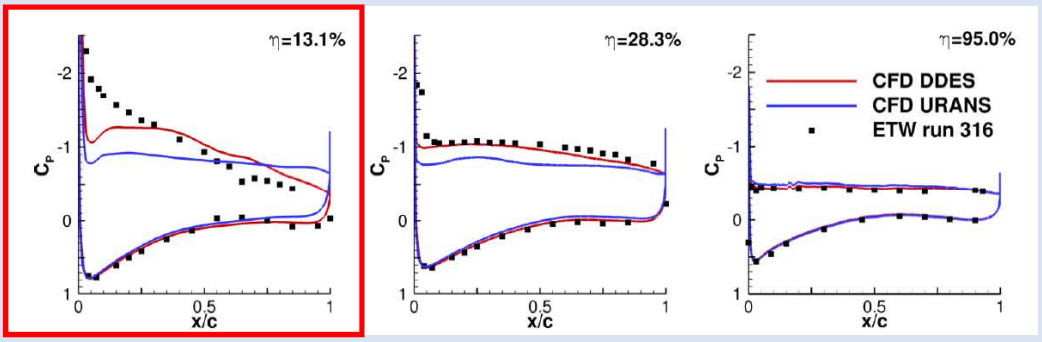

[1]

- NOT Good Match with Experiment

[1] Andreas Waldman, Philipp Gansel, Thorsten Lutz, Ewald Kramer : Unsteady Wake Flow of an Aircraft under Low-Speed Stall Conditions in DES and PIV, 53rd AIAA Aerospace Sciences Meeting, 2015

Background

HR-DDES

$$\tilde{d} = d - f_d \max(0, d - C_{DES}\Delta)$$

②0.65 is the typical choice.

➡ **0.51** is used in HR-DDES

Large C_{DES} : **Large** RANS Region

Small C_{DES} : **Large** LES Region

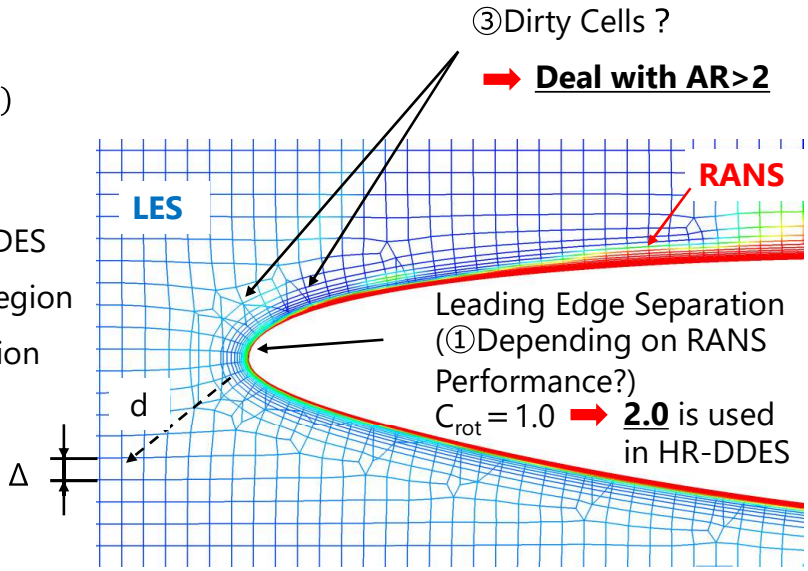

➢ $\tilde{d}/d$ is visualized around the leading edge of the main wing by color counter.
0(**Blue**) roughly corresponds to **LES** region, and 1(**Red**) is **RANS** region.

2

Background

Previous Study (Low-Speed Buffet)[2]

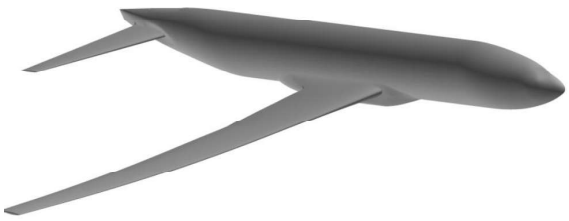

NASA CRM
22,823,905 cells

Conditions[3]		
Mach Number	:	**M = 0.25**
Reynolds Number	:	Re = 1.16×10^7
Angle of Attack	:	**α = 18 [deg.]**

Methods		
Numerical Flux	:	**SLAU**
Turbulent Model	:	DDES
Time Integration	:	LU-SGS
Slope	:	Green-Gauss
Slope Limiter	:	Hishida(vL)

[2] Kitamura Keiichi, Ogawa Suguru, Takimoto Hiroyuki, Kanamori Masashi, Hashimoto Atsushi : High-Resolution Delayed-Detached-Eddy-Simulation(HR-DDES) on Low Speed Buffet, Proceeding of the 51st Fluid Dynamics Conference / the 37th Aerospace Numerical Simulation Symposium, 2019.
[3] Andreas Waldman, Philipp Gansel, Thorsten Lutz, Ewald Kramer : Unsteady Wake Flow of an Aircraft under Low-Speed Stall Conditions in DES and PIV, 53rd AIAA Aerospace Sciences Meeting, 2015.

3

Background

Previous Study (Low-Speed Buffet)[2]

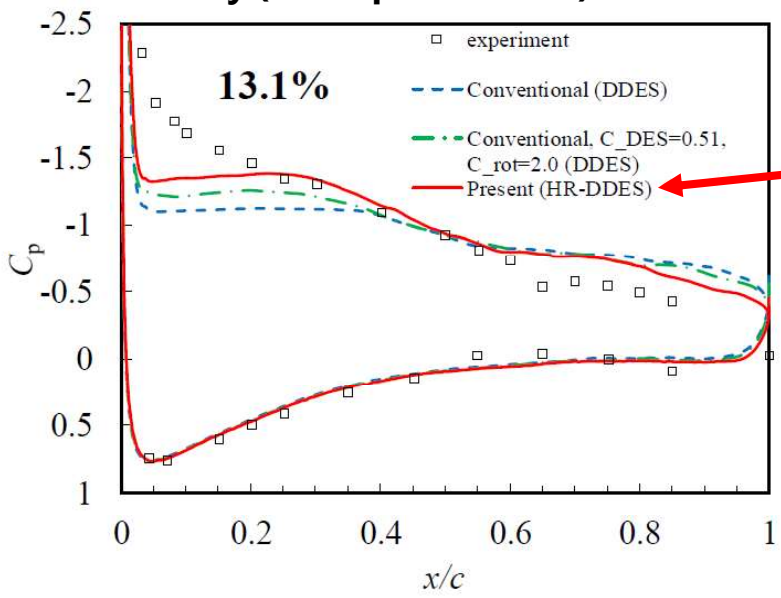

Dirty Cell Treatment(AR>2)

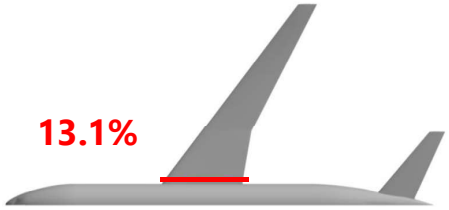

- C_{DES}=0.51, C_{rot}=2.0 and Dirty Cell Treatment(AR>2)
  - ➡ Best Match with Experiment

[2] Kitamura Keiichi, Ogawa Suguru, Takimoto Hiroyuki, Kanamori Masashi, Hashimoto Atsushi : High-Resolution Delayed-Detached-Eddy-Simulation(HR-DDES) on Low Speed Buffet, Proceeding of the 51st Fluid Dynamics Conference / the 37th Aerospace Numerical Simulation Symposium, 2019.

Objective

- Investigate the effects of the turbulence models and numerical flux functions in Unsteady NASA CRM Low-Speed Buffet Simulations

Case		
HH	:	HR-SLAU2 & HR-DDES
HS	:	HR-SLAU2 & SA-DDES
SS	:	SLAU2 & SA-DDES

HR-DDES
C_{DES} = 0.51
C_{rot} = 2.0

SA-DDES
C_{DES} = 0.65
C_{rot} = 1.0

Conditions

➢ Task 2：Unsteady simulations

Using “HexaGrid” Grid (provided by JAXA)

Conditions			
Mach Number	:	M	= 0.168
Reynolds Number	:	Re	= 1.06×10^{6}
Angle of Attack	:	α	= 11.05, 13.08 [deg.]
Time Step	:	Δt	= 0.0125 [-]
			(2.48×10^{-4} [s])

6

Conditions

➢ Task 2：Unsteady simulations

Using “HexaGrid” Grid (provided by JAXA)

Time Step Verification

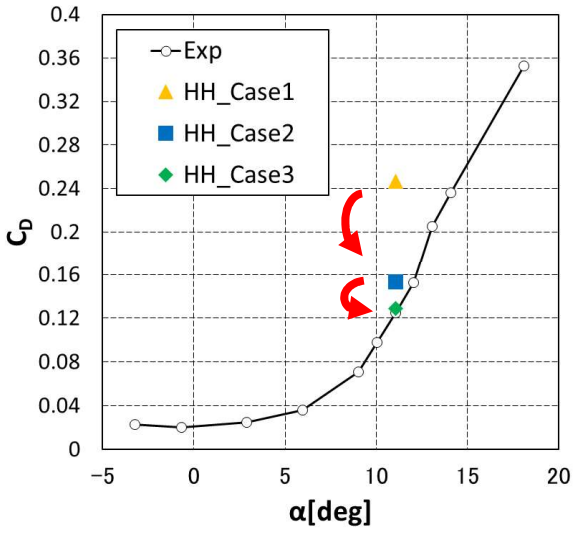

	Δt	Error [%]
HH_Case1	0.05	97.76
HH_Case2	0.025	22.81
HH_Case3	**0.0125**	**3.391**

➢ Δt=0.0125 yielded the smallest error from Exp. data

7

Conditions

➢ Task 2：Unsteady simulations

Using “HexaGrid” Grid (provided by JAXA)

Averaged duration

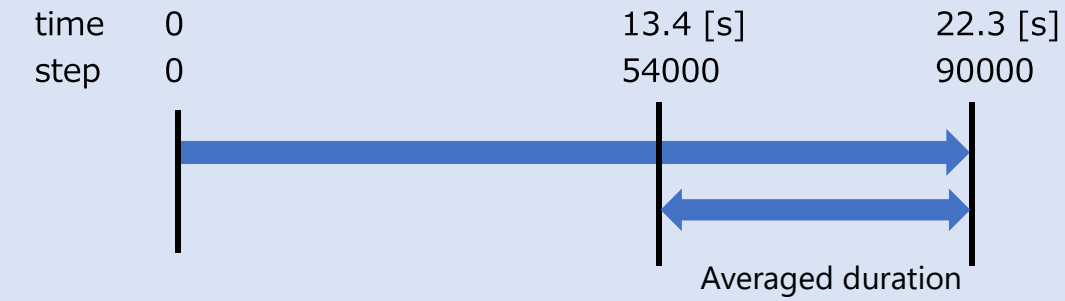

8

Methods

➢ Task 2：Unsteady simulations

Using “HexaGrid” Grid (provided by JAXA)

Methods		
Solver	:	FaSTAR
Numerical Flux	:	**SLAU2 or HR-SLAU2**
Turbulence Model	:	**HR-DDES or SA-DDES**
Time Integration	:	LU-SGS
Slope	:	Green-Gauss
Slope Limiter	:	Hishida(vL)

9

Result

Time History of Aerodynamic Coefficients (HH_AoA1105)

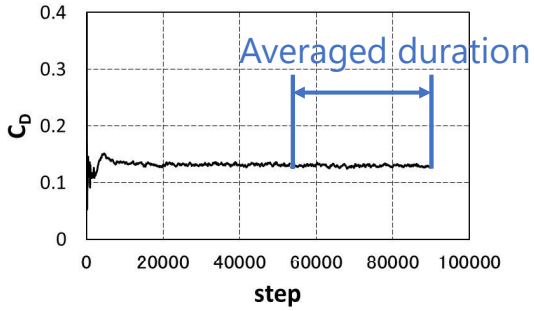

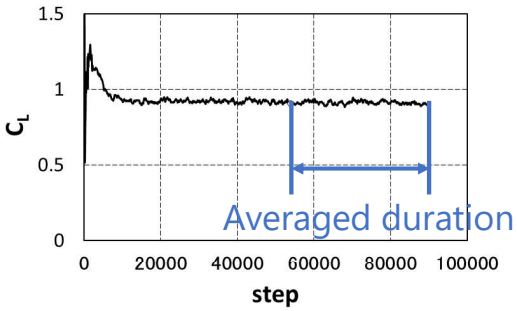

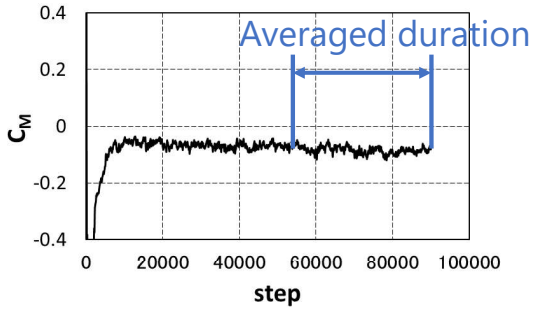

- The aerodynamic coefficients fully converge in the averaged duration

10

Result

Case		
HH	:	HR-SLAU2 & HR-DDES
HS	:	HR-SLAU2 & SA-DDES
SS	:	SLAU2 & SA-DDES

Aerodynamic Coefficients

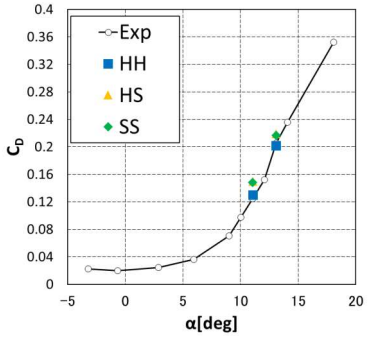

	AoA11.05		AoA13.08	
	C_D Ave.	C_D Error [%]	C_D Ave.	C_D Error [%]
HH	**0.1299**	4.139	**0.2021**	1.544
HS	0.1499	20.18	0.2187	6.527
SS	0.1484	18.98	0.2168	5.626
Exp.	0.1247		0.2053	

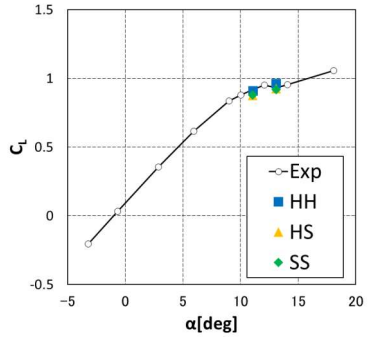

	AoA11.05		AoA13.08	
	C_L Ave.	C_L Error [%]	C_L Ave.	C_L Error [%]
HH	**0.9122**	0.5491	0.9623	3.420
HS	0.8752	4.578	**0.9238**	0.7196
SS	0.8781	4.261	0.9182	1.326
Exp.	0.9172		0.9305	

※The case closest to the Exp. is shown in **red**.

11

Result

Case		
HH	:	HR-SLAU2＆HR-DDES
HS	:	HR-SLAU2＆SA-DDES
SS	:	SLAU2＆SA-DDES

Aerodynamic Coefficients

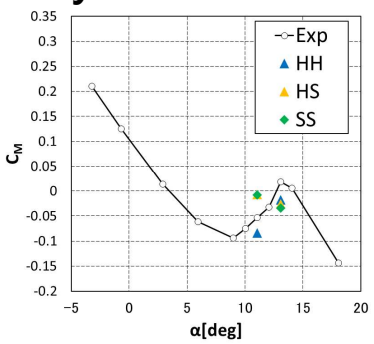

	AoA11.05		AoA13.08	
	C_M Ave.	C_M Error [%]	C_M Ave.	C_M Error [%]
HH	**-8.435×10^{-2}**	57.08	**-1.798×10^{-2}**	196.7
HS	-7.435×10^{-3}	86.15	-2.572×10^{-2}	238.3
SS	-8.294×10^{-3}	84.55	-3.448×10^{-2}	285.3
Exp.	-5.37×10^{-2}		1.86×10^{-2}	

※The case closest to the Exp. is shown in **red**.

- HH showed the closest value to the Exp. for almost all the aerodynamic coefficients compared.
- C_M showed relatively large errors from Exp. regardless of the selected methods.
- Nevertheless, only HH can capture the trend of increase of C_M with increasing angle of attack.

Result

Case		
HH	:	HR-SLAU2＆HR-DDES
HS	:	HR-SLAU2＆SA-DDES
SS	:	SLAU2＆SA-DDES

Streamlines

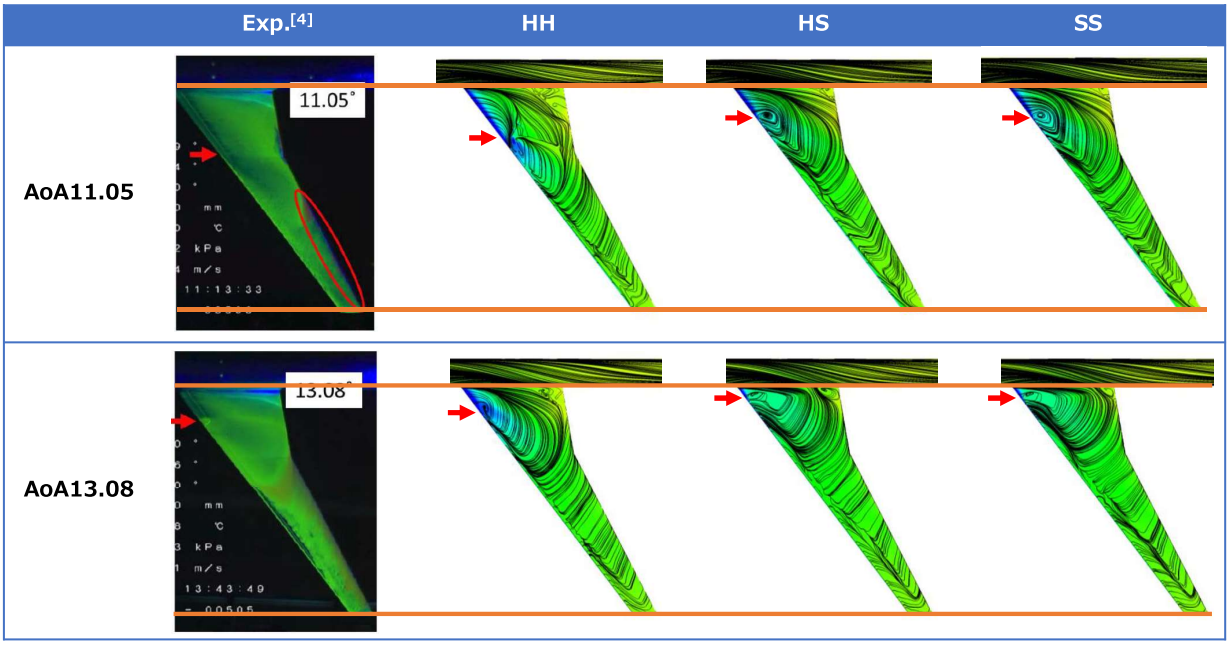

- Flow separation point predicted by HH is the closest to the Exp.

[4] Hashimoto Atsushi, Kanamori Masashi, Kirihara Ryohei, Matsuzaki Tomoaki, Nakamoto Keita, Hayashi Kenji : Steady and Unsteady computation on NASA-CRM with FaSTAR at low speeds and high angles of attack, Fluid Dynamics Conference / Aerospace Numerical Simulation Symposium 2020 Online, Sixth Aerodynamics Prediction Challenge (APC-6), 2020.

Result

Case		
HH	:	HR-SLAU2 & HR-DDES
HS	:	HR-SLAU2 & SA-DDES
SS	:	SLAU2 & SA-DDES

Q Criterion

HH_AoA11.05_Q criterion(Instant)

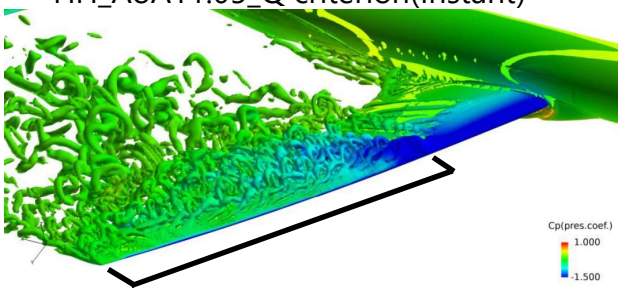

HS_AoA11.05_ Q criterion(Instant)

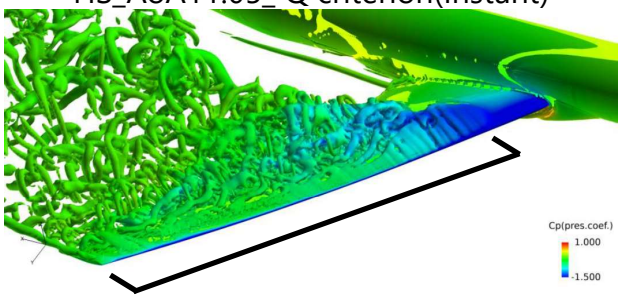

SS_AoA11.05_Q criterion(Instant)

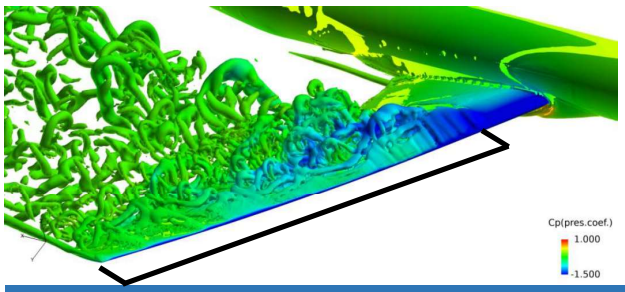

- The separation region simulated by HH is obviously different from HS and SS.

Result

Case		
HH	:	HR-SLAU2 & HR-DDES
HS	:	HR-SLAU2 & SA-DDES
SS	:	SLAU2 & SA-DDES

Wake Interference with Tail

HH_AoA11.05_Q criterion(Averaged)

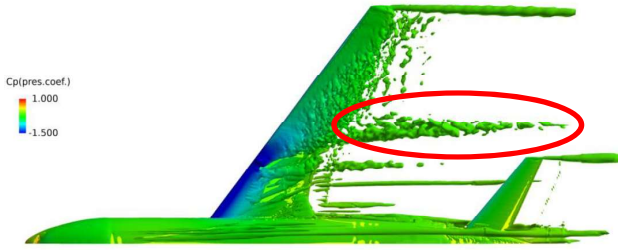

HS_AoA11.05_Q criterion(Averaged)

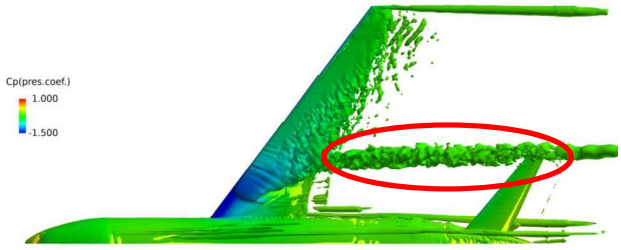

SS_AoA11.05_Q criterion(Averaged)

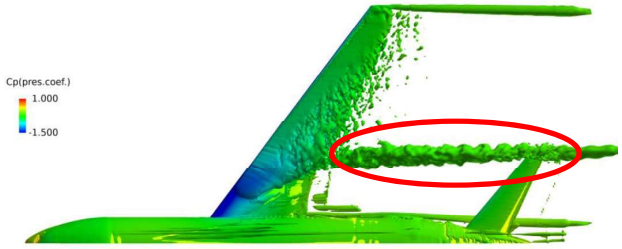

- Main wing wake is generated at the boundary between the separation and attached regions.
- In HH, the main wing wake does not interfere with the tail wing.

Result

Case		
HH	:	HR-SLAU2＆HR-DDES
HS	:	HR-SLAU2＆SA-DDES
SS	:	SLAU2＆SA-DDES

Wake Interference with Tail

HH_AoA11.05_Section YB(Averaged)

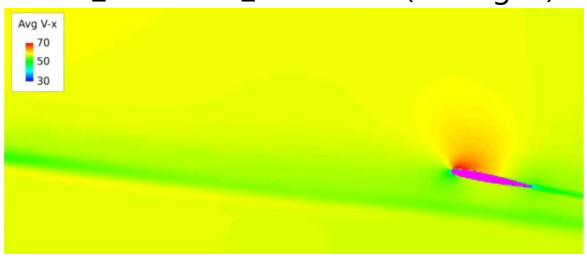

HS_AoA11.05_Section YB (Averaged)

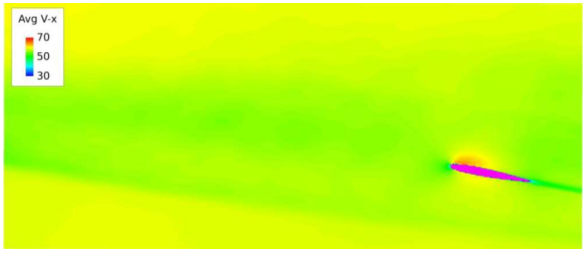

SS_AoA11.05_Section YB (Averaged)

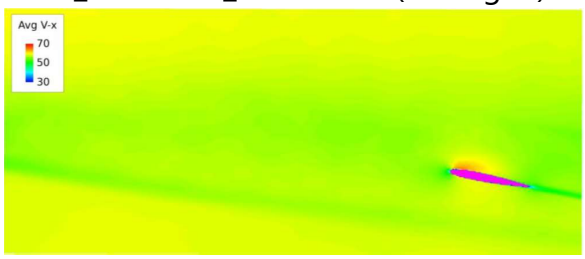

- Main wing wake is generated at the boundary between the separation and attached regions.
- In HH, the main wing wake does not interfere with the tail wing.

Result

Case		
HH	:	HR-SLAU2＆HR-DDES
HS	:	HR-SLAU2＆SA-DDES
SS	:	SLAU2＆SA-DDES

Wake Interference with Tail

HH_Tail_Cp

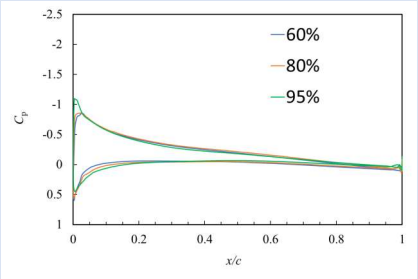

HS_Tail_Cp

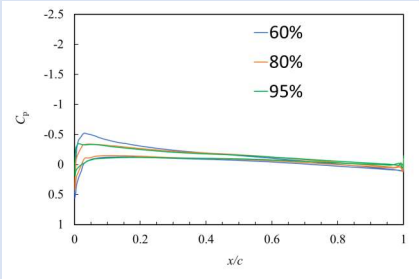

HH_AoA1105

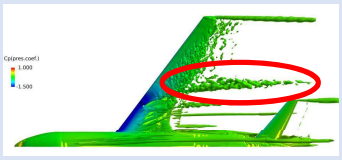

HS_AoA1105

- C_p distributions on upper surface of tail are different among cross-sections due to interference with wake.
  (large difference between 80% and 95%)
  ➡ Lift C_L is smaller in HS than in HH.

Tail C_L	
HH	HS
0.0416	0.0208

Result

Case		
HH	:	HR-SLAU2 & HR-DDES
HS	:	HR-SLAU2 & SA-DDES
SS	:	SLAU2 & SA-DDES

Wake Interference with Tail

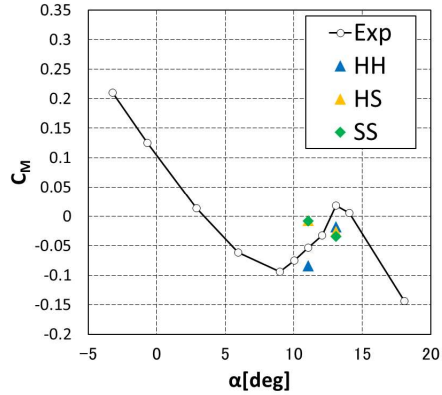

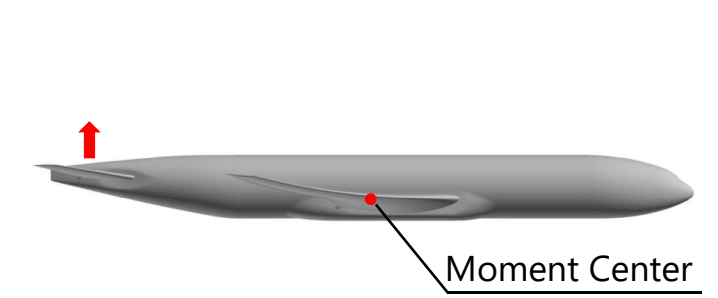

Tail C_L	
HH	HS
0.0416	0.0208

- Head-down moment is caused due to increased lift on the tail.
  - ➡ HH shows the closest value to the Exp.

18

Result

Case		
HH	:	HR-SLAU2 & HR-DDES
HS	:	HR-SLAU2 & SA-DDES
SS	:	SLAU2 & SA-DDES

C_p Distributions

AoA11.05

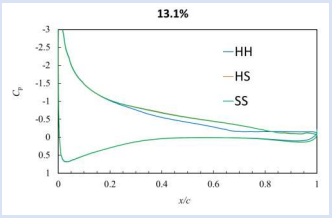

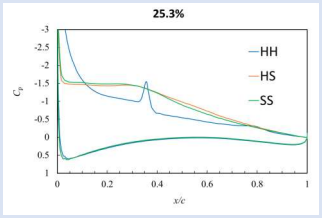

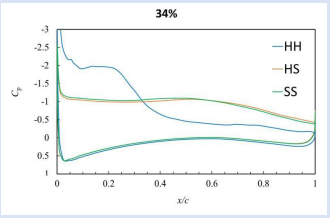

AoA13.08

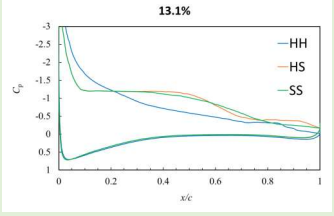

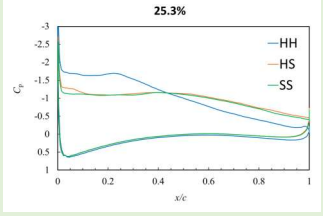

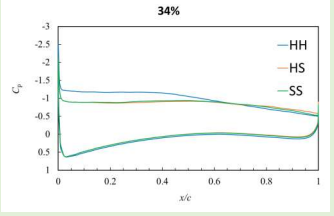

- HS and SS showed relatively similar distributions, different from HH.
- HH showed a spike of C_p around x/c = 0.35 at the 25.3% position.

19

Result

Case		
HH	:	HR-SLAU2＆HR-DDES
HS	:	HR-SLAU2＆SA-DDES
SS	:	SLAU2＆SA-DDES

C_p Distributions

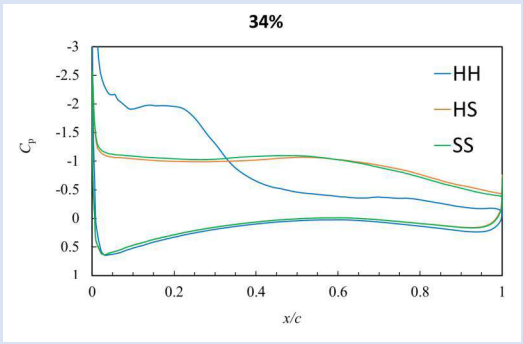

- In HH, the flow over the wing appears to begin to separate.
- In HS, the flow is completely separated.

HH_AoA11.05(Averaged)

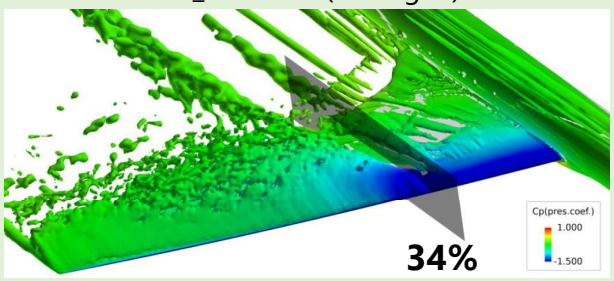

HS_AoA11.05(Averaged)

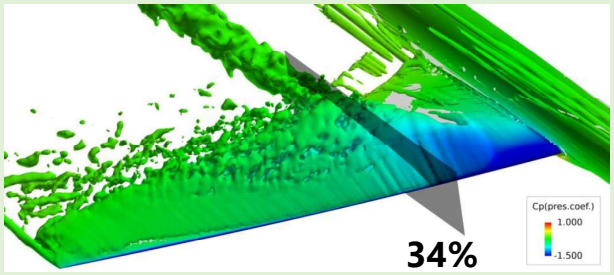

Result

Case		
HH	:	HR-SLAU2＆HR-DDES
HS	:	HR-SLAU2＆SA-DDES
SS	:	SLAU2＆SA-DDES

C_p in HH

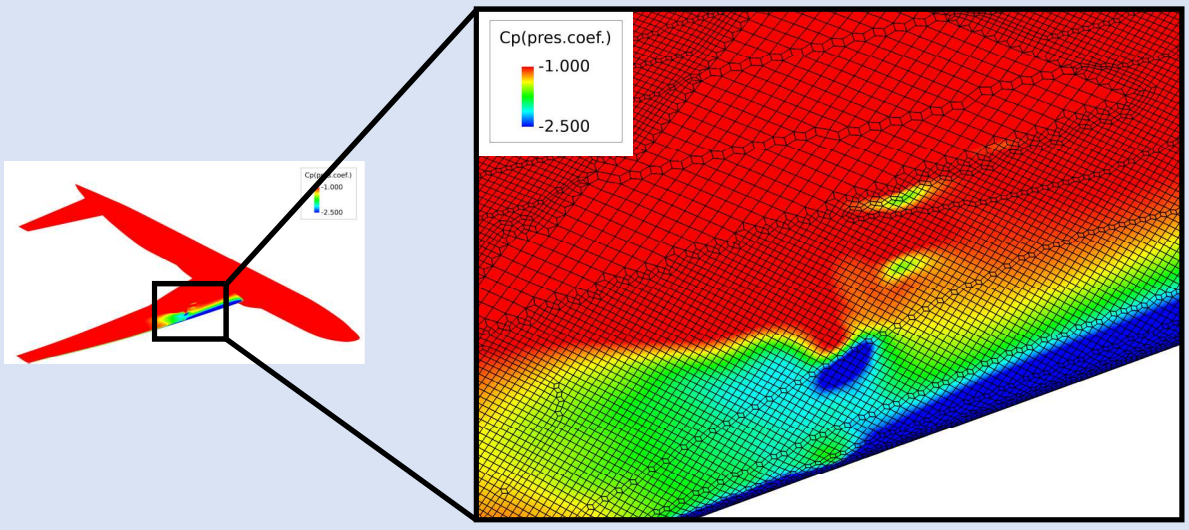

- The spike of C_p occurred at switching location of the cell sizes/geom.
- More severe cell treatment will suppress the spike?

Conclusions

Case		
HH	:	HR-SLAU2 & HR-DDES
HS	:	HR-SLAU2 & SA-DDES
SS	:	SLAU2 & SA-DDES

- HH yielded the closest aerodynamic coefficient values to the experiment.
- HH predicted the flow separation point of the experiment.
- In HH, the main wing wake did not interfere with the tail wing. This led to lift increase of the tail and its negative pitching moment.
- HS and SS showed relatively similar C_p distributions, that were different from HH.
- HH exhibit a spike in the C_p profile, originated from the switching point of cell sizes/geometries.

HH_AoA1105

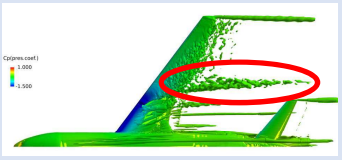

HS_AoA1105

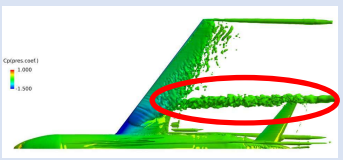

Acknowledgments

The flow solver used here was **FaSTAR** developed at JAXA, as well as the mesh generator **HexaGrid**.

The computations were conducted using JAXA's Supercomputer System(**JSS**) 3.

Mr. Ogawa, Suguru, **Mr. Takimoto, Hiroyuki**, **Mr. Harada, Toshiaki** and **Mr. Takagi, Yuya** at **Yokohama National University** performed a part of numerical cases.

We appreciate their cooperation.

1A21

Flux-Reconstruction法と壁面モデルを用いたNASA-CRMの低速・高迎角流の非定常解析

Unsteady Flow Analysis for NASA-CRM at Low-speed and High Angle-of-attack Conditions Using Flux-reconstruction Method and Wall-Model

SAKAI Ryotaro, ○HAGA Takanori, FUKUSHIMA Yuma,
MURAYAMA Mitsuhiro (JAXA),
AMEMIYA Takashi (QuickMesh), ITO Hiroyuki (Ryoyu Systems)

Objective

- To assess the prediction capability of the state-of-the-art high-order scheme (Split-FR) and the wall-stress model for practical unsteady flows, which is realized by LS-FLOW-HO solver.
- Grid dependency for WMLES
- Overset grid approach to satisfy the grid requirement with minimal increase of grid cells.
- Case 2 : Unsteady flow analysis

  Flow conditions: $M_\infty = 0.168$, $Re = 1.06 \times 10^6$
  Angle of attack: 11.05 [deg]

Solver: LS-FLOW-HO

Discretization	**Split-FR (p0-15)** [1]
Inviscid Flux	Roe
Viscous Flux	BR2 $(\eta_{BR2} = 6.0)$
SGS Model	None (Implicit LES)
Time Integration	3rd-order TVD Runge-Kutta
Shock Capturing	LAD [2] (not used in this study)
Wall Stress Model	**Equilibrium BL eqs.** [3]
Parallelism	MPI & OpenMP/OpenACC
Grid	Hex cell, **Overset**

Airframe noise: 30P30N airfoil (APC-5)

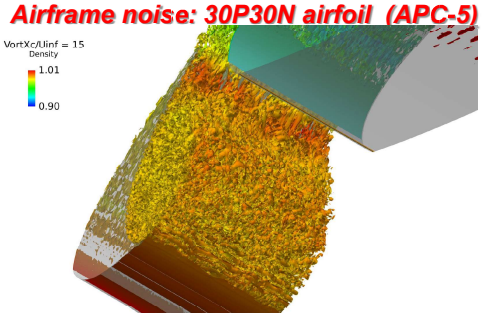

High lift flow WMLES: CRM (APC-6)

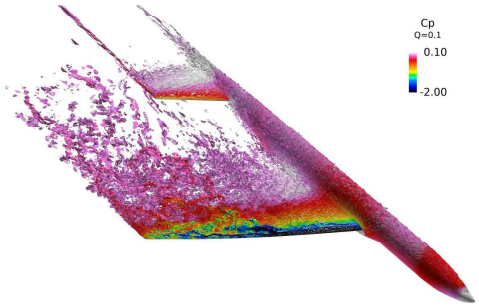

[1] Y. Abe, et al., JCP 353 193-227 (2018)
[2] T. Haga and S. Kawai, JCP 376 534-563 (2019)
[3] T. Haga and S. Kawai, The 31st CFD symposium (2017) (in Japanese)

Transition Treatment

- According to the locations of trip-dot in the wind-tunnel test, **laminar (no-slip)** or **turbulent (wall-modeled)** BCs are prescribed.

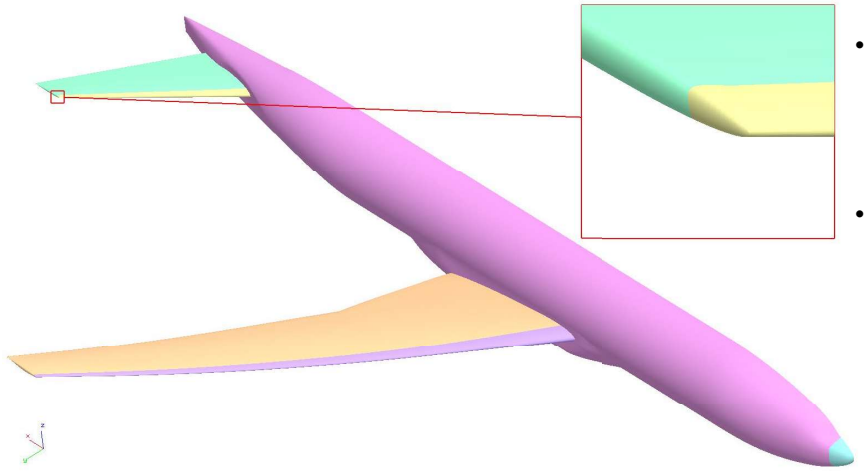

- In Exp.
  - Wings: 10% of each chord length
  - Body: 1.5% of the fuselage length
- In CFD
  - Boundary surface is split by the grid line that is close to the 10% of MAC (wings).

Computational Mesh (Structured)

- Modified the AIAA-DPW4 RNAS mesh (JAXA-Multiblock-Coarse) 2,293,988 cells

P	Points
2	62 million
3	147 million
4	287 million

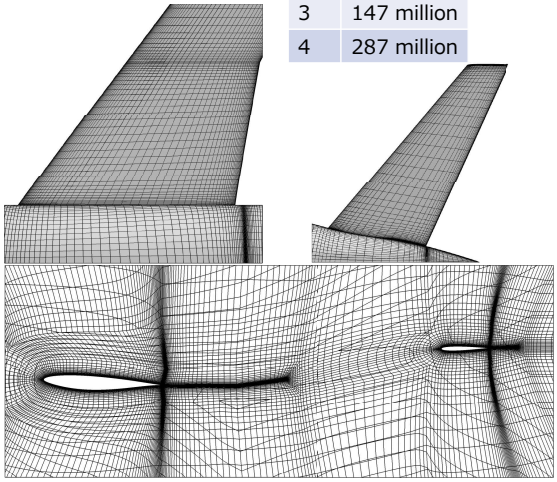

- Enlarged cell-height for WM: $\frac{\Delta h_{wall}}{c}$ =7.25e-5(y^+<10)
- Each hex was subdivided into 8 hex by ***Pointwise*** Glyph script. (Feature lines are kept exactlly)
- In the near wall (24 layers), the 8 hex were combined into a p2-element by ***QuickMesh***.
  - ➢ p2-p1 mixed mesh in Gmsh format

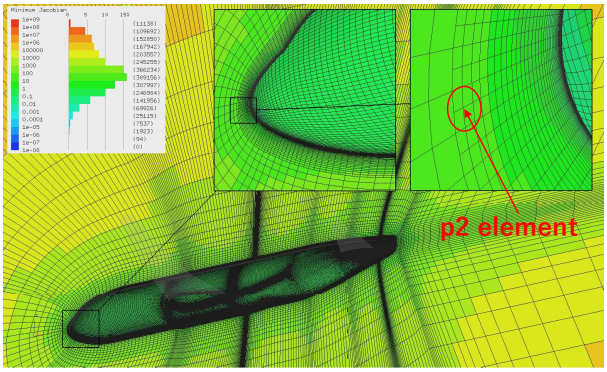

5

Overset Grid Approach

Overset Grids	Cells
01_Layer(BodyFitted)	1,004,157
02_BG(Δ=5inch)	503,401
03_BG(Δ=7inch)	792,120
04_BG(Δ=20inch)	378,906
05_BG(Δ=40～4000inch)	266,070
Total cell	2,944,654

P	Points
2	111 million
3	264 million

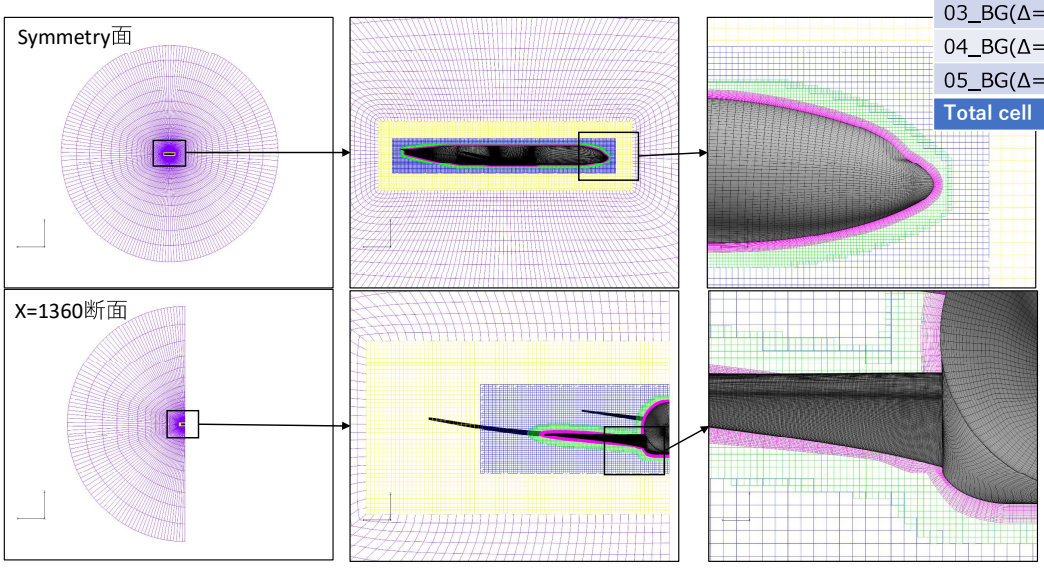

6

Computational Mesh (Overset)

- Controlled grid resolution for the layer grid (body-fitted)

LE: x/c~0.1: h_w =0.2 δ_{max}/c_{MAC}

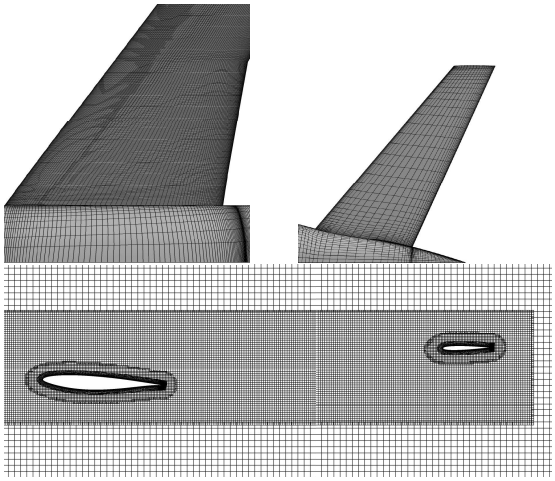

Grid Requirements by Prof. Larsson
https://wmles.umd.edu/wall-stress-models/grid-requirements/

APC7

$$\Delta x \lesssim \begin{cases} 0.05\delta - 0.10\delta & \text{, outer layer} \\ 0.6h_{\mathrm{wm}} - 1.0h_{\mathrm{wm}} & \text{, log-layer} \end{cases}$$

APC6

$$\Delta y \lesssim \begin{cases} 0.01\delta - 0.04\delta & \text{, outer layer} \\ 0.2h_{\mathrm{wm}} - 0.3h_{\mathrm{wm}} & \text{, log-layer} \end{cases}$$

$$\Delta z \lesssim \begin{cases} 0.04\delta - 0.08\delta & \text{, outer layer} \\ 0.4h_{\mathrm{wm}} - 0.8h_{\mathrm{wm}} & \text{, log-layer} \end{cases}$$

FR-p3 was validated for parallel channel flow
$\Delta x_e/\delta \approx 0.08, \Delta y_{\min,e}/\delta \approx 0.02, \Delta z_e/\delta \approx 0.05$

7

Cases and Costs

JAXA 4.32% scale model: C_{ref}=0.30262 [m], Flow through time: $C_{\mathrm{ref}}/U_\infty$=0.005104 [s]

Case	Grid	$h_{\mathrm{smp}}/C_{\mathrm{ref}}$	$\Delta t \cdot a_\infty/C_{\mathrm{ref}}$	Timesteps for $10\ C_{\mathrm{ref}}/U_\infty$	Cores (CPUs) Fujitsu FX1000	Actual elapse time [hours] for (X $C_{\mathrm{ref}}/U_\infty$)	Estimated elapse time [hours] for $10\ C_{\mathrm{ref}}/U_\infty$	Restart
P2 w/ WM	Str-2020	5.0e-4	3.0e-6	1.98e+7	4096 (128)	282 (7.46)	378	Uniform
P3 w/ WM	Str-2021	2.0e-3	↑	↑	12288 (256)	325 (6.05)	537	Uniform
P4 w/ WM	↑	↑	↑	↑	12288 (256)	368 (4.23)	868	From p3
P2 w/ WM	Overset	4.0e-3	1.2e-4	4.95e+5	12000 (250)	27.9 (9.07)	30.8	Uniform
P3 w/ WM	↑	↑	0.8e-4	7.43e+5	12000 (250)	35.0 (3.76)	93.0	Uniform

Str-2021
- Enlarged minimum edge length : slight larger dt than APC6
- Higher h_w : based on the BL thickness from p3-WM result.

Overset grid
- 26.6-40 times larger dt than Str-2021

8

Boundary Layer Thickness

From p3 w/ WM result on Str. gird

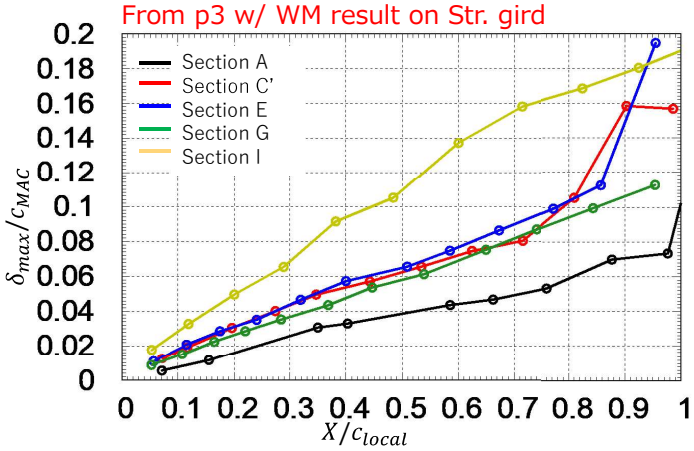

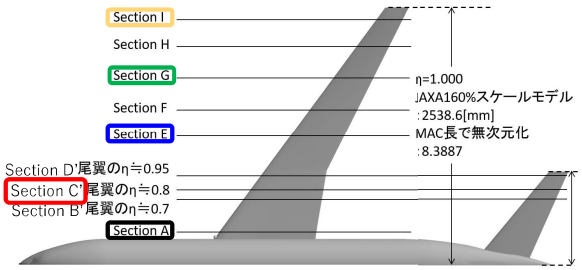

Estimated boundary layer thickness
- LE (x/c~0.1): δ_{max}/c_{MAC} ~0.02
- TE (x/c~1.0): δ_{max}/c_{MAC} ~0.1

WM sampling point（loosened grid requirement）
- LE (x/c~0.1): 0.2 δ_{max}/c_{MAC}
- TE (x/c~1.0): 0.1 δ_{max}/c_{MAC}

Effective resolutions in parallel directions

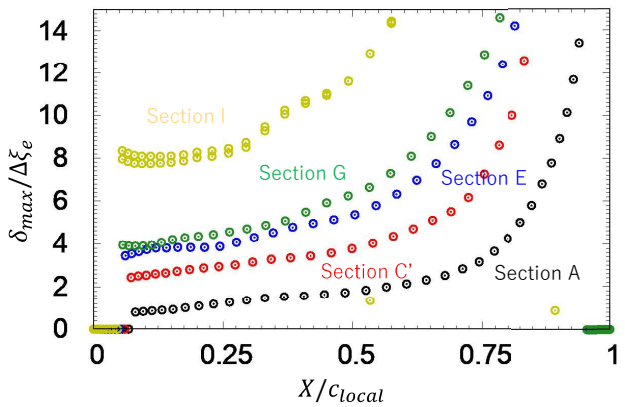

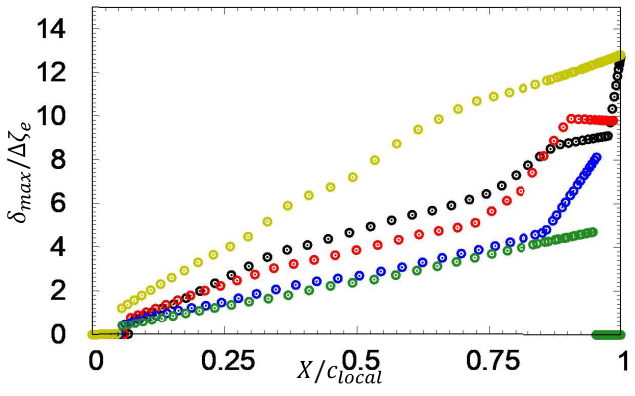

WMLES on very coarse grids

Coarse Grid WMLES(Channel flow)

- $M_b = 0.3$, $Re_\tau \approx 5{,}200$ Lee and Moser (2015)

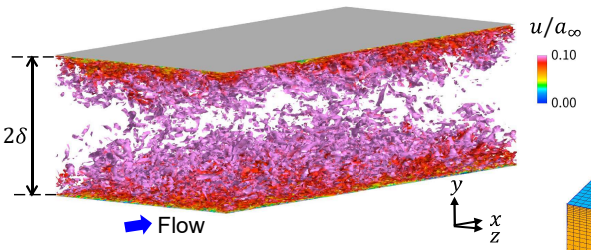

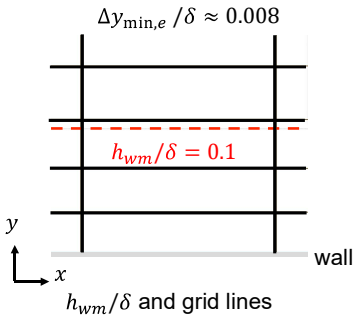

h_{wm}/δ and grid lines

	$\Delta x_e/\delta$	$\Delta y_e/\delta$	$\Delta z_e/\delta$	$\delta/\Delta x_e = \delta/\Delta z_e$
grid1	0.04	0.008-0.029	0.04	25
grid2	0.08	0.008-0.029	0.08	12.5
grid3	0.16	0.008-0.029	0.16	6.25
grid4	0.32	0.008-0.029	0.32	3.75
Larsson et al. (2016)	≲0.05-0.1	≲0.01-0.04	≲0.04-0.08	

Subscript e indicates effective resolution : grid cell size is divided by the number of solution point 4 (p3 scheme).

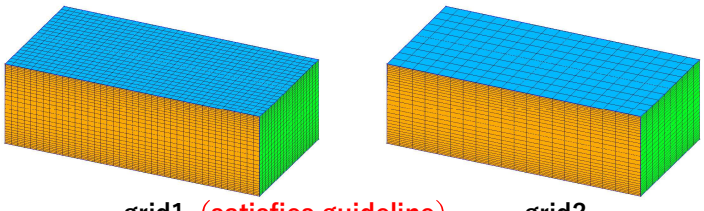

grid1（satisfies guideline） grid2

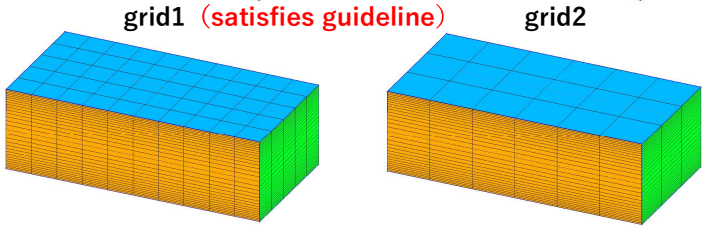

grid3 grid4（~APC6 grid）

Coarse Grid WMLES(Channel flow)

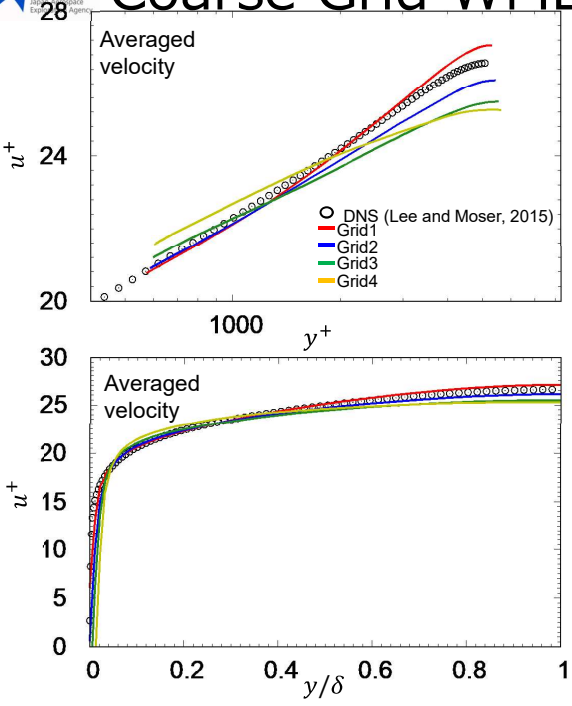

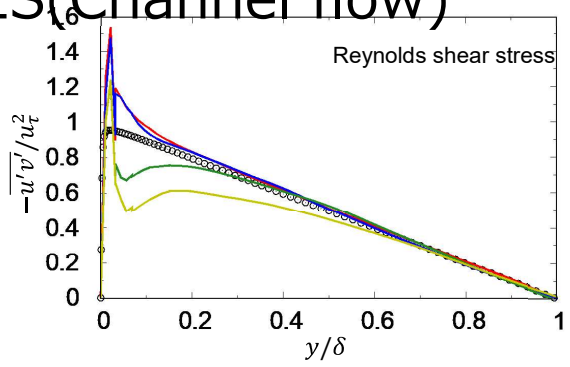

Grid information for channel flow

	$\Delta x_e/\delta$	$\Delta y_e/\delta$	$\Delta z_e/\delta$	$\delta/\Delta x_e = \delta/\Delta z_e$	C_f (DNS: 3.44 × 10^{-3})
grid1	0.04	0.008-0.029	0.04	25	3.39×10^{-3}
grid2	0.08	0.008-0.029	0.08	12.5	3.55×10^{-3}
grid3	0.16	0.008-0.029	0.16	6.25	3.65×10^{-3}
grid4	0.32	0.008-0.029	0.32	3.125	3.70×10^{-3}
Larsson et al. (2016)	≲0.05-0.1	≲0.01-0.04	≲0.04-0.08		

Subscript e indicates effective resolution : grid cell size is divided by the number of solution point 4 (p3 scheme).

Coarse Grid WMLES(periodic hill)

- $u_b = 0.2$, $Re_h \approx 37{,}000$ Gloerfelt and Cinnella (2019)
- $h_{wm}/h = 0.1$

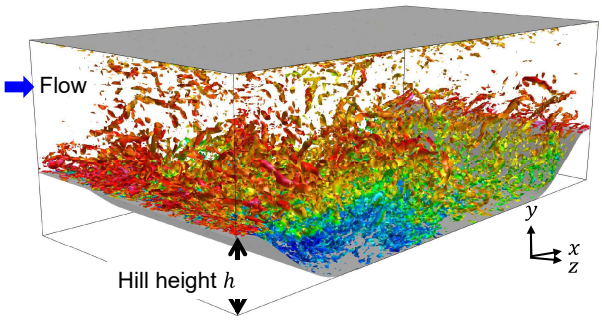

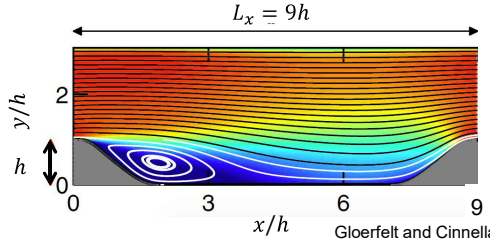

Gloerfelt and Cinnella (2019)

Grid1（Bottom surface）

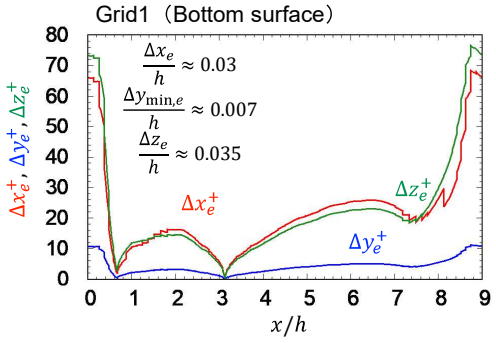

	$\Delta x_e/h$	$\Delta y_{\min,e}/h$	$\Delta z_e/h$	$h/\Delta x_e$	$h/\Delta z_e$
grid1	0.03	0.007	0.035	33.3	28.5
grid2	0.06	0.007	0.07	16.6	14.3
grid3	0.12	0.007	0.14	8.3	7.1
grid4	0.24	0.007	0.28	4.15	3.55
Larsson et al. (2016)	≲0.05-0.1	≲0.01-0.04	≲0.04-0.08		

Subscript e indicates effective resolution : grid cell size is divided by the number of solution point 4 (p3 scheme).

Coarse Grid WMLES(periodic hill)

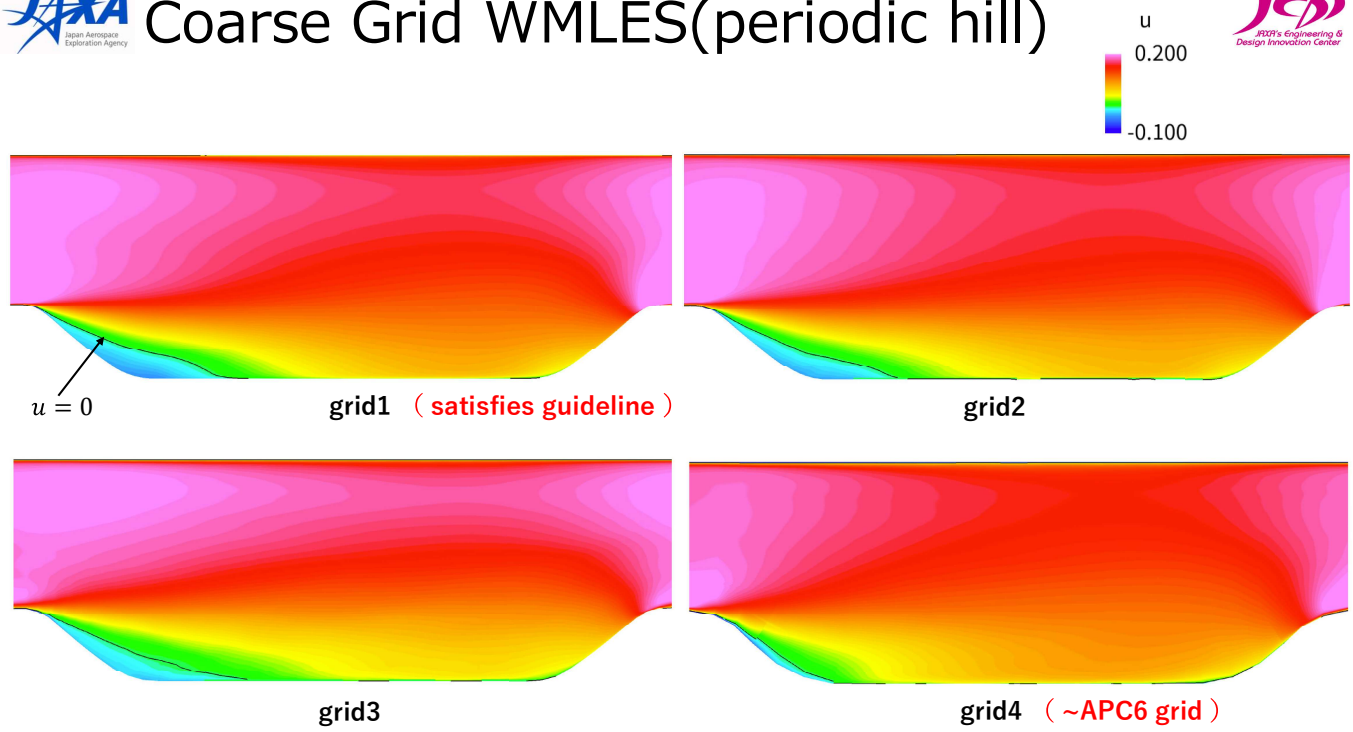

Coarse Grid WMLES(periodic hill)

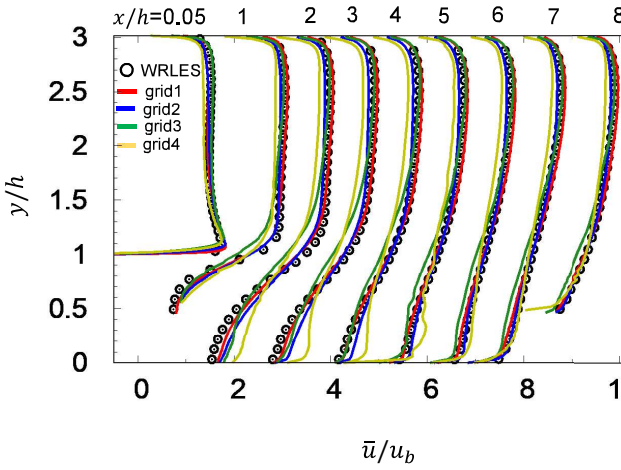

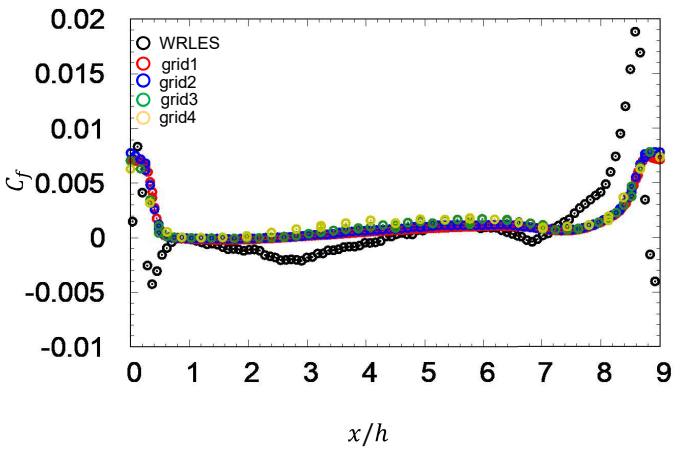

- Velocity profile: grid1 agrees well with WRLES

- Skin friction: discrepancy between WMLES and WRLES. Need improvement of the wall-model for separated flows.

APC7 Results

Force Coefficients (Averaged)

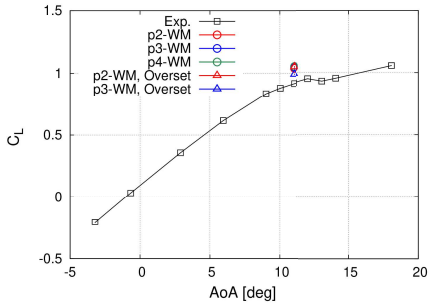

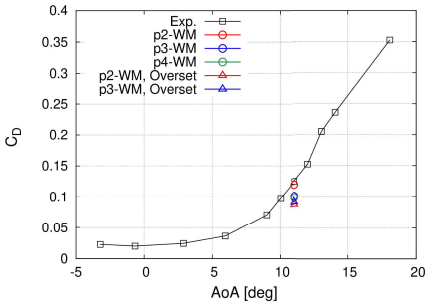

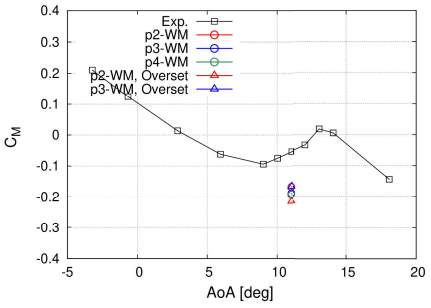

Oil Flow (Comparison with Exp.)

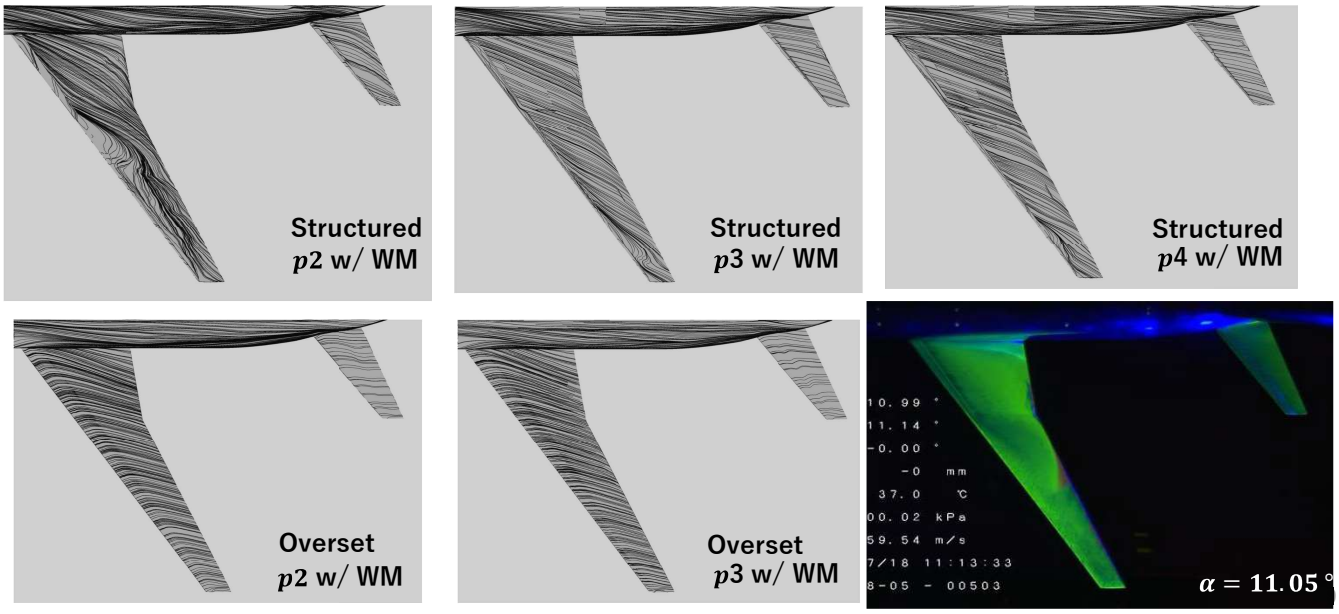

U-rms (Section HA)

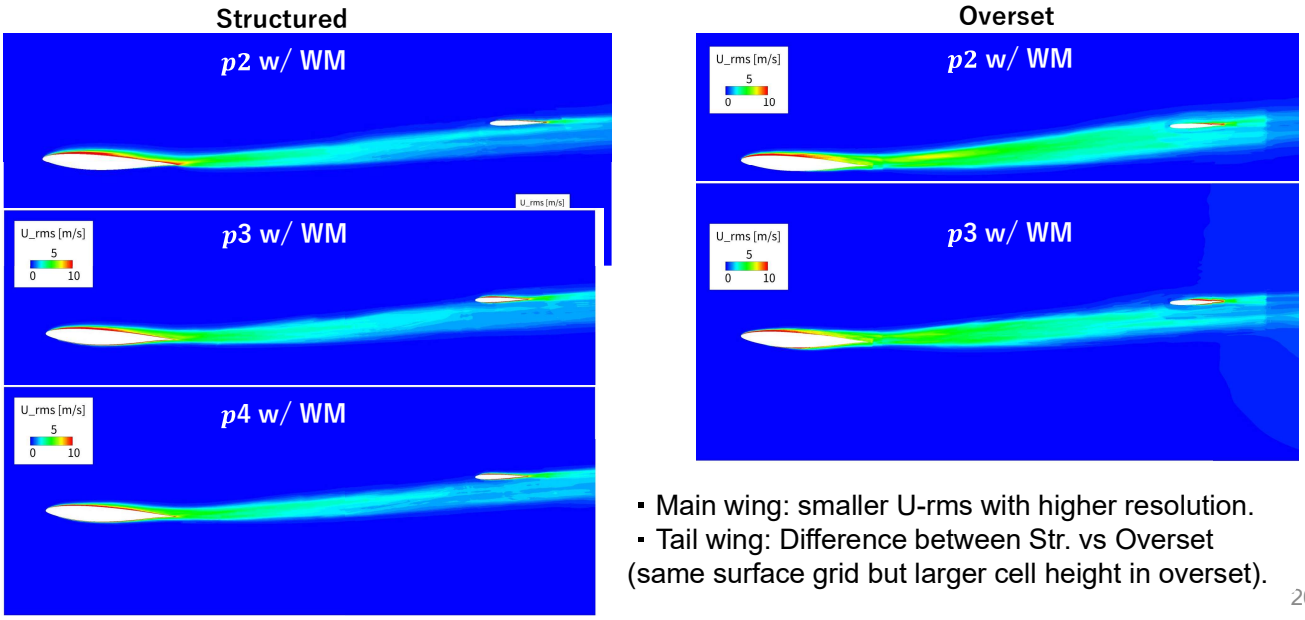

- Main wing: smaller U-rms with higher resolution.
- Tail wing: Difference between Str. vs Overset (same surface grid but larger cell height in overset).

U-rms near main wing (Section HA)

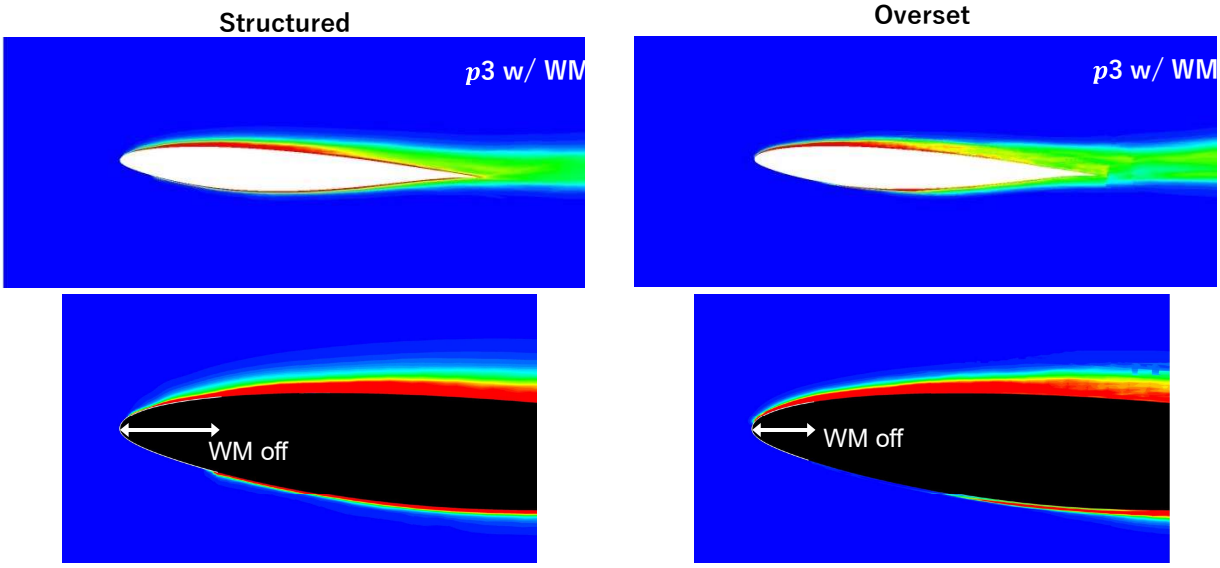

- Width of laminar B.C. depends on the grid surface. (split by a grid line close to 10% of MAC)
- Higher U-rms near L.E. on overset grid（due to insufficient grid resolution?）

21

Summary

- Robust WMLES computations for CRM were performed by LS-FLOW-HO（upto p4 (5th-order), no parameter tuning of the scheme).
- Grid dependency for WMLES was studied especially for very coarse grids. The following trend was observed:
  - Overestimate of Cf for channel flow case
  - Small separation for periodic hill case
- Overset grid is very effective to reduce total grid cells while keeping the grid requirement
- Reasonable CL, CD prediction comparing to RANS results in APC6. Slight improvement by Overset-p3 case.
- Difficult to predict oil flows in the present cases. (No separation by Overset results) Further grid dependency study is needed (strictly satisfy the guideline, near LE?)
  - h/p adaptive solver will be more effective?

22

Acknowledgments

- JAXA Supercomputing System (JSS3) was used for the computations.
- Part of this work was supported by JSPS KAKENHI Grant Number 21K14083.

The 53th Fluid Dynamics Conference/ The 39th Aerospace Numerical Simulation Symposium
30th June 2021

APC-7の集計結果
Summary of APC-7

橋本 敦 (JAXA) , APC有識者会議
Hashimoto Atsushi(JAXA), APC committee

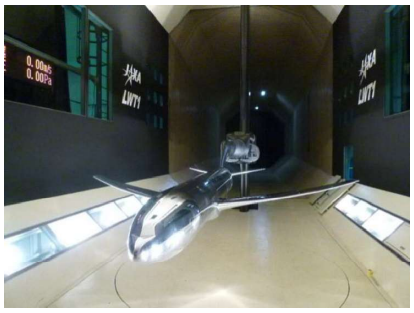

Statistics of submitted data

- Organizations and number of submitted data(total 23 data)
  - National research institutes：JAXA(11)
  - Universities: Univ. of Tokyo(6), YNU(3), Iwate Univ.(1)
  - Aerospace industries: KHI(2)
- Grids
  - JAXA：5
  - Customs：5
- Code
  - Unstructured solver(16)
  - Cartesian solver(7)
- Turbulence models
  - Steady: SA(7), SST(3)
  - Unsteady: SA(8), SST(3), ILES(2)
- Initial conditions
  - Steady: Uniform flow(10)
  - Unsteady: Uniform flow(4), Restart from the steady-state solution(8), Mapping(1)

Participants of case 1

ID	Name	Organization	Code	Grid	Turbulence Model	Initial Condition	Note
A1	橋本敦	JAXA	FaSTAR（Unstructured solver）	BOXFUN	SST-2003	Uniform flow	Hanging node
A2				UPACS	SA-noft2-R		
A3					SST-2003		
A4				MEGG3D	SA-noft2-R		
A5					SST-2003		
B1	上野 陽亮	川崎重工	Cflow（Unstructured solver）	Custom（Orthogonal octree + Body-Fitted layer grid）	SA-neg	Uniform flow	Local time step
B2							Global time step
C1	原惇	東京大学	UTCart（Cartesian solver）	Custom（Orthogonal grid）	SA-noft2-R (Crot=1)	Uniform flow	Grid #1（Number of cells is 140M）
C2				Custom（Orthogonal grid）			Grid #2（Number of cells is 90M）
D1	菅谷圭祐	東京大学	UTCart（Cartesian solver）	Custom（Orthogonal grid）	SA-noft2-R (Crot=1)	Uniform flow	

3

Participants of case 2

ID	Name	Organization	Code	Grid	Turbulence Model	Initial Condition	Note
A1	橋本敦	JAXA	FaSTAR（Unstructured solver）	BOXFUN	SST-2003 IDDES	Restart from the steady-state solution	Hanging node
A2				UPACS	SA-noft2-R IDDES		
A3					SST-2003 IDDES		
A4				MEGG3D	SA-noft2-R IDDES		
A5					SST-2003 IDDES		
C1	原惇	東京大学	UTCart（Cartesian solver）	Custom（Orthogonal grid）	SA-noft2-R (Crot=1)	RANSの収束解からリスタート	Grid #1（Number of cells is 140M）
C2				Custom（Orthogonal grid）			Grid #2（Number of cells is 90M）
D1	菅谷圭祐	東京大学	UTCart（Cartesian solver）	Custom（Orthogonal grid）	DDES-protected (SA-noft2-R Crot=1)	RANSの収束解からリスタート	
E1	坂井玲太郎	JAXA	LS-FLOW-HO（Unstructured solver）	Custom（Hexa second order element）	ILES	同じ迎角の「4次精度・wall-model無し」の解からマッピング	
F1	髙橋佑太	岩手大学	Cut-Cell Iwate（Cartesian solver）	Custom（Orthogonal grid）	ILES+Wall model	Uniform flow	
G1	安村祐哉	横浜国立大学	FaSTAR（Unstructured solver）	HexaGrid	SA-noft2-R DDES (Cdes = 0.51, Crot = 2.0)	Uniform flow	HR-SLAU2
G2					SA-noft2-R DDES (Cdes = 0.65, Crot = 1.0)		HR-SLAU2
G3					SA-noft2-R DDES (Cdes = 0.65, Crot = 1.0)		SLAU2

4

Surface grid(Wing root)

BO=BOXFUN
UP=UPACS
ME=MEGG3D
He=HexaGrid
Cu=Custom

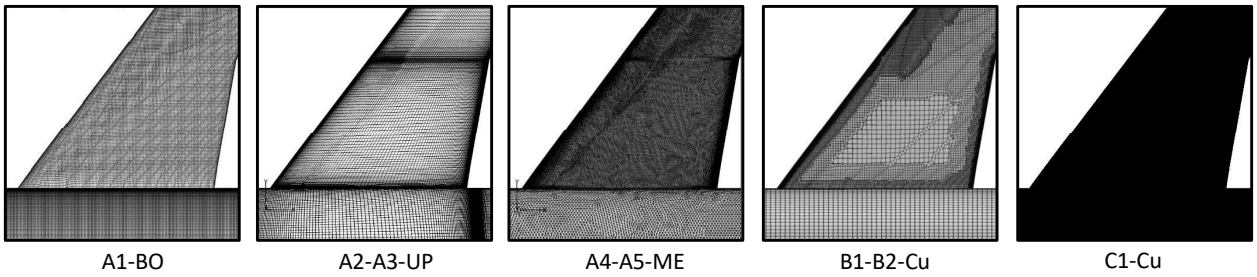

A1-BO | A2-A3-UP | A4-A5-ME | B1-B2-Cu | C1-Cu

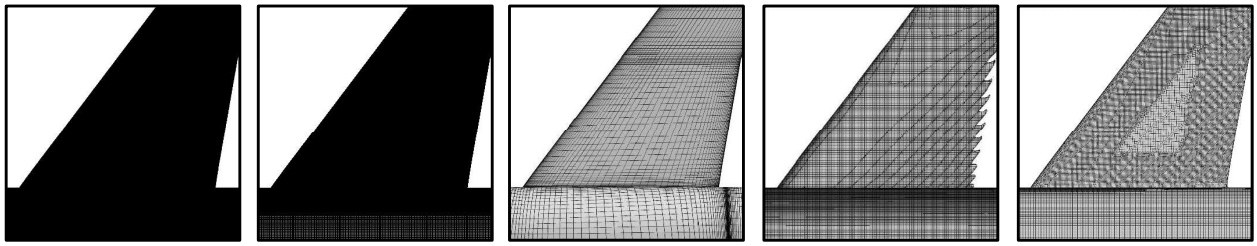

C2-Cu | D1-Cu | E1-Cu | F1-Cu | G1-G2-G3-He

5

Surface grid(Wing root)

BO=BOXFUN
UP=UPACS
ME=MEGG3D
He=HexaGrid
Cu=Custom

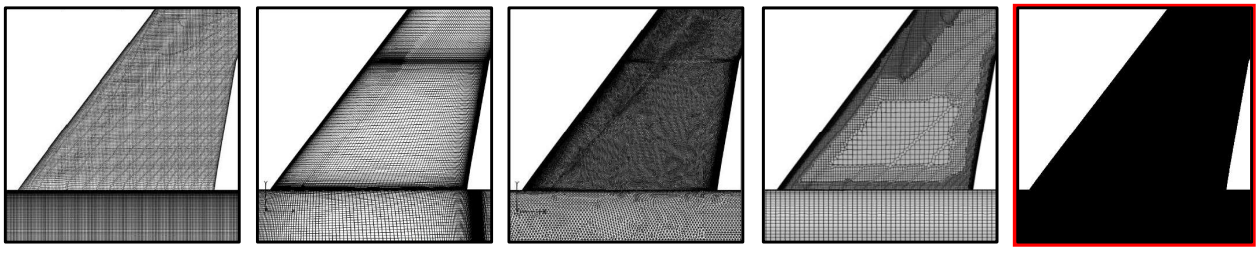

A1-BO | A2-A3-UP | A4-A5-ME | B1-B2-Cu | C1-Cu

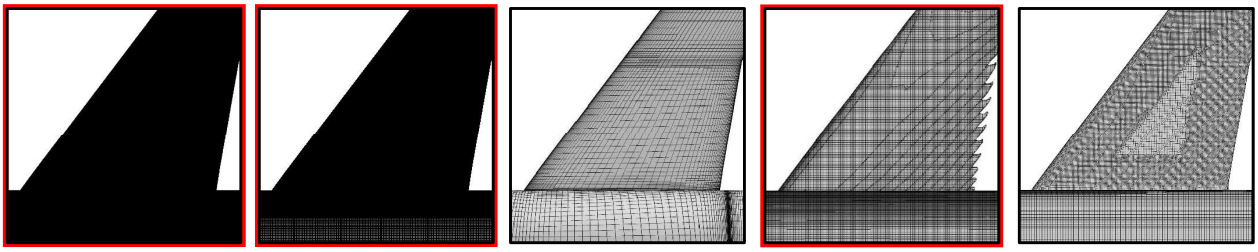

C2-Cu | D1-Cu | E1-Cu | F1-Cu | G1-G2-G3-He

6

Cartesian

Surface grid(Wing root)

Hexahedral
unstructured

BO=BOXFUN
UP=UPACS
ME=MEGG3D

He=HexaGrid
Cu=Custom

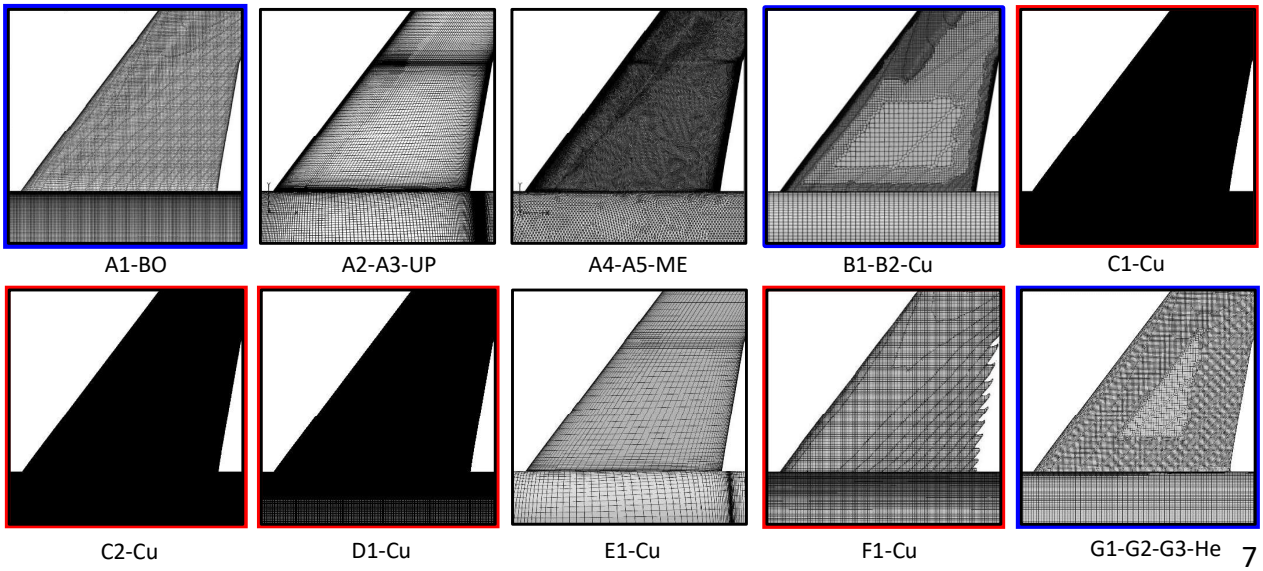

Cartesian

7

Surface grid(Wing root)

Hexahedral
unstructured

Mixed-element unstructured
(Tetra,Prism,Pyramid,Hexa)

BO=BOXFUN
UP=UPACS
ME=MEGG3D

He=HexaGrid
Cu=Custom

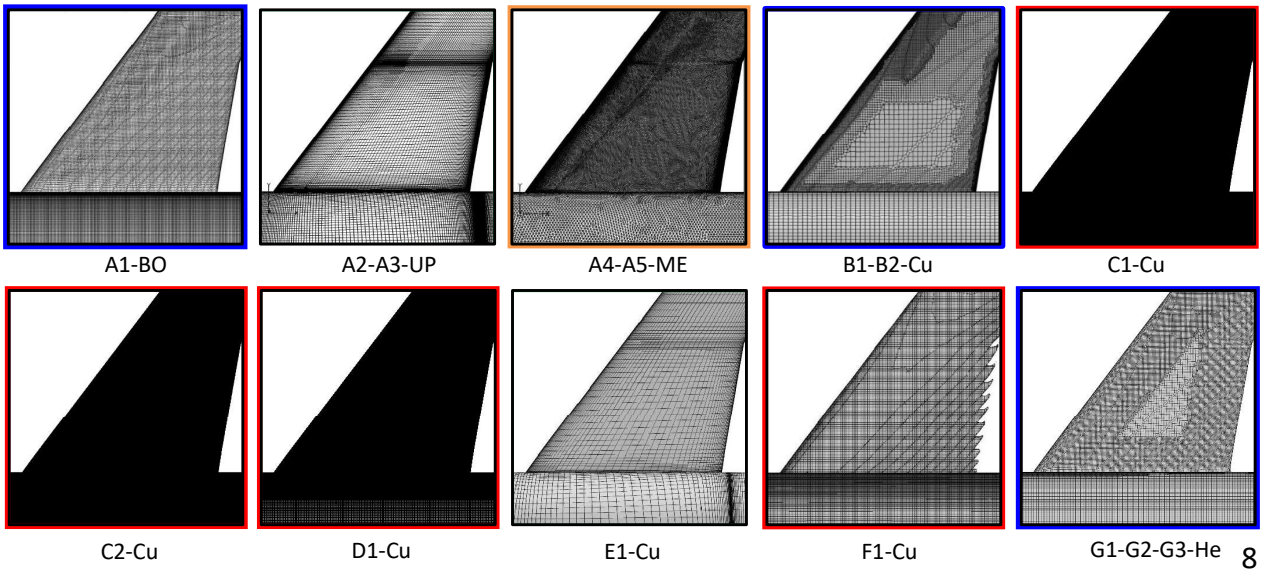

Cartesian

8

Surface grid(Wing root)

Hexahedral unstructured

Mixed-element unstructured (Tetra,Prism,Pyramid,Hexa)

BO=BOXFUN
UP=UPACS
ME=MEGG3D
He=HexaGrid
Cu=Custom

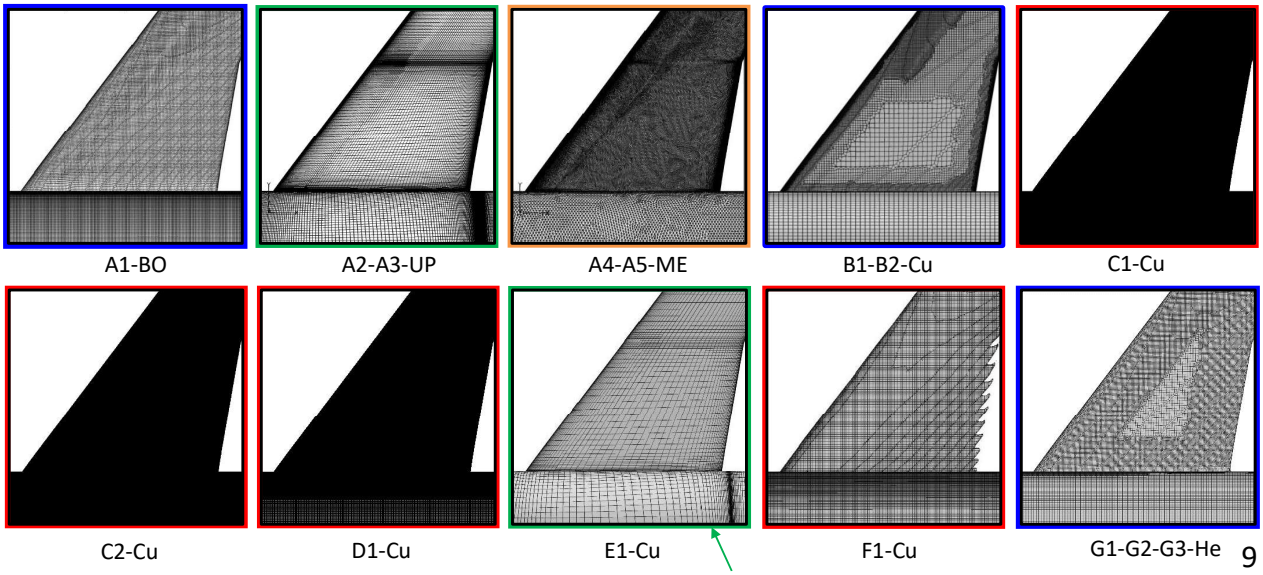

A1-BO | A2-A3-UP | A4-A5-ME | B1-B2-Cu | C1-Cu

C2-Cu | D1-Cu | E1-Cu | F1-Cu | G1-G2-G3-He

Cartesian Structured

second-order element

9

Surface grid(Tail)

BO=BOXFUN
UP=UPACS
ME=MEGG3D
He=HexaGrid
Cu=Custom

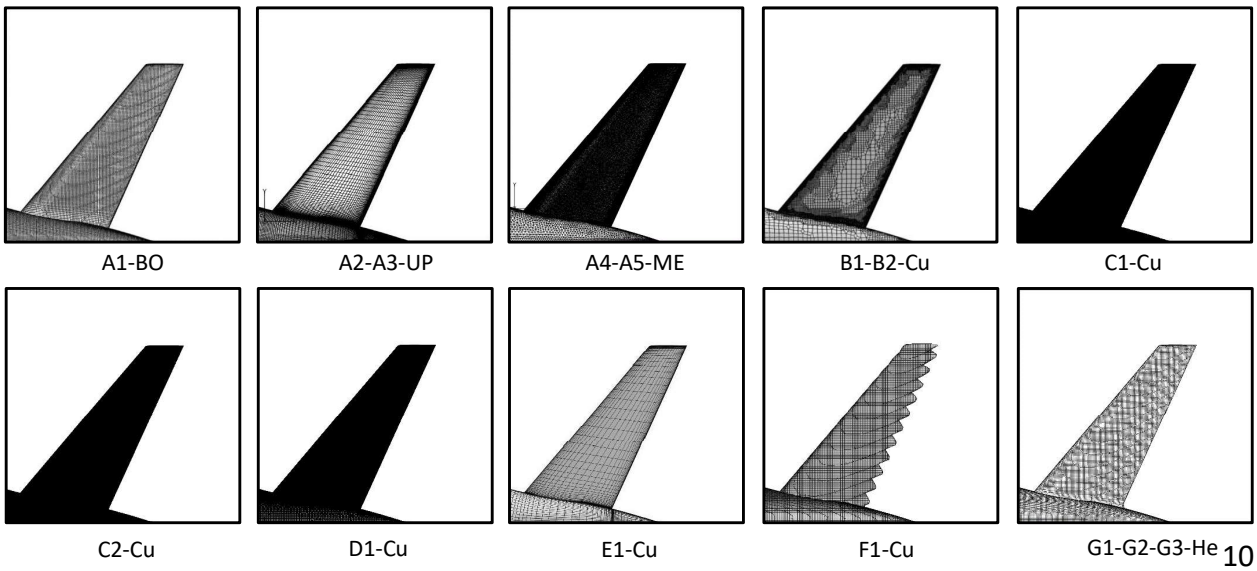

A1-BO | A2-A3-UP | A4-A5-ME | B1-B2-Cu | C1-Cu

C2-Cu | D1-Cu | E1-Cu | F1-Cu | G1-G2-G3-He

10

Cross section grid

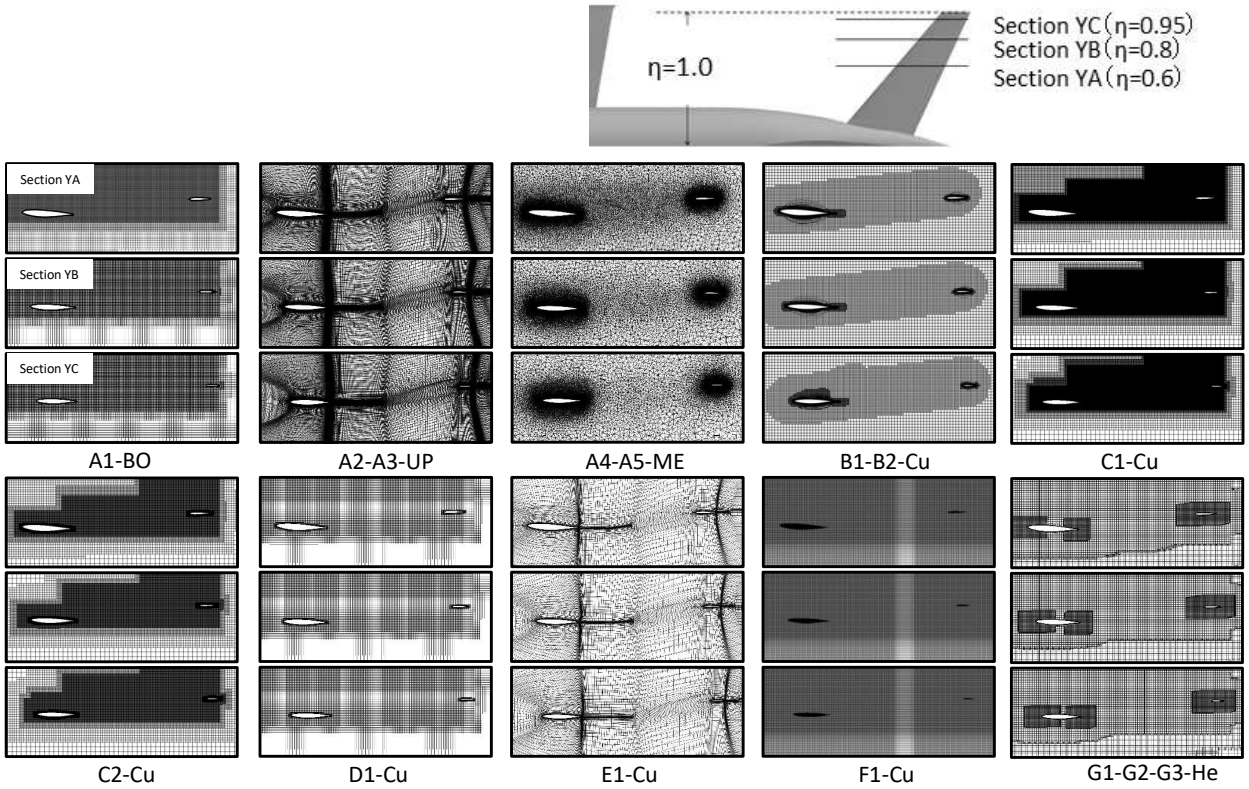

11

Case1 : Steady computation

- Aims
  - Understand the prediction accuracy of aerodynamic performance such as CL, CD, Cm at low speeds and separation characteristics (beginning of separation, separated area).
  - Understand the dependency of turbulence model, grid.

- Conditions
  - M = 0.168, Re_c = 1.06 x 10^6, T_{ref}=310K
  - AoA = -3.22, -0.67, 2.89, 5.95, 9.01, 10.03, 11.05, 12.06, 13.08, 14.08, 18.08deg

12

CL-Alpha, case1

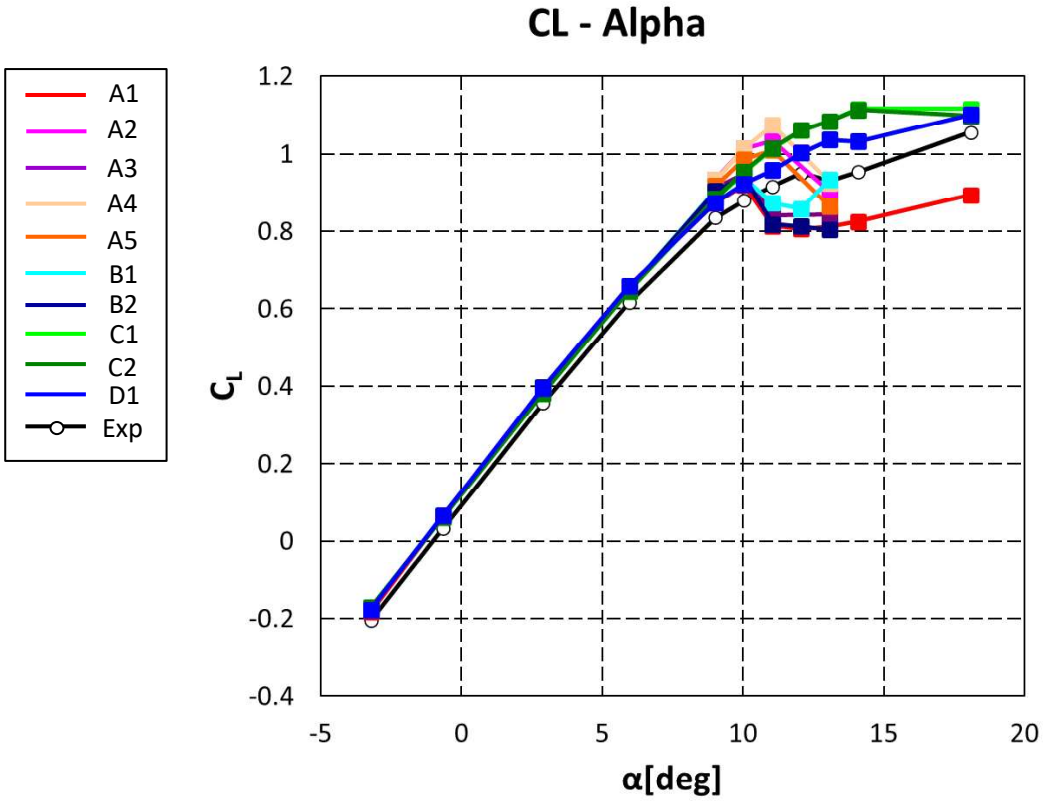

13

CL-Alpha, case1

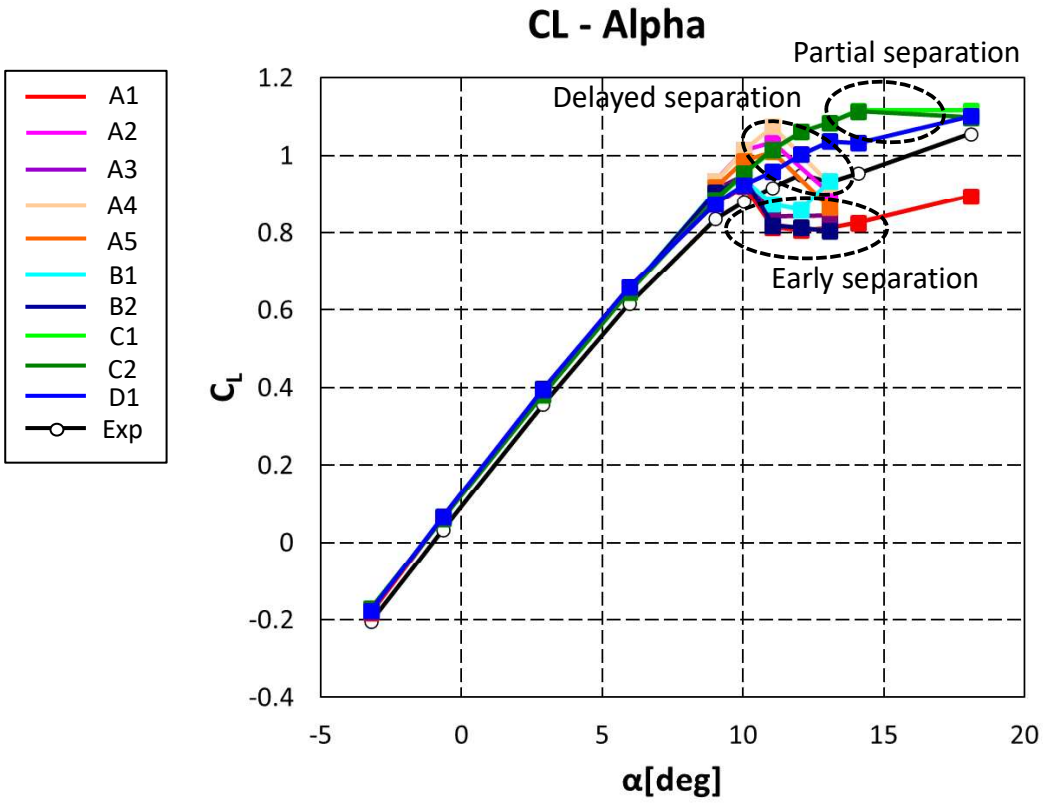

14

CD-Alpha, case1

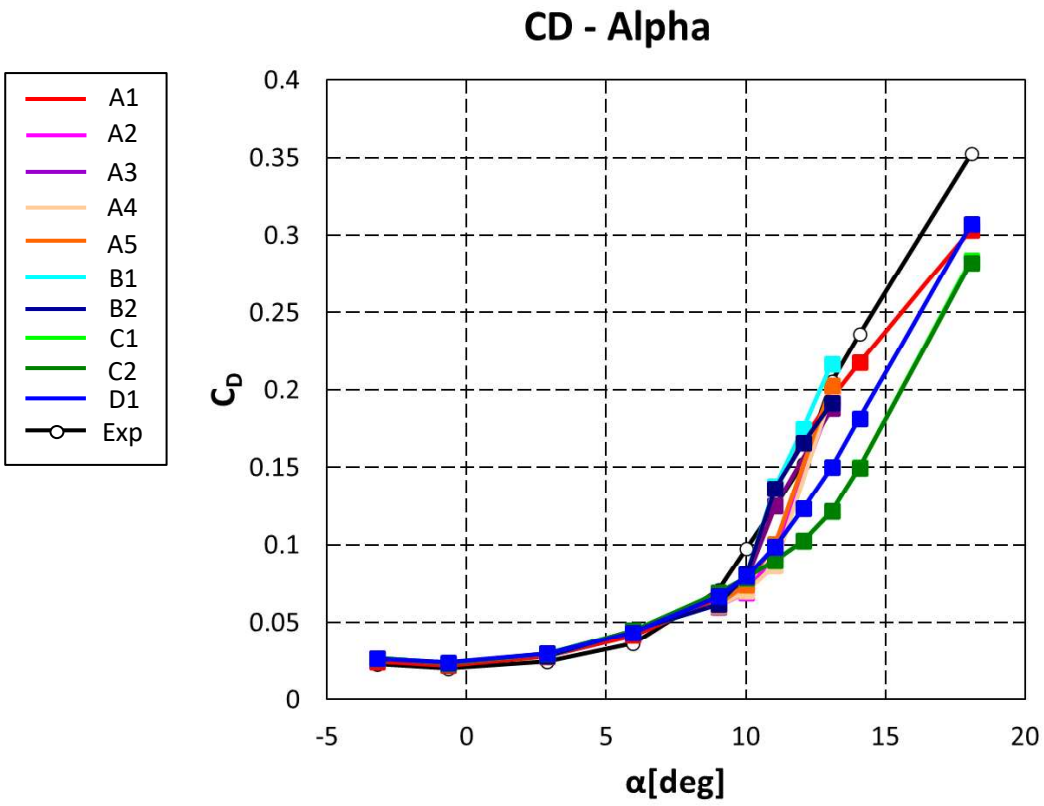

15

Cm-Alpha, case1

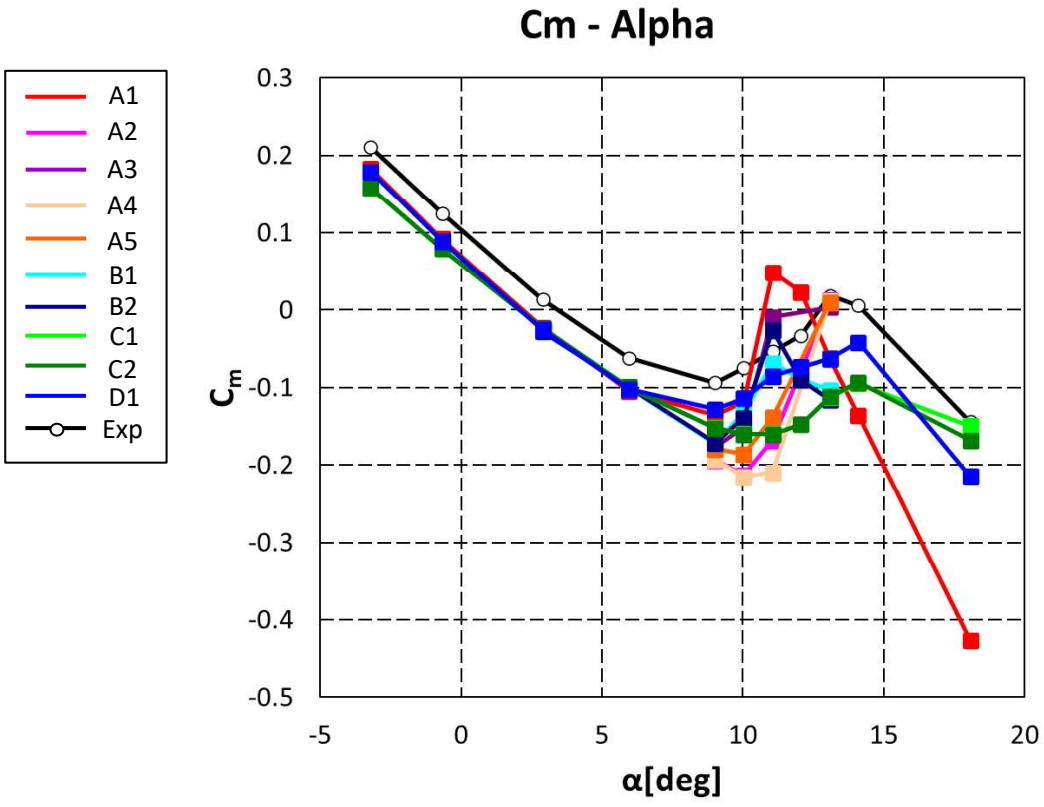

16

Surface streamline(11.05deg)

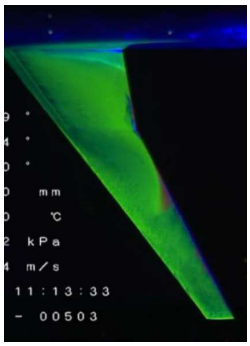

The flow tends to separate for hexahedral unstructured grid and SST model

T. Uchiyama, et al., AIAA 2019-2190

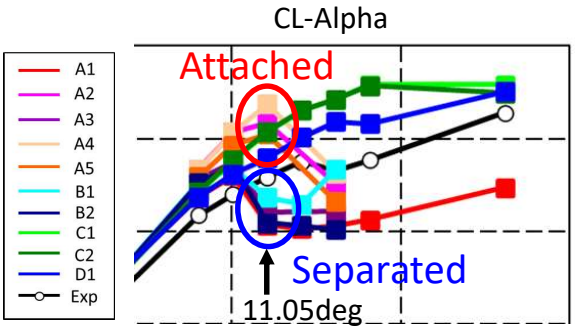

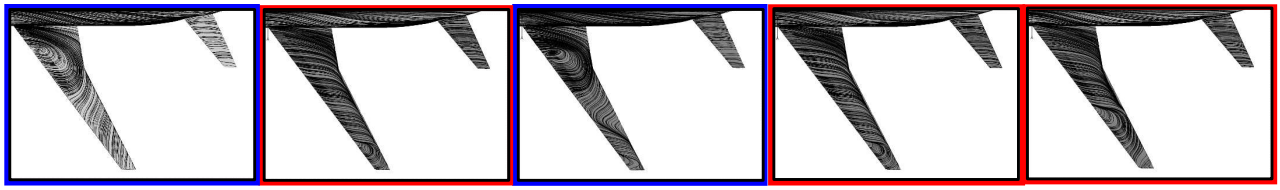

A1-BO-SST A2-UP-SA A3-UP-SST A4-ME-SA A5-ME-SST

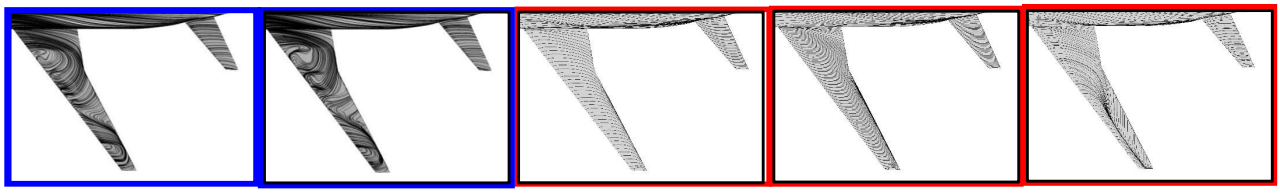

B1-Cu-SA B2-Cu-SA C1-Cu-SA C2-Cu-SA D1-Cu-SA

17

Surface streamline(13.08deg)

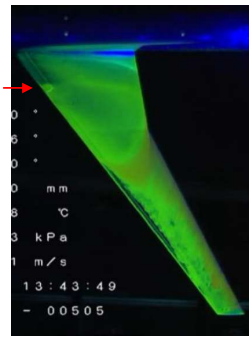

The flow tends to attach for Cartesian grid.
A4 and B1 are close to the experiment.

T. Uchiyama, et al., AIAA 2019-2190

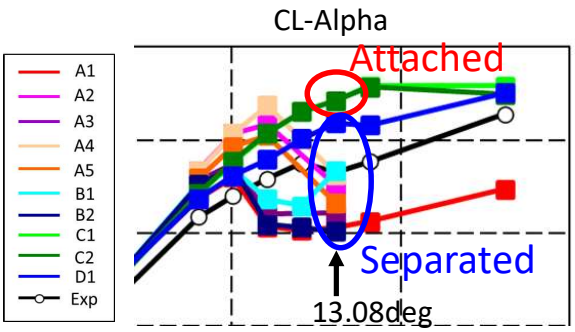

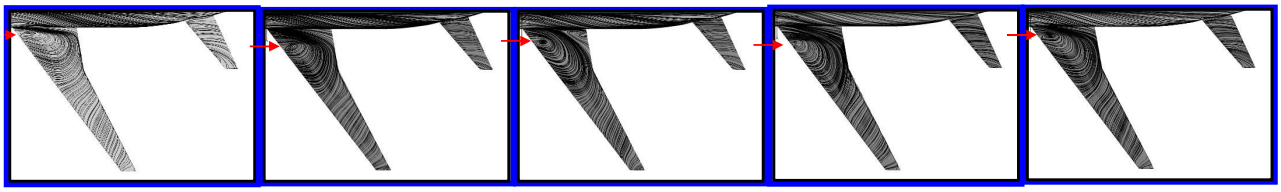

A1-BO-SST A2-UP-SA A3-UP-SST A4-ME-SA A5-ME-SST

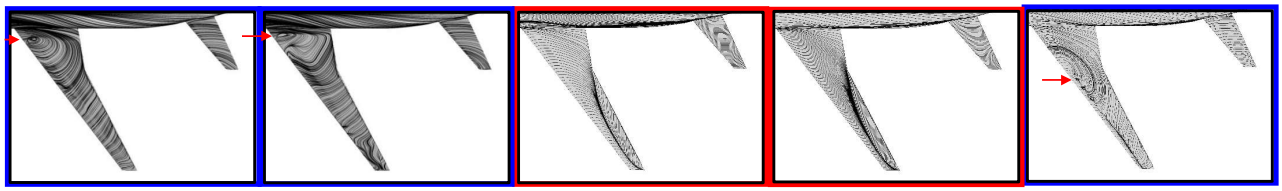

B1-Cu-SA B2-Cu-SA C1-Cu-SA C2-Cu-SA D1-Cu-SA

18

Wake interference with tail (11.05deg, Section YB)

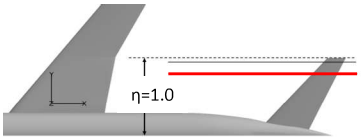

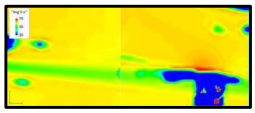

PIV（AoA=11deg）

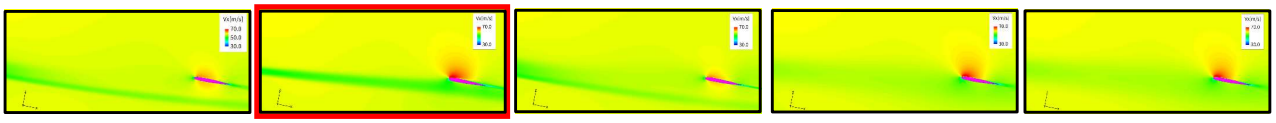

A1-BO-SST　A-UP-SA　A3-UP-SST　A4-ME-SA　A5-ME-SST

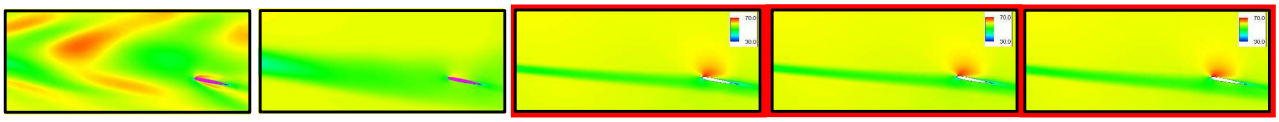

B1-Cu-SA　B2-Cu-SA　C1-Cu-SA　C2-Cu-SA　D1-Cu-SA

The attached cases are close to the experiment

19

Wake interference with tail (11.05deg, Section YC)

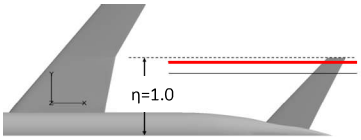

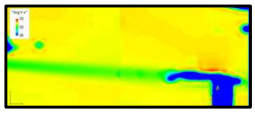

PIV（AoA=11deg）

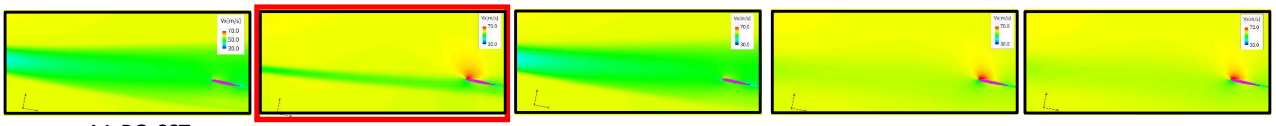

A1-BO-SST　A-UP-SA　A3-UP-SST　A4-ME-SA　A5-ME-SST

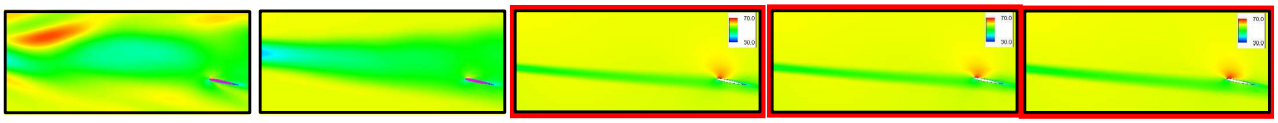

B1-Cu-SA　B2-Cu-SA　C1-Cu-SA　C2-Cu-SA　D1-Cu-SA

The attached cases are close to the experiment

20

Wake interference with tail (13.08deg, Section YB)

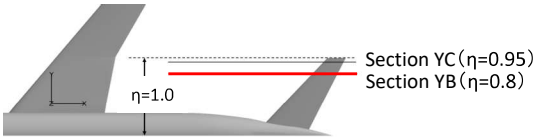

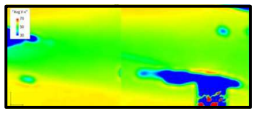

PIV（AoA=13deg）

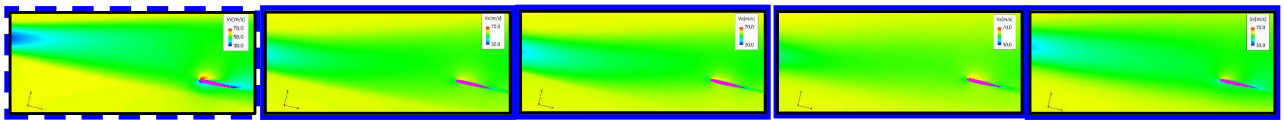

A1-BO-SST　A-UP-SA　A3-UP-SST　A4-ME-SA　A5-ME-SST

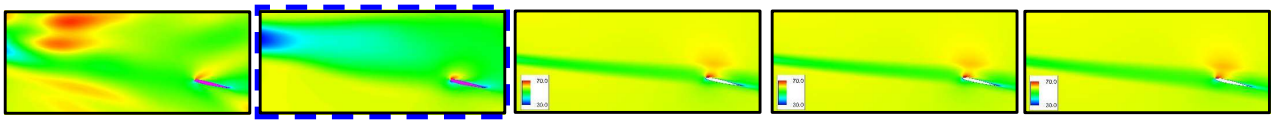

B1-Cu-SA　B2-Cu-SA　C1-Cu-SA　C2-Cu-SA　D1-Cu-SA

The separated cases are close to the experiment

21

Wake interference with tail (13.08deg, Section YC)

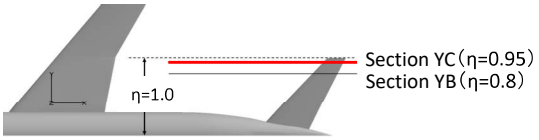

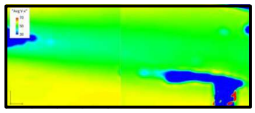

PIV（AoA=13deg）

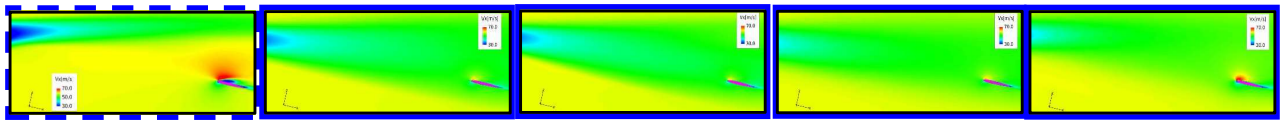

A1-BO-SST　A-UP-SA　A3-UP-SST　A4-ME-SA　A5-ME-SST

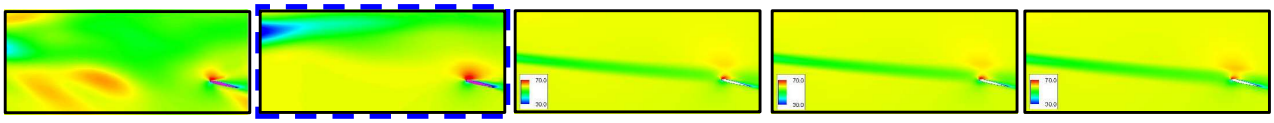

B1-Cu-SA　B2-Cu-SA　C1-Cu-SA　C2-Cu-SA　D1-Cu-SA

The separated cases are close to the experiment

22

Velocity contours (11.05deg, Section XA)

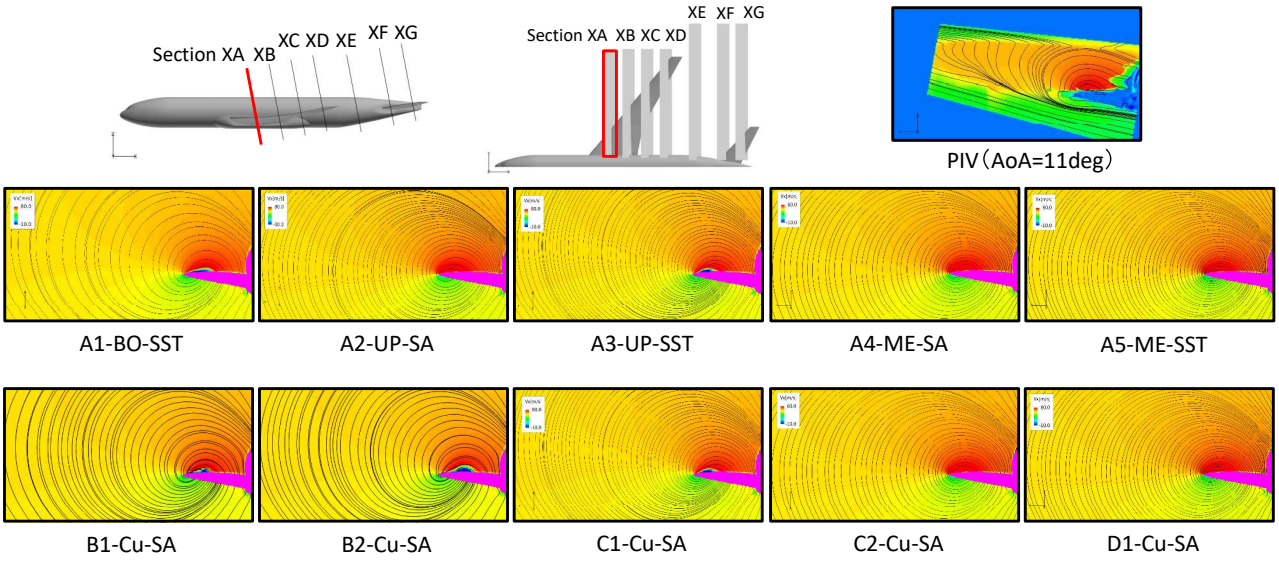

23

Velocity contours (11.05deg, Section XB)

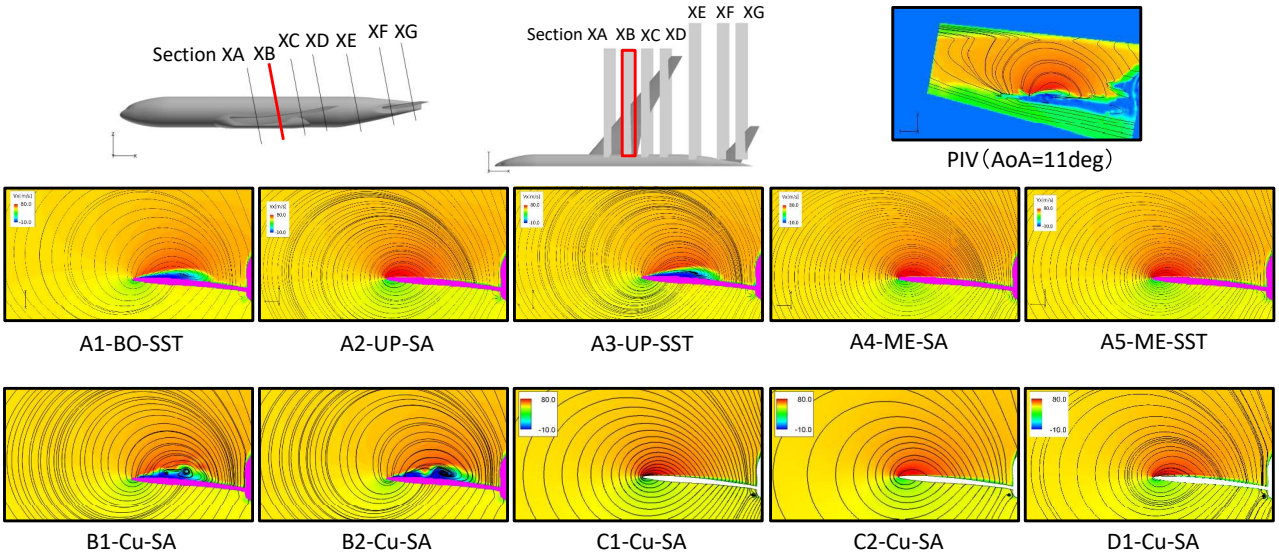

24

Velocity contours (11.05deg, Section XC)

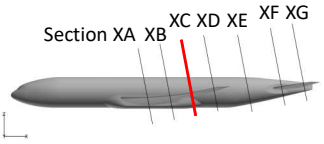

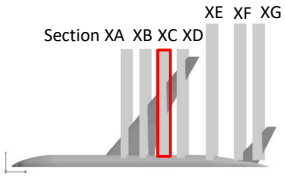

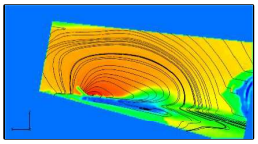

PIV（AoA=11deg）

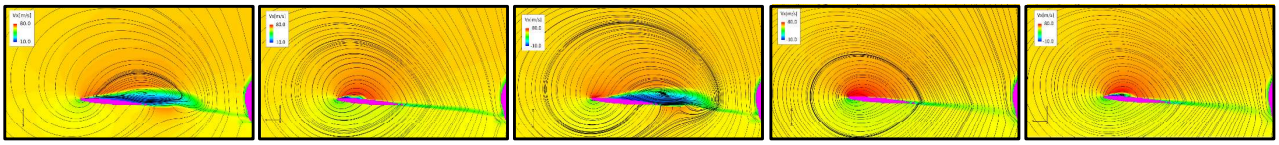

A1-BO-SST　A2-UP-SA　A3-UP-SST　A4-ME-SA　A5-ME-SST

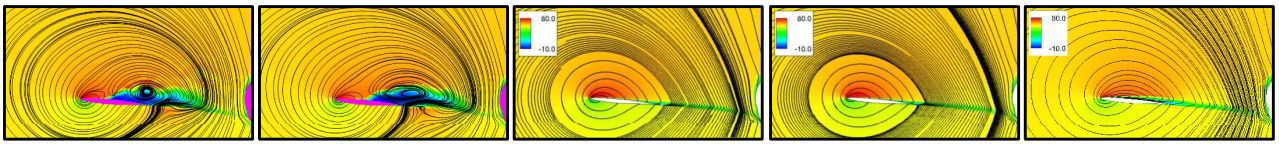

B1-Cu-SA　B2-Cu-SA　C1-Cu-SA　C2-Cu-SA　D1-Cu-SA

25

Velocity contours (11.05deg, Section XD)

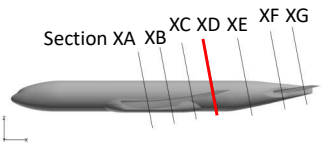

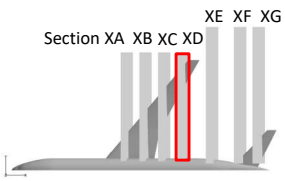

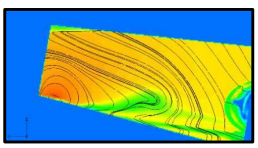

PIV（AoA=11deg）

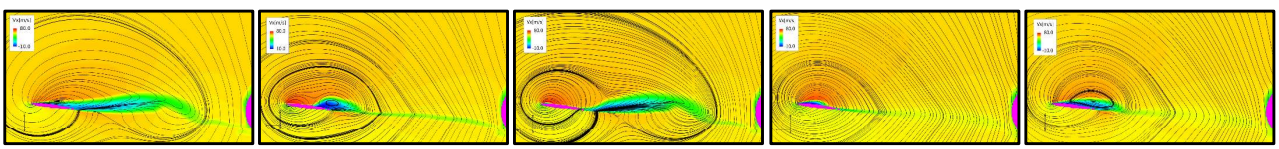

A1-BO-SST　A2-UP-SA　A3-UP-SST　A4-ME-SA　A5-ME-SST

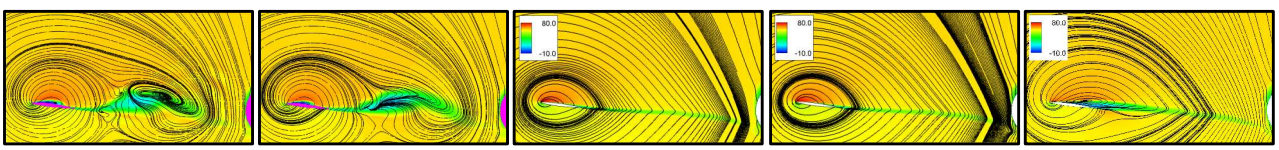

B1-Cu-SA　B2-Cu-SA　C1-Cu-SA　C2-Cu-SA　D1-Cu-SA

26

Velocity contours (11.05deg, Section XE)

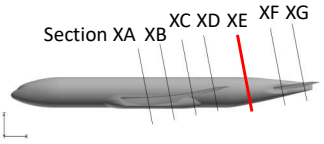

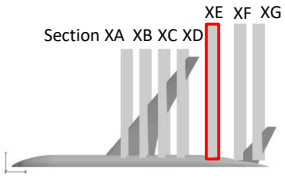

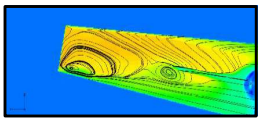

PIV（AoA=11deg）

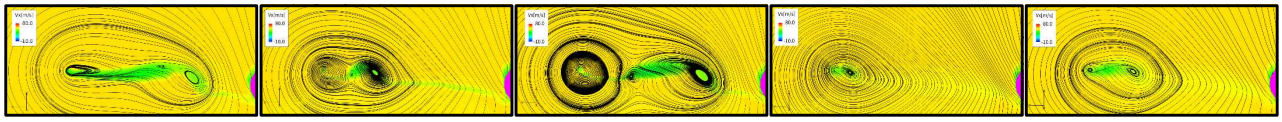

A1-BO-SST　A2-UP-SA　A3-UP-SST　A4-ME-SA　A5-ME-SST

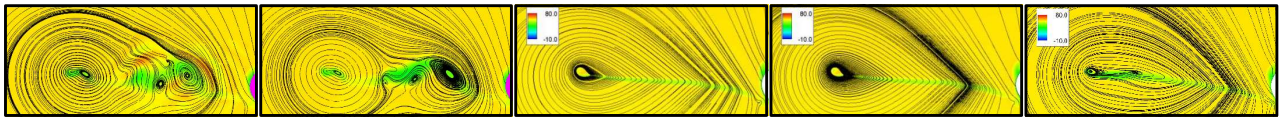

B1-Cu-SA　B2-Cu-SA　C1-Cu-SA　C2-Cu-SA　D1-Cu-SA

27

Velocity contours (11.05deg, Section XF)

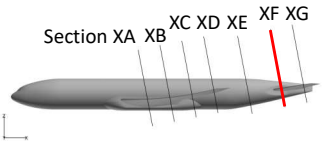

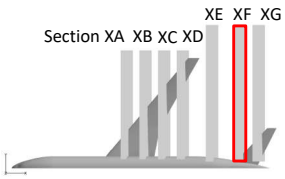

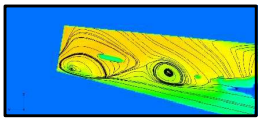

PIV（AoA=11deg）

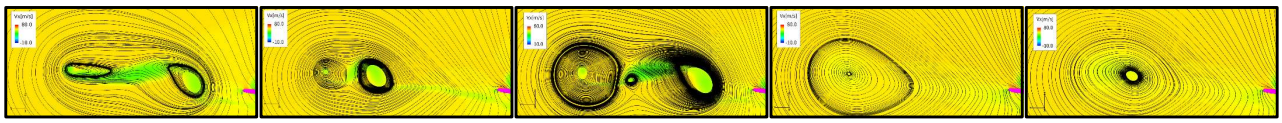

A1-BO-SST　A2-UP-SA　A3-UP-SST　A4-ME-SA　A5-ME-SST

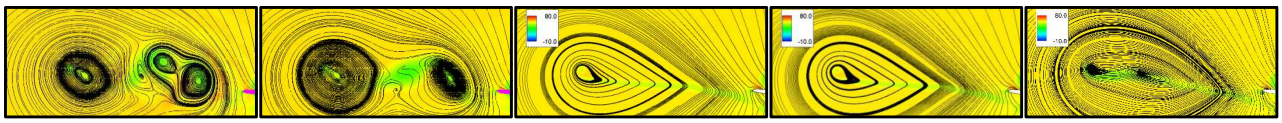

B1-Cu-SA　B2-Cu-SA　C1-Cu-SA　C2-Cu-SA　D1-Cu-SA

28

Velocity contours (11.05deg, Section XG)

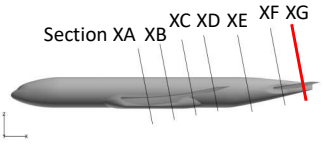

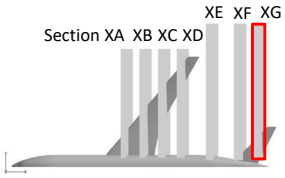

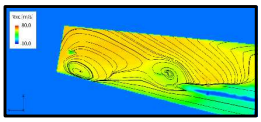

PIV（AoA=11deg）

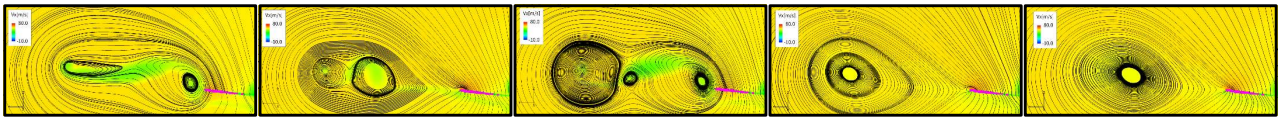

A1-BO-SST　A2-UP-SA　A3-UP-SST　A4-ME-SA　A5-ME-SST

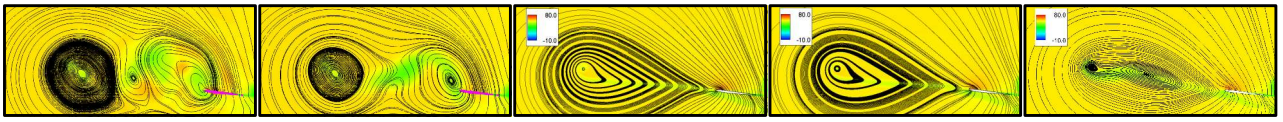

B1-Cu-SA　B2-Cu-SA　C1-Cu-SA　C2-Cu-SA　D1-Cu-SA

29

Velocity contours (13.08deg, Section XA)

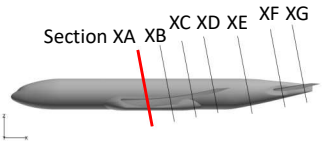

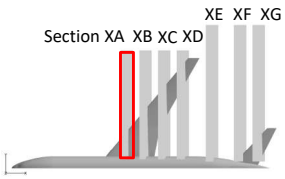

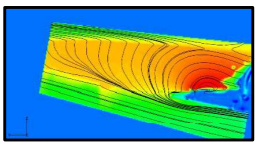

PIV（AoA=13deg）

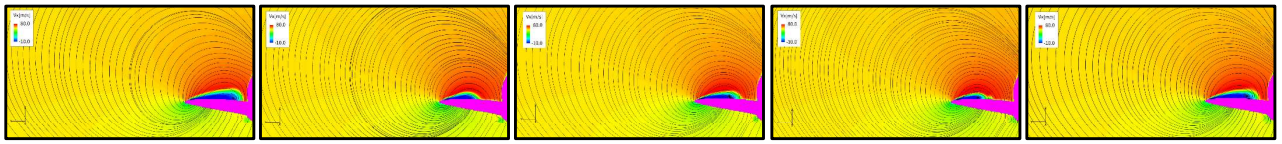

A1-BO-SST　A2-UP-SA　A3-UP-SST　A4-ME-SA　A5-ME-SST

B1-Cu-SA　B2-Cu-SA　C1-Cu-SA　C2-Cu-SA　D1-Cu-SA

30

Velocity contours (13.08deg, Section XB)

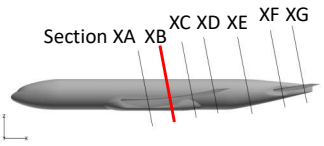

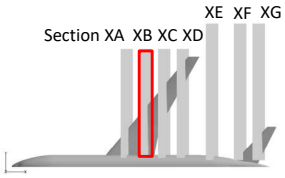

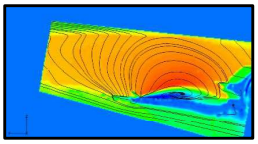

PIV（AoA=13deg）

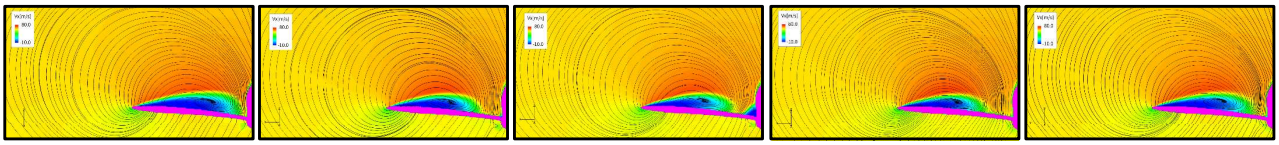

A1-BO-SST A2-UP-SA A3-UP-SST A4-ME-SA A5-ME-SST

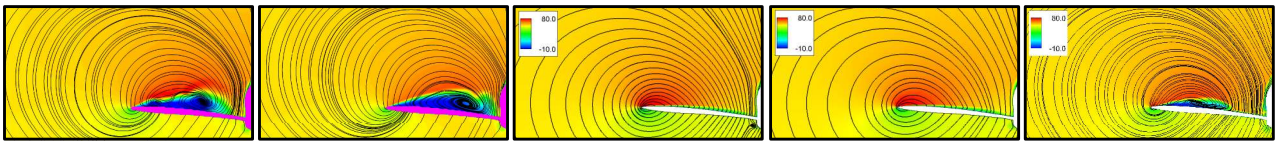

B1-Cu-SA B2-Cu-SA C1-Cu-SA C2-Cu-SA D1-Cu-SA

31

Velocity contours (13.08deg, Section XC)

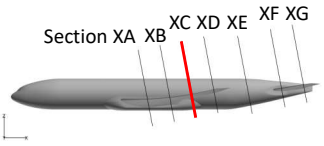

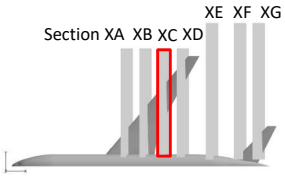

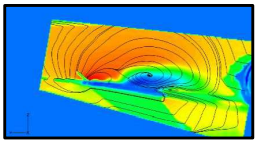

PIV（AoA=13deg）

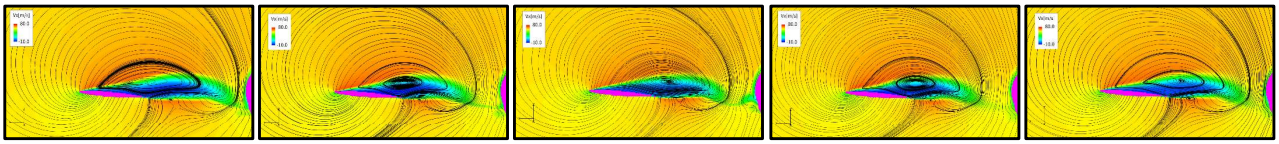

A1-BO-SST A2-UP-SA A3-UP-SST A4-ME-SA A5-ME-SST

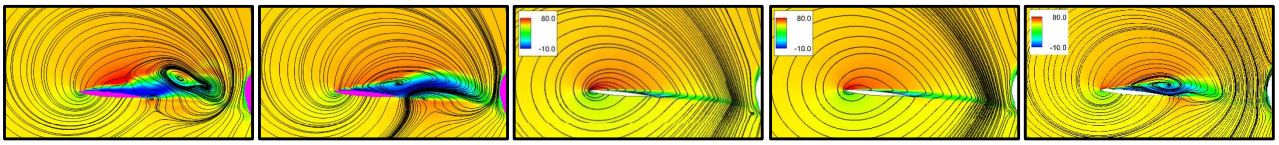

B1-Cu-SA B2-Cu-SA C1-Cu-SA C2-Cu-SA D1-Cu-SA

32

Velocity contours (13.08deg, Section XD)

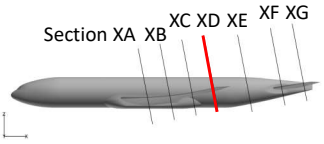

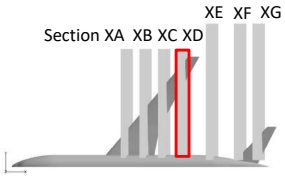

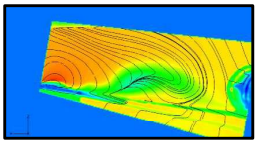

PIV（AoA=13deg）

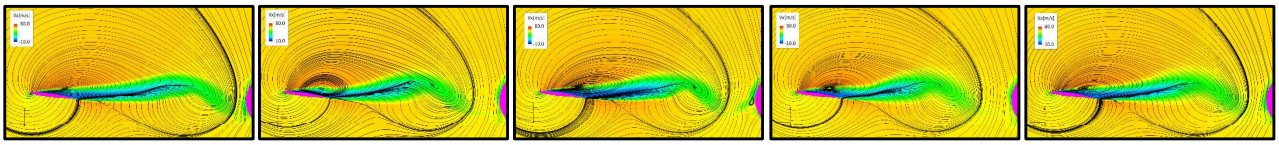

A1-BO-SST　A2-UP-SA　A3-UP-SST　A4-ME-SA　A5-ME-SST

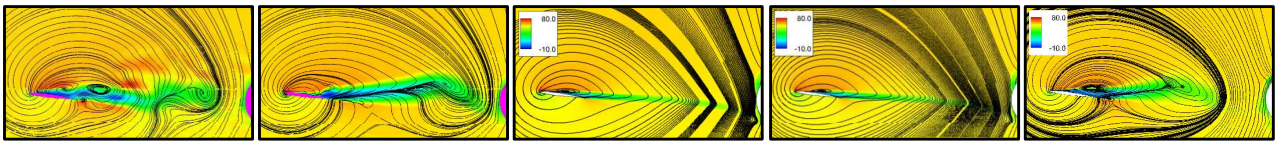

B1-Cu-SA　B2-Cu-SA　C1-Cu-SA　C2-Cu-SA　D1-Cu-SA

33

Velocity contours (13.08deg, Section XE)

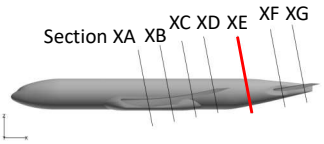

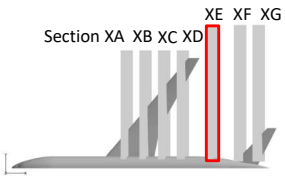

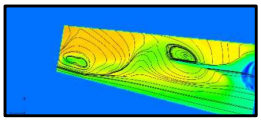

PIV（AoA=13deg）

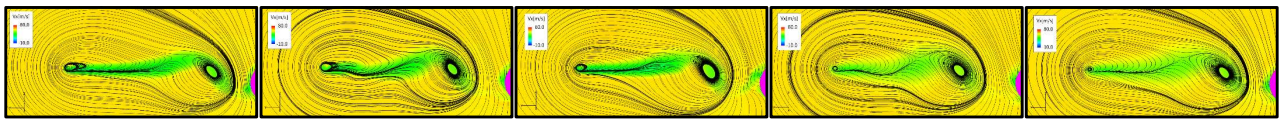

A1-BO-SST　A2-UP-SA　A3-UP-SST　A4-ME-SA　A5-ME-SST

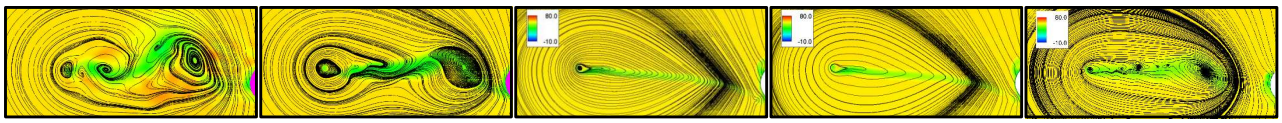

B1-Cu-SA　B2-Cu-SA　C1-Cu-SA　C2-Cu-SA　D1-Cu-SA

34

Velocity contours (13.08deg, Section XF)

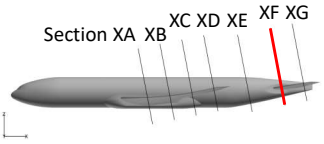

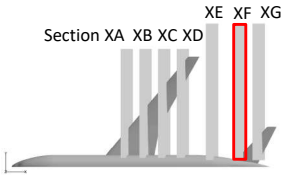

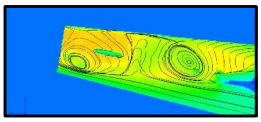

PIV（AoA=13deg）

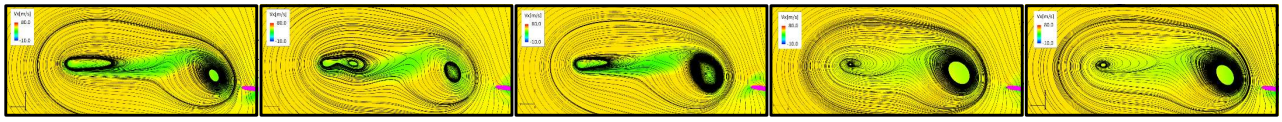

A1-BO-SST A2-UP-SA A3-UP-SST A4-ME-SA A5-ME-SST

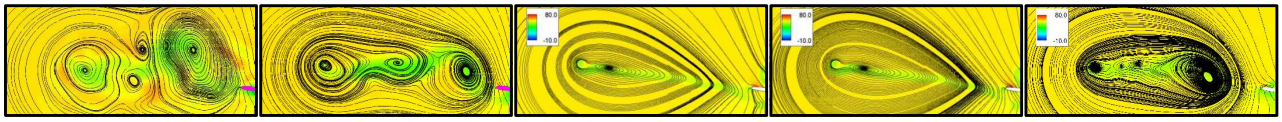

B1-Cu-SA B2-Cu-SA C1-Cu-SA C2-Cu-SA D1-Cu-SA

35

Velocity contours (13.08deg, Section XG)

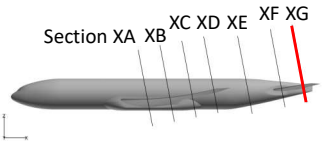

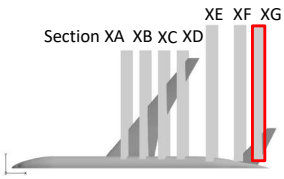

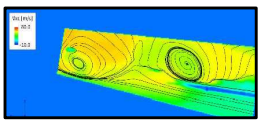

PIV（AoA=13deg）

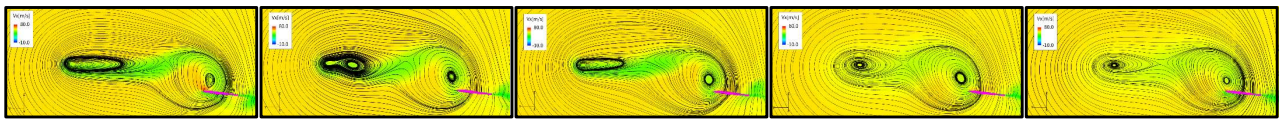

A1-BO-SST A2-UP-SA A3-UP-SST A4-ME-SA A5-ME-SST

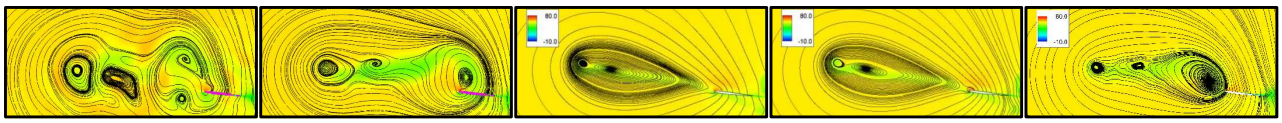

B1-Cu-SA B2-Cu-SA C1-Cu-SA C2-Cu-SA D1-Cu-SA

36

Surface Cp distribution（Tail, Section HB-HC）

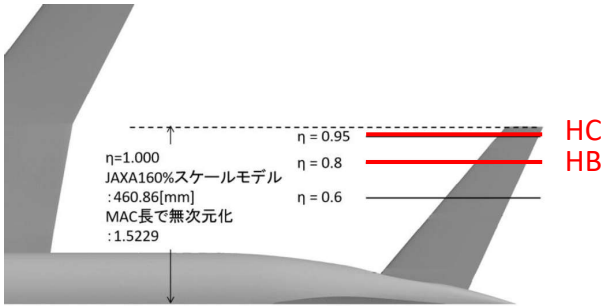

Cross section	η	y[mm]
Section HA	0.6	277
Section HB	0.8	369
Section HC	0.95	438

α[deg]	
CFD	EXP
-3.22	-3.0
-0.67	-0.5
2.89	3.0
5.95	6.0
9.01	9.0
10.03	10.0
11.05	11.0
12.06	12.1
13.08	13.0
14.08	14.1
18.08	18.1

37

Surface Cp distribution（Tail, Section HB-HC）

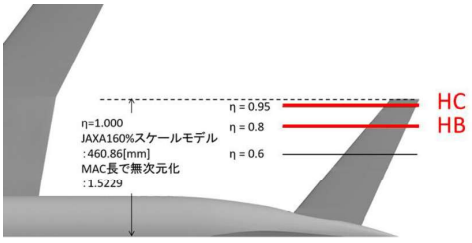

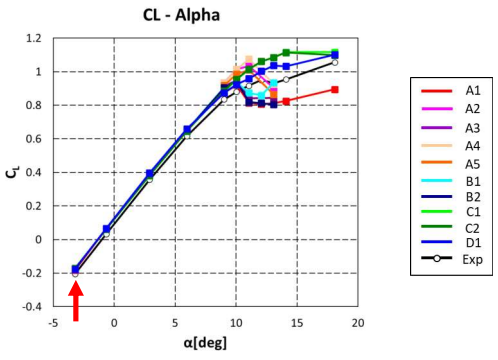

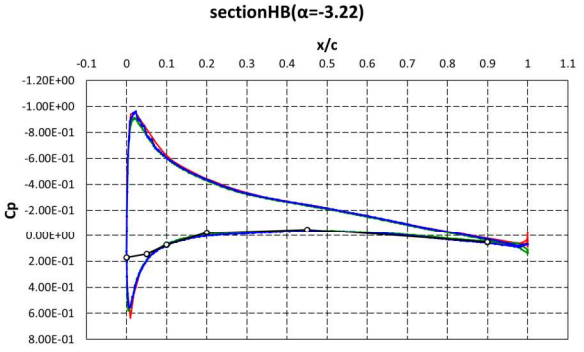

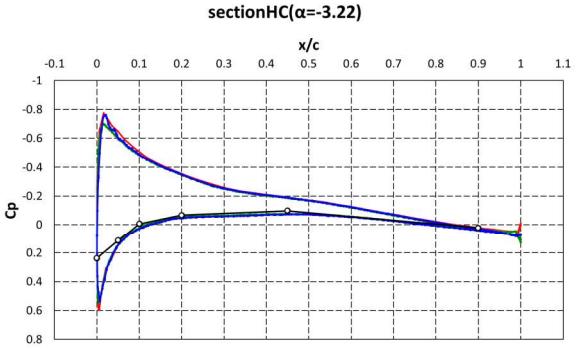

38

Surface Cp distribution（Tail, Section HB-HC）

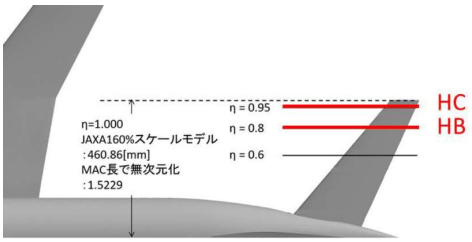

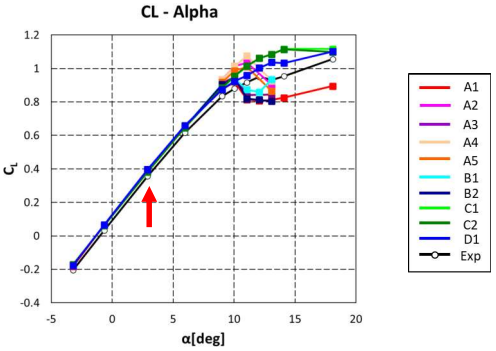

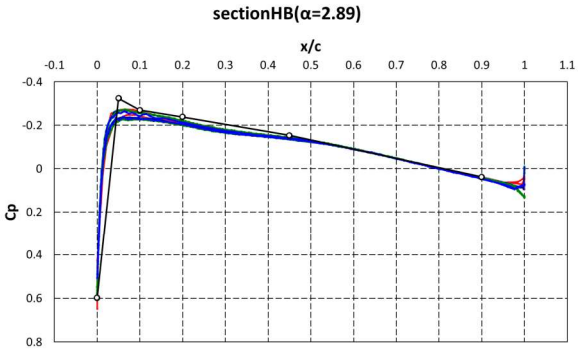

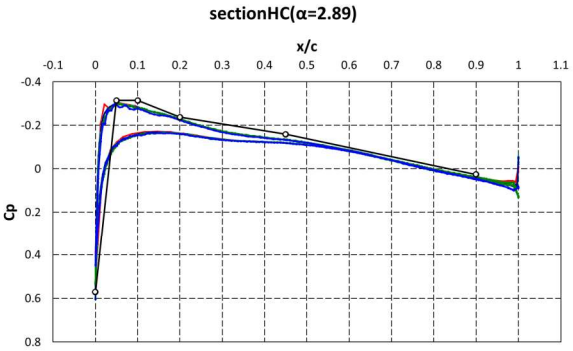

39

Surface Cp distribution（Tail, Section HB-HC）

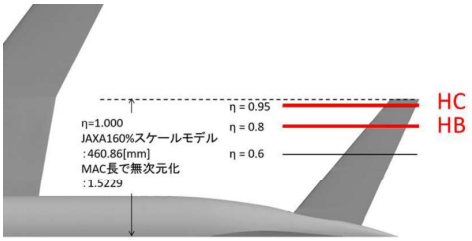

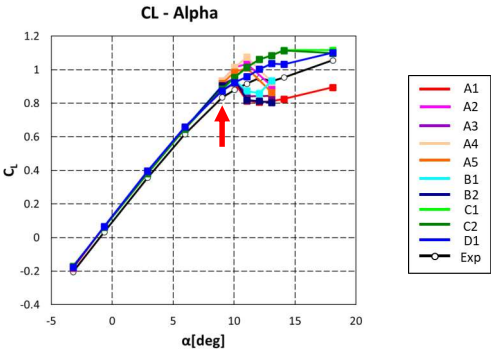

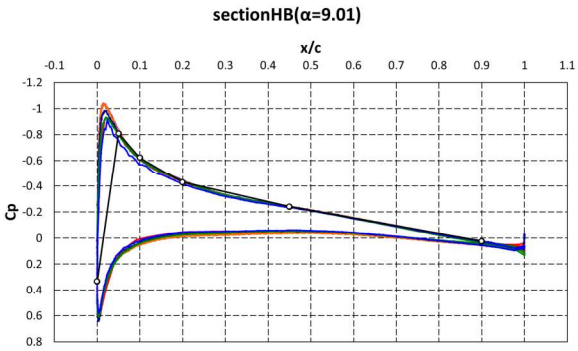

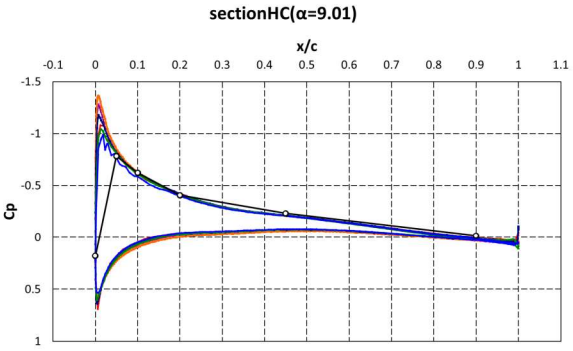

40

Surface Cp distribution（Tail, Section HB-HC）

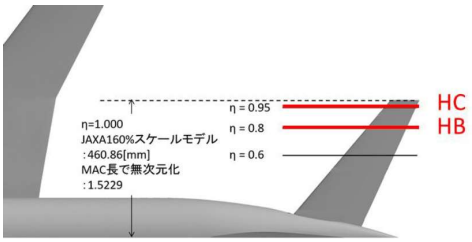

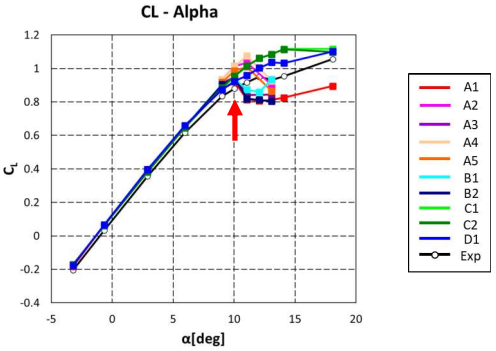

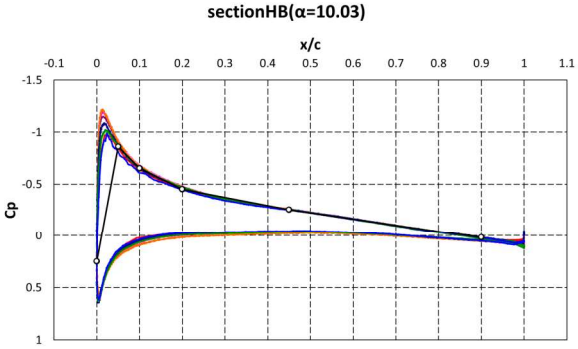

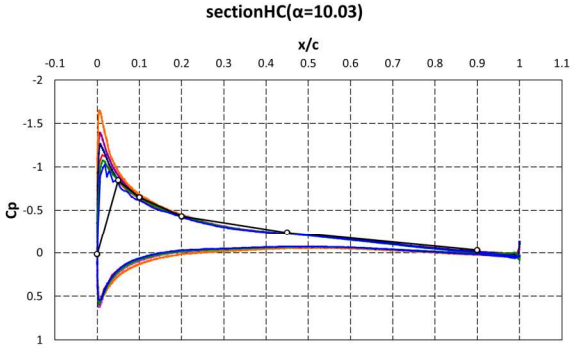

41

Surface Cp distribution（Tail, Section HB-HC）

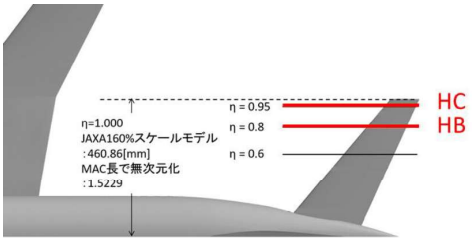

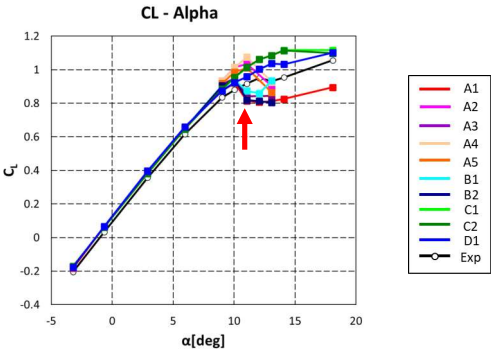

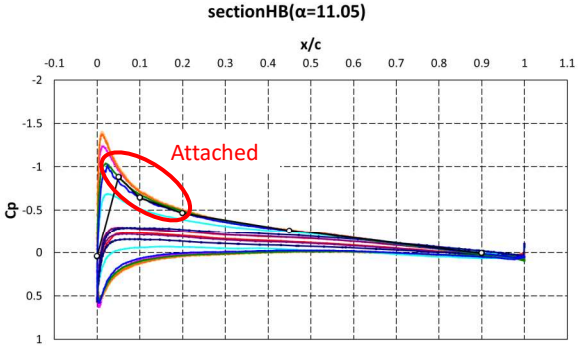

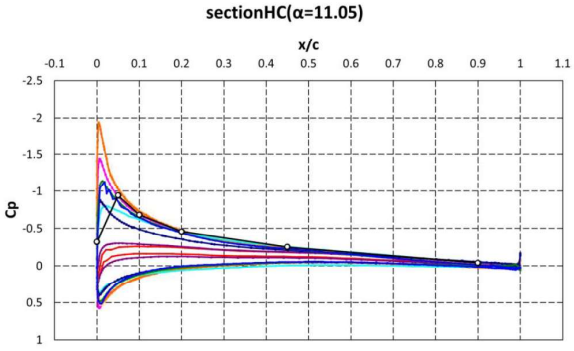

The attached cases are close to the experiment

42

Surface Cp distribution（Tail, Section HB-HC）

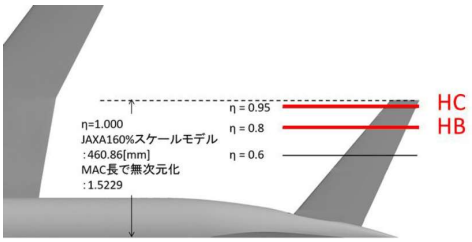

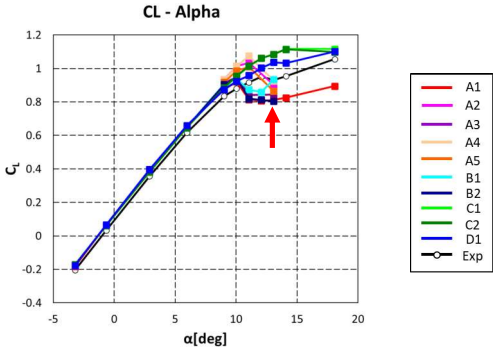

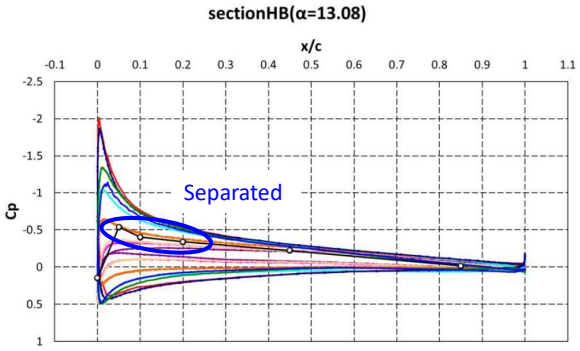

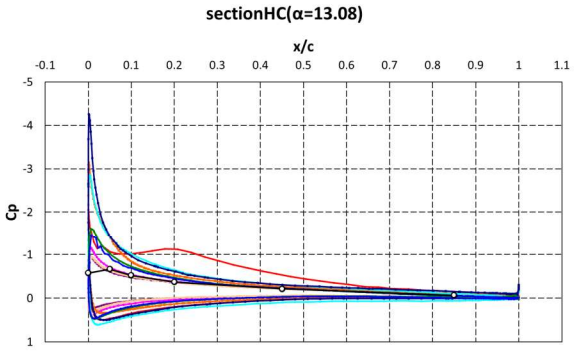

The separated cases are close to the experiment

43

Surface Cp distribution（Tail, Section HB-HC）

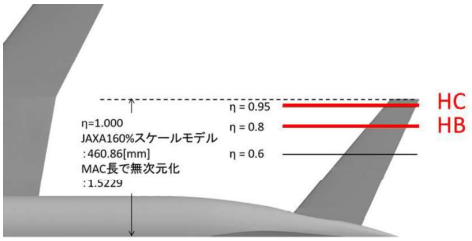

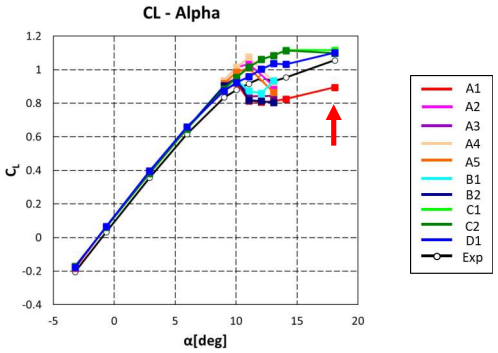

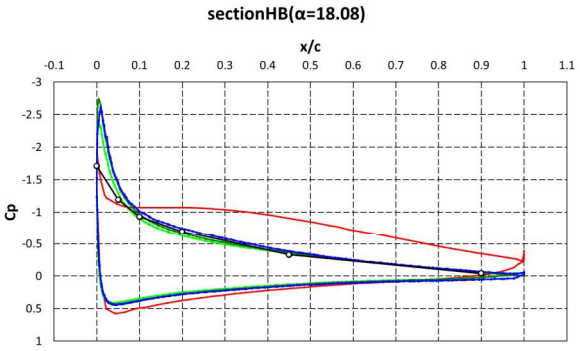

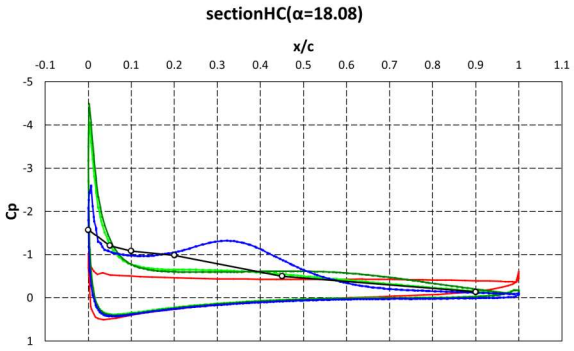

44

Case2 : Unsteady computation

- Aims
  - Understand the prediction accuracy of unsteady computation by comparing the unsteady computation with the steady computation.
  - Understand the dependency of turbulence model, grid, time step.

- Conditions
  - M = 0.168, Re_c = 1.06 x 10^6, T_{ref}=310K
  - AoA = 11.05, 13.08deg

45

CL-Alpha, case2

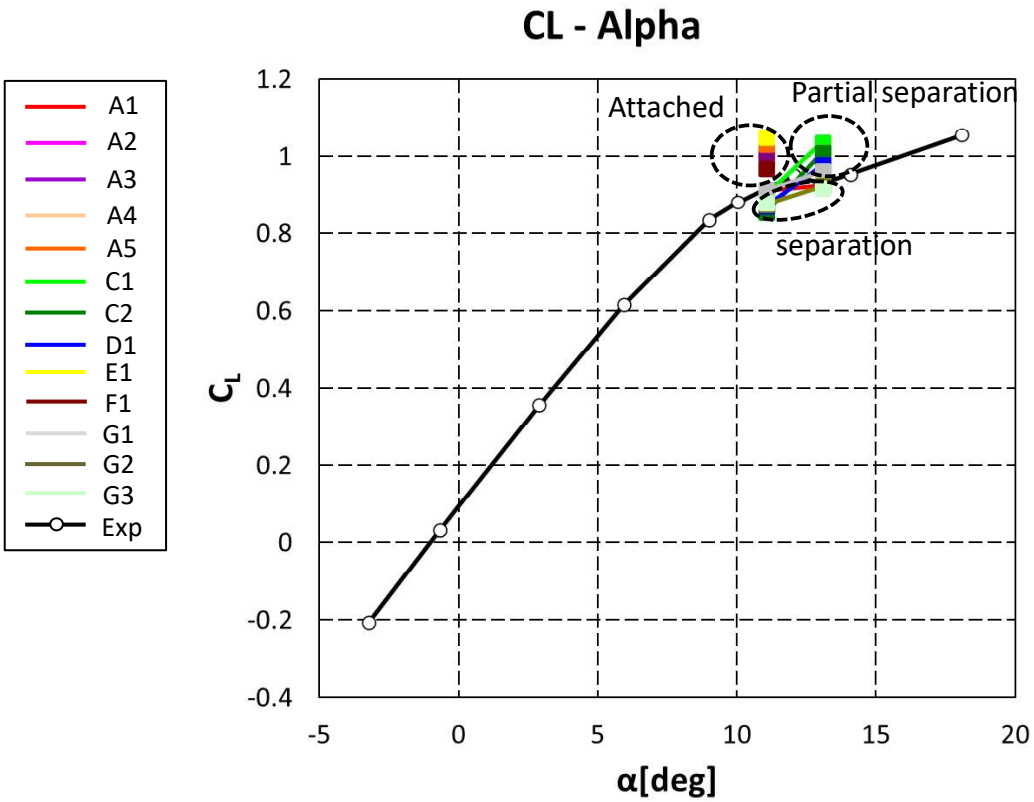

46

CD-Alpha, case2

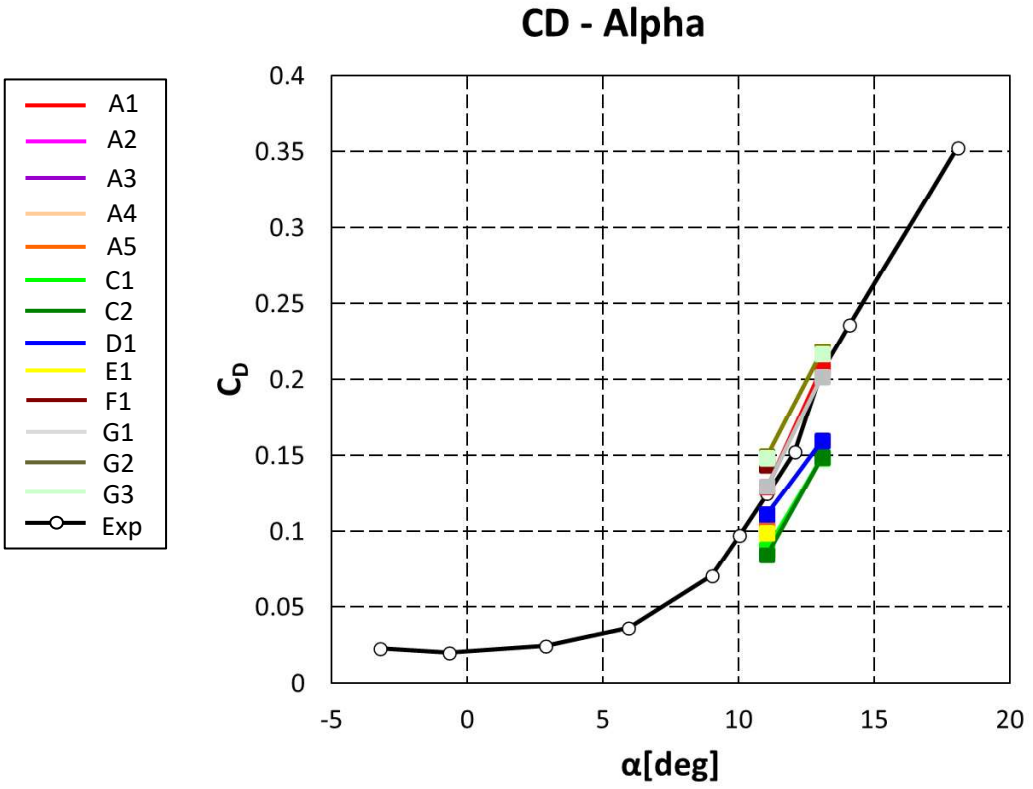

47

Cm-Alpha, case2

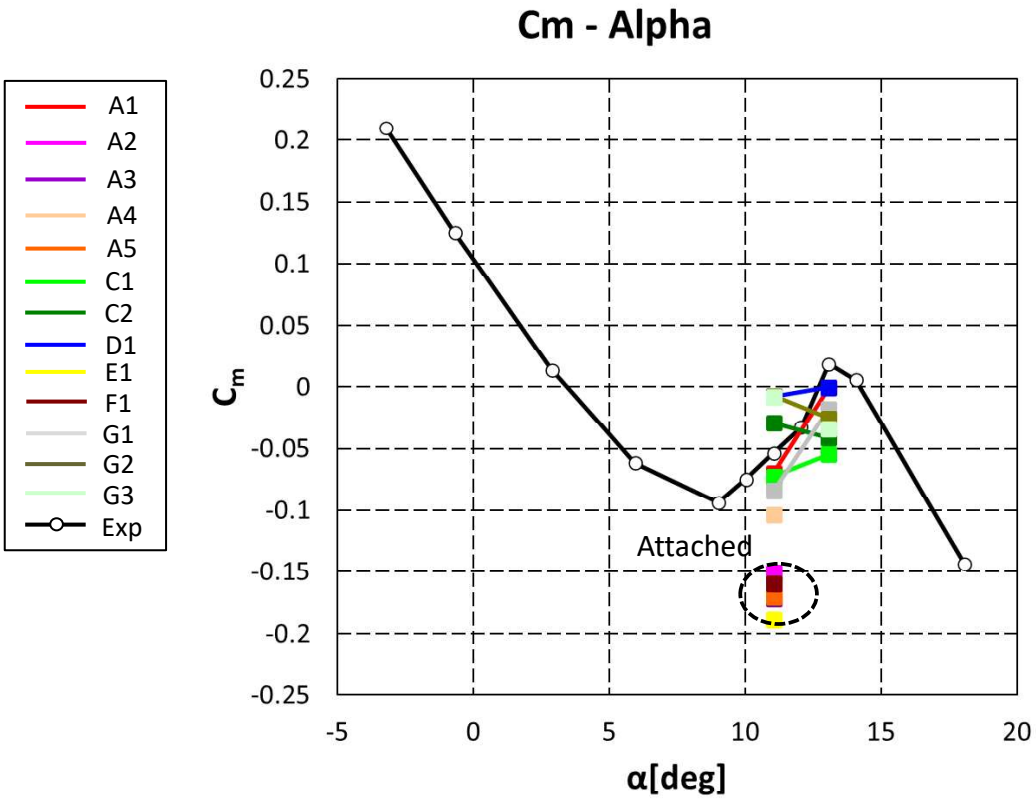

48

CL-Alpha

Steady (Case1)

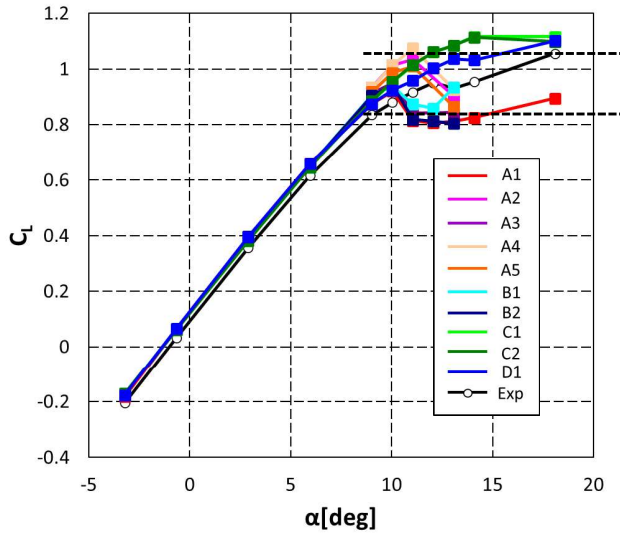

Unsteady (Case2)

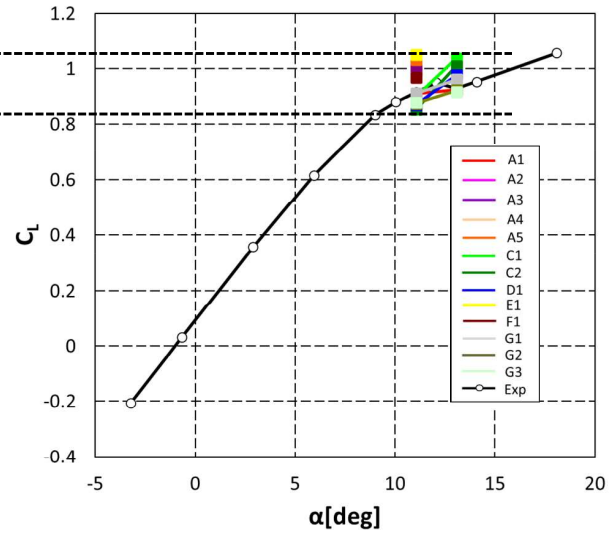

49

CL-Alpha

Steady (Case1)

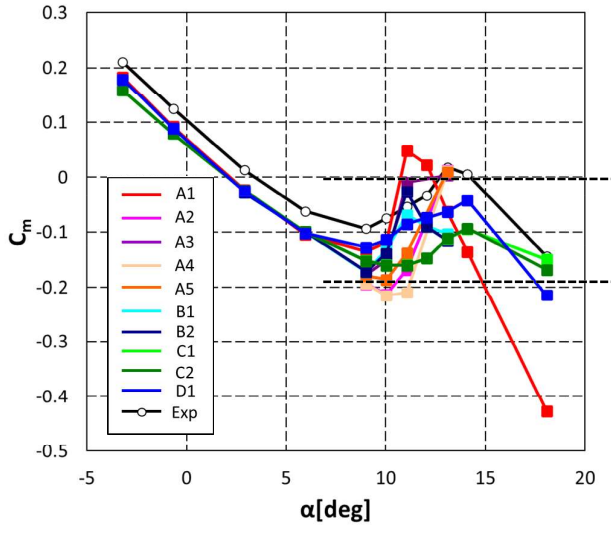

Unsteady (Case2)

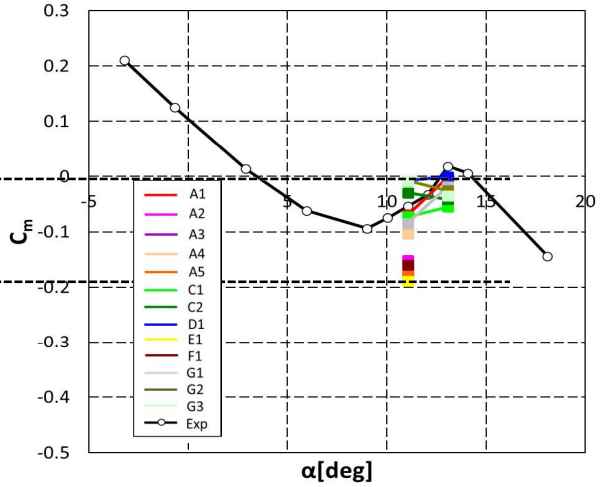

50

CL-Alpha

Steady (Case1)

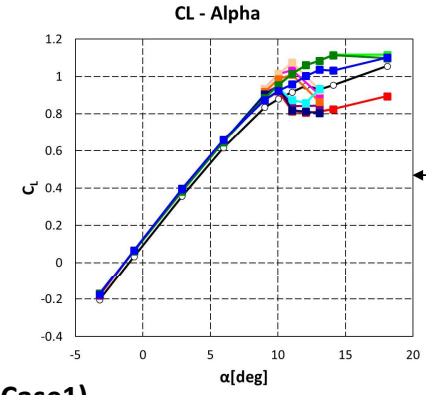

Unsteady (Case2)

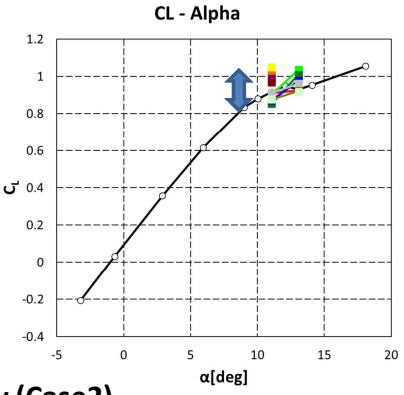

APC-7

Steady (Case1)

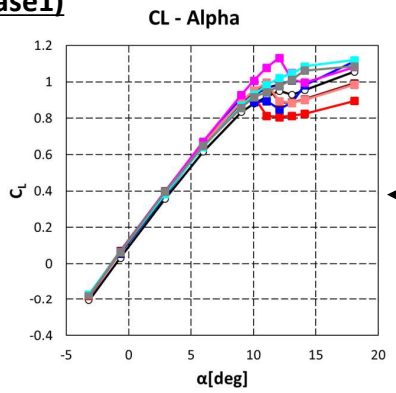

Unsteady (Case2)

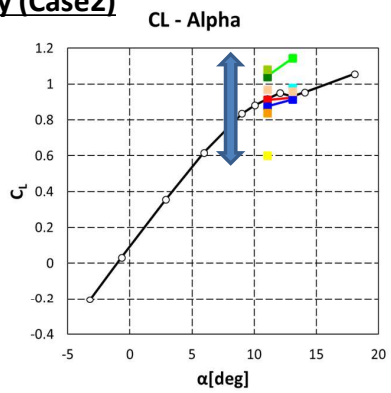

APC-6

51

Surface streamline(11.05deg, Average)

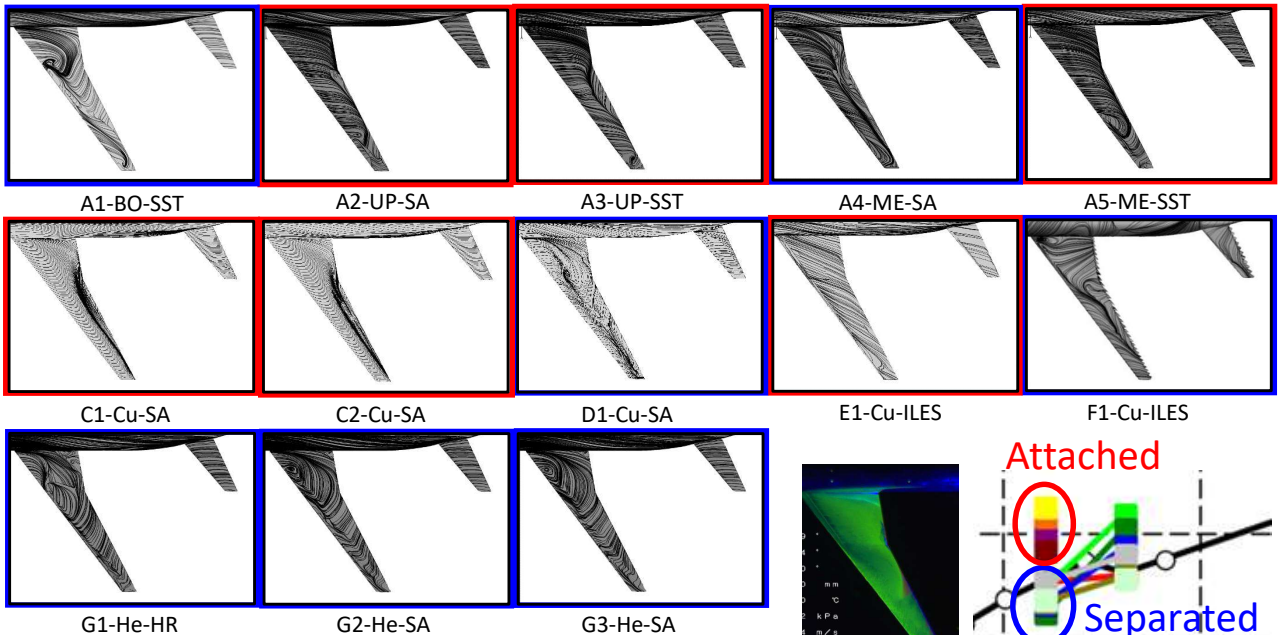

T. Uchiyama, et al., AIAA 2019-2190

52

Surface streamline(13.08deg, Average)

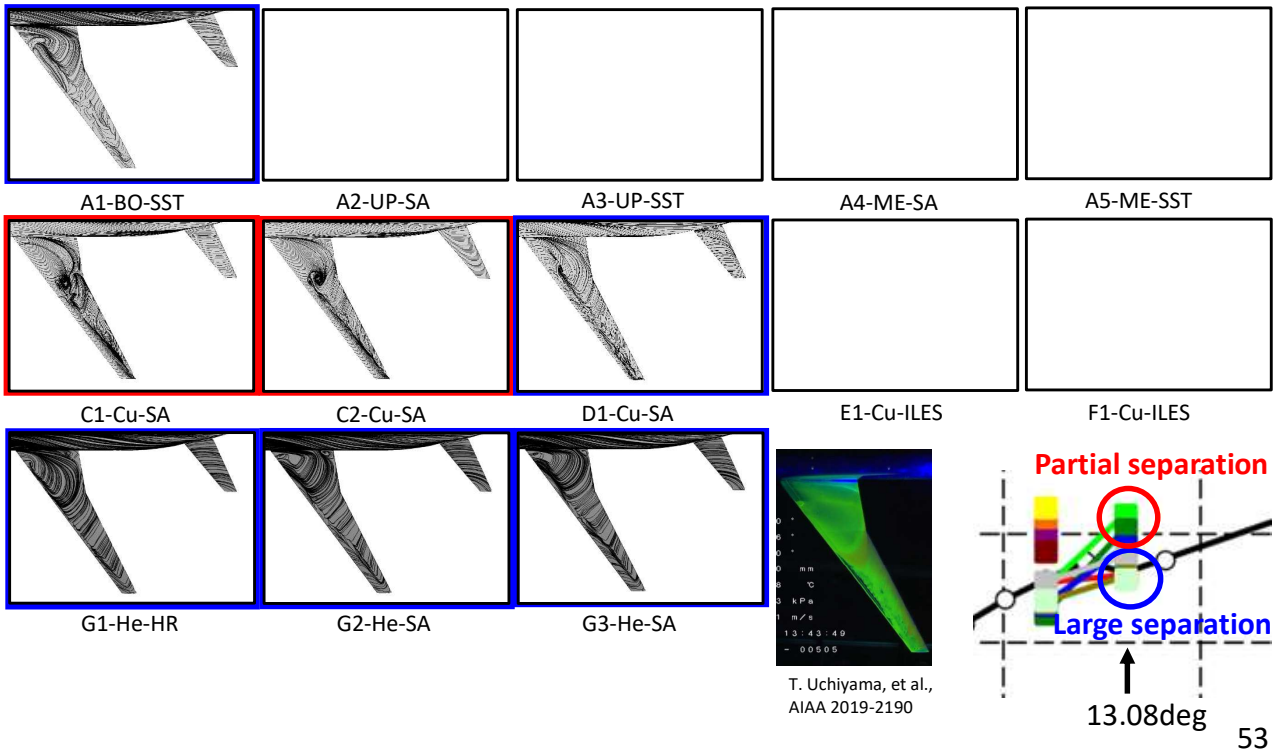

53

Wake interference with tail (11.05deg, Section YB, Average)

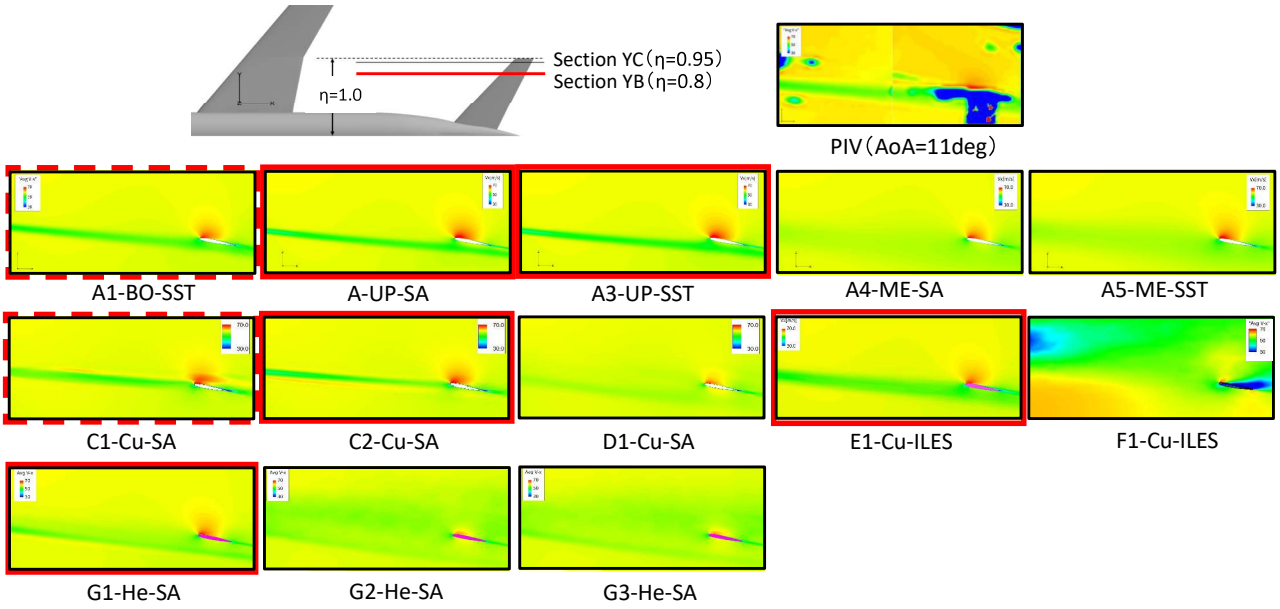

The attached cases are close to the experiment

54

Wake interference with tail (11.05deg, Section YC, Average)

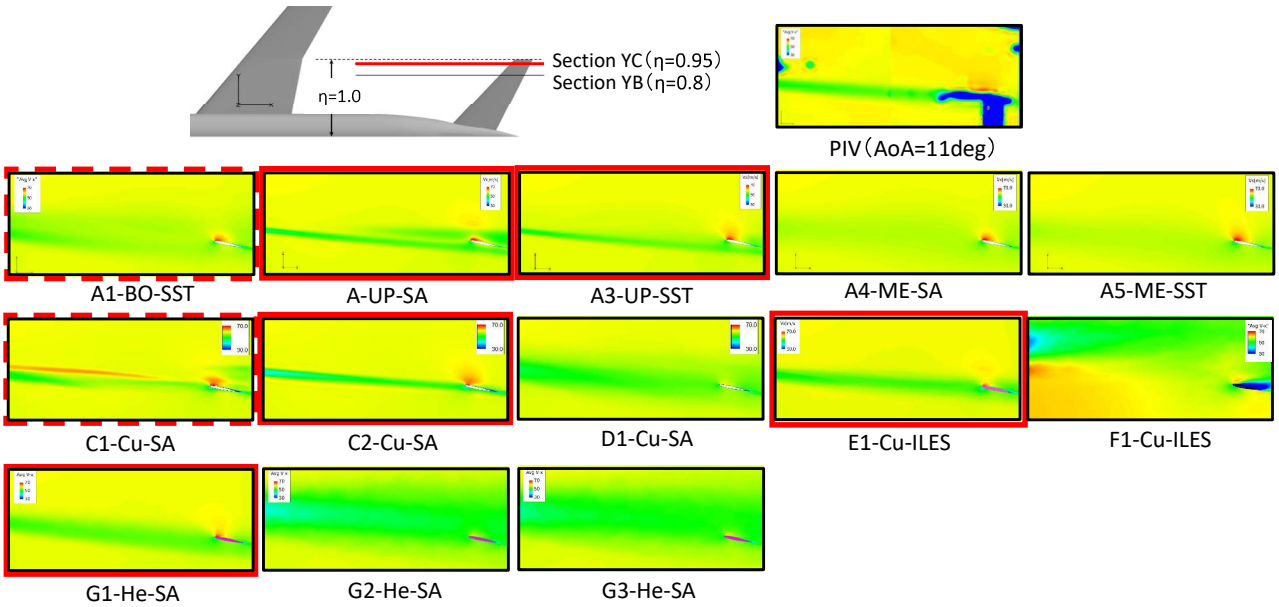

55

Wake interference with tail (13.08deg, Section YB, Average)

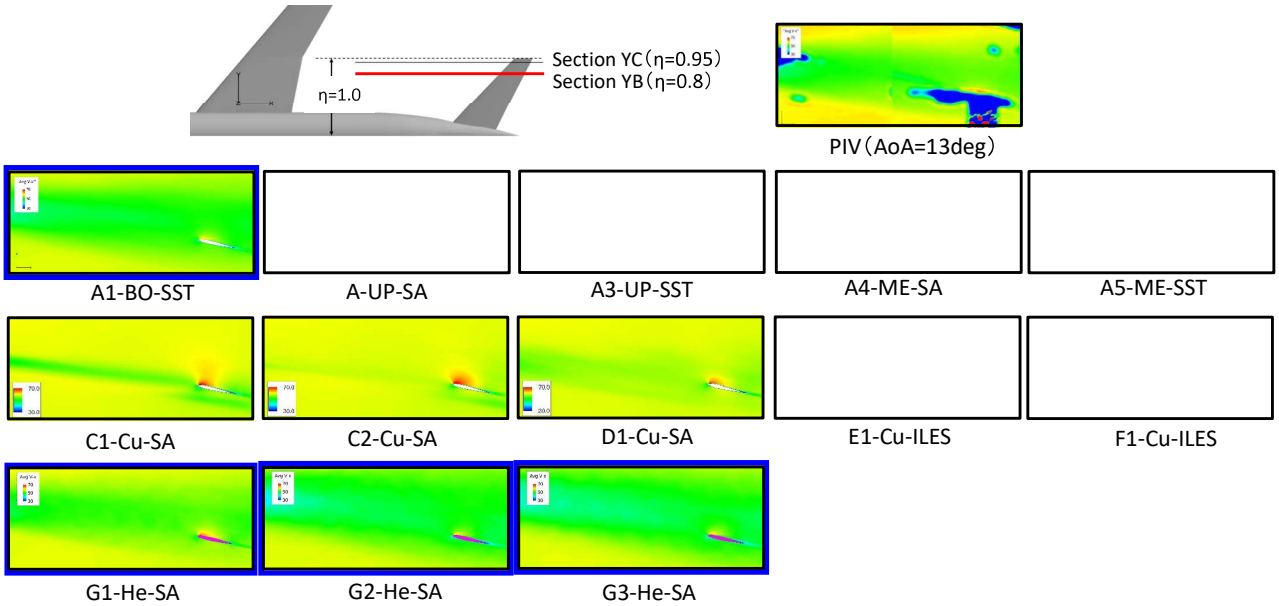

The separated cases are close to the experiment

56

Wake interference with tail (13.08deg, Section YC, Average)

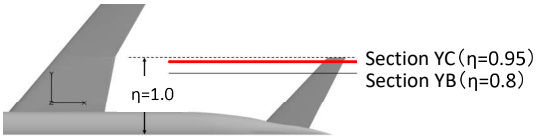

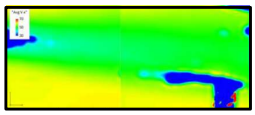

PIV（AoA=13deg）

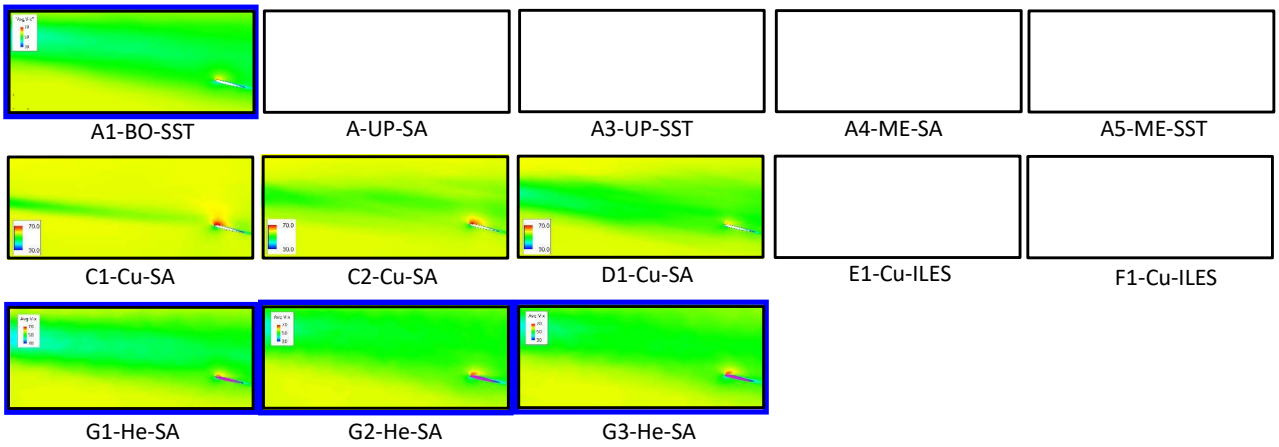

The separated cases are close to the experiment

57

Velocity contours (11.05deg, Section XA)

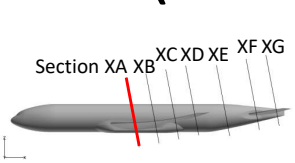

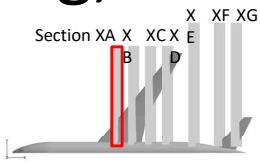

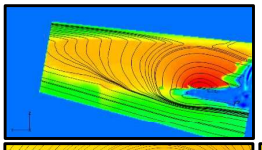

PIV（AoA=11deg）

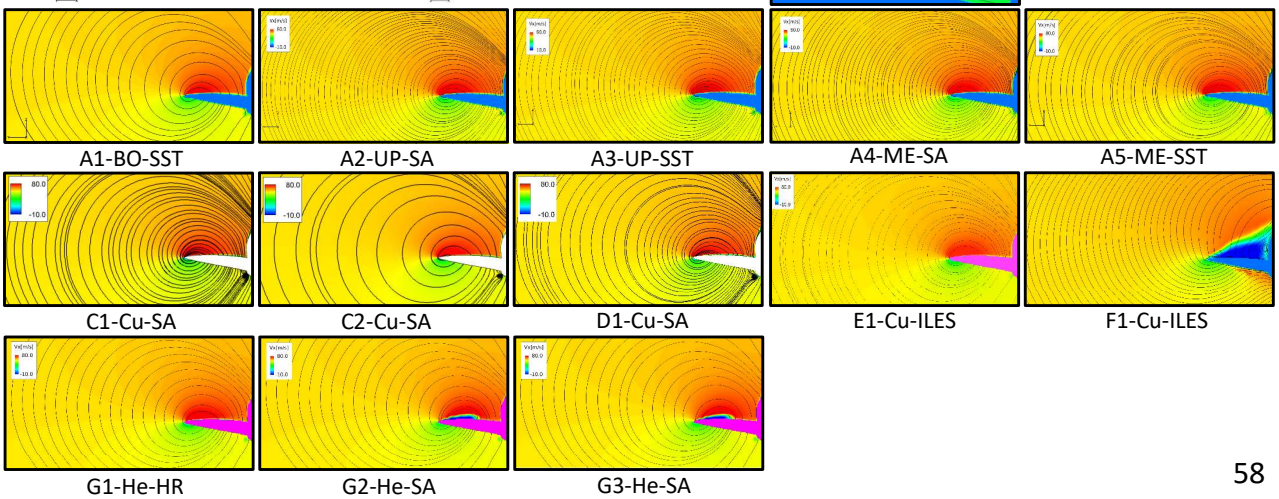

58

Velocity contours (11.05deg, Section XB)

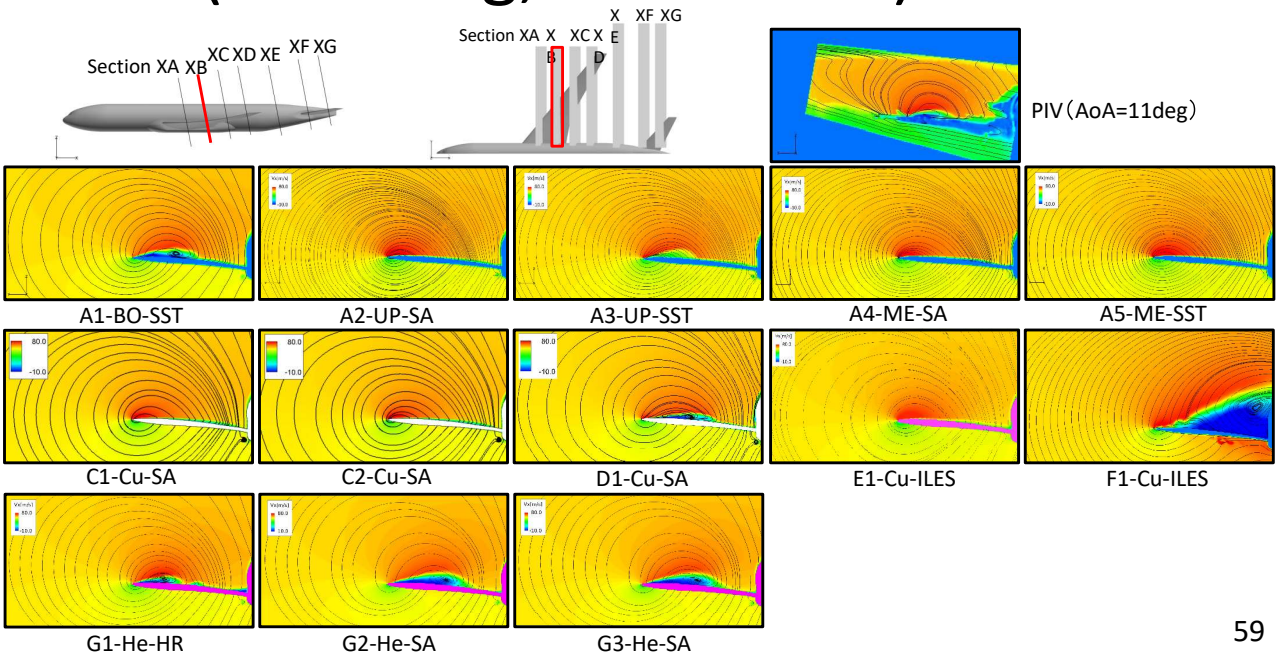

59

Velocity contours (11.05deg, Section XC)

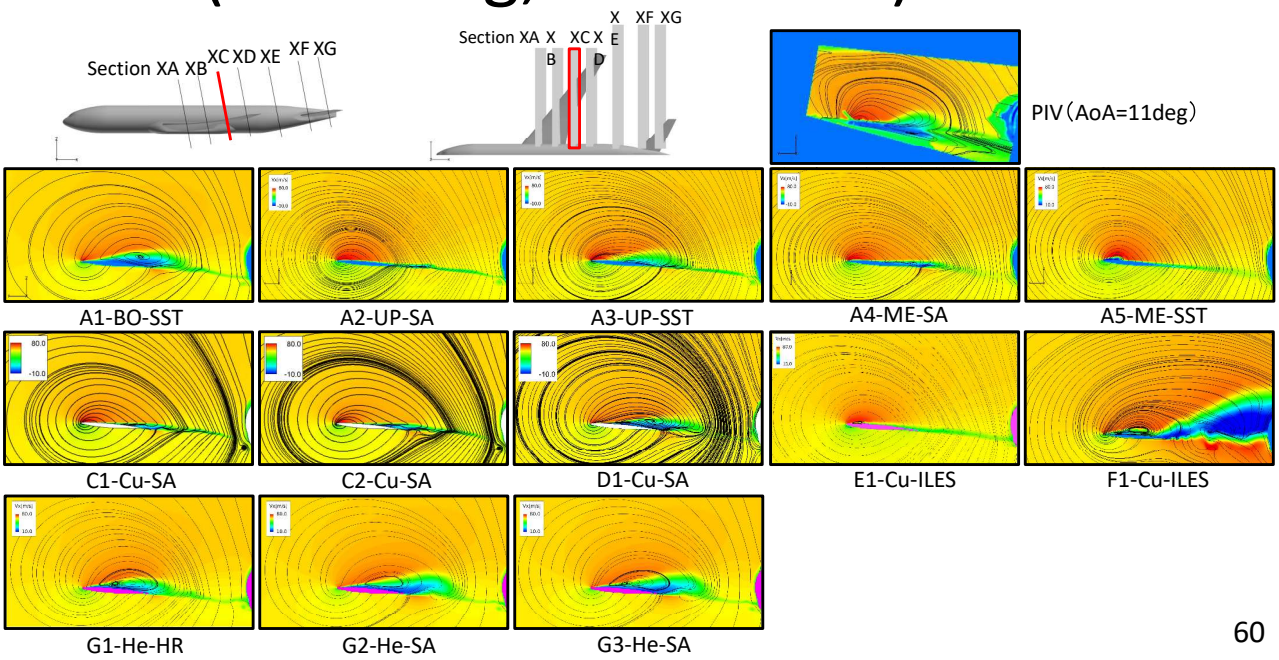

60

Velocity contours (11.05deg, Section XD)

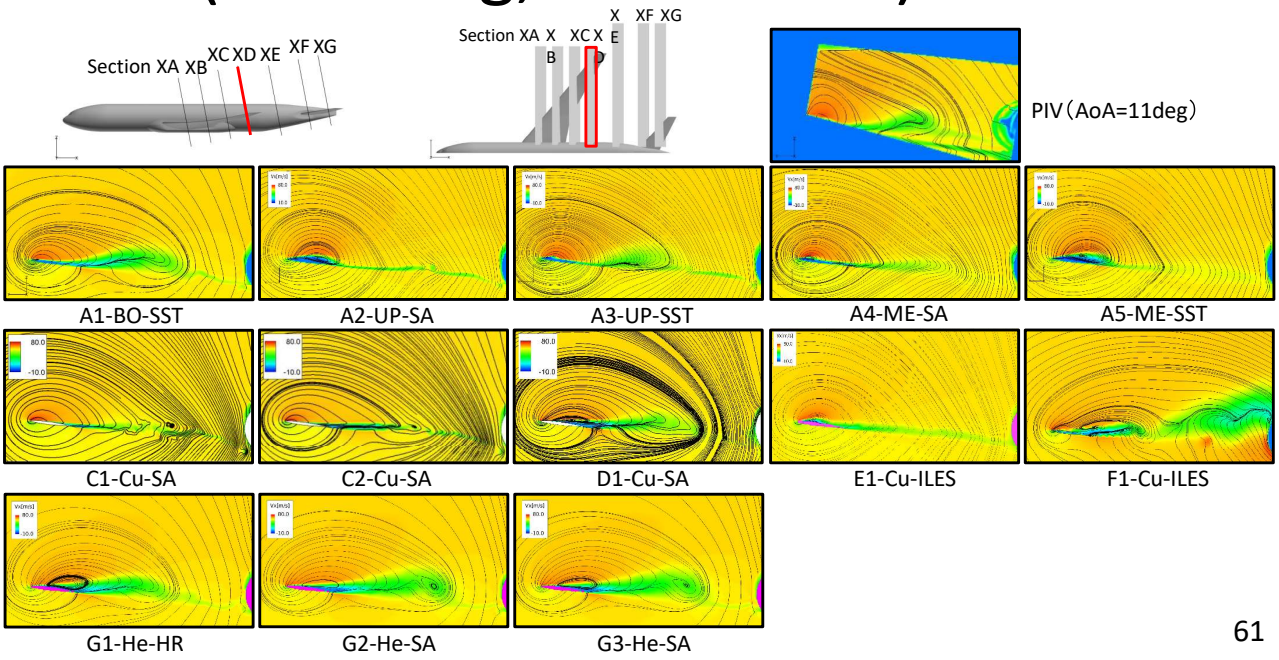

61

Velocity contours (11.05deg, Section XE)

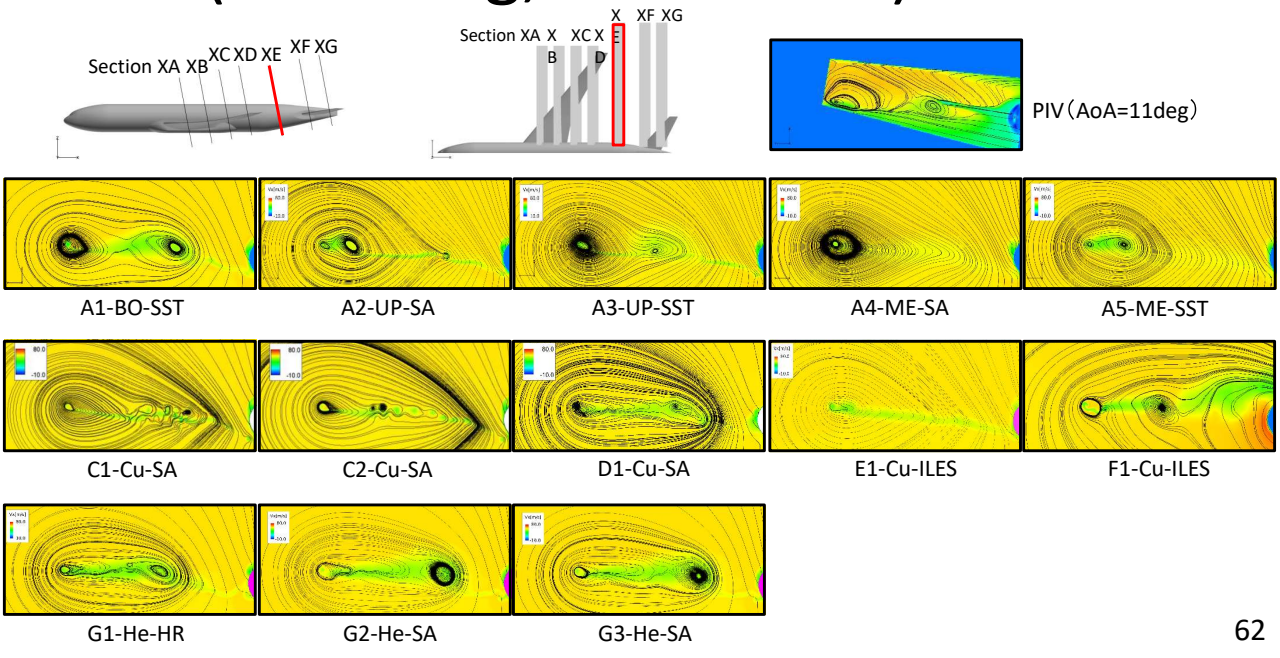

62

Velocity contours (11.05deg, Section XF)

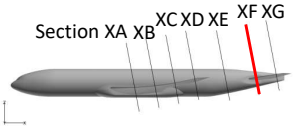

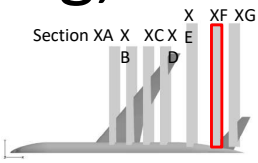

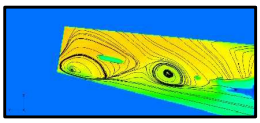

PIV（AoA=11deg）

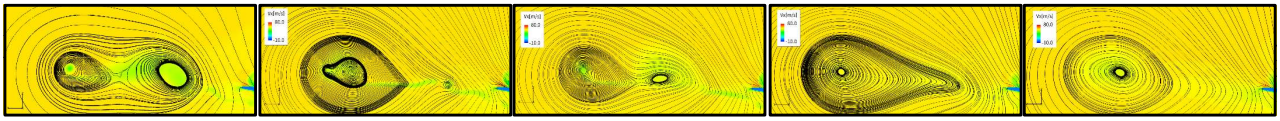

A1-BO-SST A2-UP-SA A3-UP-SST A4-ME-SA A5-ME-SST

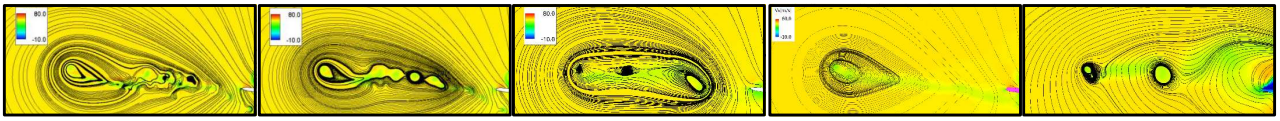

C1-Cu-SA C2-Cu-SA D1-Cu-SA E1-Cu-ILES F1-Cu-ILES

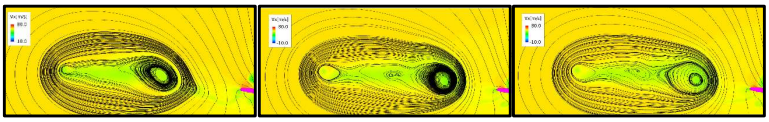

G1-He-HR G2-He-SA G3-He-SA

63

Velocity contours (11.05deg, Section XG)

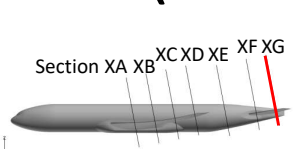

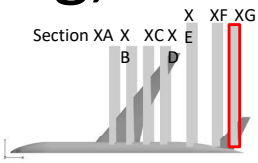

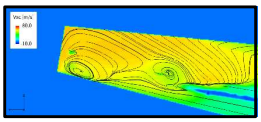

PIV（AoA=11deg）

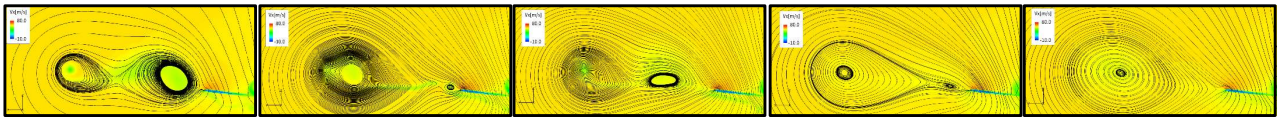

A1-BO-SST A2-UP-SA A3-UP-SST A4-ME-SA A5-ME-SST

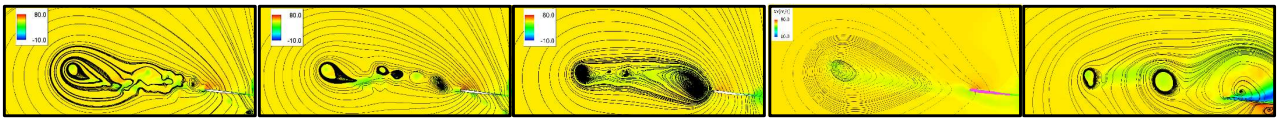

C1-Cu-SA C2-Cu-SA D1-Cu-SA E1-Cu-ILES F1-Cu-ILES

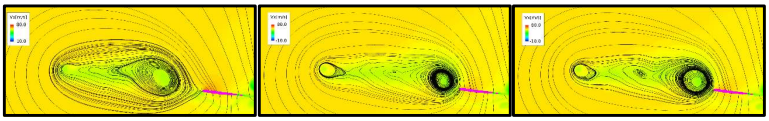

G1-He-HR G2-He-SA G3-He-SA

64

Velocity contours (13.08deg, Section XA)

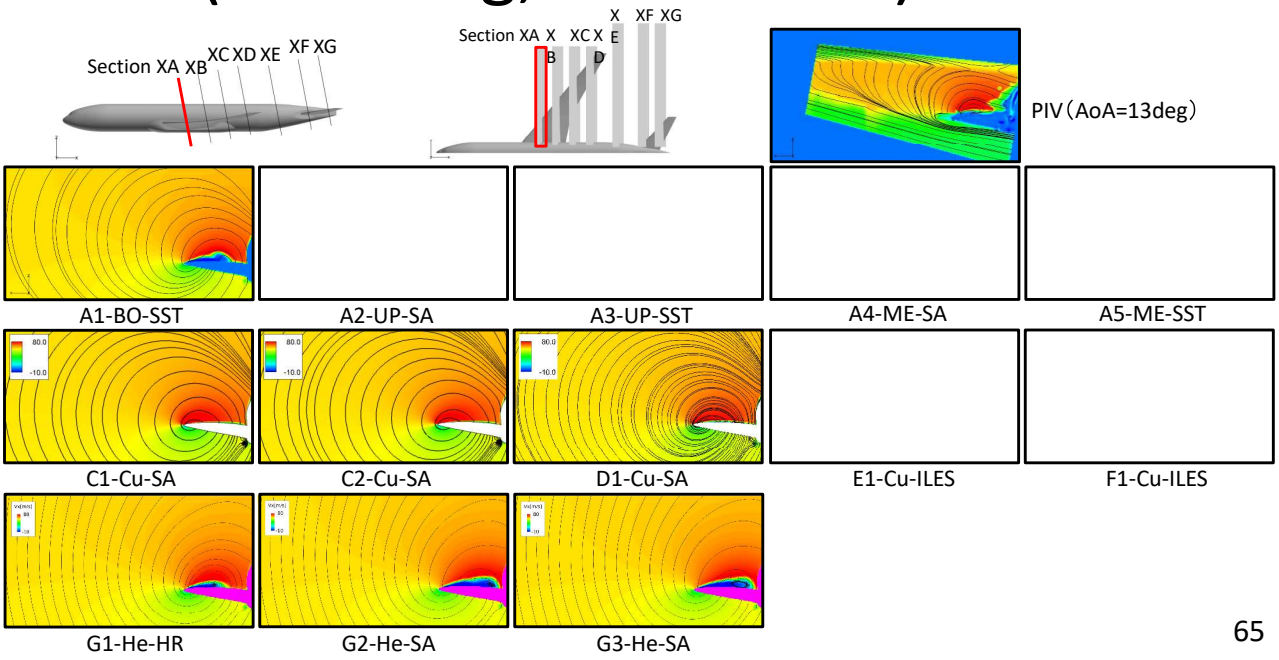

65

Velocity contours (13.08deg, Section XB)

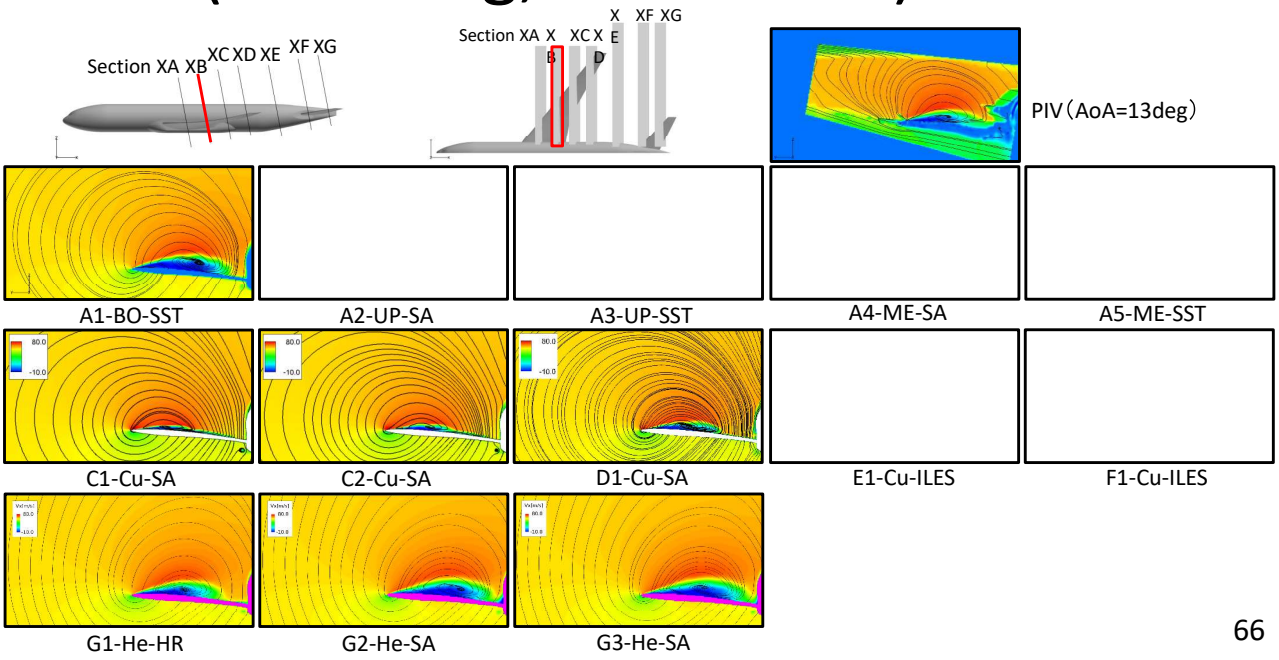

66

Velocity contours (13.08deg, Section XC)

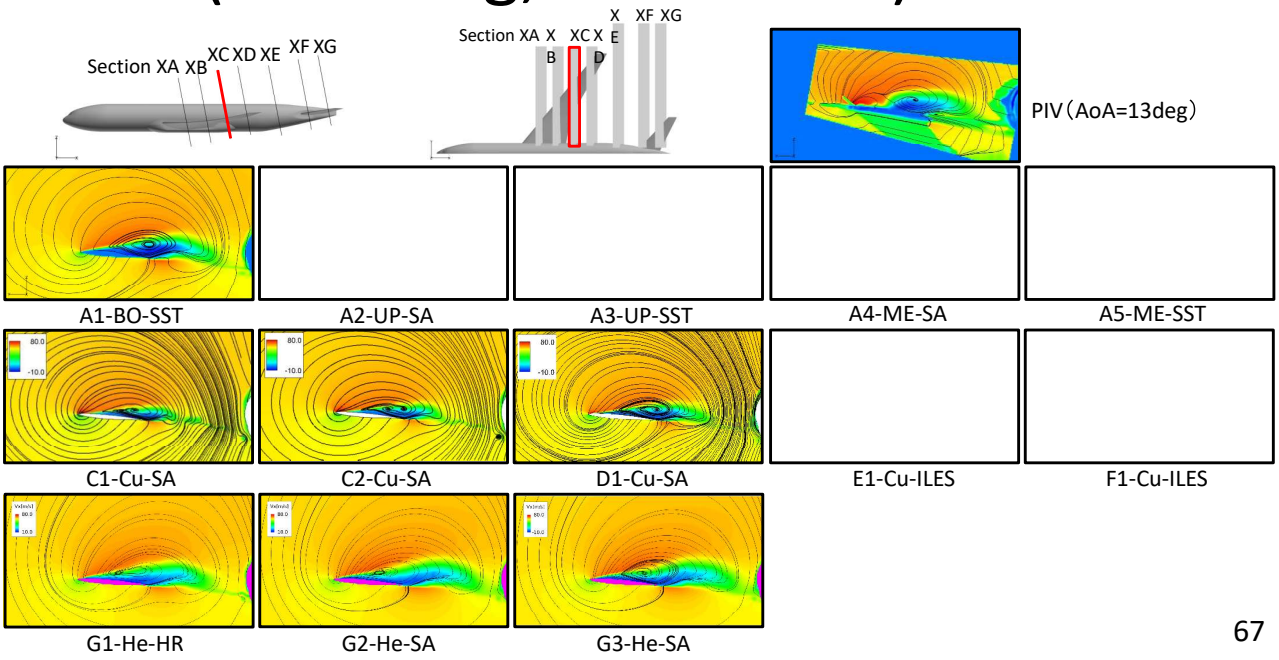

67

Velocity contours (13.08deg, Section XD)

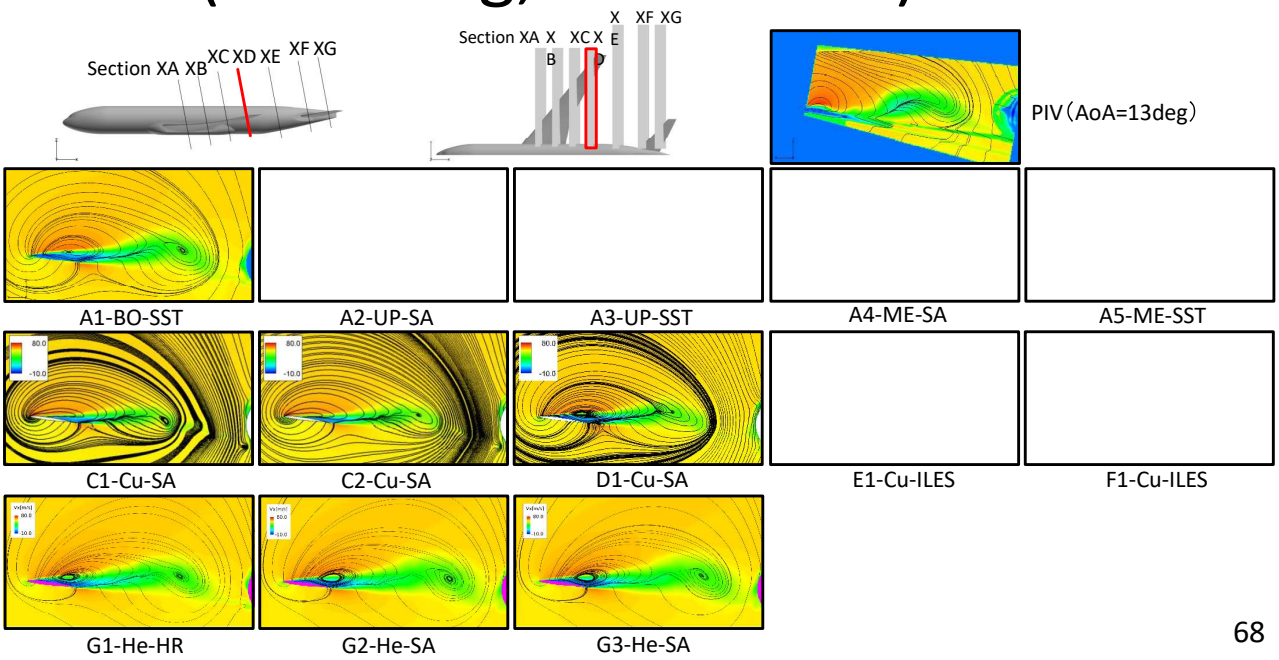

68

Velocity contours (13.08deg, Section XE)

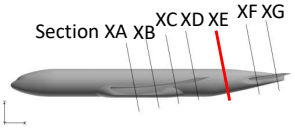

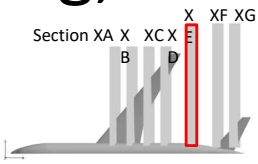

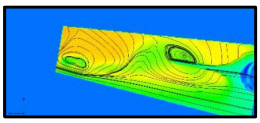

PIV（AoA=13deg）

A1-BO-SST　A2-UP-SA　A3-UP-SST　A4-ME-SA　A5-ME-SST

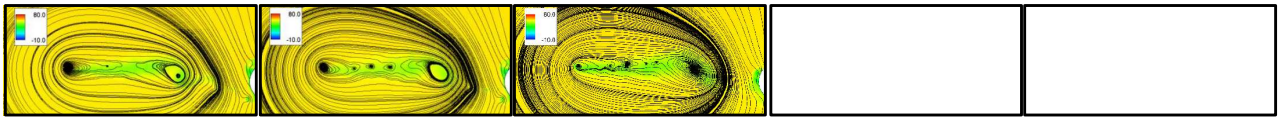

C1-Cu-SA　C2-Cu-SA　D1-Cu-SA　E1-Cu-ILES　F1-Cu-ILES

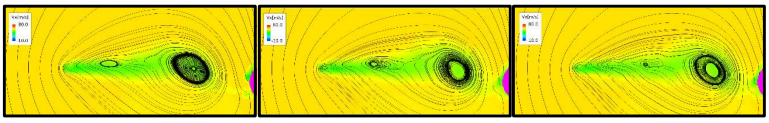

G1-He-HR　G2-He-SA　G3-He-SA

69

Velocity contours (13.08deg, Section XF)

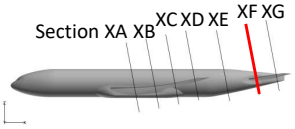

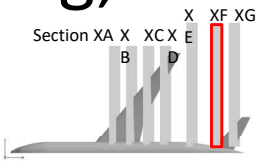

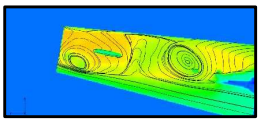

PIV（AoA=13deg）

A1-BO-SST　A2-UP-SA　A3-UP-SST　A4-ME-SA　A5-ME-SST

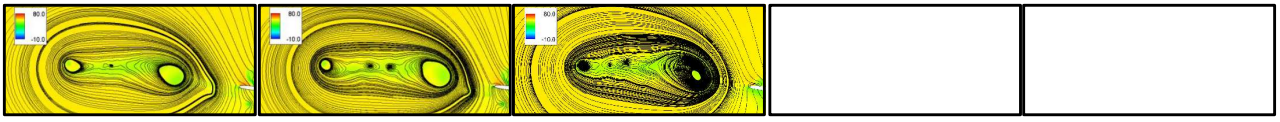

C1-Cu-SA　C2-Cu-SA　D1-Cu-SA　E1-Cu-ILES　F1-Cu-ILES

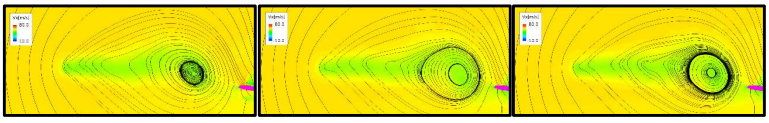

G1-He-HR　G2-He-SA　G3-He-SA

70

Velocity contours (13.08deg, Section XG)

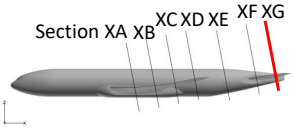

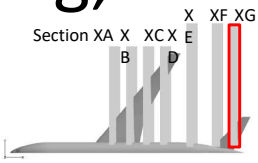

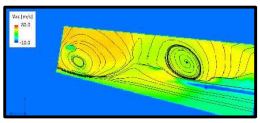

PIV（AoA=13deg）

A1-BO-SST　A2-UP-SA　A3-UP-SST　A4-ME-SA　A5-ME-SST

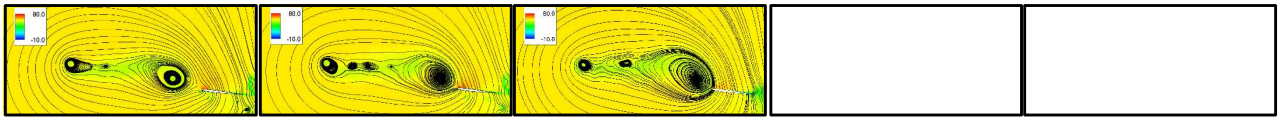

C1-Cu-SA　C2-Cu-SA　D1-Cu-SA　E1-Cu-ILES　F1-Cu-ILES

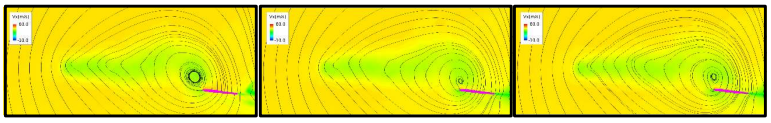

G1-He-HR　G2-He-SA　G3-He-SA

71

Surface Cp distribution（Tail, Section HB-HC）

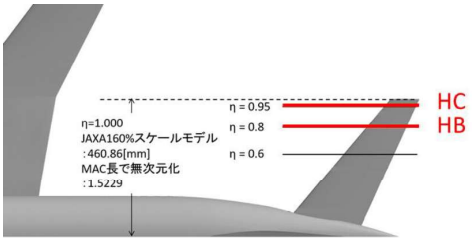

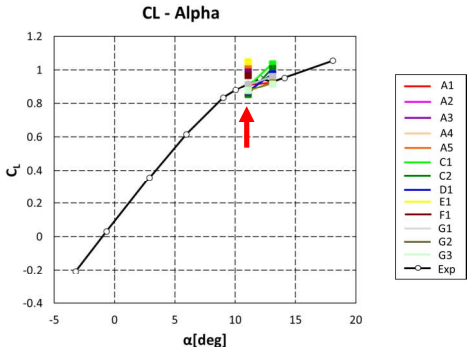

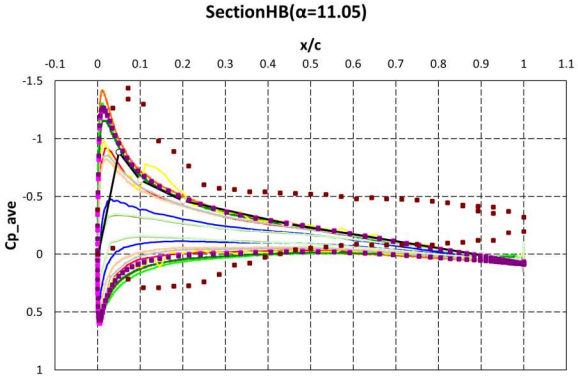

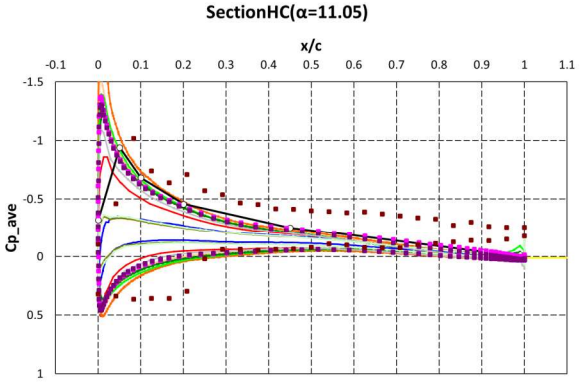

72

Surface Cp distribution（Tail, Section HB-HC）

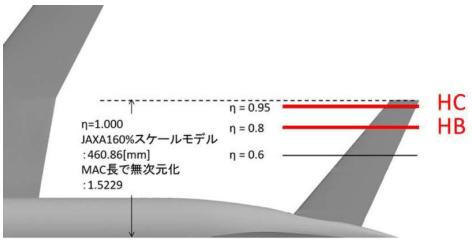

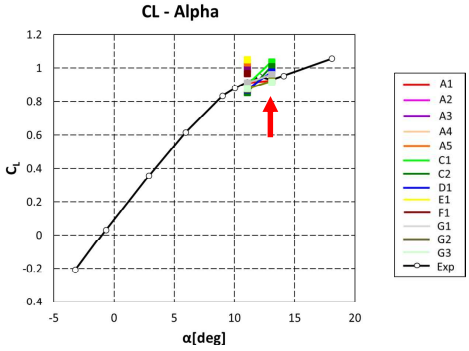

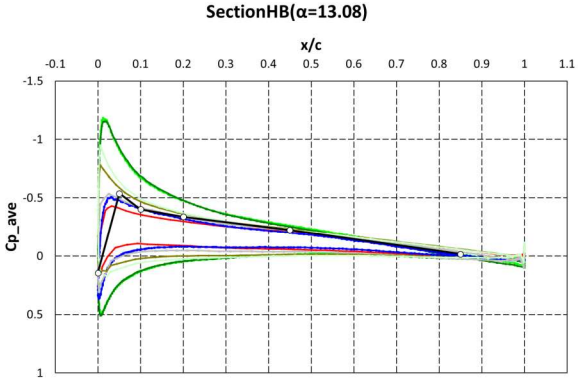

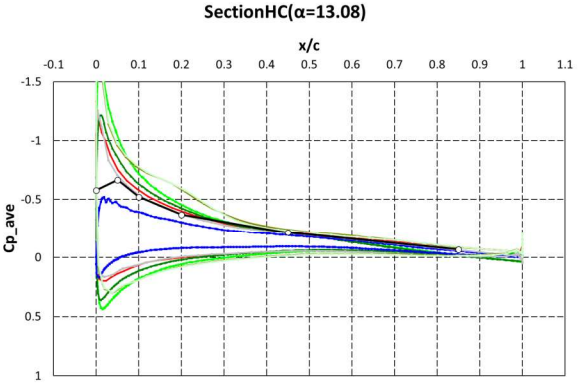

73

Surface Cp distribution（Tail, Section HB-HC）

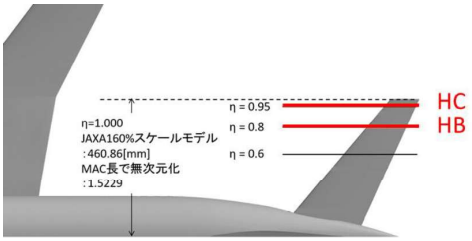

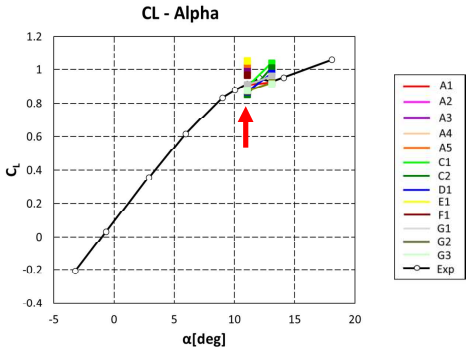

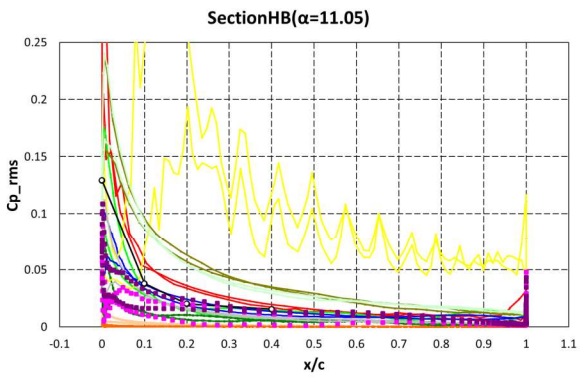

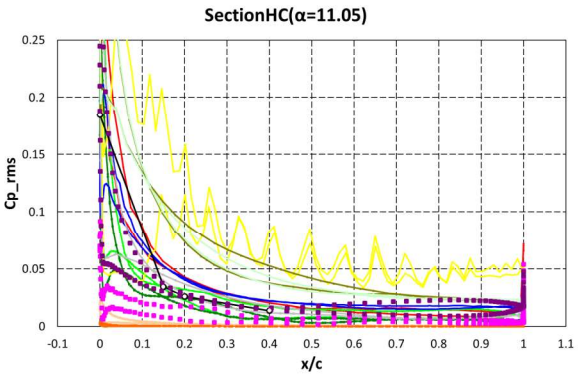

74

Surface Cp distribution（Tail, Section HB-HC）

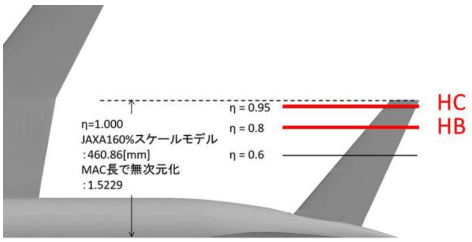

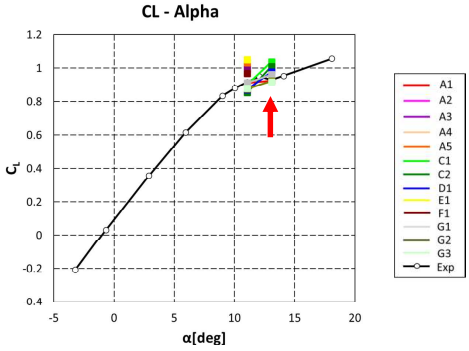

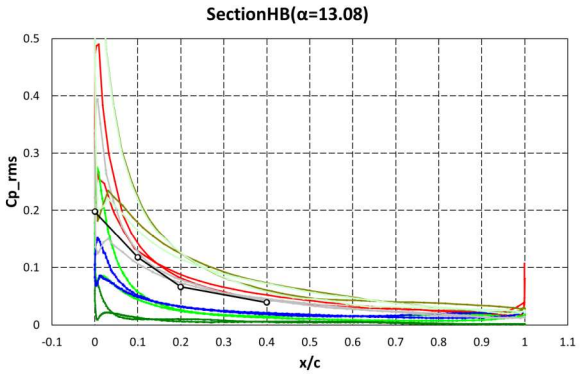

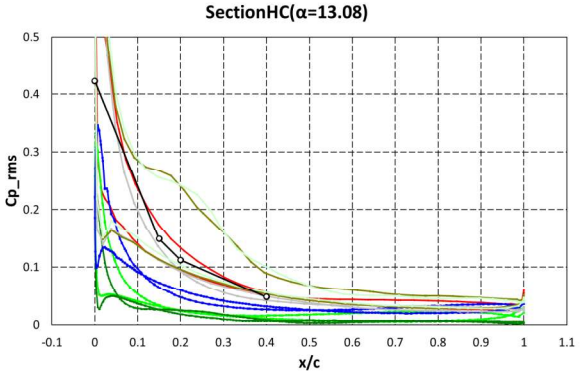

75

Surface Cp distribution（Main wing, Section B’-D’）

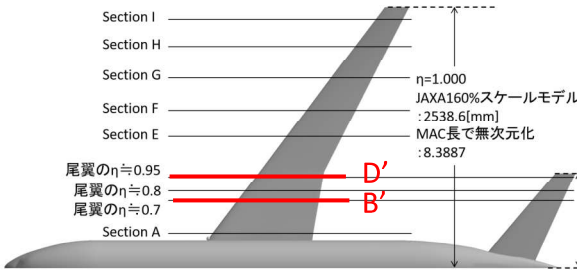

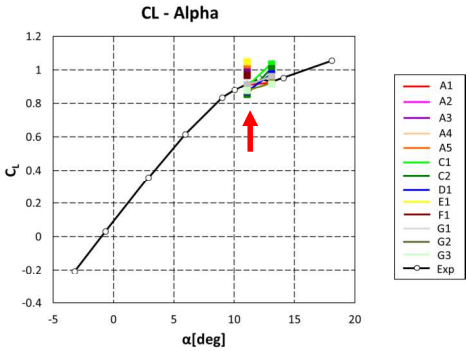

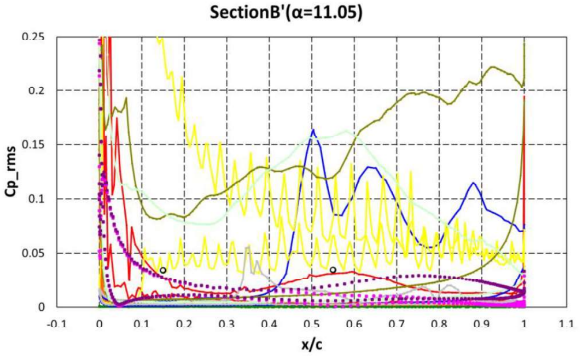

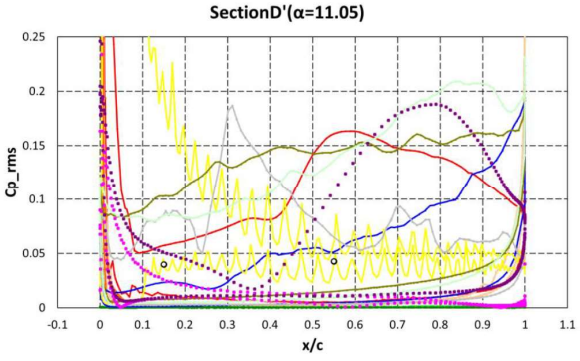

76

Surface Cp distribution（Main wing, Section B’-D’）

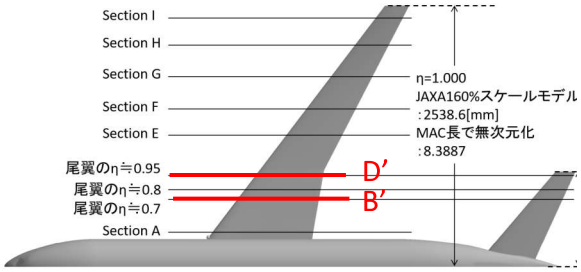

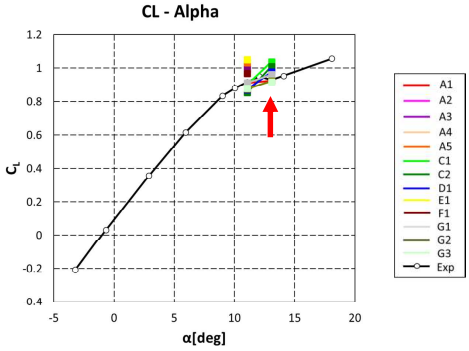

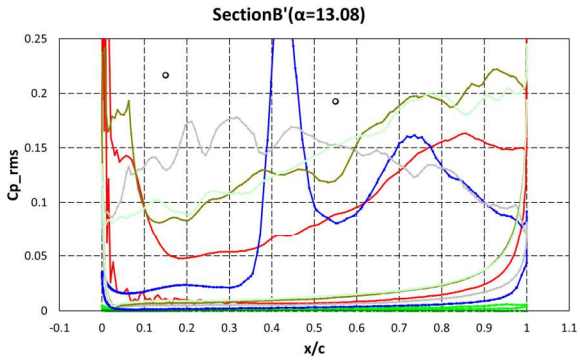

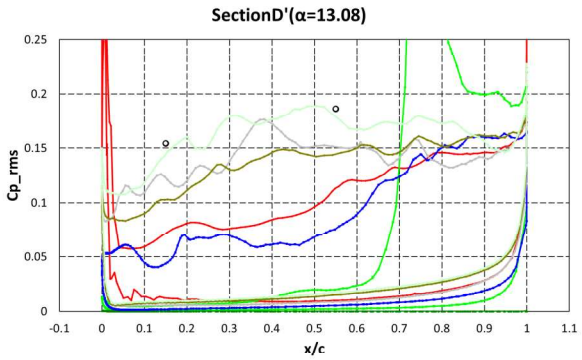

77

Summary

- The stall prediction is affected by the grid type (hexahedral/mixed-element unstructured grid, structured grid) and the boundary treatment (body-fitted grid, immersed boundary).
- The SST model predicts the stall at lower angle of attack than the SA model for various grids.
- The prediction of mild and partial separation that appears at 11deg is very challenging. The prediction of large separation at 13deg is improved by using the unsteady simulation. The variation of the predicted lift is reduced as compared with APC-6.
- The wake is diffused for the mixed-element grid that is relatively coarse between the main wing and the tail. However, for the other grids, the effect of the grid resolution on the wake profile is not clear since the wake profile is largely affected by the main wing separation.
- The rich PIV data enabled the detailed validation of three-dimensional separated flow.

78

宇宙航空研究開発機構特別資料　JAXA-SP-21-002
JAXA Special Publication
Seventh Aerodynamics Prediction Challenge（APC-7）

発　　行　　国立研究開発法人 宇宙航空研究開発機構（JAXA）
〒182-8522　東京都調布市深大寺東町7-44-1
URL: http://www.jaxa.jp/
発　行　日　　2021年11月26日
電 子 出 版 制 作　　松枝印刷株式会社